EXPERIMENTAL INVESTIGATION OF WAKES BEHIND TWO-DIMENSIONAL SLENDER BODIES AT MACH NUMBER SIX

Thesis by

Richard George Batt

In Partial Fulfillment of the Requirements

For the Degree of

Doctor of Philosophy

California Institute of Technology

Pasadena, California

1967

(Submitted May 12, 1967)

ACKNOWLEDGMENTS

The author wishes to express his sincere appreciation to Professor Toshi Kubota for his interest, patient guidance, and valuable assistance during the course of this research program. The enthusiasm and helpful suggestions of Professor Lester Lees, for which the author is deeply grateful, contributed greatly to the investigation in many ways. The author is also grateful to Messrs. S. Roman, J. Van Dijk, G. Van Halewyn, and H. Mazurowski for their assistance in conducting the wind tunnel tests; to Mr. P. Baloga under whose guidance the wind tunnel operations were performed; to Mr. G. Carlson and the staff of the GALCIT Aeronautics Shop for their skill in constructing the experimental equipment; to Mrs. Truus van Harreveld for her conscientious and proficient computational assistance; to G. Van Halewyn for his skill in preparing the illustrations; and to Mrs. E. Fox for an excellent typing of the manuscript.

A special note of appreciation goes to Professor Ernest Sechler for his initial and continued encouragement of the author's graduate career.

This thesis is dedicated to the author's wife Kay, whose inspiration and encouragement truly made it possible.

The work discussed in this thesis was carried out under the sponsorship and with the financial support of the U. S. Army Research Office and the Advanced Research Projects Agency, Contract No. DA 31 124 ARO(D) 33. This research is a part of Project DEFENDER sponsored by the Advanced Research Projects Agency.

ABSTRACT

An experimental investigation has been conducted to determine mean flow properties for both near and far wakes behind several two-dimensional slender bodies at $M_\infty = 6$. Three adiabatic wall models consisting of a flat plate model and two 20^o included angle wedge models (H = .15", H = .3") were tested. The effect of wall temperature on wake properties was examined by cooling the larger of these two wedge models with the internal flow of liquid nitrogen ($T_W/T_o = .19$). Free stream Reynolds numbers were varied from $Re_\infty/in. = .5 \times 10^5$ to 2×10^5 for each of these four configurations. In the far wake, measurements of total temperature, as determined with hot wire probes, and Pitot and static pressures were used to derive all other mean flow properties. The effect of transition on these far wake data was determined. Near wake flows were laminar for all adiabatic wall tests and at least for the two lowest test Reynolds numbers of the cold wall wedge. Base region flow field mappings and shear layer profiles were obtained for the .3"H wedge model by combining Pitot pressure data with hot wire measurements of total temperature and mass flux. These results illustrated that for slender bodies with flat bases, the basic structure for laminar near wakes is appreciably more complex for hypersonic than for supersonic flow primarily because, in hypersonic flow, the corner expansion fan extends into the separated shear layers and base region shocks now become imbedded within the viscous portion of the shear layers.

TABLE OF CONTENTS

SECTION	TITLE	PAGE
	ACKNOWLEDGMENTS	ii
	ABSTRACT	iii
	TABLE OF CONTENTS	iv
	LIST OF FIGURES	v
	LIST OF TABLES	xiii
	LIST OF SYMBOLS	xiv
I.	INTRODUCTION	1
II.	TEST APPARATUS AND EXPERIMENTAL TECHNIQUES	5
	II.1 Wind Tunnel	5
	II.2 Wind Tunnel Models	6
	II.3 Probe Design and Instrumentation	9
III.	DATA REDUCTION AND ACCURACY ESTIMATES	13
	III.1 Corrections to Measured Data	13
	III.2 Mean Flow Calculations	17
	III.3 Accuracy Estimates	20
IV.	RESULTS AND DISCUSSION	30
	IV.1 Far Wake	30
	IV.2 Near Wake	47
V.	SUMMARY OF RESULTS	71
	REFERENCES	76
	Appendix A. Hot Wire Anemometry Techniques for Mean Flow Measurements	81
	Appendix B. Data Reduction Programs	89
	Appendix C. Tabulated Mean Flow Data	151

LIST OF FIGURES

FIGURE	TITLE	PAGE
1	Schlieren Photograph of Wake behind 20°, Adiabatic Wall Wedge (H = .3) at $M_{\infty} = 6$ and $Re_{\infty H} = 5.2 \times 10^4$	179
2	Variation of Free Stream Mach Number and Temperature of Tunnel Sidewall with Free Stream Stagnation Pressure-Third Port Centerline	180
3	Variation of Free Stream Conditions along Tunnel Centerline	181
4	Variation of Free Stream Pitot Pressure in Vertical Centerplane of Tunnel	182
5a	Flat Plate Model (FP)	183
5b	20° Wedge Model-H = .15" (.15W)	184
5c	20° Wedge Model-H = .3" (.3W-1)	185
5d	20° Wedge Model-H = .3" (.3W-2)	186
6	Liquid Nitrogen Cooling System	187
7	Static and Pitot Pressure Probes	188
8	Calibration of Statham Pressure Transducer	189
9	Base Region Stagnation Point Probe	190
10	Hot Wire Probe	191
11	Simplified Schematic for Hot Wire Recording System	192
12	Probe Flow Regimes in the M-RE Plane	193
13	Nusselt Number End Loss Correction Factor	194
14	Correlation of Cylinder Heat Transfer Data	195
15a	Variation of Static Pressure along Wake Centerline at $M_{\infty} = 6$ - Flat Plate	196
15b	Variation of Static Pressure along Wake Centerline at $M_{\infty} = 6$ - 20° Wedge - H = .15	197

LIST OF FIGURES (Continued)

FIGURE	TITLE	PAGE
15c-1	Variation of Static Pressure along Wake Centerline at M_∞ = 6 - 20° Wedge - H = .3 - Adiabatic Wall	198
15c-2	Variation of Static Pressure along Wake Centerline at M_∞ = 6 - 20° Wedge - H = .3 - Adiabatic Wall	199
15d-1	Variation of Static Pressure along Wake Centerline at M_∞ = 6 - 20° Wedge - H = .3 - Cold Wall	200
15d-2	Variation of Static Pressure along Wake Centerline at M_∞ = 6 - 20° Wedge - H = .3 - Cold Wall	201
16a	Variation of Centerline Mach Number with Axial Distance at M_∞ = 6 - Flat Plate	202
16b	Variation of Centerline and Edge Mach Number with Axial Distance at M_∞ = 6 - 20° Wedge - H = .15	203
16c	Variation of Centerline and Edge Mach Number with Axial Distance at M_∞ = 6 - 20° Wedge Model - H = .3 - Adiabatic Wall	204
16d	Variation of Centerline and Edge Mach Number with Axial Distance at M_∞ = 6 - 20° Wedge Model - H = .3 - Cold Wall	205
17	Correlation of Centerline Mach Number for 20° Adiabatic Wall Wedge at M_∞ = 6	206
18a	Variation of Centerline Total Temperature with Axial Distance at M_∞ = 6 - Flat Plate	207
18b	Variation of Centerline Total Temperature with Axial Distance at M_∞ = 6 - 20° Wedge - H = .3	208
19a	Variation of Centerline Velocity with Axial Distance at M_∞ = 6 - Flat Plate	209
19b	Variation of Centerline Velocity with Axial Distance at M_∞ = 6 - 20° Wedge - H = .15	210

LIST OF FIGURES (Continued)

FIGURE	TITLE	PAGE
19c	Variation of Centerline Velocity with Axial Distance at M_∞ = 6 - 20° Wedge - H = .3 - Adiabatic Wall	211
19d	Variation of Centerline Velocity with Axial Distance at M_∞ = 6 - 20° Wedge - H = .3 - Cold Wall	212
20a	Variation of Centerline Enthalpy with Axial Distance at M_∞ = 6 - Flat Plate	213
20b	Variation of Centerline Enthalpy with Axial Distance at M_∞ = 6 - 20° Wedge - H = .15	214
20c	Variation of Centerline Enthalpy with Axial Distance at M_∞ = 6 - 20° Wedge - H = .3 - Adiabatic Wall	215
20d	Variation of Centerline Enthalpy with Axial Distance at M_∞ = 6 - 20° Wedge - H = .3 - Cold Wall	216
21a	Variation of Integral Wake Thicknesses with Axial Distance at M_∞ = 6 - Flat Plate	217
21b	Variation of Integral Wake Thicknesses with Axial Distance at M_∞ = 6 - 20° Wedge - H = .15	218
21c	Variation of Integral Wake Thicknesses with Axial Distance at M_∞ = 6 - 20° Wedge - H = .3 - Adiabatic Wall	219
21d	Variation of Integral Wake Thicknesses with Axial Distance at M_∞ = 6 - 20° Wedge - H = .3 - Cold Wall	220
22a	Variation of Wake Thickness and Wake Shock Position with Axial Distance at M_∞ = 6 - Flat Plate	221
22b	Variation of Wake Thickness and Wake Shock Position with Axial Distance at M_∞ = 6 - 20° Wedge - H = .15	222

LIST OF FIGURES (Continued)

FIGURE	TITLE	PAGE
22c	Variation of Wake Thickness and Wake Shock Position with Axial Distance at $M_\infty = 6$ - 20° Wedge - H = .3 - Adiabatic Wall	223
22d	Variation of Wake Thickness and Wake Shock Position with Axial Distance at $M_\infty = 6$ - 20° Wedge - H = .3 - Adiabatic Wall	224
23	Wake Transition Correlation at $M_\infty = 6$	225
24a	Comparison of Velocity Defect Data with Linear Theory for $M_\infty = 6$ and $Re_{\infty_L} = 4.7 \times 10^4$ - Flat Plate	226
24b	Comparison of Velocity Defect Data with Linear Theory for $M_\infty = 6$ and $Re_{\infty_H} = 1.4 \times 10^4$ - 20° Wedge - H = .15	227
24c	Comparison of Velocity Defect Data with Linear Theory for $M_\infty = 6$ and $Re_{\infty_H} = 1.4 \times 10^4$ - 20° Wedge - H = .3 - Adiabatic Wall	228
25a	Comparison of Enthalpy Excess Data with Linear Theory for $M_\infty = 6$ and $Re_{\infty_L} = 4.7 \times 10^4$ - Flat Plate	229
25b	Comparison of Enthalpy Excess Data with Linear Theory for $M_\infty = 6$ and $Re_{\infty_H} = 1.4 \times 10^4$ - 20° Wedge - H = .3 - Adiabatic Wall	230
26	Correlation of Centerline Velocity Data with Linear Theory $Re_\infty/in. = 4.7 \times 10^4$	231
27	Flow Field Mapping of Near Wake Behind Flat Plate at $M_\infty = 6$	232
28	Correlation of Near Wake Thickness Behind Flat Plate at $M_\infty = 6$	233
29	Variation of Trailing Edge and Neck Thickness with Free Stream Reynolds Number at $M_\infty = 6$	234
30	Correlation of Neck Thickness for 20° Wedges at $M_\infty = 6$	235

LIST OF FIGURES (Continued)

FIGURE	TITLE	PAGE
31	Surface Pressure Distribution Near Trailing Edge of 20^{o}, Adiabatic Wall Wedge at $M_{\infty} = 6$	236
32	Wedge Base Pressure at $M_{\infty} = 6$	237
33	Correlation of Wedge Base Pressure Data at $M_{\infty} = 6$	238
34	Correlation of Base Pressure Data for Adiabatic Wall Wedges	239
35a	Rear Stagnation Point Location for Near Wake behind 20^{o} Wedge at $M_{\infty} = 6$ (H = .3) - Adiabatic Wall	240
35b	Rear Stagnation Point Location for Near Wake behind 20^{o} Wedge at $M_{\infty} = 6$ (H = .3) - Cold Wall	241
36	Variation of Rear Stagnation Point Temperature with Wall Temperature	242
37a	Typical Shear Layer Profiles for Near Wake behind 20^{o}, Adiabatic Wall Wedge at $M_{\infty} = 6$ and $Re_{\infty_H} = 1.4 \times 10^{4}$ (H = .3) - Pitot Pressure Profiles	243
37b	Typical Shear Layer Profiles for Near Wake behind 20^{o}, Adiabatic Wall Wedge at $M_{\infty} = 6$ and $Re_{\infty_H} = 1.4 \times 10^{4}$ (H = .3) - Total Temperature Profiles	244
37c	Typical Shear Layer Profiles for Near Wake behind 20^{o}, Adiabatic Wall Wedge at $M_{\infty} = 6$ and $Re_{\infty_H} = 1.4 \times 10^{4}$ (H = .3) - Mach Number Profile	245
37d	Typical Shear Layer Profiles for Near Wake behind 20^{o}, Adiabatic Wall Wedge at $M_{\infty} = 6$ and $Re_{\infty_H} = 1.4 \times 10^{4}$ (H = .3) - Static Pressure Profiles	246
37e	Typical Shear Layer Profiles for Near Wake behind 20^{o}, Adiabatic Wall Wedge at $M_{\infty} = 6$ and $Re_{\infty_H} = 1.4 \times 10^{4}$ (H = .3) - Velocity Profiles	247

LIST OF FIGURES (Continued)

FIGURE	TITLE	PAGE
37f	Typical Shear Layer Profiles for Near Wake behind 20^{o}, Adiabatic Wall Wedge at $M_{\infty} = 6$ and $Re_{\infty_H} = 1.4 \times 10^4$ (H = .3) - Static Enthalpy Profiles	248
38a	Flow Field Mapping of Near Wake behind 20^{o}, Adiabatic Wall Wedge at $M_{\infty} = 6$ (H = .3) - $Re_{\infty_H} = 1.4 \times 10^4$	249
38b	Flow Field Mapping of Near Wake behind 20^{o}, Adiabatic Wall Wedge at $M_{\infty} = 6$ (H = .3) - $Re_{\infty_H} = 2.8 \times 10^4$	250
38c	Flow Field Mapping of Near Wake behind 20^{o}, Adiabatic Wall Wedge at $M_{\infty} = 6$ (H = .3) - $Re_{\infty_H} = 4.1 \times 10^4$	251
38d-1	Flow Field Mapping of Near Wake behind 20^{o}, Adiabatic Wall Wedge at $M_{\infty} = 6$ (H = .3) - $Re_{\infty_H} = 5.5 \times 10^4$	252
38d-2	Near Wake behind 20^{o}, Adiabatic Wall Wedge at $M_{\infty} = 6$ (H = .3) - Superposition of Flow Field Mapping ($Re_{\infty_H} = 5.5 \times 10^4$) and Schlieren Photograph ($Re_{\infty_H} = 5.2 \times 10^4$)	253
39a-1	Flow Field Mapping of Near Wake behind 20^{o}, Cold Wall Wedge at $M_{\infty} = 6$ (H = .3, $T_W/T_o = .19$) - $Re_{\infty_H} = 1.4 \times 10^4$ - $p_t/p_o)_c$	254
39a-2	Flow Field Mapping of Near Wake behind 20^{o}, Cold Wall Wedge at $M_{\infty} = 6$ (H = .3, $T_W/T_o = .19$) - $Re_{\infty_H} = 1.4 \times 10^4$ - $T_t/T_o)_c$	255
39b-1	Flow Field Mapping of Near Wake behind 20^{o}, Cold Wall Wedge at $M_{\infty} = 6$ (H = .3, $T_W/T_o = .19$) - $Re_{\infty_H} = 2.8 \times 10^4$ - $p_t/p_o)_c$	256
39b-2	Flow Field Mapping of Near Wake behind 20^{o}, Cold Wall Wedge at $M_{\infty} = 6$ (H = .3, $T_W/T_o = .19$) - $Re_{\infty_H} = 2.8 \times 10^4$ - $T_t/T_o)_c$	257
39c-1	Flow Field Mapping of Near Wake behind 20^{o}, Cold Wall Wedge at $M_{\infty} = 6$ (H = .3, $T_W/T_o = .19$) - $Re_{\infty_H} = 4.1 \times 10^4$ - $p_t/p_o)_c$	258

LIST OF FIGURES (Continued)

FIGURE	TITLE	PAGE
39c-2	Flow Field Mapping of Near Wake behind 20°, Cold Wall Wedge at M_{∞_4} = 6 (H = .3, T_W/T_o = .19) - Re_{∞_H} = 4.1 x 10^4 - $T_t/T_o)_c$	259
39d-1	Flow Field Mapping of Near Wake behind 20°, Cold Wall Wedge at M_{∞_4} = 6 (H = .3, T_W/T_o = .19) - Re_{∞_H} = 5.5 x 10^4 - $p_t/p_o)_c$	260
39d-2	Flow Field Mapping of Near Wake behind 20°, Cold Wall Wedge at M_{∞_4} = 6 (H = .3, T_W/T_o = .19) - Re_{∞_H} = 5.5 x 10^4 - $T_t/T_o)_c$	261
40	Typical Static Enthalpy Profiles for Near Wake behind 20°, Cold Wall Wedge at M_∞ = 6 and Re_{∞_H} = 5.5 x 10^4 (H = .3, T_W/T_o = .19)	262
41a	Static Enthalpy Profiles - 20° Wedge Model - H = .3 - Cold Wall	263
41b	Static Enthalpy Profiles - 20° Wedge Model - H = .3 - Cold Wall	264
42a	Shear Layer Static Pressure Profiles 20° Wedge - H = .3 - Adiabatic Wall	265
42b	Shear Layer Static Pressure Profiles 20° Wedge - H = .3 - Cold Wall	266
43a	Shear Layer Velocity Profiles - 20° Wedge - H = .3 - Adiabatic Wall	267
43b	Shear Layer Velocity Profiles - 20° Wedge - H = .3 - Cold Wall	268
44a	Pitot Pressure Profiles - Flat Plate	269
44b	Pitot Pressure Profiles - 20° Wedge - H = .15	270
44c-1	Pitot Pressure Profiles - 20° Wedge - H = .3 - Adiabatic Wall	271
44c-2	Pitot Pressure Profiles - 20° Wedge - H = .3 - Adiabatic Wall	272
44d-1	Pitot Pressure Profiles - 20° Wedge - H = .3 - Cold Wall	273

LIST OF FIGURES (Continued)

FIGURE	TITLE	PAGE
44d-2	Pitot Pressure Profiles - 20° Wedge Model - H = .3 - Cold Wall	274
45a	Total Temperature Profiles - Flat Plate	275
45b	Total Temperature Profiles - 20° Wedge - H = .3 - Adiabatic Wall	276
45c	Total Temperature Profiles - 20° Wedge Model - H = .3 - Cold Wall	277

LIST OF TABLES

TABLE	TITLE	PAGE
I	Test Summary	177
II	Accuracy Summary	178

LIST OF SYMBOLS

b	spanwise length
c	flat plate chord length
C	Chapman-Rubesin factor ($= \rho\mu/\rho_e\mu_e$)
d	hot wire diameter
D	reference length
E	wake energy thickness ($= \int_0^\infty \frac{\rho u}{\rho_e u_e}\left(1 - \frac{T_t}{T_{t_c}}\right)dy$)
g	normalized enthalpy excess $[=(h-h_e)/h_e]$
$g(s_1)$	molecular speed ratio function
h	static enthalpy
$\bar{h}$	convective heat transfer coefficient ($= q/(T_w - T_{aw})$)
H	total base height
I	hot wire current
k	conductivity
ℓ	hot wire length
ℓ_p	length of pressure tubing
L	flat plate chord length
M	Mach number
$\overline{M}$	mass of gas in given volume
Nu	Nusselt number ($= \bar{h}d/k$)
p	pressure
p_{t_2}	Pitot pressure
$p_o \equiv p_{t_\infty}$	freestream total pressure
Pr	Prandtl number
q	heat transfer rate per unit area
Q	throughput
r	recovery factor

R wire resistance

$\mathcal{R}$ gas constant

Re Reynolds number

R_r reference wire resistance for zero current and zero ^{o}C

s resistance parameter $\left(= \frac{\alpha_r T_t}{1+\alpha_r (T_{awm} - T_r)}\right)$

s_1 molecular speed ratio $(= \sqrt{\gamma/2}\, M)$

St Stanton number

t time

T temperature

$T_o \equiv T_{t_\infty} \equiv T_{t_e}$ free stream total temperature

u velocity

$\bar{u}_*$ limiting velocity ratio along dividing streamline (=.587)

U pipe flow resistance

V volume of system

w normalized velocity defect $\left(= \frac{u_e - u}{u_e}\right)$

x axial distance from model base

$\bar{x}$ transformed axial distance from model base $\left(= \int_0^x \frac{\rho_e u_e \mu_e}{\rho_\infty u_\infty \mu_\infty}\, dx\right)$

y lateral distance from wake centerline

$\bar{y}$ transformed lateral distance from wake centerline

$$\left(= \frac{\rho_e u_e}{\rho_\infty u_\infty} \sqrt{Re_{\infty H} C} \int_0^y \frac{\rho}{\rho_e}\, dy \right)$$

α accommodation coefficient

α_r slope of wire calibration curve $(R_{wm} \sim T_{wm})$ for zero current

γ specific heat ratio

δ shear layer or wake total temperature thickness

δ^* wake displacement thickness $\left(= \int_0^\infty (1 - \frac{\rho u}{\rho_e u_e}) \, dy \right)$

Δx axial distance between a zero intercept transition distance, obtained by extrapolating transition location data to infinite Reynolds number, and a transition location

η_c experimental recovery ratio for continuum flow

η_f theoretical recovery ratio for free molecule flow

η_* recovery ratio for infinite length wire $(=T_{aw*}/T_t)$

$\overline{\eta}_*$ normalized recovery ratio for infinite length wire $((\eta_*-\eta_c)/(\eta_f-\eta_c))$

θ wedge included angle

$\overline{\theta}$ wake momentum thickness $\left(= \int_0^\infty \frac{\rho u}{\rho_e u_e} (1 - \frac{u}{u_e}) \, dy \right)$,

$\overline{\theta}_{avg}$ average wake momentum thickness

μ viscosity

ν_o dimensionless quantity $\left(= \frac{\ell}{d} \sqrt{\frac{k_t}{k_w}} \, Nu_t \right)$

ρ density

τ plate thickness

$\overline{\chi}$ hypersonic viscous interaction parameter $\left(= \frac{M^3 \sqrt{C}}{\sqrt{Re_x}} \right)$

ψ streamline $(= \int_0^y \rho u dy)$

ψ_N Nusselt number end loss correction factor $(= \frac{Nu_t}{Nu_m})$

ψ_r recovery temperature end loss correction factor $(= \frac{T_{aw*}}{T_{awm}})$

ω_o dimensionless quantity $(= \frac{\tanh \nu}{\nu})$

Subscripts

aw zero heat transfer (adiabatic wall)

b base

BL boundary layer edge

c	continuum flow
C	constant
℄	centerline
e	edge
f	free molecule flow
H	total base height
m	measured
NW	near wake edge
o	initial condition
r	evaluated at reference temperature (= 273^{o}K)
s	support
sp	rear stagnation point
S	shock wave
t	local stagnation quantity
TE	trailing edge
TR	transition
w	wire
ws	wedge surface
W	wall
1	upstream of shock
2	downstream of shock
∞	free stream conditions
*	refers to infinitely long wire

I. INTRODUCTION

The wake of a body moving at high speeds through air (figure 1) has intrigued investigators for many years. Originally, because of the interest in base drag estimates, this problem was looked upon primarily as a "base pressure problem." However, with the advent of hypersonic vehicles and the necessity to understand and evaluate wake observable phenomena, attention has more recently been focused on not only the near but also the far wake regimes. To date, reasonable progress has been made in analytically treating the laminar and turbulent far wake, including the effects of transition, once initial profile data have been provided (1-7). As a result, current studies are now concentrating on the near wake (that portion of the wake upstream of and including the wake neck) with the intent of suitably evaluating the complex coupling processes that occur within the base regions of hypersonic wakes. In these regions separated shear layers, which initially may often be considered as constant pressure mixing regions, enclose a low speed, recirculating flow which extends downstream to the location where the shear layers coalesce to form the wake's rear stagnation point. In the vicinity of this point the flow recompresses as the shear layers turn parallel to the wake axis. This turning process generates the wake shock observed experimentally in hypersonic wake investigations. The wake thickness beyond the stagnation point continues to thin down because of the acceleration of the wake flow until the neck or minimum thickness location is reached. In many cases, the separated shear layers for low supersonic flows and even for hypersonic flows behind blunt

bodies, experience negligible lateral pressure gradients (8). This is not the case however for high speed flow in the base regions of slender bodies with flat bases. The rapid expansion of the boundary layer at the body's trailing edge gives rise to inviscid rotational flow phenomena with lip shocks becoming deeply imbedded within the vortical flow of the shear layer (9,10). The Chapman dividing streamline model based on conservation of mass within the recirculating flow region (11), and the significance of base region mixing due to momentum transport as outlined in the Crocco-Lees Theory (12) are indeed still applicable for the slender body near wake. However, the outer flow is highly complicated in this latter case and at the present time the complete matching procedure which joins the base region flow to the pre-separated boundary layer is not satisfactorily understood. Furthermore this coupling process is dependent on the upstream influence of the corner expansion and the pronounced profile distortion that takes place in the vicinity of the trailing edge. Thus a current need exists for experimentally investigating the near wake with emphasis on flow field mappings and shear layer profiles.

The far wake investigation reported herein has been carried out because it was realized early in the present investigation that not only did there appear to be a scarcity of such data for slender bodies with which to verify existing theory, but the effect of transition on mean flow properties, the approach of laminar wake flow to classical linear theory and the effect of model cooling on the far wake properties seemed to merit further study. In addition it was well known that the onset of transition and its proximity to the near

wake could appreciably alter the base region properties. For example, as Crocco and Lees have shown (12), the significant increase in base region mixing associated with the onset of turbulence in the separated shear layers of the base region, results in a substantial increase in the amount of recompression the flow is able to sustain. In fact, even for transitional flow a significant rise in base region mixing may occur, if the most forward location of the wake's "transition zone" is in the vicinity of the wake's "critical point". This characteristic wake location (the point where the wake goes supersonic on the "average") is located just upstream of the centerline sonic point. Since the downstream pressure appears dominated by the inviscid flow and is relatively insensitive to Reynolds number effects, the increased recompression capability results in a lowering of the base pressure with a correspondingly greater expansion of the separated shear layers. It is therefore important to determine the most forward location of the wake transition region, so that an experimental investigation of the laminar near wake can be undertaken with confidence that the flow corresponds to only laminar conditions, and does not include the additional effects of turbulent mixing phenomena. Thus the far wake results reported in Section VI.1 were obtained prior to initiating the near wake investigation discussed in Section IV.2.

It is with these ideas in mind that the present study has been undertaken. It is a study which examines experimentally the effects of free stream Reynolds number, wall temperature ratio and model geometry on the flow properties of hypersonic wakes behind two

dimensional slender bodies. Taken together the complete set of results serves not only as a means for verifying existing theory but also provides additional insight into those hypersonic wake regions which are not yet amenable to analytical treatment.

II. TEST APPARATUS AND EXPERIMENTAL TECHNIQUES

II.1 Wind Tunnel

Leg I of the GALCIT Hypersonic Wind Tunnel (13) with a nominal Mach number of 6 was used to obtain the present set of wake measurements. This tunnel is a continuous flow, closed return device with a 5''x 5'' test section. A usable test rhombus extends from 23'' (model position) to approximately 33'' downstream of the nozzle throat. Tests were made for stagnation pressures of p_o = 10, 35, 60 and 85 psig corresponding to free stream Reynolds numbers of Re_∞/in. = .465, .94, 1.42, and 1.9 x 10^5/in. A reservoir stagnation temperature of 275°F and a dew point of -40°F was maintained for all tests which satisfactorily eliminated condensation effects. Table I summarizes the various test conditions covered during the current experimental investigation.

Because of the boundary layer along the tunnel wall the Mach number in the test section varies slightly with stagnation pressure and with axial position. Pitot and static pressure surveys both in the axial and vertical centerplanes were made without a model in the tunnel ('free' tunnel) to determine the magnitude of such variations and to establish suitable corrections to measured data. The results of these surveys, which compare favorably with similar data of Dewey (8), Herzog (14), and Behrens (7), are shown in figures 2, 3 and 4. Since flow conditions were sensitive to wall boundary layer effects, the tunnel was always warmed up for approximately 2 hours before any data were taken. This provided sufficient time for the temperature of the tunnel wall (figure 2) to reach its equilibrium level.

In comparing free stream stagnation temperatures, as measured with hot wire probes, with the reservoir temperature of 408°K, a consistent deficiency of 1 to 2% was observed. Such a result was similarly found by Behrens (7). A calibration check using an iron constantan thermocouple located 1 inch upstream of the nozzle throat confirmed the accuracy of the automatic regulator which set the reservoir temperature. However some energy loss takes place as the low speed air accelerates through the nozzle and it is tentatively concluded that this is the primary cause for the noted deficiency. In any event, all results cited in this report have been suitably normalized so that this effect is relatively unimportant to final results.

II.2 Wind Tunnel Models

For the present investigation four separate models consisting of a flat plate model and three wedge models of 20° included angle, were fabricated from Ketos steel. The geometry of these models and the manner in which they were installed in the tunnel are shown in figure 5. The leading edges of all models were carefully machined to thicknesses less than .002". Alignment with the free stream flow was established either by checking the symmetry of Pitot pressure traces in the wake or by comparing the lower and upper surface pressures, as was the case for the one wedge model which had surface pressure taps (.3w-1, Table I). To minimize the interference effects from the boundary layer on the tunnel wall, fences were designed for the wedge models. These fences were triangular in shape, 1/16" in thickness, and attached perpendicular to the base. They were

located 3/4'' from the tunnel wall and extended two base heights downstream.

The first model tested was a flat plate with a 1'' chord and .0156'' thickness. Both the leading and trailing edges of the plate were tapered to a 4^{o} included angle with an edge thickness of approximately .0017''. The plate was tested while under tension to eliminate vibration.

The smallest of the wedge models, one with a base height of .15'', was the next configuration investigated. Two base taps, .0135'' in diameter, were installed on the model centerline and a base pressure lead, .042'' stainless steel tubing, was flush mounted in a groove on the base and brought out of the tunnel through one of the side ports.

In order to extend the base pressure results of this small wedge model and also to obtain surface pressure data near the trailing edge of a 20^{o} wedge, another model with the same included angle but with a base height of .3'', was machined from a solid piece of Ketos steel. Surface and base pressure taps were installed as noted in figure 5c with the pressure leads, .042'' stainless steel tubing, being flush mounted in surface grooves and led out one of the side ports.

The design of the final 20^{o} wedge was determined by the need to test a .3'' base height model, which could be cooled by the internal flow of liquid nitrogen. This model was constructed in a rib and skin configuration by first machining the upper, lower, and base surfaces and then soldering them together in the manner shown

in figure 5d. The thicknesses of the three surfaces were initially somewhat oversize so that the assembled model could be machined to the specified dimensions. Four copper constantan "Ceramo" thermocouples, each enclosed within ceramic insulation and a .040" stainless steel shroud, were spot welded to internal surfaces at locations specified in figure 5d. Cylindrical model supports, containing nitrogen coolant lines and the thermocouple leads, were soft-soldered to each end of the model. Leak free mounting was insured by soft soldering metal bellows to these supports after the model was installed in thermally insulating micarta inserts and aligned in the tunnel. These bellows proved satisfactory in not only sealing the model in its mountings under extremely cold temperature conditions, but also in allowing for the contraction and expansion of the tunnel side walls during the start and shut down operation of the tunnel. Although this model was designed primarily for cold wall testing, it was also used as an adiabatic wall model, and a complete set of wake measurements were obtained for both cold and adiabatic wall conditions. This proved important to final results since the effects of cooling on wake properties were readily discernible.

A schematic diagram of the nitrogen cooling system developed during the current investigation is presented in figure 6. The system's inlet side consisted of one nitrogen pressurizing bottle with gauge, a pressurized storage tank, and a cooling bath, all in series with the model. Similarly, a cooling bath and storage tank, vented to atmosphere, were attached in series on the outlet side. This

arrangement made it possible to cycle the nitrogen from one tank to the other with relative ease while achieving spanwise uniformity in model temperature (77°K) with only approximately 1 psig inlet pressure. Some frost buildup was observed on the model, approximately .002" after about two minutes of operation at this low temperature level. However most transverse traces took less than two minutes duration so that the effect of frost buildup would seem to be relatively unimportant. After each trace, the nitrogen flow was shut off and the subsequent heating of the model rapidly "burned" off any accumulated frost. Unfortunately some temperature gradient always existed in the chordwise direction since the leading edge could never be sufficiently cooled due to its lack of direct contact with the liquid nitrogen. This was evident in that the frost buildup always began about .1" downstream of the leading edge. Such a gradient will influence the initial boundary layer and subsequent interaction effects.

II.3 Probe Design and Instrumentation

A) Pitot Pressure Probe

Pitot pressure surveys were made for the present set of wake measurements with a .042" diameter probe flattened at the forward end to a .004" by .035" opening, figure 7. The probe positioning mechanism of the tunnel activated a Helipot potentiometer which in turn converted probe positions to linear electric signals for use in a Moseley XY recorder. A 5 psi Statham pressure transducer was used for most measurements to convert pressures to

electrical signals which were recorded, after suitable amplification, on the XY recorder. The transducer was calibrated against a mercury manometer and the results are shown in figure 8. Near the base of the various models, where measured pressures fell below the lower limit of the transducer's range of linearity, Pitot pressures on the centerline were more accurately measured by means of a silicon micromanometer. A vacuum reference pressure for this manometer was maintained at less than a .5 microns by combining a diffusion pump in series with a mechanical vacuum pump. The precision gauge on the manometer permitted reading pressure levels to within .5 mm of silicon.

B) Static Pressure Probes

Static pressures along the wake centerline were measured with the above-mentioned silicon micromanometer using pressure probes fabricated from .042'' stainless steel tubing. The conical tipped probe shown in figure 7 was identical to that designed and calibrated by Behrens (15). On this probe three pressure orifices were located ten diameters behind the shoulder of a 20^{o} cone tip. Although this probe was used for the majority of the static pressure measurements, its tip to orifice length prevented taking measurements near the base of a model, and additional probes were used to obtain near wake data for the largest wedge model tested. These probes, three in number, consisted of 2'' lengths of .042'' tubing with one end capped off. For each probe two orifices were located at a prescribed distance from the capped tip and the open end was soft-soldered to a pressure lead holder. In practice the sealed tip

of the probe was placed in contact with the base of the model on the wake centerline and the subsequent pressure recorded by the precision micromanometer. Since tip to orifice lengths were different for each of the three probes, it was then possible to obtain a distribution of static pressure on the wake centerline. Great care was exercised to maintain all probes at zero angle of attack because of the pronounced sensitivity of static pressure probes to angle of attack effects (16).

C) Stagnation Point Probe

Because of the significance in near wake studies of the rear stagnation point, a special probe (figure 9) was fabricated to aid in determining the location of this point. This probe was made from .032" stainless steel tubing and actually consisted of two pressure leads. A spanwise section of the tubing, sealed at the centerline location, was joined at each end to these leads. Pressure taps, one facing upstream and the other downstream, were located on alternate sides of the center cap. When in use the pressure leads were brought out of the tunnel through the probe strut system and attached to opposite sides of a silicon "U" tube. The probe was then maneuvered along the wake centerline in the base region until the pressure levels were equal. In principle, as the probe moved into and out of the recirculating region, the pressure levels would be unequal at every position except the rear stagnation point since, except for that location, one tap would either be experiencing "base type" flow while the other would be under impact pressure conditions, or vice versa. In this manner the location where the pressures just balanced each

other, namely the rear stagnation point, was determined.

D) Hot Wire Anemometer

The hot wire probes used for the current set of measurements were similar to those designed by Dewey (17) and modified by Herzog (14). Each probe consisted of a platinum-10% rhodium wire approximately .030" in length, soft-soldered to two needle supports, figure 10. Chromel Alumel thermocouple wires (.001") were spot welded to within .005" of one support tip for each of the probes. All wires were annealed and calibrated in the manner outlined by Dewey (17). From these calibration measurements wire resistivity coefficients (α_r) and reference resistances (R_r) for zero current were determined. Manufacturer specified resistance values for 68°F were checked against these calibration results and slight variations, less than 1% were observed.

For the actual flow measurements, the instrumentation system (figure 11) developed by Herzog (14) was used with considerable success. This system not only automatically positioned the probe in the tunnel but was also capable of measuring and recording on IBM cards the probe position, support temperature, and wire voltages corresponding to five known currents. A comprehensive description of this system is furnished by Herzog (14) and a discussion of the manner in which the measured data were reduced to furnish adiabatic wire temperatures and measured Nusselt numbers is given in Appendix A.

III. DATA REDUCTION AND ACCURACY ESTIMATES

III.1 Corrections to Measured Data

All Pitot and static pressure measurements have been adjusted so as to account for the tunnel axial gradients discussed in Section II. This was accomplished by dividing the measured pressure at a given axial location by the ratio of the pressure at the same location to the pressure at the location corresponding to the model's leading edge under "free" tunnel conditions, figure 3. Since lateral gradients in Pitot pressures under "free" tunnel conditions (figure 4) were relatively minor no corrections have been made to the measured data for these effects.

Virtual leak corrections were also made for Pitot and static pressure measurements as well as base pressure data. Because all high vacuum systems experience some outgassing or even small in-leaks, a pretest calibration of each probe was carried out using the silicon micromanometer to determine, if necessary, suitable corrections for these effects. As discussed in reference 21, such corrections are determined for a sealed system with a given volume by first measuring the change of pressure per unit time for that system. The product of the volume and this rate of pressure change can be shown to be proportional to the mass inflow rate for a sealed system. Using the perfect gas law and assuming small volume changes this follows from:

$$V \frac{dp}{dt} = \frac{d\overline{M}}{dt} \mathcal{R} T$$

The noted product is often termed the throughput in vacuum technology and given the designation Q. Under actual test conditions this mass flow is exhausted out the probe opening and, as a result, a certain pressure drop occurs along the length of pressure lead between the micromanometer and the probe orifice. Since the pressure levels for the present measurements corresponded to viscous rather than free molecular flow, it can be shown from Hagen-Poiseuille pipe flow theory that the resistance to such a mass flow is given by:

$$U = \frac{\pi D^4}{128 \mu \ell_p} \bar{p}$$

and the resultant pressure drop is then determined from:

$$\Delta p = \frac{Q}{U}$$

For many pressure measurements this virtual leak correction is relatively unimportant and can often be disregarded. On the other hand, in regions where very low pressures exist, such as base recirculation regions behind slender two dimensional bodies, this pressure loss can prove significant to final results and should be accounted for where applicable. Thus all low pressure data herein have been corrected for this effect whenever the estimated pressure drop was greater than 1% of the measured data.

A) Pitot Pressure Probes

Additional corrections to Pitot pressure data, such as those associated with angle of attack, streamline displacement and viscous effects were also investigated. Probe angles of attack were maintained within $\pm 1^{\circ}$ to the local flow direction for all measurements

except the separated shear layer and outer flow regimes of the near wake. For these cited exceptions the angle of attack varied by as much as $\pm 10^{o}$. Since the data of Matthews (22), McCarthy (16) and also Dewey (8) indicate that even for these angles, corrections to Pitot pressure data are negligible, no corrections for angle of attack effects have been applied to any of the Pitot pressure data presented herein.

Similarly, streamline displacement effects for those shear flows investigated herein were also found to be unimportant. Dewey (8) indicates that these effects become negligible when the ratio of free shear layer thickness to probe size is greater than 2. For the present set of experiments this ratio was greater than 25.

The final correction, that of viscous effects, was examined with the aid of figure 12. In this figure the different flow regimes covered during the present tests are easily discernible. Although the Reynolds numbers for those measurements in supersonic flow were sufficiently high, according to Matthews' results so as not to make necessary any viscous corrections for the supersonic data (<1%), such is not the case for the subsonic measurements. Using the data of Sherman (23) which describes the variation of the normalized viscous correction

$$\frac{p_{impact} - p_{impact\ w/o\ viscous\ effects}}{\frac{1}{2}\rho u^2}$$

as a function of Reynolds number, this correction has been applied to all subsonic Pitot pressure data measured during the current

investigation. For some of the low Reynolds number results herein this correction reduced measured data by as much as 20%.

B) Static Pressure Measurements

Since the conical probe shown in figure 7 was identical to the probe calibrated by Behrens (15), all corrections for viscous interaction effects have been carried out using the results of reference 15. In that reference Behrens indicates that the increase in pressure associated with viscous interaction phenomena is given by

$$\frac{p_m}{p} - 1 = .065\,\bar{\chi} + .040\,\bar{\chi}^2, \quad \bar{\chi} = \frac{M^3\sqrt{C}}{\sqrt{Re_x}}$$

For the present measurements the noted corrections were always less than 2%. Figure 12 indicates the various flow regions covered by this probe during the present tests and illustrates the range of applicability for the Behrens' data.

Those data taken with the base region probes have been left uncorrected for low Reynolds number effects. From the Behrens' results such corrections to probes of this diameter appear to be less than 1%. If any corrections are in order it would seem that interaction effects resulting from the probe's interference with the base recirculation region should be considered. Because of the difficulty in obtaining a quantitative measure of this correction, such an effect has not been accounted for, and there exists greater uncertainty in the resulting data (Section III.3.)

C) Rear Stagnation Point Probe

During a pretest checkout of the virtual leak effects associated with the stagnation point probe it was determined that the

required corrections to each of the two measured pressures were identical. Therefore the uncertainty in the measured location of the rear stagnation point was caused primarily by the base interference effects. No corrections were made to the data for this effect and the resultant uncertainty is discussed in Section III.3.

D) Hot Wire Probe

The hot wire probe, with the availability of suitable calibration data, has been shown to be an effective tool in carrying out mean flow measurements (17,24). By direct measurement it determines recovery temperature and heat transfer rate for a wire (cylinder) immersed normal to a fluid stream. These measurements, when corrected for end-loss effects and coupled with established calibration results, can then provide stagnation temperature and mass flux data for the flow in question. A detailed discussion of the manner in which the raw data measurements have been reduced, corrected and finally combined with recovery temperature and Nusselt number calibration data is presented in Appendix A.

III.2 Mean Flow Calculations

By suitably combining the corrected data discussed in the previous section, with the compressible flow relations (25), final mean flow calculations have been carried out for the present investigation. Because of the characteristics peculiar to the various wake regions examined, several different computation procedures were necessary. All these calculations were made on an IBM 7094 using semiprofile traces of Pitot pressure and total temperature

along with a third independently measured quantity. For the majority of the present results this third quantity was the static pressure which was assumed constant across the wake and equal to its value at the centerline. This procedure was followed not only for all far wake results herein but also for those neck and base regions within the wake shock boundaries. For comparison purposes flow field results for these latter regions were also calculated by using semi-profile traces of the mass flux data in place of static pressures. All other shear layer data were computed by similarly combining mass flux data with Pitot pressure and total temperature results. For those regions of inviscid flow located between the nose shock and the shear layer edge, as determined from total temperature profile traces, total temperatures and stagnation pressures remained constant throughout since it was assumed that all streamlines suffered the same total head loss in passing through the leading edge shock. As a result, the calculation procedure adopted herein for determining mean flow properties for these isentropic, inviscid regions combined total pressures, as calculated from the nose shock orientation and free stream conditions, with free stream total temperatures and measured Pitot pressures. Admittedly, curvature of the nose shock wave near the model's leading edge invalidates the assumption that all streamlines within such inviscid regions experience the same total head losses. In fact it is estimated that stagnation pressures along streamlines closest to shear layer edges may in some cases be 10 to 20% less than stagnation pressures based on the "straight" portion of the nose shock. However, even

with this uncertainty in stagnation pressure, derived mean flow results are still within the accuracy limits of hot wire data (Section III.3) and thus the assumption that stagnation pressures remained invariant for these outer inviscid regions was considered reasonable. For one model, the smallest wedge configuration (.15w), total temperature distributions were not measured, and calculations in this case were made by assuming that all stagnation temperatures remained constant and equal to the free stream value. Streamline calculations for the base region were performed by integrating mass flux data from the nose shock toward the wake centerline. Since near the wake centerline such a procedure results in appreciable errors, additional streamline data were obtained by integrating from the centerline out to the wake shock. For these calculations the first computation procedure described above was used wherein static pressure was assumed constant across the integration region.

All profile results for the present investigation have been normalized with respect to edge conditions. Although the definition of edge location is often somewhat nebulous, depending on whether total temperature or velocity traces are used, the values for edge properties can be established with some degree of consistency. For example, most transverse traces of Pitot pressure in the far wake exhibit the existence of a maximum value outside the viscous

wake and within the wake shock boundaries. Such a value, when present, has been used to compute edge properties. For several of the most aft locations of the smallest wedge model investigated (.15w) the "inviscid" Pitot pressure traces, instead of displaying a peak, exhibit initially a plateau followed by a gradual rise until the wake shock position is reached (Appendix C). The slight rise in Pitot pressure between the plateau region and the wake shock is believed caused by the weakening of the leading edge shock by the expansion fan generated at the base of the model. Thus streamlines in the far wake at increasing lateral distances from the centerline of the wake will exhibit lower total head losses with corresponding Pitot pressure variations. As a result the edge property data for these traces has been based on the plateau pressure level in lieu of the maximum "inviscid" value. In the near wake all edge results correspond to mean flow data as measured at the actual edge location determined from total temperature traces.

III.3 Accuracy Estimates

A) Free Stream Mach Number

The free stream Mach numbers herein were determined under "free" tunnel conditions from the ratio of measured Pitot pressures to the tunnel's reservoir pressure (25). Because the magnitudes of reservoir and free stream Pitot pressures were relatively high and thus could be measured very precisely, Mach numbers so computed were correspondingly quite accurate. However some repeatability difficulties existed due to wall boundary layer

effects, which caused the flow in the test section for a given set of measurements to deviate somewhat from that for the tunnel survey results. This effect was most pronounced at $p_o = 35$ psig since transition of the wall boundary layer occurred at this pressure. By combining measurement accuracies with repeatability difficulties it is estimated that values of the free stream Mach number, which have been used herein for flow field calculations, are accurate to within .5%.

B) Positioning and Alignment

From repeatability checks and by examining the reliability of position indicators it is estimated that probe position uncertainty was within $\pm$ .002". In order to eliminate the mechanical backlash effects, all vertical and axial positionings of a probe were carried out by moving the probe upward and forward respectively. It is interesting to note that the semiprofile results herein are perhaps even more accurate from a position standpoint than the cited $\pm$.002", since final results were established by averaging full profile data and thus any systematic offset would be compensated for in the reduction procedure.

Alignment of the pressure probes with the free stream direction was accomplished through use of a precision level. Because the tunnel used for the present investigation was designed with the flow parallel to the horizontal, this level was capable of aligning the pressure probe to within $.5^{\circ}$ of the axial flow direction.

C) Pitot Pressure Measurements

In Section III.1 it was indicated that all Pitot pressure results herein have been corrected for axial tunnel gradients,

subsonic viscous effects and even virtual leak phenomena. Presumably, therefore, the uncertainties in Pitot pressures due to these effects have been all but eliminated. On the other hand, the effects of streamline displacement, angle of attack, lateral tunnel gradients, and viscous interaction in supersonic flow have been examined and are believed to have a cumulative error amounting to less than $\pm 1\%$. Since extreme care was exercised to minimize errors caused by electronic circuitry, transducer calibration, and Moseley recording uncertainties, only an additional $\pm 1\%$ uncertainty is expected from all these effects. Admittedly, for the large pressures measured outside the viscous wake regions, the percentage error arising from recording uncertainties is much smaller than for the centerline data, and thus this latter error estimate probably should be only about $\pm .5\%$ for such data. By taking into consideration all these effects the overall error for Pitot pressure measurements is believed to be within 2%.

D) Static Pressure Measurements

As mentioned above for Pitot pressure data, corrections for low Reynolds number effects, axial tunnel gradients and virtual leak phenomena have also been made to static pressure measurements, and thus any uncertainties caused by these effects should be of negligible importance to final results. In addition the use of a precision micromanometer for measuring these pressures reduced considerably possible recording errors. Thus the primary cause for error with these data appeared to be angle of attack effects and the assumption that the static pressure was constant across the wake. Several

lateral surveys were made to check this latter assumption and slight dips in the pressure traces were observed near the wake edges for laminar flow conditions. However, since static pressure probes are exceptionally sensitive to angle of attack as brought out by McCarthy (16), it is tentatively concluded that the noted "dips" are caused by probe alignment difficulties that occur near the wake edge. As a result, static pressures across the wake have been assumed constant and equal to the value at the wake centerline for all the far wake computations herein. Since centerline data are accurate to within 2% when all uncertainty factors are considered, it is estimated that the assumption of zero lateral pressure gradient causes an error in the value used for the pressure at the wake's edge to be approximately $\pm 5\%$. Because those static pressure probes, used to measure recirculation region pressures, caused some base interference effects the resulting measured data are uncertain at the lower pressures by as much as $+7\%$.

E) Stagnation Point Measurements

Since the accuracy of the stagnation point probe in measuring the location of the rear stagnation point is dependent to a great extent on probe diameter, the smallest tubing size, .032" OD, consistent with structural requirements was used for its construction. Possible virtual leak effects for this small probe, though of importance in quantitative pressure measurements, were not significant to final comparative results because, as discussed in Section III.2, any such effects tended to be self-compensating. Therefore, recognizing the interference effects which exist when the probe is situated just

at the rear stagnation point, it is estimated that measured values of $(x/H)_{sp}$ are accurate to within one probe diameter, namely $\pm$ .032". For the .3" wedge model, the only configuration for which rear stagnation point locations were measured, this amounts to an uncertainty of within one-tenth of a base height.

F) Base and Surface Pressure Measurements

The lowest pressures measured during the present investigation were the base pressures and great care was exercised in obtaining these data. Not only were measurements made by the already mentioned precision micromanometer and virtual leak effects accounted for, but spanwise three dimensional effects were minimized, if not eliminated altogether, by use of base fences. Pronounced base pressure increases were observed at the higher tunnel pressures for the .3" wedge models when the models were tested without fences as compared to similar data with fences. Apparently the boundary layer on the tunnel sidewall, turbulent at these high pressures, caused a significant cross flow to occur because of turbulent mixing effects and the pressure differential which existed between the sidewall boundary layer and the recirculation region. Dewey (8), on the other hand, observed no difference between the base pressures with and without fences. However, the included angles of Dewey's models (45° and 30°) were larger than the present 20° case. For the .15" wedge model, with its higher aspect ratio, no indication of cross flow effects was evident since the data with and without fences were nearly identical.

In determining the suitable fence configuration for these models, it was considered necessary not only to position the fences near the edges of the sidewall boundary layers, but also to extend their length downstream to at least the wake's centerline sonic point. To determine the final spanwise separation distance of the fences (b = 3.5") measurements of base pressures and Pitot pressure profiles in the far wake were carried out for separation distances of both 2.5 and 3.5 inches. Since both sets of data were virtually identical, the 3.5 inch separation distance, with its correspondingly larger aspect ratio, was selected for the final design. Taking all the above factors into consideration it is estimated that base pressure uncertainties vary from $\pm$ 5% at the lowest pressure level tested, p_o = 10 psig, to $\pm$ 3% at p_o = 100 psig. These noted uncertainty estimates correspond to those data measured by base pressure taps. Since the wedge model designed for the cold wall tests (.3w-2) was fabricated without such base taps, all base pressure data for this model were taken with the Pitot pressure probe positioned within .001" to .002" of the base on the wake centerline. Comparison of base pressure data obtained in this manner with "tap" data for the adiabatic wall model (.3w-1) indicated that these Pitot probe data were high at the lowest pressure investigated by +7% due to base interference effects. Thus the uncertainty factors for cold wall base pressure data range from +7% for p_o = 10 psig to $\pm$ 5% at p_o = 85 psig.

Since surface pressures measured with the .3" wedge model, (.3w-1) were relatively high, it was possible to obtain data with good

accuracy. For example the small pressure error that occurred due to virtual leak effects was essentially negligible when compared to the magnitude of the measured pressure. Similarly the slight reading uncertainty that existed with the precision micromanometer was relatively unimportant in determining the overall uncertainty for the surface pressure data. Thus, based primarily on repeatability results, it is estimated that the surface pressure data herein are accurate to within $\pm$ 2%.

G) Hot Wire Anemometer Measurements

In making uncertainty estimates for hot wire data, consideration must be given to such factors as the reliability of the temperature-resistivity data for a given probe, measurement and recording procedures, probe end loss corrections, and finally wire calibration results for determining stagnation temperature and mass flux data from a wire's recovery temperature and Nusselt number. One advantage in evaluating the first of these factors is that often post-test calibrations are possible which enable a redetermination of a probe's temperature-resistivity curve. As Dewey has indicated (17), starting loads and exposure of these annealed hot wires for long periods of time at high temperature levels sometimes cause slight shifting of calibration curves. Thus post-test results offer a method for estimating any resulting uncertainties. Several wires used for the present results were therefore recalibrated after testing and changes in reference resistance due to tunnel exposure effects of less than $\pm$ .02 ohms ($\pm$ 1/2°K) were observed. No variations in resistivity coefficient (α_r) were evident however. Although on occasion some

wire calibration curves exhibited slight deviation from linearity, only those wires which had a variation of less than .02 ohms for the temperature range considered were used to obtain the results herein. Thus the overall uncertainty arising from wire calibration effects is estimated at being about $\pm$ .04 ohms, i.e., $\pm$ 1°K.

The actual hot wire data were obtained with the system designed and used by Herzog (14). Hot wire resistances as measured by this system are accurate to within $\pm$ .02 ohms. An additional uncertainty in adiabatic wire resistance of $\pm$ .02 ohms exists because of slight errors that arise when reducing the measured data (Appendix B.1). The curve fitting technique discussed in Appendix B.1 although reasonably accurate in determining the zero power intercept (adiabatic wire resistance), is however somewhat poorer when evaluating the zero current slope of the resistance power curve because of the high sensitivity of this slope to the measured data. Since measured Nusselt numbers are proportional to these slopes it is estimated that these data are thus only accurate to within $\pm$2%.

The end loss corrections to measured hot wire data herein varied between 1.05 and 1.2 for adiabatic wire temperatures and ranged from .13 to .85 for measured Nusselt numbers. Any estimate of the uncertainty associated with these corrections has to take into consideration not only the analysis of Dewey but the dependence of such corrections on other measured quantities with their own accuracy limitations. By using these accuracy estimates with an analysis of the dependence of derived parameters on measured data, uncertainties in stagnation temperatures arising from end loss

corrections have been made. These uncertainties vary from $\pm 2^{\circ}K$ for edge data to as much as $\pm 10^{\circ}K$ for those centerline measurements corresponding to cold wall, low Nusselt number conditions. In a similar manner it is estimated that uncertainties in final Nusselt numbers due to end loss corrections alone are approximately $\pm$ 3%.

The final factor of importance in evaluating hot wire accuracies is the recovery factor and Nusselt number calibration data. Dewey (17) indicates that recovery factors as determined from his correlation results have a maximum uncertainty of less than $\pm$ 1.5% for all values of Mach number and Reynolds number. On the other hand, for the Reynolds numbers covered during the present investigation and using the Nusselt-Reynolds number correlation of Kubota (Appendix A), the uncertainty in mass flux data (Reynolds number) for given values of Mach number and Nusselt number is less than $\pm$ 5%.

In determining overall accuracies for stagnation temperatures and mass flux data some improvement over the accumulated uncertainties mentioned above is possible. This was accomplished by reducing the effects of data scatter with proper curve fairing, by averaging full profile data into semiprofile results, and finally by compensating for possible systematic errors through suitably normalized final results. Several repeatability checks confirmed the acceptability of this procedure. When all these effects are considered together with the specified uncertainty factors the overall accuracies for stagnation temperature and mass flux data

are as shown in Table II. This table also summarizes uncertainty estimates for all other measurements and those derived results which are of interest to the study herein.

IV. RESULTS AND DISCUSSION

IV.1 Far Wake

A) Mean Flow Results

To initiate a discussion on the results from the present set of far wake measurements, it seems appropriate to begin by first examining data along the wake's centerline and edge for each of the four configurations under investigation. These data are indicated in figures 15 through 22, and the trends exhibited by a given flow variable are observed to be quite similar for all four cases. The one pronounced exception, as might be expected, occurs for the total temperature and enthalpy data for the highly cooled model (figures 18b and 20d) and these results will be discussed shortly.

i) Centerline Static Pressure

In figures 15a through 15d-2 static pressure data along the wake centerline are presented. Except for the flat plate results, these data illustrate the degree of recompression the flow experiences in rising from the low pressures in the base region to the downstream pressure levels. It was not possible to determine the amount of recompression for the flat plate model, since any attempt to measure centerline pressures near the model's trailing edge would result in appreciable flow disturbance (figure 15a). In any event, all pressure data indicate an initial overshoot followed by a gradual decay back to free stream conditions. A slight oscillatory feature to this decay is observed, especially downstream of the cold wall model (figure 15d-1). This type of behavior has been observed by other investigators such as Martellucci et al. (26) and

Badrinarayanan (27) and as of now there still does not exist a satisfactory explanation. It is interesting to note that the decay of the centerline pressure from its "overshoot" value seems to commence at locations closer to the base as the Reynolds number increases. As will be shown shortly, these initial decay locations, in general, coincide with the onset of the wake transition region, which likewise moves forward with increasing Reynolds number. It is not surprising then that the flow will attempt to readjust itself to free stream levels at a faster rate, once turbulent diffusion effects begin to play a more dominant role.

For the wedge data, rough estimates have been made of maximum pressures at the overshoot location and these are labeled "Inviscid Estimate" in figure 15. To obtain these approximations, inviscid flow along the wedge face was expanded to measured base pressure values and then turned through an oblique shock which would bring the flow parallel to the wake's axis. All the calculated values are seen to be within 5% of the overshoot pressures. Such a finding, in spite of the fact that base pressures vary as much as 25% for the Reynolds numbers considered, illustrates that the inviscid flow plays a significant role in downstream pressure levels.

One final observation appears worthy of comment at this time and that is the noticeable inflection in the centerline pressure curves near the bases of the adiabatic and cold wall wedges (figures 15c-2 and 15d-2). Such a trend has been similarly observed by Hama (28) in his experiments with wedges in supersonic flows. For his results Hama points out that this effect is caused by an expansion

fan emanating from the region of interaction of the base's lip shock with the wake shock. For the present set of measurements the lip shock and wake shock, as determined from transverse Pitot pressure surveys, appear to form a continuous shock structure (Section IV.2). This was found also by Hama in his experiments at high Mach numbers and occurs because the lip shock turns more toward the wake axis as the Mach number increases until eventually it appears to coalesce with the wake shock. The fact that the noted change in centerline pressure gradient occurs for Hama's high Mach number data and for the present results, suggests that some shock interaction phenomena may be taking place for these cases even though, with the current measurement resolutions, two distinct shocks are not discernible in the base regions.

ii) Centerline Mach Number

Mach numbers along the wake centerline and edge have been computed using Pitot and static pressure measurements, and these results are shown in figure 16. As discussed in Section III, static pressures at the edge have been assumed equivalent to static pressures measured on the wake's centerline. The centerline data of figure 16 illustrate a tendency to break away from the curve corresponding to the lowest Reynolds number at progressively more forward locations as the Reynolds number is increased. Such an upstream movement of the "break away" point with increasing Reynolds number reflects the influence of transition on the centerline flow. This trend has also been observed in other wake investigations.

Behrens (7) in his experiments on hypersonic wakes behind cylinders and also Sato and Kuriki (29) in their investigation of incompressible flow behind a flat plate, have compared such growth increases in centerline mean flow data with fluctuation measurements. Both investigations have shown that these pronounced centerline deviations are not necessarily indicative of fully developed turbulent flow but only of the termination of a linear growth region characterized by linear stability theory, and the initiation of a region of non-linear instabilities. The absence of any "break away" phenomena for the lowest Reynolds number data suggests that these data correspond to completely laminar flow, even to the most aft location at which measurements were made. Additional discussion of the laminar nature of these lower Reynolds number results will be made in Section IV.1-B.

Except for the cold wall model, all centerline Mach number data illustrate that the onset of the transition region is well downstream of the centerline sonic point. Since disturbances in supersonic flow cannot propagate upstream, the near wake for the adiabatic wall 20° wedge (.3w-2A) is experiencing steady, laminar flow for the present set of measurements, even for the highest Reynolds number under investigation. This result is not necessarily true for the near wake of the cold wall wedge especially at $Re_{\infty H} = 5.5 \times 10^4$ (.3w-2C). The proximity of the "break away" location to the centerline sonic point is obvious from the data of figure 16 and the possible effect of fluctuations on the base region should be kept in mind when examining the near wake results for this case.

The trend of transition to move closer to the base with cooling, however, is an effect predicted by linear stability theory (6).

In an attempt to verify the consistency of the Mach number results in figure 16, a comparison was made using the data for the two adiabatic wall wedges. Since free stream Reynolds numbers were equal for two test conditions for each model, even though base heights differed by a factor of two, it would be expected that axial Mach numbers should be in agreement. Figure 17 presents the results of this correlation and the comparison is seen to be quite favorable.

iii) Centerline Total Temperature

Corrected total temperatures along the wake centerline for both the flat plate and the large 20^{o} wedge models are shown in figure 18. Similar data for .15" base height wedge were not measured and all results specified herein for this 20^{o} wedge model correspond to the assumption of isoenergetic flow, namely $T_t = T_{t_\infty}$. Figure 18 again illustrates the increase in centerline growth rate as the flow experiences the onset of transition. The upstream movement of the most forward location of the transition region with increasing Reynolds number, is again clearly evident, and offers another illustration of the effect of turbulent diffusion on the wake's mean flow properties. Total temperature data were obtained only up to 6 inches downstream of the wedge bases because of probe support limitations. The absence of data forward of $x/H = 1.5$ for the 20^{o} wedge data (excluding the wall temperature measurement) was caused by the ineffectiveness of the hot wire probe in very low

density, low speed flow. Convective heat losses from the wire were so small that the wire temperature became dominated by probe support effects resulting in unacceptably inaccurate total temperatures. The variation of total temperature with Reynolds number and the distribution of total temperature within such a near wake region are of considerable importance to development of the wake downstream. The inability to obtain such information from the present investigation points out the necessity of other techniques for obtaining total temperature data in base flow regions. For example, several investigators have succeeded in measuring near wake temperatures behind slender bodies in both shock tubes and shock tunnels taking advantage of transient phenomena.

Examining the total temperature data of figure 18 clearly illustrates the pronounced effect which model cooling has on centerline total temperatures. Since wall temperature ratios (T_W/T_{t_∞} = .03 → .12) associated with high speed entry into the atmosphere correspond to cold wall conditions, the cold wall data (T_W/T_{t_∞} = .19) would seem to be of more practical interest than the adiabatic wall results (T_W/T_{t_∞} = .87). The measured wall temperature, incidentally, for the adiabatic wall model agrees favorably with that predicted by theory for laminar flow (r = .85) at M_∞ = 6.

iv) Centerline Velocity

Centerline velocity data for all four models used in the current investigation are presented in figure 19. Since the Mach number and total temperature data used to generate these results have already been discussed, little comment seems necessary at

this time. The typical growth increases associated with the onset of transition are again clearly evident. The comparison between linear wake theory (5) and the lowest Reynolds number data for the adiabatic wall models is seen to be quite reasonable. The results for the larger wedge model (.3w-2A) are the least favorable and this is primarily the result of applying the theory not far enough downstream where the velocity defect has become sufficiently small $(1 - \frac{u}{u_e} << 1)$ as required by linear theory. Additional discussion of the validity of using linear theory for the present results will be presented shortly.

v) Centerline Enthalpy

Another quantity which is of interest in any study of far wakes, especially with the extreme temperatures associated with high speed reentry, is that of the distribution of enthalpy along the wake centerline. Figure 20 presents the results from the current investigation and, as might be expected, an appreciable difference between the adiabatic and cold wall data is evident. All three adiabatic wall cases are quite similar in their decay characteristics, even to displaying the upstream movement of transition with increasing Reynolds number. Results of linear theory calculations are also shown on figures 20a, 20b and 20c illustrating the effects of Prandtl number and initial conditions on the computations. The cold wall results indicate a maximum centerline temperature of almost triple free stream values and in addition, for the low Reynolds number data, these relatively high temperatures persist for some distance downstream, a factor of great importance in evaluating wake observable

phenomena. The sharp temperature rise taking place in the vicinity of the base occurs primarily within the recirculating zone of the base region. This result and the fact that a maximum temperature occurs somewhat downstream of the rear stagnation point can be explained by examining the balance between thermal and kinetic energy along the wake centerline. Since the flow velocities within the recirculating zone are small, the total energy of the centerline flow initially consists primarily of thermal energy. The axial distribution of enthalpy along the centerline thus follows closely the total enthalpy variation (figure 18). However once downstream of the rear stagnation point the flow velocities increase rapidly with the result that the centerline enthalpy attains a maximum followed by a gradual decay as the kinetic energy of the flow increases and begins to account for a greater share of the centerline total enthalpy. This latter effect is clearly in evidence in the adiabatic wall cases wherein, because the total enthalpy is nearly constant in the far wake, the enthalpy decay along the centerline is just matched by the kinetic energy increase.

vi) Integral Thicknesses

Integral wake thicknesses for the present results are presented in figure 21. Integration of the boundary layer equations indicates that the expected variation for these thickness data should be as follows:

$$\frac{d}{d(x/H)}\left[\frac{\rho_e u_e^2}{\rho_e u_{e_\infty}^2}\frac{\bar{\theta}}{H}\right] = -\frac{\rho_e u_e}{\rho_\infty u_\infty^2}\frac{du_e}{d(x/H)}\frac{\delta^*}{H} = \frac{1}{\rho_\infty u_\infty^2}\frac{dp}{d(x/H)}\frac{\delta^*}{H}$$

$$\frac{d}{d(x/H)}\left[\frac{\rho_e u_e}{\rho_\infty u_\infty}\frac{E}{H}\right] = 0$$

where $$\frac{\delta^*}{H} = \int_0^\infty \left(1 - \frac{\rho u}{\rho_e u_e}\right) d(y/H)$$

$$\frac{\bar{\theta}}{H} = \int_0^\infty \frac{\rho u}{\rho_e u_e}\left(1 - \frac{u}{u_e}\right) d(y/H)$$

$$\frac{E}{H} = \int_0^\infty \frac{\rho u}{\rho_e u_e}\left(1 - \frac{T_t}{T_{te}}\right) d(y/H)$$

The slight increases in momentum thickness with axial distance are partially caused by the small axial pressure gradients depicted in figure 15 and the transverse entropy gradient characteristic of some viscous wakes. This latter effect is brought about because some of the streamlines passing through the stronger portions of the curved bow shock first enter the viscous far wake at varying distances downstream. The additional "drag" associated with these streamlines is similar to the outer wake drag typical of blunt bodies which experience extensive normal shock pressure losses. Some growth of momentum thickness (drag) with axial distance is thus not surprising.

Similar explanations based on fluid mechanical phenomena cannot be made to account for the slight increase in energy thickness of the cold wall data. Since these data should remain constant with axial distance, the small growth rate experienced by the energy

thickness in figure 21d represents a measure of the cumulative error occurring for the present results. Considering the various corrections and calibrations associated with the current measuring techniques such a result, however, is not unexpected.

vii) Wake Thickness

Figure 22 presents results of wake thickness and wake shock position for the four models used in the current investigation. The rapid change in Pitot pressure at the wake shock (figure 44) clearly determines the location of this shock. The midpoint of this sharp Pitot pressure change has been used as the wake shock position. The wake edge data of figure 22 were obtained by determining those locations where the tangent to the maximum transverse gradient in Pitot pressure intersected the edge value of Pitot pressure. This definition coincides, within the accuracy of the present results, with the total-temperature edge (figure 45). From the data in figure 22 estimates of wake neck position are possible by noting the location of the minimum thickness point. Further, these results indicate that all the wakes initially grow almost linearly with downstream distance until, except for the low Reynolds number data, some point is reached where a sudden growth rate change takes place. The new growth rate again is nearly constant. Since fluctuations bring about increases in wake growth rates, these data are good indicators of the breakdown of the steady laminar flow condition. The upstream movement of this "transition" point with increasing Reynolds number is very noticeable. Similar results for wake thickness were obtained by Demetriades (30) in his experiments on hypersonic flows behind

20^{o} wedges using hot wire probes to measure turbulent fluctuations.

B) Analysis of Transition

Wake transition distance is defined as the axial distance downstream from the base of a body to a location where the effects of transition produce a pronounced change in flow characteristics. In Demetriades' measurements behind 20^{o} wedges (30) and also Sato and Kuriki's data for incompressible flow behind a flat plate (29), the onset of increased turbulent fluctuations was designated as the beginning of transition. A similar approach has been used by Behrens for flow behind cylinders in hypersonic flow (7). The present results correspond to a transition location based on the axial distance from the model base to the position in the wake where the wake thickness growth rate shows a sudden change. These transition locations are specified in figure 22 and are replotted in figure 23 as a function of reciprocal of Reynolds number. The results therein illustrate that a linear variation exists not only when free stream Reynolds numbers are used but also when the Reynolds number is based on edge conditions. This linear variation in turn can be used to define a transition Reynolds number since the slope of the curves, for each of the models, corresponds to a Reynolds number based on the axial distance between a zero intercept distance, obtained by extrapolating the measured data to infinite Reynolds number, and the transition location. As explained by Lees (31), the noted linear variation of transition distance cannot continue indefinitely as the Reynolds number is decreased. In fact a minimum critical Reynolds number is reached below which viscous dissipation

prevents the existence of wake turbulence. Thus all curves in figure 23 would eventually curve upward if lower Reynolds number measurements had been made. Demetriades illustrates this effect in his measurements (30).

From the results of figure 23 the following transition Reynolds numbers seem appropriate:

Model	$Re_{\infty \Delta x}$	$\left(\frac{x}{H}\right)_{TR_o}$	$Re_{e \Delta x}$	$\left(\frac{x}{H}\right)_{TR_o}$
Flat Plate	50,000	35	---	---
20^o Wedge, adiabatic wall	3.5×10^5	8.5	2.8×10^5	8.5
20^o Wedge, cold wall	3.3×10^5	2.0	2.5×10^5	2.0

Although the flat plate value corresponds closely to the result which Demetriades obtained by extrapolating his wedge data to the 0^o included angle case (flat plate) [$Re_{\infty \Delta x} = 56,000$], the zero intercept distance found herein [$\left(x/H\right)_{TR_o} = 35$] differs substantially from his data [$\left(x/H\right)_{TR_o} = 15$]. H, as used both for the present correlation and Demetriades' results, represents the sum of the total boundary layer displacement thickness, as calculated, and the plate thickness. A satisfactory explanation for the noted discrepancy is not known at the present time.

On the other hand, present transition results for the adiabatic wall 20^o wedge data not only show agreement between the two different sized models, but are seen to compare favorably with those data measured by Demetriades in his turbulent fluctuation experiments. This agreement occurs both in terms of free stream transition Reynolds number ($Re_{\infty \Delta x} = 3. \times 10^5$, Demetriades) and the zero intercept

distance. In addition, transition data for flow behind sharp nosed cones at $M_\infty = 6$ indicate that a transition Reynolds number based on edge conditions ($Re_{e\Delta x} = 2.3 \times 10^5$), compares favorably with the present data. Such findings verify the use of the present mean flow technique for locating the approximate location of transition in lieu of detailed flow turbulence measurements.

It should be pointed out, however, that centerline properties apparently "sense" the onset of transition a short distance upstream of those locations of transition as defined from wake thickness results. This is evident from figure 16 by comparing these transition locations with the initial deviation of the centerline Mach number data from the low Reynolds number results. These centerline deviations become important when evaluating the forward extent of the transition zone and its relevancy to the laminar nature of the near wake. For example, from figure 16, it is questionable whether or not the near wake for the cold wall wedge at $Re_{\infty H} = 5.5 \times 10^4$ is indeed completely laminar, since the centerline Mach number data therein commence deviating as far upstream as $x/H = 3$.

Figure 23 illustrates the pronounced effect which cooling has on wake transition. The significant upstream movement of transition distance for a given Reynolds number with cooling indicates the increased flow instabilities associated with cold wall bodies.

As a final comment on these transition results, it is appropriate to reexamine the low Reynolds number data of figures 15 through 22. Since now transition Reynolds numbers are available,

it is possible to make estimates of transition distances for these cases. The results are:

Model	$x)_{TR}$
Flat Plate, L = 1 inch	7.5L
20^{o} Wedge, adiabatic wall, H = .15 inch	58.5H
20^{o} Wedge, adiabatic wall, H = .3 inch	33.5H
20^{o} Wedge, cold wall, H = .3 inch	27.5H

These results additionally substantiate the earlier claim that the low Reynolds number data were representative of laminar flow for large downstream distances. Furthermore, the absence of the "break away" phenomena in the centerline measurements also verifies that such data correspond to laminar flow even to the farthest downstream station at which measurements were made.

C) Comparison of Present Results with Linear Wake Theory

The two-dimensional linear wake theory, as derived by Kubota (4) for compressible flow and arbitrary streamwise pressure gradient, incorporates the Oseen type approximation along with the assumption that the initial velocity and enthalpy distributions correspond to delta functions. A modified version of this theory has been developed by Gold wherein arbitrary initial profiles are acceptable (5). Basically the theory requires, in addition to the necessity for the boundary layer equations to remain valid, that the velocity defect be small ($1 - \frac{u}{u_e} \ll 1$), and that both the Prandtl number and Chapman-Rubesin factor ($C = \frac{\rho_e \mu_e}{\rho \mu}$) be constant. Under these assumptions and with the additional approximation of negligible axial pressure gradient, which would seem appropriate from the far wake results

of figure 15, the linear wake theory gives the following results:

$$w \equiv \frac{u_e - u}{u} = \frac{1}{\sqrt{4\pi\bar{x}/H}} \int_{-\infty}^{\infty} w_o(\bar{\xi}/H) \exp\left[-\frac{(\bar{\xi}/H - \bar{y}/H)^2}{4\bar{x}/H}\right] d(\bar{\xi}/H)$$

$$g \equiv \frac{h - h_e}{h_e} = \sqrt{\frac{Pr}{4\pi\bar{x}/H}} \int_{-\infty}^{\infty} g_o(\bar{\xi}/H) \exp\left[-\frac{Pr(\bar{\xi}/H - \bar{y}/H)^2}{4\bar{x}/H}\right] d(\bar{\xi}/H)$$

where $\bar{y} = \frac{\rho_e u_e}{\rho_\infty u_\infty} \sqrt{Re_{\infty H} C} \int_0^y \frac{\rho}{\rho_e} dy$

$$\bar{\xi} = \frac{\rho_e u_e}{\rho_\infty u_\infty} \sqrt{Re_{\infty H} C} \int_0^\xi \frac{\rho}{\rho_e} d\xi$$

$$\bar{x} = \int_0^x \frac{\rho_e u_e \mu_e}{\rho_\infty u_\infty \mu_\infty} dx$$

$w_o(\bar{\xi}/H) = \frac{u_e - u}{u_e}$ at initial wake station where $x = x_o$

$g_o(\bar{\xi}/H) = \frac{h - h_e}{h_e}$ at initial wake station where $x = x_o$

This formulation of the linear wake solution has been programmed on the IBM 7094* and various calculations have been carried out to examine the effect of initial conditions and Prandtl number on the computations. Several results of these calculations are shown in figures 19 and 20, where centerline distributions of velocity and enthalpy for the low Reynolds number cases are compared with measured adiabatic wall data. In general, the flat plate calculations of

*Behrens, private communication

both velocity and enthalpy are in favorable agreement with the data. The velocity results, for the small base height 20° wedge (.15w), similarly agree with the data. However such agreement is not as satisfactory for the large wedge model (.3w-2A) for both velocity and enthalpy results due apparently to the use of initial conditions $\left(\frac{x}{H}\right)_o = 10$) not sufficiently far downstream where velocity defects are small enough to justify using linear theory.

The relatively large deviation between theory (Pr = .75) and data for the enthalpy results of the small wedge, figure 20b, are perhaps due mainly to the lack of measured total temperature data. The noted variations therefore should not be taken too seriously. Shown also on this figure is the effect of varying Prandtl number from .75 to 1. The Pr = 1 case, which compares quite favorably with the data, may be more realistic here since it too corresponds to constant total enthalpy.

Velocity and enthalpy profile distributions have also been calculated and these results are presented in figures 24 and 25 as functions of the transformed y coordinate. For the flat plate and small wedge models, the comparisons between predicted and measured velocities appear to be quite good. A better correlation in the case of the large wedge data (.3H-2A) for both velocity and enthalpy results would be possible if the initial stations were chosen further downstream say at $x/H)_o = 15$ instead of $x/H)_o = 10$. The flat plate enthalpy profiles, as predicted, are not in very satisfactory agreement with the measured data even though centerline results agree quite favorably. Again this indicated deviation would improve

considerably by making use of an initial station further downstream.

From linear theory it can also be shown that velocity defect results for all models should correlate well with the normalized axial distance

$$\bar{x}/Re_{\bar{\theta}_{avg}}\,\bar{\theta}_{avg}$$

The results of such a correlation are presented in figure 26 and the collapsing of the data for all three adiabatic wall models investigated verifies the use of this normalized distance.

In general, the low Reynolds number far wake data obtained during the present investigation under adiabatic wall conditions show very satisfactory agreement with linear theory. Such a finding further substantiates the laminar, steady nature of these data and illustrates the value of this theory as an effective method of analysis for the laminar far wake behind two-dimensional slender bodies.

IV.2 Near Wake

A) Near Wake Geometry for a Flat Plate in Hypersonic Flow

The flow in the vicinity of the trailing edge of a flat plate represents a problem in fluid mechanics which has been of interest to investigators for many years. Since some near wake measurements were made during the present investigation of the flat plate hypersonic wake, it was considered desirable to report on available data even though, because of inherent measurement limitations, results were limited primarily to near wake geometries. Figure 27 presents these geometry data for each of the four Reynolds numbers investigated. Shear layer and wake thicknesses were determined from total temperature distributions (figure 45) whereas both the wake and leading edge shocks were located from pilot pressure traces (figure 44). Those boundary layer edge locations indicated on the figure were calculated from the weak interaction theory (36) and the finding of Kendall (32), from his flat plate study, that $\delta^*/\delta \doteq .75$. The existence of the wake shock illustrates that the flow recompresses as it turns back to the free stream direction from its trailing edge orientation. The two degree reverse taper to the trailing edge, and the thin but finite thickness of the plate are clearly not in keeping with the infinitesimally thin flat plate assumption of analytical studies. Also shown in figure 27 are centerline sonic point locations ($x/L \doteq .2$) as determined by extrapolating the Mach number data of figure 16a.

Correlation of the wake thickness data with predicted boundary layer thicknesses are shown in figure 28. The favorable correlation indicated in figure 28 illustrates the dependence of the near wake thickness on the plate boundary layer thickness. The fact that the initial wake thickness is somewhat larger than what would be predicted from boundary layer theory can be accounted for by analyzing the mass flow balance between the boundary layer and near wake. This analysis indicates that

$$\left[\rho u\delta\left(1 - \frac{\delta^*}{\delta}\right)\right]_{BL} = \left[\rho u\delta\left(1 - \frac{\delta^*}{\delta}\right)\right]_{NW}$$

where $$\delta^* = \int_0^{\delta} \left(1 - \frac{\rho u}{\rho_e u_e}\right) dy$$

Since

$$\left(\frac{\delta^*}{\delta}\right)_{BL} \doteq \left(\frac{\delta^*}{\delta}\right)_{NW}$$

and $$u_{BL} \doteq u_{NW}$$

the mass balance equation reduces to

$$(\rho\delta)_{BL} \doteq (\rho\delta)_{NW}$$

However, assuming isentropic flow, it follows that

$$\delta_{NW} \doteq \left(\frac{p_{BL}}{p_{NW}}\right)^{1/\gamma} \delta_{BL}$$

Thus, because the near wake pressures are lower than the plate pressures (figure 15a), some increase in wake thickness over that

predicted by boundary layer theory is expected.

Another wake feature that can be determined with reasonable accuracy from the present results is the wake neck thickness. From the wake growth results of figure 22a it is estimated that the neck occurs at or near $x/L = .5$. The resulting thicknesses are presented in figure 29 as a function of free stream Reynolds numbers and a square root variation with Reynolds number is evident. The variation of the neck thickness with Reynolds number in this manner can be deduced from a mass balance analysis, similar to that described above for the initial near wake thickness, and on the dependence, according to boundary layer theory, of the thickness of the trailing edge boundary layer on the square root of Reynolds number.

B) Near Wake Behind 20^{o} Wedge

The near wake behind slender bodies has been the subject of many experimental investigations for the past several years. Both shock tunnel facilities and continuous flow wind tunnels have been used for these investigations. Mach numbers ranging from low supersonic to hypersonic values and flow regimes from all laminar through transitional to fully turbulent flow have been examined. The primary aim has been to define a physically realistic model for the flow which will be amenable to analytical study. Since many of these investigations were somewhat limited in the amount and type of measurements that could be obtained, it was felt early in the current experimental program that a reasonably detailed study of the near wake with hot wire and Pitot probes would prove meaningful even though some accuracy difficulties would be experienced. Such data, although able to provide only limited information on the base recirculation region, because of previously mentioned hot wire uncertainties in subsonic flows, would furnish an interesting supplement to the near wake data already available.

i) Neck Thickness

By examining the wake growth results of figure 22 the minimum wake thickness values have been determined for all three of the 20^{o} wedges used in the present investigation. These neck thickness results are presented in figure 29 as a function of Reynolds number and a square root variation is apparent. The mass balance analysis discussed above for the flat plate results (Section IV.2A), and which provided an explanation for the dependence of the flat plate neck

thickness on the square root of Reynolds number, is similarly applicable for these wedge data. Consistency of the adiabatic wall results is evident in that the data for both the H = .15" and H = .3" wedges coincide in a favorable manner. Also shown on the figure are trailing edge boundary layer thicknesses as measured from total temperature profiles for the three tenths base height wedge under adiabatic and cold wall conditions. From boundary layer theory these data should vary with the square root of Reynolds number and the results of figure 29 satisfactorily indicate this trend.

In conducting an investigation of this type it is of interest to determine the significant scaling parameters which play a dominant role in establishing the flow field. Although the neck thickness data in figure 29 illustrate that a correlation with Reynolds number exists, it is also indicated therein that, when presenting the data in this manner, the results for the adiabatic and cold wall wedges correspond to two separate curves. However, if the data are replotted in terms of the thickness of the trailing edge boundary layer, both the adiabatic and cold wall data collapse to one curve (figure 30). This result additionally verifies Chapman's (37) finding that the noted thickness represents an important length scale for near wake flows. Figure 30 also indicates that for flow approaching zero boundary layer thickness the neck thickness behaves properly for this inviscid limit and becomes negligibly small.

ii) Wedge Surface Pressure

The upstream influence of the low base pressure and the corner expansion on wedge surface pressures is illustrated in figure

31. These adiabatic wall data were obtained with the solid wedge model (.3w-1A) discussed in Section II and indicate that the flow first "senses" low base pressures roughly two to three boundary layer thicknesses upstream of the base. Also shown on the figure for comparison purposes are calculated trailing edge pressures as determined using Kendall's results from his investigation of hypersonic flow over a flat plate (32).

Unfortunately, the small size of the model used in the present investigation prevented making pressure distribution measurements along the model base. Hama's results for such base pressure data on 12^{o} wedges (28), clearly demonstrate that an undershoot in pressure first occurs on the base after which the flow undergoes a rise in pressure to the base pressure value. Such a trend is indicative of flow which remains attached to a surface so long as a favorable (decreasing) pressure gradient exists but then tends to separate once it senses an unfavorable (increasing) pressure gradient. Thus separation of the flow from the body does not necessarily occur just at the corner but in fact occurs some distance below the corner and only when a sufficient overexpansion takes place such that the surface pressure falls below the final base pressure level. This off-corner separation result is further substantiated from the flow field mapping results to be discussed in detail shortly. These data illustrate that zero velocity and sonic line extrapolations upstream to the base, intercept the base line below the corner in the manner depicted by Hama. This finding supports the conclusion of Hama that the lip shock in the near wake is caused by a separating boundary layer and thus

is similar to the separation shock generated in the near wake of a cylinder.

iii) Wedge Base Pressure

The results of base pressure measurements for the three wedge models are presented in figure 32. These data show the variation of base to free stream pressure ratio with trailing edge Reynolds number as determined from inviscid flow theory. Also shown in figure 32 for comparison purposes, are the adiabatic wall data of Dewey for both 30° and 45° wedges (8). General agreement in both trend and magnitude is seen to exist for all adiabatic wall results. The significant decrease in base pressure with increasing Reynolds number is again emphasized by the present results. Consistency of the present adiabatic wall data is illustrated by the correlation of results from both the small (.15w) and large (.3w-2A) 20° wedges. Figure 32 also indicates that a drop in base pressure is associated with model cooling.

Since Chapman (37) as well as others have pointed out the dependence of base pressure on the thickness of the trailing edge boundary layer, and further, because a successful correlation of both adiabatic and cold wall neck thickness data has also been achieved herein with this scaling parameter, a correlation of the base pressure data has also been made with the trailing edge thickness and the results are shown in figure 33. For the adiabatic wall data the weak interaction theory modified per Kendall's results has been used to determine $(\delta/H)_{TE_{Theory}}$. On the other hand, the cold wall trailing

edge thickness is based on Chapman-Rubesin boundary layer theory for arbitrary wall temperature (38). Base pressure estimates using Chapman's dividing streamline model (11) have been made and results for $\theta = 45^{o}$ and $\theta = 20^{o}$ are shown on figure 33. According to the idealized version of this model, the flow along the dividing streamline separating the base's recirculating flow from the outer flow, attains a maximum velocity of $u_*/u_e = \bar{u}_* = .587$ and then recompresses isentropically and instantaneously to the downstream pressure level. Thus

$$\frac{p_b}{p_\infty} = \left(\frac{p_{sp}}{p'}\,\frac{1}{\eta}\right)\left(\frac{1+\frac{\gamma-1}{2}M'^2}{1+\frac{\gamma-1}{2}\frac{M'^2}{1-\bar{u}_*^2}}\right)^{\gamma/\gamma-1}$$

Here, ( )' refers to downstream conditions determined by expanding inviscid wedge flow isentropically back to the free stream direction. Such a computation method has been found to give essentially the same results, as one where inviscid wedge flow is first overexpanded, then recompressed through a weak oblique shock back to the free stream direction. The factor, $\frac{p_{sp}}{p'}\,\frac{1}{\eta}$, represents a "recompression efficiency factor" and accounts for the uncertainties in the analysis. Although the estimates on figure 33 are invariant with Reynolds numbers, the overall levels seem to compare favorably with the measured data for an "efficiency factor" of one. This favorable magnitude result occurs even though the isentropic recompression assumption of the Chapman analysis is seen not to be realistic for the present results (figure 15).

Although the method of correlation used in figure 33 still retains the wedge angle as an important variable in the base pressure determination, it is clear that the data for each wedge scales favorably with the trailing edge thickness. Admittedly, for the adiabatic wall data, this is an expected result since it has already been shown that the base pressure varies with trailing edge Reynolds number (figure 32). However, as was found in correlating the neck thickness data discussed above, the important finding indicated by the figure 33 results is the collapsing of both the adiabatic wall and cold wall base pressure data for the present investigation to a single curve. This result further substantiates the significance of the trailing edge thickness as a suitable length scale for the base flow problem.

In an effort to determine additional characteristic parameters for the base pressure data several other combinations of variables have been attempted. One finding is that all adiabatic wall data from both Dewey's and the present studies collapse to one curve with only $\pm 7\%$ scatter by presenting p_b/p_∞ as a function of free stream Reynolds number based on the base height (figure 34). This result, indicating only minor dependence on wedge angle, was similarly found by Cheng et al. (39) in their experimental investigation of wakes behind wedges in low density flow.

iv) Rear Stagnation Point

The rear stagnation point location is the position on the wake axis where the flow stagnates and separates the reverse flow in the base region from the downstream wake. Most initial conditions for near wake calculations make use of profile data corresponding to the

location of the rear stagnation point. In addition, relatively high temperatures exist at this point, as discussed in Section IV.1, and thus electron densities can be correspondingly large in actual atmospheric entry. For the present set of measurements with the three-tenths base height wedge and for both adiabatic and cold wall conditions, the position of the rear stagnation point has been located at x/H = .75. These results are evident from the data of figure 35 wherein centerline static and Pitot pressure data were plotted as a function of axial distance. Although the location of the point where the curves coalesce (rear stagnation point) may be somewhat uncertain because of the small cross angles involved, the resulting locations of the rear stagnation points are believed to be accurate to within $\pm$ .1 H at least for all the adiabatic wall data and for those results corresponding to the two lowest Reynolds numbers of the cold wall model. An uncertainty estimate somewhat larger may seem more realistic for the two highest Reynolds number cold wall data because of the greater difficulty in accurately determining the crossover point. The $x/H)_{sp} = .75$ result was also confirmed, for the adiabatic wall condition, by use of the differential pressure probe discussed in Section II. Both of these methods for determining the rear stagnation point position have been used by Martellucci, et al. (26) in their experiments on the turbulent near wake of a cone at M = 6 and similar agreement between the two techniques was obtained. The values of $x/H)_{sp} = .75$ for the present results are in good agreement with the summary curve of reference 26 showing the variation of rear stagnation point location with trailing edge Reynolds

number. The data used by Martellucci et al. for this summary comprise measurements from not only wedges but also cones and cylinders as well under cold and adiabatic wall temperatures and even both laminar and turbulent flow conditions. A satisfactory correlation of most data and a general trend indicating a slight aft movement of the rear stagnation point with trailing edge Reynolds numbers (trailing edge boundary layer thickness) are evident. The movement aft of $x/H)_{sp}$ for the high Reynolds number cold wall data in the present investigation may appear to have occurred (figure 35b) but the noted data uncertainty prevents concluding such a trend. If such were the case however, it would be in agreement with the summary data of reference 26 for decreasing trailing edge boundary layer thickness.

v) Wall Temperature Ratio

Of interest in an experimental investigation of this nature is the comparison between already existing data and current results. One such comparison, in the case of the cold wall model, is the relationship of the temperature at the wake's rear stagnation point to the model's wall temperature. Figure 36 presents a summary of results from other investigations along with the present data showing this relationship in terms of normalized temperature ratios. The free stream stagnation temperature has been used as a normalizing parameter for the data. It is evident from figure 36 that the present cold wall results compare favorably with previous data.

vi) Typical Shear Layer Profiles

Before analyzing flow field mappings of the near wake behind the three-tenths base height wedge, it seems appropriate to discuss

briefly several typical profiles for the near wake shear layers. These profiles, all for the low Reynolds number adiabatic wall case, are plotted in figure 37 in overlap fashion with the base geometry, so as to illustrate the manner in which characteristic lines and/or regions are distinguishable. For example, figure 37a, showing transverse Pitot pressure traces, indicates that the leading edge and wake shock positions were determined from the Pitot pressure gradients occurring at these respective locations. The relatively slight change in Pitot pressure gradient indicated near the axis for the x/H = .5 trace is more suggestive of compression Mach waves, and thus has been associated with the lip shock arising from the flow separation at the base. From these data, and also the profile results of figure 44, showing all the Pitot pressure data taken during the current investigation, it can be seen that both the wake and lip shocks have substantial width $(\Delta \frac{y}{H})_S \doteq .10\ H)$. This was similarly observed by Dewey (8) in his studies of the near wake behind a cylinder. A computation was made of the orientation of the leading edge shock wave based on the assumption of weak shock-boundary-layer interaction and the existence of simple wave flow between the boundary layer edge and the shock wave. The calculated result was within $.5^{\circ}$ of the measured shock wave angle at the model's trailing edge. The u = 0 line indicated in figure 37a corresponds to those transverse locations where the static pressure, as measured on the wake's centerline, and Pitot pressure are equal. This line terminates at the rear stagnation point location which has been determined in a similar manner.

One near wake characteristic, which has not been determined to any great extent by existing near wake investigations, is the location of the shear layer edge. Figure 37b presents total temperature profiles for the near wake shear layer, and the temperature overshoot, typical of adiabatic wall boundary layer profiles, is evident. The locations where the overshoot decreases to zero, namely where the total temperature achieves equilibrium with the free stream total temperature, represents the shear layer edge. This edge, in essence, corresponds to the boundary between that portion of the flow unaffected by the temperature of the wall and that part of the flow which has been affected by the wall through the action of viscosity and heat conductivity. It will be recalled that in the far wake either Pitot pressure or total temperature results could be used to determine the wake edge. In the near wake region, downstream of the base, such use of the Pitot pressure data is not possible because of the Pitot pressure gradients associated with the expansion fan outside the shear layer. At the trailing edge, where the effect of the expansion fan on Pitot pressure is quite small, values of the boundary layer thickness based on the Pitot pressure profile compare favorably with edge data derived from total temperature traces. The one open symbol indicated in figure 37b on the model surface at $x/H = -.5$ corresponds to a calculated boundary layer thickness based on the Chapman-Rubesin compressible boundary layer theory (38) for arbitrary wall temperatures. The thickness so noted agrees favorably with similar thickness estimates based on the weak interaction theory. An interesting result of figure 37b is the location and

variation of the shear layer's edge with axial distance. Not only is the wake neck, defined as the wake's minimum thickness location, not located near the wake's rear stagnation point, but it even occurs downstream of the centerline sonic point as will be shown shortly. The tendency of the shear layer to avoid turning sharply downstream of the model base indicates that extremely low densities exist within the immediate vicinity of the base. This result is of significance to the development of the viscous sublayer postulated in many of the analytical techniques currently under investigation. Complete total temperature profile data for the current investigation are presented in figure 45 and the above comments, regarding the shear layer edge, are seen to hold true for all cases.

The Mach number distributions of figure 37c illustrate that rather high Mach numbers ($M \geq 6$) are experienced by the separated shear layers in the present near wake investigation. This constitutes a major distinction between near wakes behind slender bodies with flat bases, and near wakes behind blunt nosed bodies with rounded bases such as spheres and cylinders where shear layer Mach numbers are usually less than three (8). From figure 37c the location of the sonic line and the manner in which it fairs smoothly into the centerline sonic point is clearly apparent. Such a line is also arrived at directly by locating the position where the ratio of static pressure, assumed equal to the pressure on the centerline, to Pitot pressure corresponds to the value at Mach number unity, namely, $p/p_{t_2})_{M=1} = .5283$. This represents a satisfactory method for determining the sonic line since the static

pressure, as will be shown shortly, is nearly constant across the base region up to the wake (or lip) shock. Between the wake shock and shear layer edge, the accuracy with which certain flow data, such as Mach number, static pressure, and static temperature, have been determined is rather poor as discussed in Section III. The present method for determining these data using hot wire measurements was shown to have inherent uncertainties that limit data accuracy at high Mach numbers. This point should be kept in mind when evaluating certain trends and even data scatter. On the other hand, those data within the wake shock boundaries correspond to low Mach numbers ($M < 3$) and thus should be reasonably accurate.

Several interesting results from the present investigation have been obtained from static pressure profiles such as those shown in figures 37d and 42. All the data in figure 37d, represented by open symbols and below the shear layer edge, are the values of static pressure arrived at by combining Pitot pressures with total temperatures and mass flux data from hot-wire measurement. Within the accuracy limits specified in Table II, the results indicate that, not only is the static pressure constant from the centerline out to the wake shock and equal to the value measured at the centerline with a static pressure probe, but also that the static pressure, at least for $x/H = 1.5$, from the wake shock out to the shear layer edge is, in addition to being constant, equal to the base pressure. The data near the corner show that the effects of the corner expansion become progressively more dominant within the shear layer, until at the trailing edge, the entire shear layer

from the edge down to the zero velocity line is experiencing large lateral pressure gradients. Thus, clearly the shear layer cannot be considered as a region of constant transverse pressure until several boundary layer thicknesses downstream of the base. Such a pressure gradient exists also in the case of attached flow negotiating an expansion corner. Because these data show that the static pressure is roughly constant from the wake axis out to the base region shocks, a simplified data reduction procedure was carried out, in which all the wake profiles and the flow field mappings within the base region shock boundaries have been derived by calculations based on a zero pressure gradient assumption in a manner similar to all far wake results. Figure 37d also shows the locations of the leading and trailing rays of the corner expansion fan defined by the method of tangents indicated on the figure. Admittedly the determination of these limiting rays for the corner expansion is somewhat arbitrary. In fact it may even seem more appropriate to select the round off points experienced by these curves as more representative of the location for the leading and trailing rays. If such a technique were used, the leading and trailing rays would be displaced outward and inward respectively from the location indicated in figure 37d. However, the difficulty in consistently locating the round off points resulted in appreciable uncertainty in the final orientation of the limiting rays. Thus the present technique, based on the tangent to the maximum static pressure slope, has been adopted for determining the leading and trailing ray positions. The leading ray orientation, incidentally, as

determined in this manner agrees very well with the Mach wave angle for the inviscid wedge flow of the present investigation. Normally, since the total pressure is constant within the outer inviscid region, the leading ray can be determined from the Pitot pressure data directly. However the trailing ray, since it becomes immersed in the shear layer, cannot be located by Pitot pressure data alone, and thus the present results, using hot wire measurements, provide another characteristic line which has not been determined in most near wake measurements to date. Because the Mach number decreases in the shear layer as the trailing ray approaches the base, a slight curvature of this line is observed. The Mach wave angles for the local flow along a trailing ray have been compared with the orientation of the trailing ray itself and a satisfactory agreement was obtained. The forward extension of the leading ray of the expansion fan shows the approximate region of upstream influence to which the body boundary layer is subjected. Recognizing the fact that some outward adjustment of this estimate of the leading ray position is warranted because of the above-mentioned uncertainty in locating this line, the extent of upstream influence agrees in general with the results of the surface pressure measurements discussed earlier.

The final set of shear layer profiles, which merit some attention, are the velocity and static enthalpy results of figures 37e and 37f respectively. Results such as these are often used as initial profiles for analytical studies of the near wake. The data of figure 37e and also the complete profile results of figure 43 illustrate that

the velocity profiles experience a noticeable gradient change in the vicinity of the wake shock. The small velocity variation that occurs in the shear layer outside the wake shock, at least for the downstream stations, is not entirely unexpected since the velocity is relatively insensitive to the variations in the high Mach numbers which exist in this region of the shear layer. The enthalpy data of figure 37f point out that peak enthalpies for the near wake of an adiabatic wall model occur on the wake axis. Shortly, similar data will be presented for the near wake behind the cold wall wedge and a pronounced difference in enthalpy distribution will be in evidence.

vii) Near Wake Flow Field Mappings

Perhaps the most important set of results, from the present near wake investigation, are the flow field mappings for both the adiabatic and cold wall models shown in figures 38 and 39. The data presented in these figures not only indicate the location of the characteristic lines discussed in the previous section, but also illustrate the relative orientation of base region streamlines, constant total pressure lines and, as in the case of the cold wall wedge, lines of constant total temperature. Position accuracy for these lines is estimated to vary from $\pm$ .01H at the base station to about $\pm$ .02H at stations further downstream. The streamlines were obtained by integrating profile data from the leading edge shock down to the wake shocks, at which location they were then matched with calculated streamline values arrived at by integrating from the wake centerline using the assumption of zero pressure gradient. In an effort to verify the streamline orientation for the adiabatic case, additional

calculations of flow direction were made by combining Pitot pressure data, both upstream and downstream of the wake shock, with centerline pressure data. The resulting flow orientation angles are indicated by the short lines drawn to the shock location symbols. The comparison between the streamlines and these flow direction lines is seen to be very favorable. The tendency of the flow to be disinclined to negotiate the sharp turn at the base is clearly obvious in all the figures. Further, the small mass flow present within the lower portions of the shear layer is now well pointed out. The resulting low Reynolds numbers then suggest that any viscous layer which is developing within the shear layer will experience an appreciable growth rate. This follows by noting that, as a first approximation, the viscous layer will grow according to the flat plate boundary layer theory:

$$\frac{\delta_e}{H} \approx 5\sqrt{x/H}/\sqrt{Re_{e_H}}$$

$$\frac{d(\delta_e/H)}{d(x/H)} \sim \frac{2.5}{\sqrt{x/H}\,\sqrt{Re_{e_H}}}$$

At station $x/H = 0.1$, which is just downstream of the base separation point, the Reynolds number is of the order of 200 for the data corresponding to figure 38a. A thickness of about $\delta_e/H = 0.1$ and a growth rate $(d(\delta_e/H)/d(x/H))$ corresponding to approximately 30^o are thus calculated for this station. By making a rough estimate of the location and orientation of the inner edge of the viscous layer from the position of the sonic and $u = 0$ lines in figure 38a, it is

seen that such a viscous layer edge is in only fair agreement with the so-labeled line indicated in the figure. This line has been determined as the locus of points where the total pressure lines begin to diverge from the streamlines. However, considering the uncertainties associated with both measured and calculated results, such a discrepancy, which represents a rough estimate of the orientation and location accuracy for the viscous layer's measured edge, does not seem unreasonable. The fact that the total pressure remains almost invariant along streamlines within the shear layer and for some distance downstream of the corner, as indicated in the figure, illustrates that such a flow corresponds to an isentropic turn, so often postulated in analytical studies. Although the various data uncertainties discussed in Section III are inherent in the flow field mapping results, the consistent trends exhibited by both cold and adiabatic wall data for all Reynolds numbers investigated offer substantial verification for the noted findings. The complexity of the base region problem is now quite obvious. At one time it had been speculated that the viscous layer was contained within the wake shock boundaries and that inviscid rotational characteristic methods could then be utilized for the flow between the wake shock and shear layer edge. It is seen that this analytic model is open to question since the wake shock now appears to be imbedded within the viscous layer itself. Admittedly the viscous layer edge tends to move toward the wake shock with increasing Reynolds number and cooling, but even at the highest Reynolds number cold wall results, figure 39d-1, it still is observed to be distinctly above the wake shock itself. The

cold wall total temperature lines exhibited in figure 39-2 indicate only minor variations of total temperature along streamlines outside the base region shock boundaries. Apparently the effects of thermal diffusion and viscous dissipation compensate each other in such a manner that total temperature variations along streamlines within this viscous region are negligible.

Various other results can be deduced from the data of figures 38 and 39. For example the projection upstream of the lip shock, sonic line and zero velocity line all indicate that flow separation is apparently occurring, not at the base corner, but actually some distance below the corner, as experiments of Hama have indicated. In addition, these figures show that the shear layer edge and location of wake shocks move toward the centerline with increasing Reynolds number and model cooling. Also, with cooling, the lip shock exhibits a tendency to "originate" farther upstream than for the low Reynolds number adiabatic wall cases. This result is evident from the Pitot pressure profile data of figure 44. With regard to the lip shock strength, it has been found that at $x/H = 1.0$, the farthest downstream position where the lip shock may be estimated to exist and where it appears to be the strongest, a variation of p_2/p_1 from 1.75 to 2 exists for all the near wake results of figures 38 and 39. These values of shock strength agree very well with Hama's correlation of wedge data (28) and further substantiate his claim that the lip shocks found in near wakes behind slender bodies are not necessarily negligible but, indeed, may be quite strong. The noted shock strengths, it should be pointed out, were

obtained by ratioing centerline static pressures at x/H = 1.0 to base pressure data, since the static pressure profiles already discussed, indicated that pressures "upstream" of the lip and wake shocks were essentially equal in magnitude to base pressures, and that the pressures downstream were constant and equal to centerline values of static pressure.

Since detailed flow field mappings, such as presented in figures 38 and 39, provide a "picture" of the base region flow, a comparison can be made between such a "picture" and a Schlieren photograph of a given flow. This type of comparison is shown in figure 38d-2, where the base region mapping results for the high Reynolds number, adiabatic wall case (figure 38d-1), have been superimposed on a Schlieren photograph of the near wake behind a 20^{o} wedge under virtually the same free stream conditions. The locations of the nose and wake shocks and the leading ray of the expansion fan as determined by the detailed flow field mapping and those as shown by the Schlieren photograph are seen to be in very favorable agreement. A similar comparison regarding the wedge boundary layer was not possible because light reflection effects due to model misalignment, obscured the boundary layer along the wedge surface in the Schlieren photograph (figure 1). The large density gradients which exist in the expansion fan and which extend into the shear layer itself, as results herein have indicated, are clearly shown by the "white shading" of the Schlieren portion of figure 38d-2. The inability of Schlieren photography to locate shear layer edges in these high speed wake flows, is thus well illustrated by this figure. At lower supersonic

speeds and even for hypersonic flows behind blunt bodies where density gradients in the vicinity of and outside the shear layer edge become negligibly small, the edge of the shear layer is easily discernible. For these latter flows the corner expansion fan does not extend into the separated shear layer in the manner shown by the present flow field mappings. For slender bodies with flat bases, this result represents another major distinction between supersonic and hypersonic near wake flows.

viii) Static Enthalpy Profiles for Near Wake of Cold Wall Wedge

Of current interest to wake investigators is the temperature distribution within separated shear layers of near wakes behind high speed vehicles. It is well known that in boundary layers on a cold wall a local temperature peak, or "hot spot," exists within the boundary layer. The possible existence of similar off-axis hot spots has also been postulated in the case of near wakes behind cold wall bodies. The behavior of the static enthalpy as shown in figure 37f is quite typical of adiabatic wall boundary layer flow with the peak in enthalpy occurring on the wake centerline. Similar data for the highest Reynolds number investigated for the cold wall wedge are presented in figure 40. Not only is the off-axis peak evident in this latter figure but its initial magnitude ($\frac{h}{h_\infty} \doteq 2.8$), compares quite favorably with the maximum value as calculated by the theory of reference 38 for a laminar boundary layer with heat transfer. In addition, it appears that the location of this peak at each axial station corresponds approximately to the same streamline indicating that such "hot spots" follow along streamlines. These data also point

out the rapid rise of centerline temperature with axial distance such that the enthalpy distribution downstream of the base exhibits both two "hot spots" of approximately equal peak temperature as well as two "cold spots." Additional static enthalpy data for the other Reynolds numbers are presented in figure 41, and similar trends are indicated. These results not only confirm the existence of off axis "hot spots", but also illustrate that the peak temperatures existing within the shear layer downstream of the base are comparable to the temperatures of the flow on the wake centerline. The data of figure 41 further illustrate that the noted hot spots coalesce with centerline temperature peaks within two base heights downstream from the model base.

V. SUMMARY OF RESULTS

An experimental investigation has been conducted to determine mean flow properties for both near and far wakes behind several two-dimensional slender bodies at $M_\infty = 6$. Three adiabatic wall models, consisting of a flat plate model ($d = 1''$, $\tau = .0156''$) and two 20° included angle wedge models ($H = .15''$, $H = .3''$) were tested. The effect of wall temperature on wake properties was examined by cooling the larger of these two wedge models with the internal flow of liquid nitrogen. Free stream Reynolds number per inch were varied from $.5 \times 10^5$ to 2×10^5 for each of these four configurations.

V.1 Far Wake

The main results which have been obtained from the far wake investigation are as follows:

1. Wake transition distances based on wake thickness data agreed favorably with results from hot wire fluctuation measurements. Mean flow properties along the wake centerline, however, first deviated from laminar steady conditions somewhat upstream of "wake thickness" transition locations.

2. Transition in the far wake moved upstream with increasing Reynolds number and decreasing wall temperature.

3. Satisfactory agreement between experimental data for all low Reynolds number, adiabatic wall cases and linear wake theory confirmed that the flow in the far wake for these cases was laminar to the farthest downstream stations at which measurements were obtained.

4. Base region flows for the three adiabatic wall

configurations were laminar for all test Reynolds numbers. For the cold wall wedge, the flow in the base region was laminar at least for the two lowest test Reynolds numbers.

5. Maximum centerline pressures in the far wake for all four configurations were generally 10% higher than the free stream pressure. These "overshoot" pressures depended primarily on the inviscid flow field and, because they occurred at locations relatively far downstream, illustrated that the wake recompression process was spread out over a considerable axial distance.

6. For the cold wall wedge ($T_w/T_o = .19$) the maximum enthalpy along the wake centerline for all test Reynolds numbers occurred about two base heights downstream of the model base and was approximately triple the magnitude of the free stream enthalpy. When the far wake was laminar, the decay rate of enthalpy was extremely small.

V.2 Near Wake

The main results which were obtained from the present investigation of near wakes behind a 20^o wedge model (H = .3") under adiabatic and cold wall ($T_w/T_o = .19$) conditions are as follows:

1. Collapsing of adiabatic and cold wall data was accomplished by correlating both base pressure and wake neck thickness measurements with trailing edge boundary layer thickness. This successful correlation, which illustrated that base pressures increased with increasing trailing edge thickness, further substantiated that the thickness of the trailing edge boundary layer represents a significant length scale for the near wake problem.

2. The flow along the wake centerline became supersonic for all cases within an axial distance of two base heights.

3. Base region rear stagnation points were located at approximately three quarters of a base height downstream of the model base for all cases.

4. The temperature ratio at the rear stagnation point for the cold wall wedge for all test Reynolds numbers was approximately $T_{sp}/T_o = .34$.

5. For the cold wall wedge, peaks in static temperatures occurred in the shear layers outside the wake shock structure. Initial magnitudes of these peak temperatures agreed favorably with estimates from laminar boundary layer theory. These "hot spots" followed along streamlines and coalesced with centerline temperature peaks within two base heights downstream from the model base.

6. Wake shocks, shear layer edges, base region sonic lines, and even "viscous layer edges" moved closer to the wake centerline with increasing Reynolds number and decreasing wall temperature.

7. The boundary layer on the wedge surface was influenced by the low base pressure two to three boundary layer thicknesses upstream of the base. Separation of this boundary layer appeared to occur on the model base slightly below the corner. A "separation" shock, similar to that appearing in the near wakes of bodies with rounded bases, was generated during the separation process.

8. In this Mach number six study, the base separation shock, which "rotates" toward the wake axis with increasing Mach numbers, coalesced with the wake recompression shock to form a

single shock structure.

9. Most of the outer flow of the separated boundary layer turned very slowly in the vicinity of the base with the result that the amount of mass flow contained within the base region proper corresponded to a small fraction of the total boundary layer flow. The structures of the base regions behind the present slender bodies were thus established by flows of very low densities.

10. The supersonic turning of the separated boundary layer, though gradual, caused appreciable lateral pressure gradients in the near wake shear layers. These gradients became negligible once the flow had progressed several boundary layer thicknesses downstream of the base. The downstream boundary of this pressure gradient zone was represented, approximately, by a Mach wave originating from the vicinity of the corner. Downstream of this boundary and above the wake shock, static pressures were constant and equivalent to the base pressures. For Mach numbers appreciably higher than the present case, this region of constant pressure should decrease in extent because the noted Mach wave boundary rotates toward the wake axis with increasing Mach number.

11. Inside the wake shocks, lateral gradients in pressure were negligible.

12. Initially, during the corner turning process, the variation of total pressure along streamlines was negligible. This "isentropic turn" extended downstream to where constant total

pressure lines began diverging from streamlines. The locus of these points of divergence separated the inviscid rotational flow from the viscous flow of the shear layer. These "viscous layer edges" were positioned in the outer portions of the shear layers indicating that wake shocks were imbedded within viscous regions of the shear layers.

REFERENCES

1. Feldman, S.: "Trails of Axi-Symmetric Hypersonic Blunt Bodies Flying Through the Atmosphere," AVCO-Everett, Research Report 82, Dec. 1959; also J. Aero. Sci. 28, 433-448 (1961).

2. Lykoudis, P. S.: "Theory of Ionized Trails for Bodies at Hypersonic Speeds," Rand RM-2682-1-PR, May 1961, revised Oct. 1961.

3. Lees, L. and Hromas, L.: "Turbulent Diffusion in the Wake of a Blunt-Nosed Body at Hypersonic Speeds," J. Aero. Sci., 29, 976-993 (1962).

4. Kubota, T.: "Laminar Wake with Streamwise Pressure Gradient II," GALCIT Internal Memorandum No. 9 (April 1962).

5. Gold, H.: "Laminar Wake with Arbitrary Initial Profiles," AIAA J. 2:5, 948-949 (1964).

6. Lees, L. and Gold, H.: "Stability of Laminar Boundary Layers and Wakes at Hypersonic Speeds. Part I. Stability of Laminar Wakes," Fundamental Phenomena in Hypersonic Flow, ed. by J. Gordon Hall, Cornell Univ. Press, 310-342 (1966).

7. Behrens, W.: "Flow Field and Stability of the Far Wake behind Cylinders at Hypersonic Speeds," Ph.D. Thesis, Calif. Inst. of Tech., Pasadena, Calif. (1966).

8. Dewey, C. F., Jr.: "Near Wake of a Blunt Body at Hypersonic Speeds," AIAA J. 3:6, 1001-1010 (1965).

   Also Dewey, C. F., Jr.: "Measurements in Highly Dissipative Regions of Hypersonic Flows. Part II. The Near Wake of a Blunt Body at Hypersonic Speeds," Ph.D. Thesis, Calif.

Inst. of Tech., Pasadena, Calif. (1963).

9. Weinbaum, S.: "Rapid Expansion of a Supersonic Boundary Layer and Its Application to the Near Wake," AIAA J. 4:2, 217-226 (1966).

10. Weiss, R. F. and Weinbaum, S.: "Hypersonic Boundary Layer Separation and Base Flow Problem," AIAA J. 4:8, 1321-1330 (1966).

11. Chapman, D. R., Kuehn, D. M. and Larson, H. K.: "Investigation of Separated Flows in Supersonic and Subsonic Streams with Emphasis on the Effect of Transition," NACA Report 1356 (1958).

12. Crocco, L. and Lees, L.: "A Mixing Theory for the Interaction Between Dissipative Flows and Nearly Isentropic Streams," JAS 19:10, 649-676 (1952).

13. Baloga, P. E. and Nagamatsu, H. T.: "Instrumentation of GALCIT Hypersonic Wind Tunnels," GALCIT Memorandum No. 29 (July 31, 1955).

14. Herzog, R. R.: "Nitrogen Injection into the Base Region of a Hypersonic Body," GALCIT Hypersonic Research Project, Memorandum No. 71 (August 1964).

15. Behrens, W.: "Viscous Interaction Effects on a Static Pressure Probe at M = 6," AIAA J. 1:12, 2364-2366 (1963).

16. McCarthy, J. F., Jr.: "Hypersonic Wakes," GALCIT Hypersonic Research Project, Memorandum No. 67 (July 1962).

17. Dewey, C. F., Jr.: "Hot Wire Measurements in Low Reynolds Number Hypersonic Flows," ARS J., 1709-1718 (Dec. 1961).

Also Dewey, C. F., Jr., "A Correlation of Convective Heat Transfer and Recovery Temperature Data for Cylinders in Compressible Flow," Int. J. Heat Transfer, 8, 245-252 (1965).

Also Dewey, C. F., Jr.: "Hot Wire Measurements in Low Reynolds Number Hypersonic Flows," GALCIT Hypersonic Research Project, Memorandum No. 63 (September 1961).

18. Vrebalovich, T.: "Heat Loss from Hot Wires in Transonic Flow," JPL Research Summary No. 36-14 (May 1, 1962).

19. Christiansen, W. H.: "Development and Calibration of a Cold Wire Probe for Use in Shock Tubes," GALCIT Memorandum No. 62 (1961).

20. Sherman, F. S.: " A Survey of Experimental Results and Methods for the Transition Regime of Rarefied Gas Dynamics," International Symposium on Rarefied Gas Dynamics, Vol. II, Academic Press, New York (1963).

21. Guthrie, A.: "Vacuum Technology," John Wiley and Sons, Inc., (1963).

22. Mathews, M. L.: "An Experimental Investigation of Viscous Effects on Static and Impact Pressure Probes in Hypersonic Flow," GALCIT Hypersonic Research Project, Memorandum No. 44 (June 1958).

23. Sherman, F. S.: "New Experiments on Impact-Pressure Interpretation in Supersonic and Subsonic Rarefied Air Streams," NACA TN 2995 (1953).

24. Laufer, J. and McClellan, R.: "Measurements of Heat Transfer from Fine Wires in Supersonic Flows," JFM 1:3, 276-289, (September 1956).

25. Ames Research Staff: "Equations, Tables and Charts for Compressible Flow," NACA Report 1135 (1953).

26. Martellucci, A., Trucco, H. and Agnone, A.: "Measurements of the Turbulent Near Wake of a Cone at Mach 6," AIAA J. 4:3, 385-391 (1966).

27. Badrinarayanan, M. A., "An Experimental Investigation of Base Flows at Supersonic Speeds," J. Roy. Aeronaut. Soc. 65, 475-482 (July 1961).

28. Hama, F. R.: "Experimental Investigations of Wedge Base Pressure and Lip Shock," Jet Propulsion Laboratory, TR No. 32-1033 (Dec. 1966).

29. Sato, H. and Kuriki, K.: "The Mechanism of Transition in the Wake of a Thin Flat Plate Placed Parallel to a Uniform Flow," JFM II:3, 321-352 (November 1961).

30. Demetriades, A.: "Hot Wire Measurements in the Hypersonic Wakes of Slender Bodies," AIAA J. 2:2, 245-250 (1964).

31. Lees, L.: "Hypersonic Wakes and Trails," AIAA J. 2:3, 417-428 (1964).

32. Kendall, J. M., Jr.: "An Experimental Investigation of Leading-Edge Shock-Wave Boundary Layer Interaction at $M_{\infty} = 5.8$," JAS 24, 47-56 (1957).

33. Muntz, E. P. and Softley, E. J.: "A Study of Laminar Near Wakes," AIAA J. 4:6, 961-968 (1966).

34. Cresci, R. J. and Zakkay, V.: "An Experimental Investigation of the Near Wake of a Slender Cone at M = 8 and 12," Aerospace Research Laboratories 65-87 (May 1965).

35. Todisco, A. and Pallone, A.: "Near Wake Flow Field Measurements," AIAA Paper 65-53 (Jan. 1965).

36. Hayes, W. D. and Probstein, R. F.: "Hypersonic Flow Theory," Academic Press, New York and London (1959).

37. Chapman, D. R.: "An Analysis of Base Pressure at Supersonic Velocities and Comparison with Experiment," NACA Report 1051 (May 1950).

38. Chapman, D. R. and Rubesin, M. W.: "Temperature and Velocity Profiles in the Compressible Laminar Boundary Layer with Arbitrary Distribution of Surface Temperature," JAS 16:9, 547-565 (1949).

39. Cheng, R., Schaaf, S. A. and Hurlbut, F. C.: "The Measurement of Base Pressure as Wedges in Supersonic Low Density Flow," Institute of Engineering Research, University of California (Berkeley) Report No. AS-64 17 (Nov. 1964).

APPENDIX A

HOT WIRE ANEMOMETRY TECHNIQUES FOR MEAN FLOW MEASUREMENTS

A.1 Raw Data Measurements

Hot wire raw data are obtained by exposing a short, small diameter wire to a given flow condition, and measuring the wire resistance corresponding to each of several heating currents. By extrapolating the variation of resistance with wire power (I^2R), i.e., wire heat loss, to zero power, the adiabatic wire resistance is obtained. A pretest calibration giving the correlation between wire resistance and temperature then enables the determination of the adiabatic wire temperature. Measured Nusselt number is also determined from the resistance-power curve since it is proportional to the slope of this curve at zero power (17). Appendix B.1 describes the computer program by which both the zero-power resistance and slope were determined for the present results.

A.2 End Loss Analysis

In using hot wire probes it is often necessary to carry out end loss corrections to account for the conduction of heat from the wire to the probe supports so that results correspond to infinite wire data. These corrections were formulated by Dewey (17) from his analysis of the conduction of heat from a finite length wire to two end supports at a temperature, T_s. The wire was assumed to be in uniform flow with uniform temperature existing at each cross-section. Additionally it was assumed that the thermal conductivity

of the wire remained constant and that the electrical resistance varied linearly with temperature. His results are

$$T_{aw_*} = \psi_r \, T_{awm}$$

$$Nu_t = \psi_N \, Nu_m$$

where ψ_r and ψ_N, recovery ratio and Nusselt number end loss correction factors respectively, are given by:

$$\psi_r = \frac{1 - \frac{T_s}{T_{awm}} \omega_o}{1 - \omega_o}$$

$$\psi_N = (1-\omega_o)\left[1 + \frac{st_s}{2} \; \frac{\left\{(2\omega_o - 1)\omega_o - \frac{1}{\cosh^2 \nu_o}\right\}}{(1-\omega_o)^2}\right]$$

The Nusselt number end loss correction factor stated here is that derived by Behrens (7) as a corrected version to the one formulated by Dewey. Examination of these formulae indicates that an iterative scheme using infinite wire calibration results, to be discussed shortly, is necessary for solution since the Nusselt number itself is a required input to both correction factors.

In many experiments both static and Pitot pressure measurements are carried out jointly, and only one of the two measurements provided by the hot wire probe is necessary since three independently measured quantities are sufficient to define completely the flow at a given location. This redundancy in measured data makes it possible to compare the Nusselt number correction factor, as measured, with that derived through Dewey's end loss analysis.

From measured values of static pressure, Pitot pressure and adiabatic wire temperature and using the iterative calculation procedure described in Appendix B.3 the complete flow field was determined for various transverse traces across the wake behind a slender body at $M_\infty = 6$. Values of Nusselt numbers obtained with these data were then ratioed to measured Nusselt numbers to determine measured end loss correction factors. When these factors, for a given wire, were plotted as a function of the dimensionless quantity ω_o, plots such as shown in figure 13 resulted. Here ω_o is given by

$$\omega_o = \frac{\tanh \nu_o}{\nu_o}$$

where

$$\nu_o = \sqrt{\left(\frac{\ell}{d}\right)^2 \frac{k_t}{k_w} Nu_t}$$

The functional form shown in figure 13 was considered appropriate for comparing measured with predicted values of Nusselt number end loss correction factors because the formula for ψ_N indicated that ψ_N depended more strongly on ω_o than on the resistance parameter s, or the nondimensional support temperature t_s. In general, noticeable differences were observed to exist between measured and predicted results. The tendency of all the data for one wire to describe a single curve (within $\pm 5\%$), suggested possible systematic errors were involved. Replotting the correction factor data as a function of ν_o, instead of ω_o, illustrated that these measured results appeared to be consistently offset from the Behrens' curve

by a nearly constant percentage of ν_o. This offset can perhaps best be explained by noting that inaccuracies in wire conductivity and wire aspect ratio exist because of measurement difficulties. For example the function ν_o, being directly proportional to the aspect ratio, is thus subject to question and would be off by a constant percentage amount for a given percentage error in aspect ratio. In any event, the measured results demonstrate that a calibration curve, showing the variation of Nusselt number correction factor with the function ω_o, can be established for each wire in lieu of the Behrens' formula. Such curves were obtained for all the wires used in the present investigation. To check the suitability of using these calibration curves in conjunction with measured Nusselt numbers to determine mean flow data, comparison calculations were made for representative profile results. Both stagnation temperature and Nusselt number were calculated using Pitot pressure, adiabatic wire temperature and either static pressure or measured Nusselt number with a corresponding wire calibration curve for the Nusselt number correction factor. The results indicated that stagnation temperatures compared to within 1% whereas Nusselt number results differed by at most 5%. Such a favorable comparison confirmed the acceptability of this calibration procedure for determining Nusselt number data in regions of the flow where static pressure measurements were unavailable. All shear layer data presented herein were obtained in this manner since the large pressure gradients for these layers prevented making static pressure measurements.

It should be pointed out that this method of calibrating Nusselt number correction factors in a known flow is similar, in certain respects, to the flow calibration technique proposed by Demetriades* for flows where $M \geq 3$. This latter procedure is based on establishing, for each hot wire, a calibration curve showing the variation of measured Nusselt number with Reynolds number. Such a correlation is obtained by carrying out hot wire measurements in free stream flow under varying Reynolds number conditions. For small changes in support temperature and local stagnation temperature this approach was shown to be quite accurate in determining Reynolds number. For many of the present results for $M > 3$ the Nusselt number correction factor shows only minor dependence on Mach number and support temperature. Furthermore when air and wire conductivity undergo only slight changes, the correlation results shown in figure 13, which indicate that

$$\psi_N = \frac{Nu_t}{Nu_m} = \psi_N \left(\omega_o = \frac{\tanh \nu_o}{\nu_o} \right)$$

$$= \psi_N \left(\nu_o = \sqrt{\left(\frac{\ell}{d}\right)^2 \frac{k_t}{k_w} Nu_t} \right)$$

also suggest the following simplified relationship

$$Nu_m = Nu_m (Nu_t) \quad .$$

---

* Private communication

Thus, since it has been shown (7, 24) that for $M \geq 2$ the Nusselt-Reynolds number correlation is independent of Mach number, it follows that, as in Demetriades' case for $M \geq 3$,

$$Nu_m = Nu_m(Re_t) \quad .$$

It should be emphasized, however, that for this calibration technique to be applicable, the above noted assumptions should be valid. For those flows where appreciable stagnation and support temperature gradients exist and especially for $M < 2$, the present method (figure 13) would seem more appropriate.

A.3 Infinite Wire Calibrations

In using the hot wire probe to conduct mean flow measurements the investigator relies on established calibration data for a perfectly conducting cylinder (wire) infinite in extent. Such data, consisting of recovery factor (T_{aw_*}/T_t) and Nusselt number given as functions of Mach number and Reynolds number, in combination with end-loss corrections, permit the determination of local stagnation temperatures and mass flow rates from hot-wire measurements. Many experimental and theoretical studies have been made to determine such calibration data, and a comprehensive review is given by Dewey (17). Figure 12 shows the range of test conditions for the hot-wire probes used in the present investigation and it is evident that most of the measurements fell within the transitional regime. Furthermore, many measurements occurred at low supersonic speeds and thus the recovery factor and heat transfer correlation of Behrens (7) were not applicable, since his data were not only

independent of Mach number but also were valid only for $M \geq 2$.

i) Normalized Recovery Factor

Dewey, by combining the data of several investigators with his own measurements (17), found that a single curve ($\pm$ .1 in $\overline{\eta}_*$) could satisfactorily describe the variation of a normalized recovery factor with Knudsen number from continuum flow to free molecule flow for all Mach numbers greater than approximately .7. This normalized recovery factor has been used herein and is given by:

$$\overline{\eta}_* = \frac{\eta_* - \eta_c}{\eta_f - \eta_c}$$

where η_c and η_f are the continuum and free molecule recovery factors respectively.

ii) Nusselt-Reynolds Number Correlation

Sherman (20), in examining heat transfer data for spheres in subsonic flow, found that a single curve of the form

$$St/St_f = \frac{1}{1 + \frac{St_f}{St_c}}$$

correlated data from continuum flow through free-molecule flow. Such a result suggested that perhaps a similar correlation may exist even for higher Mach numbers. Kubota* in re-examining the data used by Dewey for his heat transfer correlation found that, indeed, such a correlation existed. By normalizing Nusselt number with the Nusselt number for free molecular flow ($\alpha = 1$)

---

* Private communication

$$Nu_f = \frac{\bar{h}d}{k_t} = \frac{\gamma - 1}{2(\pi)^{3/2}\gamma} \alpha \, Re_t \, Pr_t \left(\frac{g(s_1)}{s_1}\right)^*$$

and plotting the result as a function of the normalized Nusselt number for incompressible continuum flow (Nu_c / Nu_f) (the M = 0 curve in Dewey's correlation), Kubota found the results shown in figure 14. Not only did a single curve seem appropriate for correlating the data but one form which appeared reasonable for correlation purposes

$$\frac{Nu_t}{Nu_f} = \frac{1}{1 + \frac{Nu_f}{Nu_c}}$$

was identical to that of Sherman. Although this correlated curve did show noticeable deviation (+15%) from the Dewey measurements as the continuum flow regime is approached ($Nu_c/Nu_f < 1$, $Re_t > 10$) it seemed satisfactory for the present calculations since it was always within 5% of Dewey's results for the range of Reynolds numbers covered in the present tests ($Re_t < 4$, $Nu_c/Nu_f > 1.91$). This form for the Nusselt-Reynolds number correlation also was much simpler than that established by Dewey and thus proved easier to check out and use in machine computations. For Mach numbers greater than 1 these results are believed within -5% of measured data. For lower Mach numbers and for Reynolds numbers greater than 4.0 the correlation results of Dewey would seem more appropriate.

---

*This formula was misquoted in reference (17).

APPENDIX B

DATA REDUCTION PROGRAMS

B.1) Raw Data Program

Although some modifications have been made in the hot wire raw data program as established by Herzog (14), the basic purpose, input requirements and output data for this program remain the same. The input data to this program consist of punched IBM cards representing initial hot wire measurements as recorded by the Automatic Hot Wire Recording System. The data for a given input card lists hot wire position, probe support temperature, and attenuated hot wire voltages corresponding to each of 5 currents and 5 bucking voltages. In the raw data program these hot wire voltages are transformed from their digitized form to mv readings using system calibration data, and the known wire currents and bucking voltages. Conversion of these data in turn to hot wire resistance (R_m) and power (I^2R) results is straightforward. Once in this form the wire resistance (R_{awm}) and curve slope ($\frac{dR_m}{dI^2R}$) corresponding to zero power are determined by fitting a parabolic curve to the data with a least squares procedure. Often more accurate and consistent results were possible if only those data corresponding to the lowest four currents were used to obtain this fit. After completing several additional calculations, the program, as output for each probe position, lists and punches out on IBM cards such results as normalized probe position, adiabatic wire resistance and temperature, zero power slope of the resistance power curve, and probe support temperature. These cards are then used directly as input data to the plotting and end loss programs.

B.1a) Raw Data Program ID Listing

NPT	NPT	number of data points to be used in calculation of slope (dR/dI^2R) and R_{awm}
IARRAY	IARRAY	code name (hot wire, or Run No)
ID	ID	identification number
ALPHA	α_r	slope of calibration curve of $R_{wm}(\Omega)$ versus T_{wm} (^oC) for zero current, ($1/^oK$)
RR	R_r	reference resistance as calibrated for zero current and zero ^oC, Ω
L	ℓ/d	wire aspect ratio
CO(I),	I = 11,15	voltage calibration factors for each of five currents
CO(I),	I = 16,20	bucking voltages for each of five currents, mv
CO(I),	I = 21,25	constant current values (five), mv
PCI	%	% injection
XD	x/D	probe tip position in axial direction
CO(1)	y_o	centerline probe position in transverse direction relative to a standard position, in.
Q1	y	probe position in transverse direction relative to a standard position, in.
A(J),J=1,5	$C(\Delta E_{HW})$	attenuated hot wire voltage decrement, mv
Q7	T_s	support temperature, ^oC
CORN	CORN	card number
VC	V_c	support temperature correction factor
SC	S_c	support temperature correction decrement, ^oC
DR	D	reference diameter, in.
B(J),J=1,5	ΔE_{HW}	hot wire voltage decrement for each of five currents, mv
C(J), J=1,5	E_m	measured hot wire voltage for each of five currents, Mv

D(J),J=1,5	R_{wm}	measured hot wire resistance for each of five currents, Ω
E(J),J=1,5	I^2R_{wm}	measured hot wire power for each of five currents, $(ma)^2$ Ω
Z1	y/D	normalized axial distance
Z2	R_{awm}	wire resistance for zero current, Ω
Z3	$[dR_{wm}/dI^2R_{wm}]_{I=0}$	slope of resistance-power curve at I = 0, $(ma)^{-2}$
Z4	T_{awm}	wire temperature for zero current, ^oK
Z5	$Nu_m k_t$	product of measured Nusselt number and air conductivity, $\Omega(ma)^2/^oC$ in.
Z6	T_s	corrected support temperature, ^oK

B. 1b) Typical Input Data for Raw Data Program

```
$DATA
4
HOT WI 013  1597    2410    0282    12900   11865   10600   07501   05000
013 15488  12423  08738  05874  03441  4900   4060   302    2077   12354
1
RUN NO       PCI 0.0 XH  150 5786
5789 491 268 301 223 182 0874                                    11680430I2

$END JOB
```

B. 1c) Typical Output Data for Raw Data Program

```
                HOT WI 013  1597    2410    0282    12900   11865   10600   07501   05000
PCI  0.   XD   1.50  Z1 THRU Z6      0.003000   28.328848   0.006042  383.075325  71.900972  360.599998  ID  13  C.N./ 12  0.003
     0.32900795E 02      0.31381729E 02      0.29960502E 02      0.29086529E 02      0.28589930E 02
     0.78994809E 03      0.51728385E 03      0.27379491E 03      0.12547722E 03      0.43634327E 02
```

B. 1d) Fortran Listing of Raw Data Program

```
$IBFTC MAIN     DECK
C FIRST CARD MUST HAVE IN COL 1  3,4, OR5 FOR NO OF POINTS
      REAL L, NUKO, NUKMIN, NUKMAX
      DATA NAME / 6HHOT WI/, NRUN / 6HRUN NO/
      INTEGER CORNO
      DIMENSION A(5),B(5),C(5),D(5),E(5),CO(30),IARRAY(13),TITLE(10),
     1 X(200), TM(200), NUKO(200)
      DIMENSION DIF(5)
      DIMENSION SLOPE(5)
      DIMENSION COEF(3)
      READ(5,610) NPT
  610 FORMAT(I1)
   10 READ (5,502) IARRAY
      WRITE (6,516) IARRAY
  516 FORMAT(1H1 20X13A6)
      IF(IARRAY(1).EQ.NAME) GO TO 16
   15 IF(IARRAY(1).NE.NRUN) GO TO 17
      GO TO 19
   16 READ 503, IARRAY,ID,ALPHA,RR,L,(CO(I),I = 11,15)
      READ (5,504) (CO(I),I=16,25)
      READ (5,507)  VC, SC , DR
      CO(3) = ALPHA *.001
      CO(2) = RR
      CO(6) = L
      READ (5,502) IARRAY
      GO TO 15
   17 CONTINUE
C ERROR RETURN - PACK MUST START WITH NEW PCI, XD, CO(1)
      WRITE (6,510)
      STOP
C BEGINNING OF PACK - READ PER CENT INJECTION, X/D, C.P.
C
   19 CONTINUE
      READ  505,IARRAY, PCI, XD, CO(1)
      PRES = 0.
      K = 0
   20 READ (5,500)Q1, (A(J),J=1, 5), Q7,CORNO
      IF(Q1.EQ.0.0) GO TO 60
      DO 30 J = 1, 5
      B(J) = A(J) * CO(J+10)
      C(J) = B(J) + CO(J+15)
      D(J) = C(J) / CO(J+20)
      E(J) = C(J) * CO(J+20)
   30 CONTINUE
      CALL LSTSQ(E,D,NPT,SLOPE,X1,COEF)
      IN = 6 - NPT
      DO 35 J = IN,5
      DEVAL = COEF(1) + COEF(2)*E(J) + COEF(3) * E(J) * E(J)
      DIF(J) = D(J) - DEVAL
   35 CONTINUE
      DIFMAX = DIF(IN)
      IJ = IN+1
      DO 36 J = IJ,5
      IF(ABS(DIFMAX) .GT. ABS(DIF(J))) GO TO 36
      DIFMAX = DIF(J)
   36 CONTINUE
      Z1 = (Q1 - CO(1))/ DR
      Z2 = X1
      Z3 = SLOPE(1)
      Z4 = 273.2 + (Z2-CO(2)) / (CO(2)*CO(3))
      Z5 = CO(2) * CO(3) / (3.14159265*CO(6) *Z3)
```

```
      Z6 = Q7*(1.- VC) - SC + 273.2
      WRITE (6,515) PCI,XD,Z1,Z2,Z3,Z4,Z5,Z6,      ID,CORNO ,DIFMAX
  515 FORMAT(1X3HPCI 2XF3.1,2X2HXD2XF5.2,2X10HZ1 THRU Z6  2X6F12.6,
     1         2X2HID2XI3,2X4HC.N. 1XI3,1X F8.5)
      PUNCH 600,     PCI, XD, Z1, Z2, Z3, Z4, Z5, Z6,          ID ,
     1 CORNO
      WRITE (6,520) (D(J), J=1,5)
      WRITE (6,520) (E(J),J=1,5)
  520 FORMAT (5E20.8)
      GO TO 20
  500 FORMAT(F4.3,5F4.3,F5.1,48X13)
  502 FORMAT(13A6)
  503 FORMAT          (7X13,2XF8.7,F8.6,F8.8,5F8.6)
  504 FORMAT(4X5F7.4,5F7.6)
  510 FORMAT(//10X47HERROR RETURN - PACK MUST START WITH PCI, XD, CP// )
  505 FORMAT(15X F5.2,3XF5.3,F5.4)
  507 FORMAT (F4.3,1XF4.1, 1XF4.3)
  600 FORMAT(F3.1,  F5.2,1XF6.3,1XF5.2,1XF8.6,1X       F5.1,1XE11.5,
     11XF5.1, 18X   1XI3,1XI3)
   60 CONTINUE
      GO TO 10
       END
```

```
$IBFTC LST      DECK
       SUBROUTINE LSTSQ(X,Y,N,SLOPE,YINCEP,B)
       DIMENSION X(5), Y(5), C(10), A(50,3), B(50,1)
       DIMENSION SLOPE(5)
       NO=3
       IF (N.EQ.2) NO=2
       DO 10 I = 1,10
    10 C(I) = 0.
       IN = 6-N
       DO 20 I = IN,5
       X2 = X(I) * X(I)
       C(1) = C(1) + X(I)
       C(2) = C(2) + X2
       C(3) = C(3) + X2*X(I)
       C(4) = C(4) + X2*X2
       C(5) = C(5) + Y(I)
       C(6) = C(6) + X(I) * Y(I)
       C(7) = C(7) + X2*Y(I)
    20 CONTINUE
       A(1,1) = N
       A(1,2) = C(1)
       A(1,3) = C(2)
       A(2,1) = C(1)
       A(2,2) = C(2)
       A(2,3) = C(3)
       A(3,1) = C(2)
       A(3,2) = C(3)
       A(3,3) = C(4)
       B(1,1) = C(5)
       B(2,1) = C(6)
       B(3,1) = C(7)
       CALL MATINV(A,NO,B,1,DET)
       YINCEP = B(1,1)
       SLOPE(1) = B(2,1)
       RETURN
       END
```

B.2 Raw Data Plotting Program

Currently this program has the capability of plotting, as a function of y/H, adiabatic wire temperature, probe support temperature, and zero power slope of the resistance-power curve. Punched output from the raw data program are used directly as input to this program. Some flexibility is possible in the plotting routines since three different models or variable ranges in y/H and T_{awm} are made available. These were necessary in order to scrutinize the raw data not only for both the adiabatic and cold wall wedge models but also for the flat plate configuration.

B.2a) Plot Program ID Listing

NUK	$Nu_m k_t$	product of measured Nusselt number and air conductivity, $\Omega\,(ma)^2/(^oK\ in)$
PCI	%	% injection
YD	y/D	normalized transverse distance
TM	T_{awm}	wire temperature for zero current, ^oK
TS	T_s	support temperature, ^oK
XD	x/D	normalized axial distance
ID	ID	identification number
SLP	$[dR/dI^2R]_{I=0}$	slope of resistance-power curve at zero power, $(ma)^{-2}$
MODEL		plotting format, 1, 2 or 3
PR		plot request - PR > 2 implies only "SLP" data will be plotted

B. 2b) Fortran Listing of Hot Wire Plot Program

```
$IBFTC PLO      DECK
C       PUT ONE BLANK CARD BETWEEN EACH SET OF DATA.
C       PUT AN ADDITIONAL BLANK CARD TO SEPARATE TWO MODELS.
C       ADD ONE MORE BLANK CARD AT END OF ALL DATA (TOTAL 3)
C
C       MODEL 1 PLOTS 1 SHEET FOR EACH 3 SETS
C               PLUS 1 SHEET FOR REMAINING SETS
C       MODEL 2 PLOTS 1 SHEET FOR EACH 7 SETS
C               PLUS 1 SHEET FOR REMAINING SETS
C       MODEL 3 PLOTS 1 SHEET FOR EACH 7 SETS
C               PLUS 1 SHEET FOR REMAINING SETS
C
      REAL NUK
      DIMENSION PCI(40),          YD(4000), TM(4000), SLP(4000), NN(40),
     1 TITLE(12),X(200),Y(200)
      DIMENSION XDD(40), TS(4000), TX(200)
       DIMENSION DATMIN(3),DATMAX(3),DELTA(3), NPLOT(3)
       DIMENSION DAXMIN(3),DAXMAX(3)
       DATA (DAXMIN(I),DAXMAX(I), I=1,3) / -1.,1.,-1.,1.,-.2,.2 /
       DATA (DATMIN(I), DATMAX(I), DELTA(I), I=1,3) / -450.,300.,250.,
     1 -500.,250.,100.,-500.,250.,100. /
       DATA (NPLOT(I), I=1,3) / 3,7,7 /
       DATA (TITLE(I), I=1,12) / 6H      , 6H      , 6H      , 6H      ,
     1 6H      , 6H      , 6H      , 6H      , 6H      , 6H      ,
     2 6H      , 6H      /
    5 CONTINUE
       READ (5,524) MODEL,PR
       IF (MODEL .EQ. 0) STOP
       WRITE (6,600) MODEL
       XMIN = DAXMIN(MODEL)
       XMAX = DAXMAX(MODEL)
      J = 1
      N = 0
   10 N = N + 1
      READ (5,500) PERCEN, XD, YD(N),SLP(N),TM(N),TS(N),ID
      IF(ID .EQ. 0 ) GO TO 20
      SLP=SLP(N)
      SLP=SLP*(10.**5.)
      SLP(N)=SLP
      XDD(J) = XD
      PCI(J) = PERCEN
      GO TO 10
   20 CONTINUE
      NN(J) = N - 1
      J = J + 1
      IF(J.GT. 40) STOP
      READ (5,500) PERCEN, XD, YD(N),SLP(N),TM(N),TS(N),ID
      SLP=SLP(N)
      SLP=SLP*(10.**5.)
      SLP(N)=SLP
      IF(ID .NE. 0  ) GO TO 10
      J = J - 1
      IF (PR-1.) 21,21,61
   21 JK = 0
      N2 = 0
      WRITE (6,1001) (NN(LL),LL = 1,J)
      IN = 0
       TMIN = DATMIN(MODEL)
       TMAX = DATMAX (MODEL)
      ISET = 0
       CALL PPLOT1
```

```
      DO 60 I = 1, J
      ISET = ISET +1
      IN = IN+1
      IF (IN.EQ.1) GO TO 42
      GO TO 46
   42 CONTINUE
      LAB = 0
       TMIN = DATMIN(MODEL)
       TMAX = DATMAX (MODEL)
   46 CONTINUE
       NPT = NN(I) - JK
       IF (NPT .GT. 200) STOP
       DO 52 KK = 1,NPT
       JJ = JK + KK
      X(KK) = YD(JJ)
      Y(KK) =-TM(JJ)
      TX(KK) = -TS(JJ)
   52  CONTINUE
      WRITE (6,510) XDD(I), PCI(I)
       CALL XYPLT(NPT,Y,X ,TMIN,TMAX,XMIN,XMAX,TITLE,LAB)
       IF (IN .EQ. NPLOT(MODEL)) GO TO 45
      IF(ISET.EQ.J) GO TO 45
      GO TO 47
   45 CONTINUE
      IN = 0
       LAB = 1
   47 CONTINUE
       CALL XYPLT(NPT,TX,X ,TMIN,TMAX,XMIN,XMAX,TITLE,LAB)
       TMIN = TMIN - DELTA(MODEL)
       TMAX = TMAX - DELTA(MODEL)
      JK = NN(I)
       IF (LAB .EQ. 1) CALL PPLOT4
       IF (LAB .EQ. 1 .AND. I .NE. J) CALL PPLOT1
   60 CONTINUE
   61 JK = 0
      N2 = 0
      IN = 0
      ISET = 0
      CALL PPLOT1
      DO 60 I = 1, J
      ISET = ISET +1
      IN = IN+1
      IF (IN .EQ. 1 .AND. ISET .EQ. J) GO TO 69
      IF(IN.EQ.4) GO TO 65
      IF(ISET.EQ. J) GO TO 65
      IF(IN.EQ.1) GO TO 67
      GO TO 68
   69 LAB = 1
      IN = 0
      YMINK = -800.
      YMAXK = 2200.
      GO TO 68
   67 CONTINUE
      LAB = 0
      YMINK = -800.
      YMAXK = 2200.
      GO TO 68
   65 CONTINUE
      LAB = 1
      IN = 0
   68 CONTINUE
```

```
      N3 = NN(I) -JK
      Y(1) = YMAXK+10.
      Y(2) = Y(1)
      DO 70 KK = 1,N3
      JJ = JK +KK
      X(KK) = YD(JJ)
      Y(KK) =-SLP(JJ)
   70 CONTINUE
      WRITE (6,511) XDD(I), PCI(I)
      CALL  XYPLT(N3,Y,X,YMINK,YMAXK,XMIN,XMAX,TITLE,LAB)
      YMINK = YMINK - 750.
      YMAXK = YMAXK - 750.
      JK = NN(I)
      IF (LAB .EQ. 1) CALL PPLOT4
      IF (LAB .EQ. 1 .AND. I .NE. J) CALL PPLOT1
   80 CONTINUE
      GO TO 5
  500 FORMAT(F3.1,  F5.2,1XF6.3,7XF8.6,1XF5.1,13XF5.1,19XI3)
  501 FORMAT(6F10.0)
  510 FORMAT(/ 10X6HX/D = F10.2,10X 21HPER CENT INJECTION = F10.2,
     1 10X  16HPLOT OF T VS Y/D )
  511 FORMAT(/ 10X6HX/D = F10.2, 10X 21HPER CENT INJECTION = F10.2,
     1 10X 20HPLOT OF NUKQ VS Y/D   )
  524   FORMAT (5X, I2,3XF5.0)
  600   FORMAT (1H1, //, 10X, 5HMODEL, I2, //)
  605   FORMAT (1H0)
  610   FORMAT (5X, 6E20.4)
  630   FORMAT (1H0, //, 10X, 6HPPLOT1 /)
  640   FORMAT (1H0, 10X, 6HPPLOT4 /)
  650   FORMAT (1H0, 10X, 2A6 /)
 1000 FORMAT(5X4HX =   F12.2,10X4HY = E15.8,10X4HX = F12.2,10X4HY = E15.
     1 8)
 1001 FORMAT(5(I10,10X))
C       USE CONTROL CARDS.
C       $IBLDR*MJCPPI
C       $IBLDR*MLLXYR (INSTEAD OF MLLXYP)
        END
$IBLDR*MJCPPI
$IBLDR*MLLXYR
5
```

B.3 Hot Wire End Loss Program--Static Pressure Version

The purpose of this program is to determine total temperatures by making suitable end loss corrections to measured adiabatic wire temperatures using the end loss analysis developed by Dewey (17). The present program is actually an updated version of Dewey's original end loss program as modified by Herzog (14). Current input requirements consist of adiabatic wire resistance, probe support temperature, wire calibration data, tabulated semiprofiles of Pitot pressure, and centerline static pressures which have been corrected for viscous and tunnel gradient effects. An interpolation procedure determines the Pitot pressure corresponding to each probe position. IBM punched cards from the raw data program are used directly to furnish probe position, adiabatic wire resistance, and probe support temperature data. Since Mach number is readily determined from the Pitot and static pressures, all other flow quantities involved in the end loss analysis can be computed once an initial trial value of stagnation temperature is selected. The end loss correction factor corresponding to this initial estimate then determines a revised stagnation temperature value. The computation is cycled until a specified convergence criterion is met. In general, convergence based on a differential between trial and calculated stagnation temperatures of $.04^{\circ}K$ is possible within 5 iterations.

B.3a) End Loss Program ID Listing
(Static and Nusselt number version)

Q1	%	% injection
Q2	x/D	normalized axial distance
Q3	y/D	normalized transverse distance
Q4	$Nu_m k_t$	product of measured Nusselt number and air conductivity (based on local total temperature), $\Omega\ (ma)^2/^oK$ in
Q5		open
Q6	p_{t_2}	local measured Pitot pressure, mmHg
Q7	T_s	support temperature, ^oK
Q8	$(p_{t_2}/p_o)x10^2$	measured local Pitot pressure, normalized to free stream total pressure
Q9	$(p/p_o)_c x10^2$	corrected local static pressure, as normalized to free stream total pressure $\left(\frac{p}{p_o}\right)_m \left(\frac{p}{p_m}\right)_v \left(\frac{p_{LE}}{p_x}\right)_\infty \left(\frac{p_{t_{2_x}}}{p_{t_{2_{LE}}}}\right)_\infty$
Q10	$p_o = p_{t_\infty}$	free stream total pressure, mmHg
Q11	$\eta_s = T_s/T_t$,	support temperature ratio
Q12	ID	hot wire identification number
Q13	R_r	reference resistance as calibrated for zero current and zero ^oC,
Q14	ℓ/d	wire aspect ratio
Q15	d	wire diameter, cm
Q16	α_r	slope of wire calibration curve, $1/^oK$
Z18	Nu_t	Nusselt number for wire of infinite length
Z19	$\overline{\eta}_* = \frac{(\eta_* - \eta_c)}{\eta_f - \eta_c}$	normalized recovery ratio for infinite wire
Z20	M	Mach number
Z21	T_t	corrected local total temperature, ^oK

Z22	ρu	local mass flow, gmm/cm^{2}sec
Z23	u	local velocity, cm/sec
Z24	T_∞	free stream static temperature, ^oK
Z25	Re_{td}	Reynolds number based on local total temperature and wire diameter
Z26	Re_d	Reynolds number based on local static temperature and wire diameter
Z27	T_*	recovery temperature for infinite wire, ^oK
Z28	$Kn = \sqrt{\frac{\pi\gamma}{2}}\, M/Re$	local Knudsen number
Z29		open
Z30	$\psi_r = \frac{\eta_*}{\eta} = \frac{T_*}{T_m}$	recovery ratio end loss correction factor
Z31	$\overline{\psi}_r = \overline{\eta}_*/\overline{\eta}_m$	normalized form of recovery ratio end loss correction factor
Z32	$\psi_N = Nu_t/Nu_m$	Nusselt number end loss correction factor
Z33	$(p/p_{t2})_c$	Rayleigh-Pitot ratio (w/correction)
Z34	T_{awm}	measured adiabatic wall temperature for finite length wire, ^oK
Z35	Z35	number of iterations
Z37	Z37	convergence code
Z98	p_t/p_o	ratio of local total to free stream total pressure
Z99	p/p_o	ratio of local static to free stream total pressure
C1	C_1	constant in wire conductivity relation
C2	C_2	constant in wire conductivity relation
C5	η_{m_i}	initial value for η_m
C40	R	gas constant, cm^2/sec ^oK
C41	γ	specific heat ratio

C42	T_R	reference temperature (273°K), °K
EPS	$\epsilon = \eta_* - \eta_m$	generated
ETAS	$\eta_* = T_*/T_o$	recovery ratio for infinite wire
FKO	k_t	conductivity of air based on local total temperature
FKW	k_w	wire conductivity, cal/sec cm°K
FMUN	$\eta_m = T_{awm}/T_t$	measured recovery ratio
FMUO	μ_t	viscosity of air based on local total temperature, gmm/cm sec
FNBR	$\bar{\eta}_m = \frac{\eta_m - \eta_c}{\eta_f - \eta_c}$	normalized recovery ratio for finite length wire
FNU	$\nu = \frac{\ell}{d}\sqrt{\frac{k_t}{k_w}}\,Nu_t$	
FNUC	η_c	experimental recovery ratio for continuum flow
FNUF	η_f	theoretical recovery ratio for free molecule flow
S	$\alpha_r T_t/[1+\alpha_r(T_{awm}-T_R)]$	generated
SS	$\sqrt{\gamma/2}\,M$	generated
TAW	$f_1(ss)$	table
TSBZ	$g_1(ss)$	table
TS	$\tau_s = \eta_s - \eta_m$	generated
VISIN	μ_∞	viscosity based on local static temperature, gm/cm sec
WO	$\omega_o = \tanh \nu_o/\nu_o$	generated
SLP	$[dR_{wm}/dI^2 R_{wm}]_{I=0}$	slope of resistance-power curve at I = 0, $(ma)^{-2}$

DYD	DYD	correction constant for transverse coordinate
RAWM	R_{awm}	wire resistance for zero current, Ω
D		open
F17		open
Y1	Y1	storage for η_m
Y2	Y2	storage for Nu_t
Y3	Y3	storage for M
Y6		open
NX35	NX35	iteration number for PRLCM subroutine
NUCO	Nu_c	Nusselt number for continuum flow
IDXX	IDXX	input integer code (1 or 2) to indicate input location of $(p_t'/p_{o_\infty})_m \times 10^2$
NOP	NOP	number of entires in table of $(p_{t_2}/p_o) \times 10^2$ versus y/D
IQ12	IQ12	hot wire number
Q20		open
NUFM	Nu_f	Nusselt number for free molecule flow
Q17		open
Q18		open
Q19	$Re_t \mu_t \sqrt{T_t}/p_{t_2}$	Mach number function
FNUM	Nu_m	measured Nusselt number
NZ35	NZ35	iteration number for main program
NY35	NY35	iteration number for Mach number program
Q8V	$(p_{t_2}/p_o)_m \times 10^2$	measured local Pitot pressure, normalized to free stream total pressure (table)

B.3b) Typical Input Data for Hot Wire End Loss Program--Static Pressure Version

```
$DATA
  2        1261.1     282.        .001597   24.10      .06489      -.004             16
 .0   .01  .02  .03  .04  .05  .06  .07  .08  .09  .1   .11  .12  .15  .2   .15
 .34  .35  .37  .41  .49  .61  .77 1.01 1.39 1.89 2.36 2.56 2.64 2.74 2.77 2.3
 CO. 1.50 0.003 28.33 0.006042 383.1 0.71901E 02 360.6                       13  12

$END JOB
```

B.3c) Typical Output Data for Hot Wire End Loss Program--Static Pressure Version

```
NN 13              XD   0.1500E 01 YD    0.3000E-02 Z35  5  X35  2   M    0.1924E 01 U    0.5606E 05 RHOU 0.1008E-00 TINF 0.2111E 03
RO   C.3675E 03 PINF 0.6489E-01 PO    0.4510E-00 REO  0.1191E-CC RINF C.184CE-0C PSIR 0.11C2E 01 T*   0.4220E 03 NUO  0.2384E-01
PT   C.341CE-CC N*BR 0.1CC0E C1 KINF  0.1551E 02 PSIB 0.2185E C1 NU   C.1396E 01 NMBR C.4577E-C0 NC   0.9531E 00 NF   0.1148E 01
PSIM C.2639E-C0 NUM  0.9031E-01 NO    0.6337E 00 NM   0.1043E C1 TM   C.3831E 03 NS   C.9813E 00 TS   0.3606E 03 RR   0.2410E 02
ALPA C.1597E-02 N*   0.1148E C1 CYD  -0.4000E-02
```

B.3d) Fortran Listing of Hot Wire End Loss Program--Static Pressure Version

```
$IBFTC MAI     DECK
C                    MAIN PROGRAM
      DIMENSION TBL1(46),TBL1P(46),TBL3(46),TBL3P(46),TBL4(13),
     1 TBL4P(13),TBL5(43),TBL5P(43),TBL6(45),TBL6P(45),TBL6PP(45),
     2 TBL7(91),TBL7P(91),TBL8(40),TBL8P(40),YD(100),Q8V(100)
      DIMENSION Z37(3)
      COMMON Z18,Z19,Z20,Z21,Z22,Z23,Z24,Z25,Z26,Z27,Z28,Z30,Z31,Z32,
     1Z33,Z34,Z35,Z37,C1,C2,C5,C40,C41,C42,Q1,Q2,Q3,Q4,Q5,Q6,Q7,Q8,
     2Q10,Q11,Q12,Q13,Q14,Q15,Q16,Q17,Q18,Q19,Q20,Q9,D,EPS,ETAS,FKQ,
     3FKW,FMUN,FMUQ,FNBR,FNU,FNUC,FNUF,FNUM,FI7,NZ35,SO,SS,TAW,TS,
     4TSBZ,VISIN,WQ,Y1,Y2,Y3,Y6,NX35,NUCQ,RAWM,SLP,DYD
      COMMON /CONST/TBL1,TBL1P,TBL3,TBL3P,TBL4,TBL4P,TBL5,TBL6,TBL6P,
     1 TBL6PP, TBL5P, TBL7, TBL7P, TBL8, TBL8P
   50 READ (5,51) IDXX,Q10,Q14,Q16,Q13,Q9,DYD,NOP
   51 FORMAT (I4,6X6F10.0,3XI3)
      GO TO (310,320),IDXX
  320 READ (5,13) (YD(I),I=1,NOP)
   13 FORMAT (16F5.5)
      READ (5,14) (Q8V(I),I=1,NOP)
   14 FORMAT (16F5.4)
   10 READ (5,12) Q1,Q2,Q3,RAWM,SLP,Q7,IQ12
   12 FORMAT(F3.1,1XF4.2,1XF6.3,1XF5.2,1XF8.6,19XF5.1,19XI3)
      YD1=Q3+DYD
      YD12=YD1*YD1
      YD1=SQRT(YD12)
      CALL TBLKP (YD1,YD,Q8,Q8V,NOP)
      GO TO 330
  310 READ (5,11) Q1, Q2, Q3,RAWM,SLP, Q7, Q8, Q9, IQ12
   11 FORMAT(F3.1,1XF4.2,1XF6.3,1XF5.2,1XF8.6,19XF5.1,  1XF5.4,1XF4.4,
     1 8XI3)
  330 IF (RAWM.EQ.0.) GO TO 50
      Q12 = IQ12
C     SET CONSTANTS AND INITIAL VALUES
      C40 = 2871000.0
      C41 = 1.4
      C42 = 273.2
      Q15 = .000254
      Z18 = 0.1
      Z34=273.2+(RAWM-Q13)/(Q16*Q13)
      Q4=(Q13*Q16)/(3.14159265*Q14*SLP*.0001)
      REAL NUCQ
      NUCQ = 0.5
      FKW = 0.072 + (Z34 - C42)*0.0000077
      Z33 = Q9/Q8
      NO = 91
      CALL TBLKP (Z33,TBL7,Z20,TBL7P,NO)
      Q6 = Q10*Q8/100.
      SS = Z20*SQRT(0.5*C41)
      NO = 45
      CALL TBLKP (SS,TBL6,TAW,TBL6P,NO)
      CALL TBLKP (SS,TBL6,TSBZ,TBL6PP,NO)
      NO1 = 40
      CALL TBLKP (Z20,TBL4,FNUC,TBL4P,NO1)
      FNUF = (TAW/TSBZ) /(1.0 + .5 *(Z20**2.) * (C41-1.0))
C     COMPUTE
      NZ35 = 1
      FMUN=.95
      Z21=Z34/FMUN
      CALL PRLCM
      ETASG=ETAS
      ETASF=(FMUN)*Z30
```

```
      HETAS0=ETASG-ETASF
      FMUN = 2.0
   20 Z21=Z34/FMUN
      CALL PRLCM
      ETASG=ETAS
      ETASF=FMUN*Z30
      HETAS1=ETASG-ETASF
      FMUN1=FMUN+((FMUN1-.95)/(HETAS0-HETAS1))*HETAS1
      NZ35=NZ35+1
      IF (ABS((FMUN-FMUN1)/FMUN1)-.0001) 25,25,30
   25 FMUN=FMUN1
      Z21=Z34/FMUN
      CALL PRLCM
      GO TO 200
   30 IF (NZ35-20) 40,200,200
   40 IF (FMUN1-3.5) 41,200,200
   41 FMUN = FMUN1
      GO TO 20
  200 CALL OUTPUT
      GO TO (310,10), IDXX
      END
```

```
$IBFTC PRL      DECK
       SUBROUTINE PRLCM
       DIMENSION TBL1(46),TBL1P(46),TBL3(46),TBL3P(46),TBL4(13),
      1 TBL4P(13),TBL5(43),TBL5P(43),TBL6(45),TBL6P(45),TBL6PP(45),
      2 TBL7(91),TBL7P(91),TBL8(40),TBL8P(40)
       DIMENSION Z37(3)
       COMMON Z18,Z19,Z20,Z21,Z22,Z23,Z24,Z25,Z26,Z27,Z28,Z30,Z31,Z32,
      1Z33,Z34,Z35,Z37,C1,C2,C5,C40,C41,C42,Q1,Q2,Q3,Q4,Q5,Q6,Q7,Q8,
      2Q10,Q11,Q12,Q13,Q14,Q15,Q16,Q17,Q18,Q19,Q20,Q9,D,EPS,ETAS,FKO,
      3FKW,FMUN,FMUO,FNBR,FNU,FNUC,FNUF,FNUM,FI7,NZ35,SO,SS,TAW,TS,
      4TSBZ,VISIN,WO,Y1,Y2,Y3,Y6,NX35,NUCO,RAWM,SLP
       COMMON /CONST/TBL1,TBL1P,TBL3,TBL3P,TBL4,TBL4P,TBL5,TBL6,TBL6P,
      1 TBL6PP, TBL5P, TBL7, TBL7P, TBL8, TBL8P
       NO = 46
       CALL TBLKP(Z21,TBL1,FKO,TBL1P,NO)
       FKO=FKO*(0.00001)
       Q11 = Q7 / Z21
       NO1=46
       CALL TBLKP(Z21,TBL3,FMUO,TBL3P,NO1)
       FMUO=FMUO*(0.0000001)
       Z24=Z21/(1.0+0.5*(C41-1.0)*(Z20**2))
       CALL TBLKP(Z24,TBL3,VISIN,TBL3P,NO1)
       VISIN=VISIN*(0.0000001)
       IF (Z20-1.) 10,11,11
   10  Z25=((.3386*Q6)/(FMUO*SQRT((C41+1.)*C40*Z21/(2.*C41))))*(((C41
      1+1.)*Z20*Z20/2.)**.5)*(1./((1.+(C41-1.)*Z20*Z20/2.)**((C41+1.)/
      2(2.*(C41-1.)))))
       GO TO 12
   11  Z25=((.3386*Q6)/(FMUO*SQRT((C41+1.)*C40*Z21/(2.*C41))))*(1./((C41
      1+1.)*Z20*Z20/2.)**((C41+1.)/(2.*(C41-1.))))*(((2.*C41*Z20*Z20-C41
      2+1.)/(C41+1.))**(1./(C41-1.)))*((1.+(C41-1.)*Z20*Z20/2.)**.5)
   12  Z28=(VISIN*Z20/(Z25*FMUO))*SQRT(0.5*C41*3.1415927)
       REAL NUCO
       REAL NUFM
       REAL NUC1
       NX35 = 1
   13  IF (NX35-20) 15,15,14
   14  NZ35 = 20
       GO TO 990
   15  FRNU = -Z25+1.45*(NUCO**(.128*((2.-NUCO)**4.)+2.67))
       DFRN= Z25*((.128*((2.-NUCO)**4.)+2.67)/NUCO-.512*
      1((2.-NUCO)**3.)*ALOG(NUCO))
       NUC1=NUCO-FRNU/DFRN
       NX35=NX35+1
       IF (ABS((NUC1-NUCO)/NUC1)-.0001) 30,30,20
   20  NUCO=NUC1
       GO TO 13
   30  NUCO=NUC1
       NUFM=.01796*(TSBZ/SS)*Z25
       Z18 = NUCO/(1.+(NUCO/NUFM))
       FNU = SQRT((Q14**2.)*(FKO/FKW)*Z18)
       WO =(EXP(2.0*FNU)-1.0)/(FNU*(EXP(FNU*2.0)+1.0))
       NO1=43
       CALL TBLKP(Z28,TBL5,Z19,TBL5P,NO1)
       Z31 = 1.0 + WO * (1.0+(FNUC-Q11) / (FMUN-FNUC)) /(1.-WO)
       ETAS=Z19*(FNUF-FNUC) + FNUC
       Z30=(1.-(Q7*WO/Z34))/(1.-WO)
  990  RETURN
       END
```

```
$IBFTC OUT      DECK
      SUBROUTINE OUTPUT
      DIMENSION TBL1(46),TBL1P(46),TBL3(46),TBL3P(46),TBL4(13),
     1 TBL4P(13),TBL5(43),TBL5P(43),TBL6(45),TBL6P(45),TBL6PP(45),
     2 TBL7(91),TBL7P(91),TBL8(40),TBL8P(40)
      DIMENSION Z37(3)
      COMMON Z18,Z19,Z20,Z21,Z22,Z23,Z24,Z25,Z26,Z27,Z28,Z30,Z31,Z32,
     1Z33,Z34,Z35,Z37,C1,C2,C5,C40,C41,C42,Q1,Q2,Q3,Q4,Q5,Q6,Q7,Q8,
     2Q10,Q11,Q12,Q13,Q14,Q15,Q16,Q17,Q18,Q19,Q20,Q9,D,EPS,ETAS,FKO,
     3FKW,FMUN,FMUO,FNBR,FNU,FNUC,FNUF,FNUM,FI7,NZ35,SO,SS,TAW,TS,
     4TSBZ,VISIN,WO,Y1,Y2,Y3,Y6,NX35,NUCO,RAWM,SLP,DYD
      COMMON /CONST/TBL1,TBL1P,TBL3,TBL3P,TBL4,TBL4P,TBL5,TBL6,TBL6P,
     1 TBL6PP, TBL5P, TBL7, TBL7P, TBL8, TBL8P
      Z23=Z20*SQRT(C41*C40*Z24)
      Z22 = Z25 * FMUO / Q15
      Z26=Z25*FMUO/VISIN
      Z27=Z21*(FNUC+(FNUF-FNUC)*Z19)
      Z30=(1.0-WO*(Q11/FMUN))/(1.0-WO)
      Z99 = Q9
      FNUM = (Q4/(FKO*4.187*2.54)) * 1.0E-6
      Z32=Z18/FNUM
      FNBR=Z19/Z31
      IF(Z20-1.0) 31,31,32
   31 Z98 = Q8
      GO TO 40
   32 Z98 = Q8 /((6.0*Z20*Z20/(Z20*Z20+5.0))*(36.0*Z20*Z20/((Z20*Z20
     1 + 5.0)*(7.0*Z20*Z20-1.0)))**2.5 )
   40 ID = Q12 + .01
      WRITE (6,500) ID,Q2,Q3, NZ35,                NX35,Z20,Z23,Z22,
     1 Z24,Z21,Z99,Z98,Z25,Z26,Z30,Z27,Z18,Q8 ,Z19,Z28,Z31,FNU,FNBR,
     2 FNUC,FNUF,Z32,FNUM,WO,FMUN,Z34,Q11,Q7,     Q13,Q16,ETAS,DYD
  500 FORMAT(2HHWI3,11X4HXD  E11.4,1X4HYD  E11.4,1X4HZ35 I2,2X4HX35 I2,
     1 2X4HM   E11.4,1X4HU   E11.4,1X4HRHQUE11.4,1X4HTINFE11.4/,
     24HTO  E11.4,1X4HPINFE11.4,1X4HPO  E11.4,1X4HREO E11.4,
     31X4HRINFE11.4,1X4HPSIRE11.4,1X4HT*  E11.4,1X4HNUO E11.4/,
     44HPT  E11.4,1X4HN*BRE11.4,1X4HKINFE11.4,1X4HPSIBE11.4,
     51X4HNU  E11.4,1X4HNMBRE11.4,1X4HNC  E11.4,1X4HNF  E11.4/,
     64HPSINE11.4,1X4HNUM E11.4,1X4HWO  E11.4,1X4HNM  E11.4,
     71X4HTM  E11.4,1X4HNS  E11.4,1X4HTS  E11.4,1X4HRR  E11.4/,
     84HALPAE11.4,1X4HN*  E11.4,1X4HDYD E11.4//)
      RETURN
      END
```

```
$IBFTC BLO     DECK
       BLOCK DATA
       DIMENSION TBL1(46),TBL1P(46),TBL3(46),TBL3P(46),TBL4(13),
      1 TBL4P(13),TBL5(43),TBL5P(43),TBL6(45),TBL6P(45),TBL6PP(45),
      2 TBL7(91),TBL7P(91),TBL8(40),TBL8P(40)
       DIMENSION Z37(3)
       COMMON /CONST/TBL1,TBL1P,TBL3,TBL3P,TBL4,TBL4P,TBL5,TBL6,TBL6P,
      1 TBL6PP, TBL5P, TBL7, TBL7P, TBL8, TBL8P
       DATA (TBL1(I),I = 1,41)/     30.,40.,50.,60.,70.,80.,90.,100.,110.
      1 ,120.,130.,140.,150.,160.,170.,180.,190.,200.,210.,220.,230.,240.
      2 ,250.,260.,270.,280.,290.,300.,310.,320.,330.,340.,350.,360.,370.
      3 ,380.,390.,400.,410.,420.,430./
       DATA (TBL1(I),I = 42,46)/440.,450.,460.,470.,480./
       DATA (TBL1P(I),I = 1,41)/    0.7039,0.9117,1.131,1.350,1.558,1.784
      1 ,1.996,2.210,2.425,2.640,2.855,3.068,3.281,3.492,3.703,3.912,4.11
      2 9,4.324,4.527,4.729,4.929,5.127,5.323,5.517,5.709,5.897,6.087,6.2
      3 72,6.457,6.641,6.820,6.999,7.178,7.357,7.530,7.703,7.876,8.043,8.
      4 211,8.378,8.545/
       DATA (TBL1P(I),I = 42,46)/8.706,8.868,9.030,9.192,9.347/
       DATA (TBL3(I),I = 1,46)/     30.,40.,50.,60.,70.,80.,90.,100.,110.
      1 ,120.,130.,140.,150.,160.,170.,180.,190.,200.,210.,220.,230.,240.
      2 ,250.,260.,270.,280.,290.,300.,310.,320.,330.,340.,350.,360.,370.
      3 ,380.,390.,400.,410.,420.,430.,440.,450.,460.,470.,480./
       DATA (TBL3P(I),I = 1,46)/    215.7,281.1,347.3,416.3,485.6,555.1,6
      1 22.9,692.9,763.3,831.9,899.0,964.6,1029.,1091.,1152.,1212.,1271.,
      2 1329.,1385.,1440.,1494.,1547.,1599.,1650.,1700.,1750.,1798.,1846.
      3 ,1893.,1939.,1985.,2030.,2075.,2118.,2160.,2202.,2245.,2286.,2327
      4 .,2366.,2406.,2445.,2485.,2520.,2560.,2595./
       DATA (TBL4(I),I = 1,13)/     0.,0.2,0.4,0.6,0.8,1.0,1.2,1.4,1.6,1.
      1 8,2.0,2.2,8.0/
       DATA (TBL4P(I),I = 1,13)/    1.0,0.998,0.995,0.991,0.985,0.977,0.9
      1 70,0.964,0.959,0.955,0.952,0.950,0.950/
       DATA (TBL5(I),I = 1,43)/     0.05,0.06,0.07,0.08,0.09,0.10,0.11,0.
      1 12,0.14,0.15,0.17,0.19,0.20,0.23,0.25,0.30,0.35,0.40,0.50,0.60,0.
      2 70,0.80,0.90,1.0,1.1,1.2,1.3,1.4,1.5,1.7,1.9,2.0,2.5,3.0,3.5,4.0,
      3 5.0,6.0,7.0,8.0,10.0,12.0,20./
       DATA (TBL5P(I),I = 1,43)/    0.02,0.03,0.042,0.054,0.068,0.082,0.0
      1 97,0.112,0.144,0.158,0.188,0.218,0.232,0.272,0.294,0.350,0.397,0.
      2 437,0.505,0.558,0.603,0.640,0.672,0.700,0.724,0.744,0.765,0.783,0
      3 .800,0.826,0.849,0.858,0.895,0.916,0.932,0.944,0.960,0.970,0.977,
      4 0.982,0.990,1.0,1.0/
       DATA (TBL6(I),I = 1,45)/     0.2,0.4,0.6,0.8,1.0,1.2,1.4,1.6,1.8,2
      1 .0,2.2,2.4,2.6,2.8,3.0,3.2,3.4,3.6,3.8,4.0,4.2,4.4,4.6,4.8,5.0,5.
      2 2,5.4,5.6,5.8,6.0,6.2,6.4,6.6,6.8,7.0,7.2,7.4,7.6,7.8,8.0,8.2,
      38.4,8.6,8.8,9.0/
       DATA (TBL6P(I),I = 1,45)/    9.80271,10.94784,12.89399,15.69746,19
      1 .43609,24.20781,30.12863,37.32923,45.95230,56.14932,68.07771,81.8
      2 9947,97.77902,115.88287,136.37821,159.43361,185.21769,213.89927,2
      3 45.64801,280.63340,319.02474,360.99204,406.70528,456.33364,510.04
      4 756,568.01730,630.41182,697.40229,769.31,845.89,927.63,
      5 1014.61,1107.11,1205.2,1309.1,1418.8,1534.7,1656.7,1785.2,
      6 1920.4,2062.2,2210.9,2367.0,2530.2,2700.7/
       DATA (TBL6PP(I),I = 1,45)/   9.61234,10.16410,11.04924,12.22282,13
      1 .63288,15.22758,16.96068,18.79408,20.69872,22.65358,24.64392,26.6
      2 5990,28.69470,30.74382,32.80398,34.87300,36.94914,39.03112,41.118
      3 00,43.20904,45.30354,47.40108,49.50126,51.60366,53.70808,55.81428
      4 ,57.92200,60.03114,62.141,64.248,66.359,68.467,70.580,72.692,
      5 74.802,76.910,79.025,81.130,83.242,85.352,87.461,89.561,91.676,
      6 93.782,95.886/
       DATA(TBL7P(I),I = 1,91)/ 8.0,7.95,7.90,7.85,7.80,7.75,7.70,7.65,
      1 7.60,7.55,7.5,7.4,7.3,7.2,7.1,7.0,6.9,6.8,6.7,6.6,6.5,6.4,6.3,
```

```
     2 6.2,6.1,6.0,5.9,5.8,5.7,5.6,5.5,5.4,5.3,5.2,5.1,5.0,4.9,4.8,4.7,
     3 4.6,4.5,4.4,4.3,4.2,4.1,4.0,3.9,3.8,3.7,3.6,3.5,3.4,3.3,3.2,3.1,
     4 3.0,2.9,2.8,2.7,2.6,2.5,2.4,2.3,2.2,2.1,2.0,1.9,1.8,1.7,1.6,1.5,
     5 1.4,1.3,1.2,1.1,1.0,.9,.8,.7,.6,.5,.4,.35,.3,.25,.2,.15,.1,.05,
     6 .03,.0 /
      DATA (TBL7(I),I = 1,91)/.01207, .01222,.01237,.01253,.01269,
     1 .01285,.01302,.01319,.01336,.01354,.01372,.01409,.01448,.01488,
     2 .01530,.01574,.01619,.01667,.01716,.01768,.01823,.01880,.01939,
     3 .02002,.02067,.02136,.02208,.02284,.02364,.02449,.02537,.02631,
     4 .02730,.02834,.02945,.03062,.03187,.03319,.03459,.03609,.03768,
     5 .03938,.04120,.04314,.04523,.04747,.04987,.05247,.05526,.05829,
     6 .06157,.06513,.06900,.07323,.07785,.08291,.08848,.09461,.1014,
     7 .1089,.1173,.1266,.1371,.1489,.1622,.1773,.1945,.2142,.2368,
     8 .2628,.2930,.3280,.3685,.4159,.4689,.5283,.5913,.6560,.7209,
     9 .7640,.8430,.8956,.9183,.9395,.9575,.9725,.9844,.9930,.9983,
     1 .9994,1.0/
       END
```

```
$IBFTC TBL      DECK
       SUBROUTINE TBLKP(VO,VAR,FO,FCN,NO)
       DIMENSION VAR(100),FCN(100)
C              THIS SUBROUTINE PERFORMS TABLE LOOK-UP OPERATIONS.
       DO 100 I=1,NO
       VAR1=VAR(I)
       IF (VO-VAR1) 200,150,100
  100  CONTINUE
       WRITE (6,900)VO,NO
  900  FORMAT (34H VARIABLE EXCEEDS TABLE FOR VALUE E11.4,13H TABLE SIZE
      1=I5)
       FO =FCN(NO)
       GO TO 300
  150  FO=FCN(I)
       GO TO 300
  200  IF (I-1) 210,290,210
  210  I1=I-1
       TEMP=VO-VAR(I1)
       TEM1=VAR(I)-VAR(I1)
       RATIO=TEMP/TEM1
       FO=RATIO*(FCN(I)-FCN(I1))+FCN(I1)
       GO TO 300
  290  FO=FCN(I)
  300  RETURN
       END
```

B.4 Hot Wire End Loss Program--Nusselt Number Version

As Dewey (17) and Herzog (14) have already indicated, considerable difficulty was experienced in the initial set up and check out of this extensive end loss program. This difficulty arose because the method of successive substitution was used to compute local Mach numbers from Pitot pressures and Reynolds numbers, and this computation procedure did not always converge. It was therefore necessary to establish a double iteration procedure based on Newton's method to calculate simultaneously end loss corrections both for adiabatic wire temperature and Nusselt number. The input data for this program consist of Pitot pressures, adiabatic wire resistances, probe support temperatures, measured slopes of wire resistance-power curve corresponding to zero power (dR/dI^2R), and wire calibration data including Nusselt number correction factors (Appendix A) determined with the aid of the previous program. Input values of R_{awm}, T_s and dR/dI^2R are obtained directly from the punched card output of the raw data program. Pitot pressure input data at a given axial location consist of tabulated semiprofiles of pressures, and values corresponding to specific probe positions are determined by interpolation. Starting with initial trial values for stagnation temperature and Nusselt number, the computation is cycled until a convergence criterion is met. In most cases satisfactory convergence takes place within 5 to 6 iterations.

B.4a) Typical Input Data for Hot Wire End Loss Program--Nusselt Number Version

```
$DATA
  2        1261.1     282.       .001597    24.10                          -.004          16
.900 .852 .800 .720 .650 .565 .495 .440 .390 .345 .295 .250 .205 .165 .13  .11
.1   .05  .0
.0   .01  .02  .03  .04  .05  .06  .07  .08  .09  .1   .11  .12  .15  .2   .15
.34  .35  .37  .41  .49  .61  .77  1.01 1.39 1.88 2.36 2.56 2.64 2.74 2.77 2.8
0.   1.50  0.003 28.33 0.006042 383.1 0.71901E 02 360.6                   13  12

$END JOB
```

B.4b) Typical Output Data for Hot Wire End Loss Program--Nusselt Number Version

```
[illegible] 13          XD   0.1500E 01 YD   0.3000E-02 Z35  8  Y35  1  M    0.1897E 01 U    0.5539E 05 RHOU 0.1014E-00 TINF 0.2136E 03
[illegible]  C.3674E 03 PINF 0.6650E-03 PO   0.4436E-02 REO  0.1199E-00 RINF 0.1834E-00 PSIR 0.1101E 01 T*   0.4217E 03 MUO  0.2405E-01
[illegible]T C.341CE-02 N*BR 0.1CC0E 01 KINF 0.1534E 02 PSIB C.2179E C1 NU   C.14C2E 01 NNBR 0.4589E-C0 NC   0.9535E C0 NF   0.1148E 01
[illegible]SIA C.2663E-CC NLP 0.9C32E-C1 hC  0.6318E C0 NM   C.1043E C1 TM   C.3831E 03 AS   C.9814E 00 TS   0.3606E 03 RR   0.2410E 02
[illegible]LPA C.1597E-02 N*  0.1148E 01 DYD -0.4000E-02 RAWM 0.2833E C2 SLP  C.6042E-02
```

B.4c) Fortran Listing of Hot Wire End Loss Program--Nusselt Number Version

```
$IBFTC MAI      DECK
       DIMENSION TBL1(46),TBL1P(46),TBL3(46),TBL3P(46),TBL4(13),TBL4P(13)
      1,TBL5(43),TBL5P(43),TBL6(45),TBL6P(45),TBL6PP(45),TBL7(19),TBL7P
      2(19),YD(100),Q8V(100)
       DIMENSION Z37(3)
       COMMON Z18,Z19,Z20,Z21,Z22,Z23,Z24,Z25,Z26,Z27,Z28,Z30,Z31,Z32,
      1Z33,Z34,Z35,Z37,C1,C2,C5,C40,C41,C42,Q1,Q2,Q3,Q4,Q5,Q6,Q7,Q8,
      2Q10,Q11,Q12,Q13,Q14,Q15,Q16,Q17,Q18,Q19,Q20,Q9,D,EPS,ETAS,FKO,
      3FKW,FMUN,FMUO,FNBR,FNU,FNUC,FNUF,FNUM,FI7,NZ35,SO,SS,TAW,TS,
      4TSBZ,VISIN,WO,Y1,Y2,Y3,Y6,NY35,NUCO,RAWM,SLP,DYD
       COMMON /CONST/TBL1,TBL1P,TBL3,TBL3P,TBL4,TBL4P,TBL5,TBL6,TBL6P,
       1 TBL6PP,TBL5P,TBL7,TBL7P
C              MAIN PROGRAM
    50 READ (5,51) IDXX,Q10,Q14,Q16,Q13,Q9,DYD,NOP
    51 FORMAT (I4,6X6F10.0,3XI3)
       READ (5,500) TBL7P
   500 FORMAT (16F5.2)
       GO TO (310,320),IDXX
   320 READ (5,13) (YD(I),I=1,NOP)
    13 FORMAT (16F5.5)
       READ (5,14) (Q8V(I),I=1,NOP)
    14 FORMAT (16F5.4)
    10 READ (5,12) Q1,Q2,Q3,RAWM,SLP,Q7,IQ12
    12 FORMAT(F3.1,1XF4.2,1XF6.3,1XF5.2,1XF8.6,19XF5.1,19XI3)
       YD1=Q3+DYD
       YD12=YD1*YD1
       YD1=SQRT(YD12)
       CALL TBLKP (YD1,YD,Q8,Q8V,NOP)
       GO TO 330
   310 READ (5,11) Q1, Q2, Q3,RAWM,SLP, Q7, Q8, Q9, IQ12
    11 FORMAT(F3.1,1XF4.2,1XF6.3,1XF5.2,1XF8.6,19XF5.1,  1XF5.4,1XF4.4,
      1 8XI3)
   330 IF (RAWM.EQ.0.) GO TO 50
       Q12 = IQ12
       NZ35=1
    20 CALL FSTCM
    30 CALL PRLCM
       CALL M22
    80 IF (ABS((Z20-Y3)/Z20)-.01) 150,150,100
   100 IF (NZ35-20) 120,200,200
   120 NZ35=NZ35+1
       CALL ADDCM
       GO TO 30
   150 IF (ABS((FMUN-Y1)/FMUN)-.0005) 170,100,100
   170 IF (ABS((Z18-Y2)/Z18)-.0005) 200,200,100
   200 Q19 = Z25*FMUO*SQRT(Z21)/Q6
       IF (Q19-.0000855) 201,201,202
   201 Q19=.0000855
       Z20=7.0
       SS = Z20*SQRT(0.5*C41)
       NO = 45
       CALL TBLKP (SS,TBL6,TAW,TBL6P,NO)
       CALL TBLKP (SS,TBL6,TSBZ,TBL6PP,NO)
       NO1 = 40
       CALL TBLKP (Z20,TBL4,FNUC,TBL4P,NO1)
       FNUF = (TAW/TSBZ) /(1.0 + .5 *(Z20**2.) * (C41-1.0))
C      COMPUTE
       NZ35 = 1
       FMUN=.95
       Z21=Z34/FMUN
       CALL PRLCM
```

```
      ETASG=ETAS
      ETASF=(FMUN)*Z30
      HETAS0=ETASG-ETASF
      FMUN = 2.0
  220 Z21=Z34/FMUN
      CALL PRLCM
      ETASG=ETAS
      ETASF=FMUN*Z30
      HETAS1=ETASG-ETASF
      FMUN1=FMUN+((FMUN1-.95)/(HETAS0-HETAS1))*HETAS1
      NZ35=NZ35+1
      IF (ABS((FMUN-FMUN1)/FMUN1)-.0001) 225,225,230
  225 FMUN=FMUN1
      Z21=Z34/FMUN
      CALL PRLCM
      GO TO 202
  230 IF (NZ35-20) 240,202,202
  240 IF (FMUN1-3.5) 241,202,202
  241 FMUN = FMUN1
      GO TO 220
  202 CALL OUTPUT
      GO TO (310,10), IDXX
      END
```

```
$IBFTC FST      DECK
      SUBROUTINE FSTCM
      DIMENSION TBL1(46),TBL1P(46),TBL3(46),TBL3P(46),TBL4(13),TBL4P(13)
     1,TBL5(43),TBL5P(43),TBL6(45),TBL6P(45),TBL6PP(45),TBL7(19),TBL7P
     2(19)
      DIMENSION Z37(3)
      COMMON Z18,Z19,Z20,Z21,Z22,Z23,Z24,Z25,Z26,Z27,Z28,Z30,Z31,Z32,
     1Z33,Z34,Z35,Z37,C1,C2,C5,C40,C41,C42,Q1,Q2,Q3,Q4,Q5,Q6,Q7,Q8,
     2Q10,Q11,Q12,Q13,Q14,Q15,Q16,Q17,Q18,Q19,Q20,Q9,D,EPS,ETAS,FKO,
     3FKW,FMUN,FMUO,FNBR,FNU,FNUC,FNUF,FNUM,FI7,NZ35,SO,SS,TAW,TS,
     4ISBZ,VISIN,WO,Y1,Y2,Y3,Y6,NY35,NUCO,RAWM,SLP
      COMMON /CONST/TBL1,TBL1P,TBL3,TBL3P,TBL4,TBL4P,TBL5,TBL6,TBL6P,
     1 TBL6PP,TBL5P,TBL7,TBL7P
C                              SET CONSTANTS
      REAL NUCO
      C1=0.072
      C2=0.0000077
      C5=1.025
      C40=2871000.0
      C41=1.4
      C42=273.0
      Q15 = .000254
C                              SET INITIAL VALUES
      EPS=0.06
      FNU = 1.5
      FMUN = 1.025
      NZ35=1
      Y1=C5
      SO=0.5
      Y3 = 2.
      Z20 = 2.
      NUCO = .5
      Q19 = 0.0
C                              COMPUTE
      Z34=273.2+(RAWM-Q13)/(Q16*Q13)
      Q4=(Q13*Q16)/(3.14159265*Q14*SLP*.0001)
      FKW=C1+(Z34-C42)*C2
      Z21=Z34/FMUN
      NO=46
      CALL TBLKP(Z21,TBL1,FKO,TBL1P,NO)
      FKO=FKO*(0.00001)
      FNUM = (Q4/(FKO*4.187*2.54)) * 1.0E-6
      Q6 = Q10 * Q8 / 100.
      Q11 = Q7 / Z21
      TS = (Q7-Z34) / Z21
      CALL BSIT
      NO1=46
      CALL TBLKP(Z21,TBL3,FMUO,TBL3P,NO1)
      FMUO=FMUO*(0.0000001)
      RETURN
      END
```

```
$IBFTC PRL      DECK
       SUBROUTINE PRLCM
       DIMENSION TBL1(46),TBL1P(46),TBL3(46),TBL3P(46),TBL4(13),TBL4P(13)
      1,TBL5(43),TBL5P(43),TBL6(45),TBL6P(45),TBL6PP(45),TBL7(19),TBL7P
      2(19)
       DIMENSION Z37(3)
       COMMON Z18,Z19,Z20,Z21,Z22,Z23,Z24,Z25,Z26,Z27,Z28,Z30,Z31,Z32,
      1Z33,Z34,Z35,Z37,C1,C2,C5,C40,C41,C42,Q1,Q2,Q3,Q4,Q5,Q6,Q7,Q8,
      2Q10,Q11,Q12,Q13,Q14,Q15,Q16,Q17,Q18,Q19,Q20,Q9,D,EPS,ETAS,FKO,
      3FKW,FMUN,FMUO,FNBR,FNU,FNUC,FNUF,FNUM,FI7,NZ35,SO,SS,TAW,TS,
      4TSBZ,VISIN,WO,Y1,Y2,Y3,Y6,NY35,NUCO,RAWM,SLP
       COMMON /CONST/TBL1,TBL1P,TBL3,TBL3P,TBL4,TBL4P,TBL5,TBL6,TBL6P,
      1 TBL6PP,TBL5P,TBL7,TBL7P
       IF (ABS((Q19-.0000855)/.0000855)-.000001) 10,10,11
   11 WO =(EXP(2.0*FNU)-1.0)/(FNU*(EXP(FNU*2.0)+1.0))
       TS = (Q7-Z34) / Z21
       SO=(Q16*Z21)/(1.0+Q16*(Z34-C42))
       NO1 = 19
       CALL TBLKP(WO,TBL7,Z32,TBL7P,NO1)
       Z18=Z32*FNUM
       FNU=SQRT(Q14*Q14*Z18*FKO/FKW)
       WO =(EXP(2.0*FNU)-1.0)/(FNU*(EXP(FNU*2.0)+1.0))
       NO1=46
       CALL TBLKP(Z21,TBL3,FMUO,TBL3P,NO1)
       FMUO=FMUO*(0.0000001)
       Z24=Z21/(1.0+0.5*(C41-1.0)*(Z20**2))
       CALL TBLKP(Z24,TBL3,VISIN,TBL3P,NO1)
       VISIN=VISIN*(0.0000001)
       CALL NUOREO
       Z28=(VISIN*Z20/(Z25*FMUO))*SQRT(0.5*C41*3.1415927)
       NO1 = 43
       CALL TBLKP(Z28,TBL5,Z19,TBL5P,NO1)
       NO1 = 13
       CALL TBLKP (Z20,TBL4,FNUC,TBL4P,NO1)
       Z31=1.0+WO*(1.0+(FNUC-Q11)/(Y1-FNUC))/(1.0-WO)
       SS=Z20*SQRT(0.5*C41)
       NO = 45
       CALL TBLKP(SS,TBL6,TAW,TBL6P,NO)
       CALL TBLKP(SS,TBL6,TSBZ,TBL6PP,NO)
       FNUF=(TAW/TSBZ)/(1.0+.5*(Z20**2)*(C41-1.0))
       ETAS=Z19*(FNUF-FNUC)+FNUC
       Z30=(1.-(Q7*WO/Z34))/(1.-WO)
       FMUN=ETAS/Z30
       FNBR=Z19/Z31
       GO TO 50
   10 NO = 46
       CALL TBLKP(Z21,TBL1,FKO,TBL1P,NO)
       FKO=FKO*(0.00001)
       Q11 = Q7 / Z21
       NO1=46
       CALL TBLKP(Z21,TBL3,FMUO,TBL3P,NO1)
       FMUO=FMUO*(0.0000001)
       Z24=Z21/(1.0+0.5*(C41-1.0)*(Z20**2))
       CALL TBLKP(Z24,TBL3,VISIN,TBL3P,NO1)
       VISIN=VISIN*(0.0000001)
       Z25 = Q19*Q6/(FMUO*SQRT(Z21))
   12 Z28=(VISIN*Z20/(Z25*FMUO))*SQRT(0.5*C41*3.1415927)
       REAL NUCO
       REAL NUFM
       REAL NUC1
       NX35 = 1
```

```
   13 IF (NX35-20) 15,15,14
   14 NZ35 = 20
      GO TO 50
   15 FRNU = -Z25+1.45*(NUCO**(.128*((2.-NUCO)**4.)+2.67))
      DFRN= Z25*((.128*((2.-NUCO)**4.)+2.67)/NUCO-.512*
     1((2.-NUCO)**3.)*ALOG(NUCO))
      NUC1=NUCO-FRNU/DFRN
      NX35=NX35+1
      IF (ABS((NUC1-NUCO)/NUC1)-.0001) 30,30,20
   20 NUCO=NUC1
      GO TO 13
   30 NUCO=NUC1
      NUFM=.01796*(TSBZ/SS)*Z25
      Z18 = NUCO/(1.+(NUCO/NUFM))
      FNU = SQRT((Q14**2.)*(FKO/FKW)*Z18)
      WO =(EXP(2.0*FNU)-1.0)/(FNU*(EXP(FNU*2.0)+1.0))
      NO1=43
      CALL TBLKP(Z28,TBL5,Z19,TBL5P,NO1)
      Z31 = 1.0 + WO * (1.0+(FNUC-Q11) / (FMUN-FNUC)) /(1.-WO)
      ETAS=Z19*(FNUF-FNUC) + FNUC
      Z30=(1.-(Q7*WO/Z34))/(1.-WO)
   50 RETURN
      END
```

```
$IBFTC OUT     DECK
      SUBROUTINE OUTPUT
      DIMENSION TBL1(46),TBL1P(46),TBL3(46),TBL3P(46),TBL4(13),TBL4P(13)
     1,TBL5(43),TBL5P(43),TBL6(45),TBL6P(45),TBL6PP(45),TBL7(19),TBL7P
     2(19)
      DIMENSION Z37(3)
      COMMON Z18,Z19,Z20,Z21,Z22,Z23,Z24,Z25,Z26,Z27,Z28,Z30,Z31,Z32,
     1Z33,Z34,Z35,Z37,C1,C2,C5,C40,C41,C42,Q1,Q2,Q3,Q4,Q5,Q6,Q7,Q8,
     2Q10,Q11,Q12,Q13,Q14,Q15,Q16,Q17,Q18,Q19,Q20,Q9,D,EPS,ETAS,FKO,
     3FKW,FMUN,FMUO,FNBR,FNU,FNUC,FNUF,FNUM,FI7,NZ35,SO,SS,TAW,TS,
     4TSBZ,VISIN,WO,Y1,Y2,Y3,Y6,NY35,NUCO,RAWM,SLP,DYD
      COMMON /CONST/TBL1,TBL1P,TBL3,TBL3P,TBL4,TBL4P,TBL5,TBL6,TBL6P,
     1 TBL6PP,TBL5P,TBL7,TBL7P
      IF (ABS((Q19-.0000855)/.0000855)-.000001) 10,10,20
   20 CALL ADDCM
      CALL PRLCM
      CALL M22
   10 Z21 = Z34/FMUN
      Z22 = Z25 * FMUO / Q15
      Q20=Q6*(((7.*Z20*Z20-1.)/(6.*Z20*Z20))**2.5)* 491.67
      Z23 = 2.*Q20/Z22
      Z26=Z25*FMUO/VISIN
      Z27=Z21*(FNUC+(FNUF-FNUC)*Z19)
      Z30=(1.0-WO*(Q11/FMUN))/(1.0-WO)
   40 IF (Z20-1.0) 41,41,42
   41 Z99 = (Q6/Q10)/
     1     (1.0+.5*(C41-1.0)*Z20*Z20)**(C41/(C41-1.0))
      Z98 = Q6/Q10
      GO TO 50
   42 Z99=((.5*(C41+1.0)*Z20*Z20)**(C41/(C41-1.0))*((C41+1.0)/(2.0*C41*Z
     120*Z20-C41+1.0))**(1.0/(C41-1.0)))**(-1.0)*Q6/Q10
      Q8 = Q8/100.0
      Z98 = Q8 /((6.0*Z20*Z20/(Z20*Z20+5.0))*(36.0*Z20*Z20/((Z20*Z20
     1 + 5.0)*(7.0*Z20*Z20-1.0)))**2.5 )
   50 ID = Q12 + .01
      WRITE (6,500) ID,Q2,Q3, NZ35,                NY35,Z20,Z23,Z22,
     1 Z24,Z21,Z99,Z98,Z25,Z26,Z30,Z27,Z18,Q8 ,Z19,Z28,Z31,FNU,FNBR,
     2 FNUC,FNUF,Z32,FNUM,WO,FMUN,Z34,Q11,Q7,     Q13,Q16,ETAS,DYD,
     3RAWM,SLP
  500 FORMAT(2HHWI3,11X4HXD  E11.4,1X4HYD  E11.4,1X4HZ35 I2,2X4HY35 I2,
     1 2X4HM   E11.4,1X4HU   E11.4,1X4HRHOUE11.4,1X4HTINFE11.4/,
     24HTO  E11.4,1X4HPINFE11.4,1X4HPO  E11.4,1X4HREO E11.4,
     31X4HRINFE11.4,1X4HPSIRE11.4,1X4HT*  E11.4,1X4HNUO E11.4/,
     44HPT  E11.4,1X4HN*BRE11.4,1X4HKINFE11.4,1X4HPSIBE11.4,
     51X4HNU  E11.4,1X4HNMBRE11.4,1X4HNC  E11.4,1X4HNF  E11.4/,
     64HPSINE11.4,1X4HNUM E11.4,1X4HWO  E11.4,1X4HNM  E11.4,
     71X4HTM  E11.4,1X4HNS  E11.4,1X4HTS  E11.4,1X4HRR  E11.4/,
     84HALPAE11.4,1X4HN*  E11.4,1X4HDYD E11.4,1X4HRAWME11.4,
     91X4HSLP E11.4//)
      RETURN
      END
```

```
$IBFTC ADD    DECK
       SUBROUTINE ADDCM
       DIMENSION TBL1(46),TBL1P(46),TBL3(46),TBL3P(46),TBL4(13),TBL4P(13)
      1,TBL5(43),TBL5P(43),TBL6(45),TBL6P(45),TBL6PP(45),TBL7(19),TBL7P
      2(19)
       DIMENSION Z37(3)
       COMMON Z18,Z19,Z20,Z21,Z22,Z23,Z24,Z25,Z26,Z27,Z28,Z30,Z31,Z32,
      1Z33,Z34,Z35,Z37,C1,C2,C5,C40,C41,C42,Q1,Q2,Q3,Q4,Q5,Q6,Q7,Q8,
      2Q10,Q11,Q12,Q13,Q14,Q15,Q16,Q17,Q18,Q19,Q20,Q9,D,EPS,ETAS,FKO,
      3FKW,FMUN,FMUO,FNBR,FNU,FNUC,FNUF,FNUM,FI7,NZ35,SO,SS,TAW,TS,
      4ISBZ,VISIN,WQ,Y1,Y2,Y3,Y6,NY35,NUCO,RAWM,SLP
       COMMON /CONST/TBL1,TBL1P,TBL3,TBL3P,TBL4,TBL4P,TBL5,TBL6,TBL6P,
      1 TBL6PP,TBL5P,TBL7,TBL7P
       Z21=Z34/FMUN
       NO=46
       CALL TBLKP(Z21,TBL1,FKO,TBL1P,NO)
       FKO=FKO*(0.00001)
       FNUM = (Q4/(FKO*4.187*2.54)) * 1.0E-6
       Z27=Z21*(FNUC+(FNUF-FNUC)*Z19)
       Q11 = Q7 / Z21
       Z30=(1.0-WQ*(Q11/FMUN))/(1.0-WQ)
       ETAS=Z27/Z21
       EPS=ETAS-FMUN
       FNU = SQRT(Q14*Q14*Z18*FKO/FKW)
       Y3=Z20
       Y1=FMUN
       Y2=Z18
       RETURN
       END
```

```
$IBFTC M22      DECK
      SUBROUTINE M22
      DIMENSION TBL1(46),TBL1P(46),TBL3(46),TBL3P(46),TBL4(13),TBL4P(13)
     1,TBL5(43),TBL5P(43),TBL6(45),TBL6P(45),TBL6PP(45),TBL7(19),TBL7P
     2(19)
      DIMENSION Z37(3)
      COMMON Z18,Z19,Z20,Z21,Z22,Z23,Z24,Z25,Z26,Z27,Z28,Z30,Z31,Z32,
     1Z33,Z34,Z35,Z37,C1,C2,C5,C40,C41,C42,Q1,Q2,Q3,Q4,Q5,Q6,Q7,Q8,
     2Q10,Q11,Q12,Q13,Q14,Q15,Q16,Q17,Q18,Q19,Q20,Q9,D,EPS,ETAS,FKO,
     3FKW,FMUN,FMUO,FNBR,FNU,FNUC,FNUF,FNUM,FI7,NZ35,SO,SS,TAW,TS,
     4TSBZ,VISIN,WO,Y1,Y2,Y3,Y6,NY35,NUCO,RAWM,SLP
      COMMON /CONST/TBL1,TBL1P,TBL3,TBL3P,TBL4,TBL4P,TBL5,TBL6,TBL6P,
     1 TBL6PP,TBL5P,TBL7,TBL7P
      NY35 = 1
      IF (NZ35-1) 13,13,10
   13 Y4 = 1.0
      Y5=2.0
   10 IF (NY35-20) 11,200,200
   11 Z20 = Y4
      CALL NUOREO
      G4=((Z25*FMUO*SQRT(C40*Z21*(C41+1.0)/(2.0*C41)))/(0.3386*Q6))**2
      IF (Z20-1.) 14,14,15
   14 F4=(.5*(C41+1.)*Z20*Z20)*(1.+.5*(C41-1.)*Z20*Z20)**(-(C41+1.)/(C41
     1-1.0))
      GO TO 16
   15 F4=(1.+.5*(C41-1.)*(Z20**2))*(.5*(C41+1.)*(Z20**2))**(-(C41+1.)/
     1(C41-1.))*((2.*C41*Z20*Z20-C41+1.)/(C41+1.))**(2./(C41-1.))
   16 Z20=Y5
      CALL NUOREO
      G5=((Z25*FMUO*SQRT(C40*Z21*(C41+1.0)/(2.0*C41)))/(0.3386*Q6))**2
      IF (Z20-1.) 17,17,18
   17 F5=(.5*(C41+1.)*Z20*Z20)*(1.+.5*(C41-1.)*Z20*Z20)**(-(C41+1.)/(C41
     1-1.0))
      GO TO 19
   18 F5=(1.+.5*(C41-1.)*(Z20**2))*(.5*(C41+1.)*(Z20**2))**(-(C41+1.)/
     1(C41-1.))*((2.*C41*Z20*Z20-C41+1.)/(C41+1.))**(2./(C41-1.))
   19 Z20 = Y5-(G5-F5)*(Y5-Y4)/(G5-F5-G4+F4)
      IF (ABS(Z20-Y5)-.005) 40,40,20
   20 IF (Z20-Y5) 30,40,50
   30 IF (ABS(Z20-Y4)-.005) 60,60,70
   70 IF (Z20-Y4) 80,60,90
   80 NY35 = NY35+1
      IF (Z20-1.) 69,72,73
   69 IF (Z20-.2) 71,71,502
   71 Y5 = 1.
      Z20 = Y5
      CALL NUOREO
      G5=((Z25*FMUO*SQRT(C40*Z21*(C41+1.0)/(2.0*C41)))/(0.3386*Q6))**2
      F5=(.5*(C41+1.)*Z20*Z20)*(1.+.5*(C41-1.)*Z20*Z20)**(-(C41+1.)/(C41
     1-1.))
      Z20 = .3
  703 CALL NUOREO
      Y4 = Z20
      G4=((Z25*FMUO*SQRT(C40*Z21*(C41+1.0)/(2.0*C41)))/(0.3386*Q6))**2
      F4=(.5*(C41+1.)*Z20*Z20)*(1.+.5*(C41-1.)*Z20*Z20)**(-(C41+1.)/(C41
     1-1.))
      IF (G4-F4) 503,60,706
  706 IF (Z20-1.0) 709,200,200
  709 Z20 = Z20+.10
      GO TO 703
  502 Y4 = Z20
```

```
      CALL NUOREO
      G4=((Z25*FMUO*SQRT(C40*Z21*(C41+1.0)/(2.0*C41)))/(0.3386*Q6))**2
      F4=(.5*(C41+1.)*Z20*Z20)*(1.+.5*(C41-1.)*Z20*Z20)**(-(C41+1.)/(C41
     1-1.))
      Y5 = 1.0
      Z20 = Y5
      CALL NUOREO
      G5=((Z25*FMUO*SQRT(C40*Z21*(C41+1.0)/(2.0*C41)))/(0.3386*Q6))**2
      F5=(.5*(C41+1.)*Z20*Z20)*(1.+.5*(C41-1.)*Z20*Z20)**(-(C41+1.)/(C41
     1-1.))
      IF (G4-F4) 503,60,71
  503 IF (G5-F5) 200,72,504
  504 Z20 = Y5-(G5-F5)*(Y5-Y4)/(G5-F5-G4+F4)
      IF (NY35-12) 505,505,200
  505 IF (ABS(Z20-Y4)-.002) 990,990,506
  506 Y4=Z20
      CALL NUOREO
      G4=((Z25*FMUO*SQRT(C40*Z21*(C41+1.0)/(2.0*C41)))/(0.3386*Q6))**2
      F4=(.5*(C41+1.)*Z20*Z20)*(1.+.5*(C41-1.)*Z20*Z20)**(-(C41+1.)/(C41
     1-1.))
      NY35 = NY35+1
      GO TO 504
   72 Z20 = 1.0
      GO TO 990
   73 Y5 = Y4
      Y4 = Z20
      GO TO 10
   60 Z20 = Y4
      GO TO 990
   90 Y4 = Z20
      NY35 = NY35 + 1
      GO TO 10
   40 Z20 = Y5
      GO TO 990
   50 Y4 = Y5
      Y5 = Z20
      NY35 = NY35 + 1
      IF (Z20-10.) 10,990,990
  200 NZ35 = 20
      GO TO 990
  990 IF (Z20-10.) 992,992,993
  993 Z20 = 10.0
      Y4=2.
      Y5 = 10.
  992 GO TO 994
  994 CALL NUOREO
      RETURN
       END
```

```
$IBFTC BSI      DECK
      SUBROUTINE BSIT
      DIMENSION TBL1(46),TBL1P(46),TBL3(46),TBL3P(46),TBL4(13),TBL4P(13)
     1,TBL5(43),TBL5P(43),TBL6(45),TBL6P(45),TBL6PP(45),TBL7(19),TBL7P
     2(19)
      DIMENSION Z37(3)
      COMMON Z18,Z19,Z20,Z21,Z22,Z23,Z24,Z25,Z26,Z27,Z28,Z30,Z31,Z32,
     1Z33,Z34,Z35,Z37,C1,C2,C5,C40,C41,C42,Q1,Q2,Q3,Q4,Q5,Q6,Q7,Q8,
     2Q10,Q11,Q12,Q13,Q14,Q15,Q16,Q17,Q18,Q19,Q20,Q9,D,EPS,ETAS,FKO,
     3FKW,FMUN,FMUO,FNBR,FNU,FNUC,FNUF,FNUM,FI7,NZ35,SO,SS,TAW,TS,
     4ISBZ,VISIN,WO,Y1,Y2,Y3,Y6,NY35,NUCO,RAWM,SLP
      COMMON /CONST/TBL1,TBL1P,TBL3,TBL3P,TBL4,TBL4P,TBL5,TBL6,TBL6P,
     1 TBL6PP,TBL5P,TBL7,TBL7P
C               THIS IS A DIRECT BISECTION FOR FNU
   20 IF (FNU-8.0) 40,40,950
   40 IF (0.8-FNU) 60,60,960
   60 WO=((EXP(2.0*FNU)-1.0)/(EXP(2.0*FNU)+1.0))/FNU
      CON = (FKO/FKW)*FNUM*((Q14)**2.)
      NO1 = 19
      CALL TBLKP(WO,TBL7,Z32,TBL7P,NO1)
      FTN = (FNU**2.)/Z32
      X1=ABS(FTN-CON)
      IF (X1-.0002) 990,990,80
   80 IF (FTN-CON) 100,990,200
  100 TOP=8.0
      BOTT=FNU
      GO TO 300
  200 TOP=FNU
      BOTT = 0.8
      GO TO 300
  300 V=.5*(TOP+BOTT)
  301 IF (V-7.995) 302,302,950
  302 IF (V-0.805) 960,303,303
  303 FWO=((EXP(2.0*V)-1.0)/(EXP(2.0*V)+1.0))/V
      NO1 = 19
      CALL TBLKP(FWO,TBL7,Z32,TBL7P,NO1)
      FV = (V**2.)/Z32
      X2=ABS(FV-CON)
      IF (X2-.0002) 900,900,310
  310 IF (FV-CON) 400,900,500
  400 BOTT=V
      GO TO 300
  500 TOP=V
      GO TO 300
  900 FNU=V
      GO TO 990
  950 WRITE (6,951)
  951 FORMAT (15H NU EXCEEDS 8.0)
      FNU=7.99
      GO TO 990
  960 WRITE (6,961)
  961 FORMAT (13H NU BELOW 0.8)
      FNU = .81
      GO TO 990
  990 RETURN
      END
```

```
$IBFTC NUR      DECK
       SUBROUTINE NUOREO
       DIMENSION TBL1(46),TBL1P(46),TBL3(46),TBL3P(46),TBL4(13),TBL4P(13)
      1,TBL5(43),TBL5P(43),TBL6(45),TBL6P(45),TBL6PP(45),TBL7(19),TBL7P
      2(19)
       DIMENSION Z37(3)
       COMMON Z18,Z19,Z20,Z21,Z22,Z23,Z24,Z25,Z26,Z27,Z28,Z30,Z31,Z32,
      1Z33,Z34,Z35,Z37,C1,C2,C5,C40,C41,C42,Q1,Q2,Q3,Q4,Q5,Q6,Q7,Q8,
      2Q10,Q11,Q12,Q13,Q14,Q15,Q16,Q17,Q18,Q19,Q20,Q9,D,EPS,ETAS,FKO,
      3FKW,FMUN,FMUO,FNBR,FNU,FNUC,FNUF,FNUM,FI7,NZ35,SO,SS,TAW,TS,
      4TSBZ,VISIN,WQ,Y1,Y2,Y3,Y6,NY35,NUCO,RAWM,SLP
       COMMON /CONST/TBL1,TBL1P,TBL3,TBL3P,TBL4,TBL4P,TBL5,TBL6,TBL6P,
      1 TBL6PP,TBL5P,TBL7,TBL7P
       REAL NUCO
       REAL NUC1
       REAL NUFM
       IF (Z18 - .01) 950,950,5
     5 IF (Z18 - 5. ) 6,6,960
     6 SS = Z20*SQRT(.5*C41)
       NO = 45
       CALL TBLKP (SS,TBL6,TSBZ,TBL6PP,NO)
       NX35=1
    10 IF (NX35-20) 11,11,12
    11 NUFM=(.02604)*(TSBZ/SS)*NUCO**(.128*((2.-NUCO)**4.)+2.67)
       FNUS=-Z18+NUCO/(1.+(NUCO/NUFM))
       DNUS=((1.+(NUCO/NUFM))**(-2.))*(1.+(NUCO/NUFM)*(.128*((2.-NUCO)
      1**4.)+2.67-.512*NUCO*((2.-NUCO)**3.)*ALOG(NUCO)))
       NUC1 = NUCO -FNUS/DNUS
       NX35=NX35+1
       IF (ABS((NUCO-NUC1)/NUC1)-.0001)  30,30,20
    20 NUCO = NUC1
       GO TO 10
    12 NZ35 = 20
       GO TO 990
   950 WRITE (6,951)
   951 FORMAT (19H NUO LESS THAN 0.01)
       Z25 = .05
       GO TO 990
   960 WRITE (6,961)
   961 FORMAT (16H NUO EXCEEDS 5.0)
       Z25 = 20.0
       GO TO 990
    30 NUCO = NUC1
       Z25 = 1.45*NUCO**(.128*((2.-NUCO)**4.)+2.67)
   990 RETURN
       END
```

```
$IBFTC BLO      DECK
       BLOCK DATA
      DIMENSION TBL1(46),TBL1P(46),TBL3(46),TBL3P(46),TBL4(13),TBL4P(13)
     1,TBL5(43),TBL5P(43),TBL6(45),TBL6P(45),TBL6PP(45),TBL7(19),TBL7P
     2(19)
      DIMENSION Z37(3)
      COMMON /CONST/TBL1,TBL1P,TBL3,TBL3P,TBL4,TBL4P,TBL5,TBL6,TBL6P,
     1 TBL6PP,TBL5P,TBL7,TBL7P
      DATA (TBL1(I),I = 1,46)/      30.,40.,50.,60.,70.,80.,90.,100.,110.
     1 ,120.,130.,140.,150.,160.,170.,180.,190.,200.,210.,220.,230.,240.
     2 ,250.,260.,270.,280.,290.,300.,310.,320.,330.,340.,350.,360.,370.
     3 ,380.,390.,400.,410.,420.,430.,440.,450.,460.,470.,480./
      DATA (TBL1P(I),I = 1,46)/     0.7039,0.9117,1.131,1.350,1.558,1.784
     1 ,1.996,2.210,2.425,2.640,2.855,3.068,3.281,3.492,3.703,3.912,4.11
     2 9,4.324,4.527,4.729,4.929,5.127,5.323,5.517,5.709,5.897,6.087,6.2
     3 72,6.457,6.641,6.820,6.999,7.178,7.357,7.530,7.703,7.876,8.043,8.
     4 211,8.378,8.545,8.706,8.868,9.030,9.192,9.347/
      DATA (TBL3(I),I = 1,46)/      30.,40.,50.,60.,70.,80.,90.,100.,110.
     1 ,120.,130.,140.,150.,160.,170.,180.,190.,200.,210.,220.,230.,240.
     2 ,250.,260.,270.,280.,290.,300.,310.,320.,330.,340.,350.,360.,370.
     3 ,380.,390.,400.,410.,420.,430.,440.,450.,460.,470.,480./
      DATA (TBL3P(I),I = 1,46)/     215.7,281.1,347.3,416.3,485.6,555.1,6
     1 22.9,692.9,763.3,831.9,899.0,964.6,1029.,1091.,1152.,1212.,1271.,
     2 1329.,1385.,1440.,1494.,1547.,1599.,1650.,1700.,1750.,1798.,1846.
     3 ,1893.,1939.,1985.,2030.,2075.,2118.,2160.,2202.,2245.,2286.,2327
     4 .,2366.,2406.,2445.,2485.,2520.,2560.,2595./
      DATA (TBL4(I),I = 1,13)/      0.,0.2,0.4,0.6,0.8,1.0,1.2,1.4,1.6,1.
     1 8,2.0,2.2,10./
      DATA (TBL4P(I),I = 1,13)/     1.0,0.998,0.995,0.991,0.985,0.977,0.9
     1 70,0.964,0.959,0.955,0.952,0.950,0.950/
      DATA (TBL5(I),I = 1,43)/      0.05,0.06,0.07,0.08,0.09,0.10,0.11,0.
     1 12,0.14,0.15,0.17,0.19,0.20,0.23,0.25,0.30,0.35,0.40,0.50,0.60,0.
     2 70,0.80,0.90,1.0,1.1,1.2,1.3,1.4,1.5,1.7,1.9,2.0,2.5,3.0,3.5,4.0,
     3 5.0,6.0,7.0,8.0,10.0,12.0,25.0/
      DATA (TBL5P(I),I = 1,43)/     0.02,0.03,0.042,0.054,0.068,0.082,0.0
     1 97,0.112,0.144,0.158,0.188,0.218,0.232,0.272,0.294,0.350,0.397,0.
     2 437,0.505,0.558,0.603,0.640,0.672,0.700,0.724,0.744,0.765,0.783,0
     3 .800,0.826,0.849,0.858,0.895,0.916,0.932,0.944,0.960,0.970,0.977,
     4 0.982,0.990,1.0,1.0/
      DATA (TBL6(I),I = 1,45)/      0.2,0.4,0.6,0.8,1.0,1.2,1.4,1.6,1.8,2
     1 .0,2.2,2.4,2.6,2.8,3.0,3.2,3.4,3.6,3.8,4.0,4.2,4.4,4.6,4.8,5.0,5.
     2 2,5.4,5.6,5.8,6.0,6.2,6.4,6.6,6.8,7.0,7.2,7.4,7.6,7.8,8.0,8.2,
     3 8.4,8.6,8.8,9.0/
      DATA (TBL6P(I),I = 1,45)/     9.80271,10.94784,12.89399,15.69746,19
     1 .43609,24.20781,30.12863,37.32923,45.95230,56.14932,68.07771,81.8
     2 9947,97.77902,115.88287,136.37821,159.43361,185.21769,213.89927,2
     3 45.64801,280.63340,319.02474,360.99204,406.70528,456.33364,510.04
     4 756,568.01730,630.41182,697.40229,769.31,845.89,927.63,
     5 1014.61,1107.11,1205.2,1309.1,1418.8,1534.7,1656.7,1785.2,
     6 1920.4,2062.2,2210.9,2367.0,2530.2,2700.7/
      DATA (TBL6PP(I),I = 1,45)/    9.61234,10.16410,11.04924,12.22282,13
     1 .63288,15.22758,16.96068,18.79408,20.69872,22.65358,24.64392,26.6
     2 5990,28.69470,30.74382,32.80398,34.87300,36.94914,39.03112,41.118
     3 00,43.20904,45.30354,47.40108,49.50126,51.60366,53.70808,55.81428
     4 ,57.92200,60.03114,62.141,64.248,66.359,68.467,70.580,72.692,
     5 74.802,76.910,79.025,81.130,83.242,85.352,87.461,89.561,91.676,
     6 93.782,95.886/
      DATA (TBL7(I),I = 1,19)/      0.1,.15,.2,.25,.3,.35,.4,.45,
     1 .5,.55,.6,.65,.7,.75,.8,.85,.9,.95,1./
       END
```

```
$IBFTC TBL      DECK
       SUBROUTINE TBLKP(VO,VAR,FO,FCN,NO)
       DIMENSION VAR(100),FCN(100)
C                THIS SUBROUTINE PERFORMS TABLE LOOK-UP OPERATIONS.
       DO 100 I=1,NO
       VAR1=VAR(I)
       IF (VO-VAR1) 200,150,100
  100  CONTINUE
       WRITE (6,900)VO,NO
  900  FORMAT (34H VARIABLE EXCEEDS TABLE FOR VALUE E11.4,13H TABLE SIZE
      1=I5)
       FO =FCN(NO)
       GO TO 300
  150  FO=FCN(I)
       GO TO 300
  200  IF (I-1) 210,290,210
  210  I1=I-1
       TEMP=VO-VAR(I1)
       TEM1=VAR(I)-VAR(I1)
       RATIO=TEMP/TEM1
       FO=RATIO*(FCN(I)-FCN(I1))+FCN(I1)
       GO TO 300
  290  FO=FCN(I)
  300  RETURN
       END
```

B.5 Mean Flow Program

This program calculates the local flow properties in a fluid stream from three independent flow properties using the compressible flow relations (25). Either one of three sets of input data may be used in the program. All sets use Pitot pressure and total temperature data, and the distinction between input types exists because the third input property might be centerline static pressure, total pressure downstream of the nose shock, or mass flux data. As mentioned in Section II, this variation in input data was necessary because the static pressures could not be measured directly in the vicinity of the base. Therefore, the third independent measurement in those base regions was either mass flux data in the base shear layers or the total pressure in the inviscid isentropic region outside the shear layer. Unfortunately, double roots difficulty in solving for Mach number from the measured data requires that the mass flux version of the mean flow program be used only for $M \geq 1$.

B.5a) Mean Flow Program ID Listing

PO	$p_o \equiv p_{t_\infty}$	free stream total pressure, mmHg
TO	$T_o = T_{t_\infty} = T_{t_e}$	free stream total temperature, ^oK
MFS	M_∞	free stream Mach number
REOFS	Re_{t_∞}	free stream Reynolds number based on free stream mass flux, reference length and viscosity corresponding to free stream total temperature
TFS	T_∞	free stream static temperature, ^oK
DO	ρ_{t_∞}	free stream stagnation density, gmm/cm^3
PFS	p_∞	free stream static pressure, mmHg
QFS	q_∞	free stream dynamic pressure, gmf/cm^2
DFS	ρ_∞	free stream static density, gmm/cm^3
UFS	u_∞	free stream velocity, cm/sec
DUFS	$\rho_\infty u_\infty$	free stream mass flux, gmm/cm^2 sec
DIA	D	reference length, cm
REFS	Re_∞	Reynolds number corresponding to free stream mass flux, viscosity based on free stream static temperature, and a given reference length
MUFS	μ_∞	viscosity based on free stream static temperature, gmm/sec cm
MUO	μ_{t_∞}	viscosity based on free stream total temperature, gmm/sec cm
NOSP	NOSP	number (integer) of profiles for data set
NTYPE	NTYPE	integer (1 or 2) indicating mean flow calculation procedure; mass flux version (1) or static pressure version (2)
NPTS	NPTS	number (integer) of data points for given profile
XD	x/D	axial distance from base ratioed to reference length

YD	y/D	lateral distance from centerline ratioed to reference length
TT	T_t	local total temperature, ^oK
PPM	$(p_{t2}/p_o)_m$	measured Pitot pressure ratioed to free stream total pressure
PIBM	$(\frac{p}{p_o})_m (\frac{p}{p_m})_v (\frac{p_{LE}}{p_x})_\infty (\frac{p_{t_{2_x}}}{p_{t_{2LE}}})_\infty$	product of corrected (viscous interaction and tunnel gradient) static pressure, Pitot pressure tunnel gradient factor, and reciprocal of free stream total pressure; the ratio of PIBM to PPM gives corrected Rayleigh-Pitot ratio for determining Mach number
REOM	$Re_{t_{d_m}}$	measured local Reynolds number based on wire diameter and viscosity corresponding to local total temperature
PPG	$(p_{t_{2_x}}/p_{t_{2_{LE}}})_\infty$	free stream Pitot pressure axial gradient
M	M	local Mach number
Q	q	local dynamic pressure, gmf/cm^2
P	p/p_∞	ratio of local static pressure to free stream static pressure
PT	p_t/p_o	ratio of local total pressure to free stream total pressure
TTTTE	T_t/T_o	ratio of local total temperature to free stream total temperature
UUE	u/u_e	ratio of local velocity to edge velocity
TTE	T/T_e	ratio of local static temperature to edge static temperature
DDE	ρ/ρ_e	ratio of local density to edge density
DUDUE	$\rho u/\rho_e u_e$	ratio of local mass flux to edge mass flux
KN	$Kn = \sqrt{\frac{\pi\gamma}{2}}\, M/Re$	local Knudsen number

UE	u_e/u_∞	ratio of edge velocity to free stream velocity
DE	ρ_e/ρ_∞	ratio of edge density to free stream density
TE	T_e/T_∞	ratio of edge static temperature to free stream static temperature
TTOE	$T_{t_e} \equiv T_{t_\infty} \equiv T_o$	edge total temperature, ^oK
RET	Re_{tD}	local Reynolds number based on reference length and total temperature
W	UDEL	
H	TDEL	
MUE	μ_e	viscosity based on edge static temperature, gmm/sec cm
MU	μ	viscosity based on local static temperature, gmm/sec cm
MUT	μ_t	viscosity based on local total temperature, gmm/sec cm
C	$\rho\mu/\rho_e\mu_e$	ratio of local density-viscosity product to edge density-viscosity product
PTM	p_t/p_o	ratio of local total pressure to free stream total pressure for region between shear layer edge and leading edge shock
PPPT	p_{t_2}/p_t	ratio of local Pitot pressure to local total pressure
PPP	p/p_t	ratio of local static pressure to local Pitot pressure
PPC	$\left(p_{t_2}/p_o\right)_c$	ratio, as corrected for tunnel gradient, of local Pitot pressure to free stream total pressure
FM	$Re_t\mu\sqrt{T_t}/p_{t_2}$	Mach number function
MDEF	$\frac{\rho u}{\rho_e u_e}\left(\frac{u_e-u}{u_e}\right)$	generated
EDEF	$\left(\frac{T_{t_e}-T_t}{T_{t_e}}\right)\frac{\rho u}{\rho_e u_e}$	generated

RE	Re_D	local Reynolds number based on reference length and static temperature
UDEF	$(u-u_{\ell})/(u_e-u_{\ell})$	ratio of local-centerline velocity defect to edge-centerline velocity defect
DDEF	$(\rho-\rho_{\ell})/(\rho_e-\rho_{\ell})$	ratio of local-centerline density defect to edge-centerline defect
TDEF	$(T_{\ell}-T)/(T_{\ell}-T_e)$	ratio of centerline-local static temperature excess to centerline-edge static temperature excess
TTDEF	$(T_t-T_{t_{\ell}})/(T_o-T_{t_{\ell}})$	ratio of local-centerline total temperature defect to edge-centerline total temperature defect
UDIF	$(u_e-u)/(u_e-u_{\ell})$	ratio of edge-local velocity difference to edge-centerline density difference
DDIF	$(\rho_e-\rho)/(\rho_e-\rho_{\ell})$	ratio of edge-local density difference to edge-centerline density difference
TDIF	$(T-T_e)/(T_{\ell}-T_e)$	ratio of local-edge static temperature difference to centerline-edge static temperature difference
TTDIF	$(T_{t_e}-T_t)/(T_o-T_{t_{\ell}})$	ratio of edge-local total temperature difference to edge-centerline total temperature difference
UDEL	$(u_e-u)/u_e$	ratio of edge-local velocity defect to edge velocity
DDEL	$(\rho_e-\rho)/\rho_e$	ratio of edge-local density defect to edge density
TDEL	$(T-T_e)/T_e$	ratio of local-edge static temperature excess to edge static temperature
TTFS	T/T_{∞}	ratio of local static temperature to free stream static temperature
UUFS	u/u_{∞}	ratio of local velocity to free stream velocity
DDFS	ρ/ρ_{∞}	ratio of local density to free stream density
DUDUFS	$\rho u/\rho_{\infty}u_{\infty}$	ratio of local mass flux to free stream mass flux

DIST $\int_0^\infty \left(1 - \frac{\rho u}{\rho_e u_e}\right) d\left(\frac{y}{D}\right)$ ratio of displacement thickness to reference length, δ^*/D

MOMT $\int_0^\infty \frac{\rho u}{\rho_e u_e} \left(1 - \frac{u}{u_e}\right) d\left(\frac{y}{D}\right)$

ratio of momentum thickness to reference length, $\overline{\theta}/D$

EMT $\int_0^\infty \left(1 - \frac{T_t}{T_{te}}\right) \frac{\rho u}{\rho_e u_e} d\left(\frac{y}{D}\right)$

ratio of energy thickness to reference length, E/D

DMUDMU $\rho u \mu / \rho_\infty u_\infty \mu_\infty$ ratio of local mass flux-viscosity product to free stream mass flux-viscosity product

YB $\frac{\overline{y}}{D} = \frac{\rho_e u_e}{\rho_\infty u_\infty} \sqrt{Re_{\infty_D}} \int_0^\infty \frac{\rho}{\rho_e} d\left(\frac{y}{D}\right)$

ratio of transformed y coordinate to reference length

DEL1 δ_e/D ratio of wake total temperature semi-thickness (¢-e) to reference length

DEL2 $\left(\frac{\overline{x}}{D} + \frac{\overline{x}_o}{D}\right)_u^{1/2}$ square root of ratio of transformed axial distance (based on Kubota's linear wake theory) plus "effective origin" of wake from centerline velocity extrapolation, to reference length

DEL3 $\left(\frac{\overline{x}}{D} + \frac{\overline{x}_o}{D}\right)_h^{1/2}$ square root of ratio of transformed axial distance (based on Kubota's linear wake theory) plus "effective origin" of wake from centerline static temperature extrapolation, to reference length

DEL4 $\frac{\overline{y}}{D}\Big)_{UDIF = .5}$ ratio of wake semi-thickness in terms of transformed lateral distance and based on UDIF = .5 location, to reference length

DEL5 $\frac{\overline{y}}{D}\Big)_{TDIF = .5}$ ratio of wake semi-thickness in terms of transformed lateral distance and based on TDIF = .5 location, to reference length

YDEL1 y/δ_e ratio of lateral distance to wake semi-thickness

YBDEL1 YBDEL2 YBDEL3 YBDEL4 YBDEL5	$\bar{y}$/DEL 1→5	generated
XOU	$\left(\frac{\bar{x}}{D} + \frac{\bar{x}_o}{D}\right)_u$ -x/D	generated
XOT	$\left(\frac{\bar{x}}{D} + \frac{\bar{x}_o}{D}\right)_x$ -x/D	generated
SF	SF	code number 0, 2, or 101 for use in base region (NTYPE = 1) describing calculation procedure for streamline determination (mass flux integration from leading edge shock 2, 101 or centerline 0) and method of calculating mean flow (use of Reynolds number 2 or total pressure behind leading edge shock 101)
REOO	Re_∞	Reynolds number code which instructs program to calculate mean flow quantities from total pressure behind leading edge shock when measured Reynolds number is both greater than REOO and exceeds edge Reynolds number
YBC	YBC	for NTYPE = 1, SF > 1 implies lateral position of data point from centerline in terms of y/D; for NTYPE = 2, and NTYPE = 1, SF < 1.0 implies YB $\overline{C}$
UCL	u_ℓ/u_∞	ratio of centerline velocity to free stream velocity
DCL	ρ_ℓ/ρ_∞	ratio of centerline density to free stream density
TCL	T_ℓ/T_∞	ratio of centerline static temperature to free stream static temperature
TTCL	$T_{t\ell}$	centerline total temperature, ^oK
RW2	$\left(1 - \frac{u_\ell}{u_e}\right)^{-2}$	square of ratio of edge velocity to edge-centerline velocity defect
RH2	$\left(\frac{T_\ell}{T_e} - 1\right)^{-2}$	square of ratio of edge static temperature to centerline-edge static temperature excess

QMOMT $\dfrac{\rho_e u_e^2}{\rho_\infty u_\infty^2} \dfrac{\bar{\theta}}{D}$ product of ratio of momentum thickness to reference length with ratio of edge dynamic pressure to free stream dynamic pressure

EMTM $\dfrac{\rho_e u_e}{\rho_\infty u_\infty} \dfrac{E}{D}$ product of ratio of energy thickness to reference length with ratio of edge mass flux to free stream mass flux

PSI1 $\dfrac{\psi}{\rho_\infty u_\infty D} = \displaystyle\int_0^y \dfrac{\rho u}{\rho_\infty u_\infty} \, d\left(\dfrac{y}{D}\right)$ integrated mass flux from centerline to data point location as ratioed to free stream mass flux

PSI $\dfrac{\psi}{\rho_\infty u_\infty D} = \dfrac{y_S}{D} + \displaystyle\int_{y_S}^y \dfrac{\rho u}{\rho_\infty u_\infty} \, d\left(\dfrac{y}{D}\right)$ integrated mass flux from centerline to data point as ratioed to free stream mass flux; for this case integration starts at leading edge shock, i.e., SF > 1

B.5b) Typical Input Data for Mean Flow Program (NTYPE 1)

```
$DATA
     1      1 5153.     402.        6.14        .762        2.          .7442
0.1         1.                     14
1.045.0     .045 .145 .245 .345 .415 .455 .47  .495 .520 .545 .57  .595
4.9   6.21 6.21 6.1856.0855.94 4.9  2.2  1.4  .63  .37  .218 .13  .08
402. 402. 402. 402. 402. 402. 402. 406. 402. 388. 382. 372. 367. 362.
4.91 4.91 4.91 4.91 4.91 4.91 4.91 2.25 1.5  .73  .46  .29  .19  .13
$ENDJOB
```

B.5c) Typical Output Data for Mean Flow Program (NTYPE 1)

```
 NOSP= 1  NTYPE= 1  PO=  0.5153E 04    TO=  0.4020E 03   MFS=  0.6140E 01  CIA=  0.7620E 00  SF=  0.2000E 01    PTM  0.7442E 00
RECFS=  0.7832E 04  REFS=  0.5480E 05  TFS=  0.4707E 02  DO=  C.5951E-02  PFS=  0.2831E 01  QFS=  0.1016E 03  DFS=  0.2792E-04
LFS=  0.8446E 05    DLFS=  C.2358E 01

XC=  0.1CCCE-CO  PPG=  C.1CCOE 01  NPTS=   14  XCL= -C.          XCI= -C.          RECO= -0.
   YC              TT              PPM             PIBM            REOM            M               C               P               PT              TTTTE
   LLE             TTE             CDE             CUCUE           KN              RE              RET             LDEF            CDEF            TTFS
   LLFS            CCFS            CLDUFS          FPP             PPC             MDEF            EDEF            CIST            MOMT            EMT
   YB              PSII            MUT             FM              YCEL1           CEL5            YBCEL3          TDEF            UDEL            CCEL
   TCEL            LCIF            CCIF            TCIF            CEL3            CEL4            CMLDML          YBDEL4          YBDEL5          CEL2
   TTDEF           TTCIF           YBCEL2          RW2             RH2             PSI             CMOMT           EMTM            C               YBC

  C.1C45E C1    0.4C20E C3    0.4900E-01   -C.3534E-16   C.491CE C1    C.4917E 01    C.1839E 03    C.2823E 01    0.7446E 00    0.1C00E 01
  C.1CCOE C1    C.1C0CE C1    0.1C00E 01    C.1CC0E C1   C.3113E-CC    C.7C26E 05    0.1464E 05   -C.3534E-16   -0.3534E-16    0.1463E 01
  C.5688E CC    0.1525E C1    0.1869E C1    C.3165E-01   C.49CCE-C1    C.            C.            C.            0.            0.
  C.            -C.3534E-16   0.2294E-03   -C.3534E-16   0.1CCCE C1    0.1CCCE 01   -C.3534E-16   -C.3534E-16   -0.3534E-16   -0.3534E-16
 -C.3534E-16   -0.3534E-16   -0.3534E-16   -C.3534E-16   C.3162E-CC    C.1CC0E 01    0.2723E C1   -0.3534E-16   -0.3534E-16    0.3162E-00
 -C.3534E-16   -0.3534E-16   -0.3534E-16   -0.3534E-16   -C.3534E-16   -C.3534E-16   -C.3534E-16   -C.3534E-16   -0.3534E-16   -0.3534E-16

 -C.            0.4C2CE C3    0.6210E-01   -C.3534E-16   C.491CE C1    C.4618E 01    C.2327E 03    C.4048E C1    0.7446E 00    0.1000E 01
  C.5887E CC    0.11C9E C1    0.1294E 01    0.1279E C1   C.2534E-CC    C.81C7E 05    C.1872E 05    C.            -0.           C.1622E 01
  C.5579E CC    0.2496E C1    0.2390E 01    C.3582E-01   C.621CE-C1    C.1444E-01    C.            C.            0.            0.
  C.            -0.           0.2294E-03   -0.3534E-16   -C.           C.1CCCE 01   -C.3534E-16    C.            0.1128E-01   -0.2939E-00
  C.1085E-CC    0.1C0CE C1    0.1C00E C1    0.1CCCE C1   C.3162E-CC    C.1CCCE 01    0.3862E 01   -C.3534E-16   -0.3534E-16    0.3162E-00
  C.            0.1CCCE C1   -0.3534E-16    0.7852E 04   C.849CE C2    C.1C45E 01    0.            C.            0.1434E 01    0.1045E 01

  C.45C0E-C1    0.4C2CE C3    0.6210E-01   -C.3534E-16   C.491CE 01    C.4618E 01    C.2327E 03    C.4048E 01    0.7446E 00    0.1C00E 01
  C.5887E CC    0.11C9E C1    0.1294E C1    0.1279E C1   C.2534E-CC    C.81C7E 05    C.1872E 05    C.            -0.           0.1622E 01
  C.5579E CC    0.2496E C1    0.2390E 01    C.3582E-01   C.621CE-C1    C.1444E-01    C.            -C.1257E-01   0.6496E-03    0.
  C.2547E C2    0.1C76E-C0    0.2294E-03   -0.3534E-16   C.43C6E-01    C.1CCCE 01    0.8C54E 02    C.            0.1128E-01   -0.2939E-00
  C.1085E-CC    0.1C00E C1    0.1C00E 01    0.1CC0E C1   C.3162E-CC    C.1CC0E 01    0.3862E 01    C.2547E 02    0.2547E 02    0.3162E-00
  C.            C.1CCCE C1    C.8054E C2    0.7852E 04   C.849CE C2    C.9374E CC    C.1176E-02    C.            0.1434E 01    1.0000E 00

  C.145CE-CC    0.4C2CE C3    0.6185E-01   -C.3534E-16   C.491CE C1    C.4623E 01    0.2317E 03    0.4023E 01    0.7447E 00    0.1000E 01
  C.9885E CC    0.1107E C1    0.1288E C1    0.1274E 01   C.2543E-CC    C.8C88E 05    C.1864E 05    C.186CE-01    0.1942E-01    0.1619E 01
  C.5581E CC    0.2485E C1    0.2380E C1    0.3574E-01   C.6185E-C1    C.1411E-01    C.            -C.4022E-01   0.2077E-02    0.
  C.8154E C2    0.3461E-CC    0.2294E-03   -C.3534E-16   C.1388E-CC    C.1CCCE 01    0.2591E 03    0.185CE-01    0.1108E-01   -0.2882E-00
  C.1C65E-CC    0.9814E C0    0.9806E C0    0.9815E C0   C.3162E-CC    C.1CCCE 01    0.3839E 01    0.8194E 02    0.8194E 02    0.3162E-00
  C.            0.1C0CE C1    0.2591E C3    0.7852E 04   C.849CE C2    0.6989E 0C    0.376CE-02    C.            0.1426E 01    0.9C00E 00

  C.245CE-CC    0.4C2CE C3    0.6085E-01   -C.3534E-16   C.491CE C1    C.4643E 01    0.2280E C3    0.3924E 01    0.7449E 00    0.1C00E 01
  C.5858E CC    0.1C99E C1    0.1265E 01    0.1252E C1   C.2575E-CC    C.8C1CE 05    0.1833E 05    0.925CE-01    0.9692E-01    0.1608E 01
  C.5589E CC    0.2441E C1    0.2340E 01    0.3543E-01   C.6085E-C1    C.1283E-01    0.            -0.6654E-01   0.3424E-02    0.
  C.1378E C3    0.5821E CC    0.2294E-03   -0.3534E-16   C.2344E-CC    C.1CCCE 01    0.4357E 03    C.92C3E-01    0.1024E-01   -0.2654E-00
  C.5854E-C1    C.9C75E CC    0.9031E CC    C.9080E CC   C.3162E-CC    C.1CCCE 01    0.3747E 01    0.1378E 03    0.1378E 03    0.3162E-00
  C.            C.1C0CE C1    0.4357E C3    0.7852E 04   C.849CE C2    C.4629E-00    0.6198E-02    C.            0.1390E 01    0.8C00E 00

  C.345CE-CC    0.4C2CE C3    0.5940E-01   -C.3534E-16   C.491CE C1    C.4673E 01    C.2226E 03    C.3782E C1    0.7448E 00    0.1C00E 01
  C.591CE CC    0.1C87E C1    0.1233E 01    0.1221E C1   C.2634E-CC    C.7893E 05    0.1788E C5    C.1983E-C0    0.2087E-0C    0.1591E 01
  0.9600E 00    0.2377E 01    0.2282E 01    0.3498E-01   0.5940E-01    0.1105E-01    0.            -0.9023E-01   0.4617E-02    G.
  0.1924E 03    0.8133E 00    0.2294E-03   -0.3534E-16   0.3301E-00    0.1000E 01    0.6085E 03    0.1973E-00    0.9048E-02   -0.2325E-00
  C.8711E-01    0.8C17E C0    0.7913E C0    0.8027E C0   0.3162E-CC    C.1CC0E 01    0.3616E 01    C.1924E 03    0.1924E 03    0.3162E-00
  C.            0.1CCCE C1    0.6085E 03    0.7852E 04   C.849CE C2    C.2317E-0C    0.8359E-02    C.            0.1340E 01    0.7000E 00

  C.415CE-CC    0.4C2CE C3    0.4900E-01   -C.3534E-16   C.491CE C1    C.4917E 01    C.1839E 03    C.2823E 01    0.7446E 00    0.1C00E 01
  C.1CCCE C1    C.1CCCE C1    0.1C00E C1    C.1CCCE 01   C.3113E-CC    C.7C26E 05    C.1464E 05    C.1CCCE C1    0.1C00E 01    0.1463E 01
  C.5688E CC    0.1525E C1    0.1869E C1    C.3165E-C1   C.49CCE-C1    C.            0.            -C.9798E-01   C.5004E-02    0.
  C.2266E C3    C.5586E CC    0.2294E-03   -0.3534E-16   C.3971E-CC    C.1CCCE 01    C.7166E 03    C.1CCCE 01    C.            0.
  C.            C.            0.            0.           C.3162E-CC    C.1CCCE 01    0.2723E 01    C.2266E 03    0.2266E 03    0.3162E-00
  C.            C.1CCCE C1    0.7166E C3    0.7852E C4   C.849CE C2    C.8644E-01    C.9C59E-02    C.            0.1CC0E 01    0.6300E 00

  C.455CE-CC    0.4C6CE C3    0.2200E-01   -C.3534E-16   C.225CE C1    C.3913E 01    C.8188E 02    C.1984E C1    0.1473E-0C    0.1010E 01
  C.9585E CC    0.1451E C1    0.4845E-00    C.4644E-CC   C.7731E CC    C.2252E 05    0.6748E 04   -C.2675E 01    0.2754E 01    0.2123E 01
  C.5286E CC    0.5345E C0    0.8678E C0    0.4955E-C1   C.22CCE-C1    C.1926E-01   -C.4621E-02   -C.8727E-01    0.5389E-02   -0.9241E-04
```

C.2356E C3	C.1C13E C1	C.2311E-03	C.524CE-04	C.4354E-CC	C.1CCCE 01	C.7576E C3	-C.3154E 01	C.4147E-01	C.3155E 00
C.45C8E-CC	C.3675E C1	-C.1754E 01	C.4154E C1	C.3162E-CC	C.1CCCE 01	C.1832E 01	C.2396E C3	C.2396E C3	C.3162E-00
C.	C.1CCCE C1	C.7576E 03	C.7852E 04	C.849CE C2	C.3172E-01	C.9756E-02	-C.1727E-03	C.7020E 00	C.5900E 00
C.47CCE-CC	C.4C2CE C3	C.14CCE-01	-C.3534E-16	C.15CCE C1	C.3344E 01	C.5165E C2	C.1714E C1	C.5741E-01	C.1CCCE 01
C.5132E CC	C.18C3E C1	C.3368E-C0	C.3075E-CC	C.1235E C1	C.12CCE 05	C.45C1E 04	-C.6695E C1	C.3257E 01	C.2633E 01
C.8847E CC	C.6455E CC	C.5746E C0	C.6727E-01	C.14CCE-C1	C.267CE-C1	C.	-C.78C5E-01	C.5734E-02	-C.1271E-03
C.2423E C3	C.1C24E C1	C.2294E-C3	C.9564E-C4	C.4458E-CC	C.1CCCE 01	C.7661E C3	-C.64C3E C1	C.8684E-01	C.6632E 00
C.8034E CC	C.7655E C1	-C.2257E 01	C.74C3E C1	C.3162E-CC	C.1CCCE 01	C.15C7E C1	C.2423E C3	C.2423E C3	C.3162E-00
C.	C.1CCCE C1	C.7661E 03	C.7852E 04	C.849CE C2	C.2C9CE-01	C.1C38E-C1	-C.2374E-C3	C.6062E 00	C.5750E 00
C.455CE-CC	C.388CE C3	C.6300E-02	-C.3534E-16	C.73CCE CC	C.2928E 01	C.23C2E C2	C.9958E 00	C.1804E-C1	C.5652E 00
C.8578E CC	C.2C75E C1	C.1701E-C0	C.1459E-CC	C.2616E C1	C.4981E 04	C.219CE C4	-C.1160E 02	C.3824E C1	C.3036E 01
C.831CE CC	C.328CE-CC	C.2726E-C0	C.8684E-01	C.63CCE-C2	C.2C75E-01	C.5C8CE-C2	-C.5872E-C1	C.6327E-02	-C.6357E-04
C.245CE C3	C.1C35E C1	C.2236E-03	C.59C6E-04	C.4737E-CC	C.1CCCE 01	C.7749E C3	-C.89C1E 01	C.1422E-00	C.8299E 00
C.1C75E C1	C.1260E C2	-C.2824E 01	C.5901E 01	C.3162E-CC	C.1CCCE 01	C.8173E CC	C.245CE 03	C.2450E 03	C.3162E-00
-C.	C.1CCCE C1	C.7749E C3	C.7852E C4	C.849CE C2	C.1C31E-01	C.1145E-01	-C.1188E-C3	C.3499E-CC	C.5500E 00
C.52CCE CC	C.382CE C3	C.370CE-02	-C.3534E-16	C.46CCE-CC	C.2464E 01	C.133CE C2	C.7994E CC	C.7321E-02	C.9502E 00
C.7955E CC	C.2482E C1	C.1141E-C0	C.9081E-C1	C.4197E C1	C.2633E 04	C.1379E C4	-C.17C8E C2	C.4015E C1	C.3632E C1
C.7711E CC	C.22C1E-CC	C.1697E-C0	C.1187E-CC	C.37CCE-C2	C.1853E-01	C.4518E-C2	-C.3668E-C1	C.6818E-02	C.5641E-04
C.2466E C3	C.1C4CE C1	C.2211E-03	C.1042E-C3	C.497EE-CC	C.1CCCE 01	C.7798E C3	-C.1266E C2	C.2041E-00	C.8859E 00
C.1482E C1	C.1E08E C2	-C.3015E C1	C.1366E C2	C.3162E-CC	C.1CCCE 01	C.5592E CC	C.2466E C3	C.2466E C3	C.3162E-C0
-C.	C.1CCCE C1	C.7798E 03	C.7852E 04	C.849CE 02	C.4782E-02	C.1234E-C1	C.1054E-03	C.2765E-00	C.5250E 00
C.545CE CC	C.372CE C3	C.218CE-C2	-C.3534E-16	C.29CCE-CC	C.224CE 01	C.7727E 01	C.5715E CC	C.3573E-02	C.9254E 00
C.7479E CC	C.2696E C1	C.7511E-01	C.5617E-C1	C.6581E C1	C.1514E 04	C.8698E C3	-C.2134E C2	C.4147E 01	C.3945E 01
C.7245E CC	C.1445E-C0	C.1C50E-C0	C.1440E-CC	C.218CE-C2	C.1416E-01	C.4192E-02	-C.1352E-C1	C.7227E-02	C.1653E-03
C.2476E C3	C.1044E C1	C.2168E-C3	C.1080E-03	C.5215E CC	C.1CCCE 01	C.7831E C3	-C.1462E C2	C.2521E-00	C.9249E 00
C.1656E C1	C.2234E C2	-C.3147E 01	C.1562E 02	C.3162E-CC	C.1CCCE 01	C.3987E-0C	C.2476E C3	C.2476E C3	C.3162E-00
-C.	C.1CCCE C1	C.7831E C3	C.7852E C4	C.849CE C2	C.1348E-02	C.13C8E-C1	C.3C88E-C3	C.1958E-00	C.5000E-00
C.57CCE CC	C.367CE C3	C.1300E-02	-C.3534E-16	C.19CCE-CC	C.1814E 01	C.4433E 01	C.4997E-0C	C.1612E-02	C.9129E 00
C.6613E CC	C.3213E C1	C.5510E-01	C.3644E-01	C.9546E C1	C.8455E C3	C.5698E C3	-C.29C1E C2	C.4215E C1	C.4701E 01
C.64C7E CC	C.1C63E-CC	C.6809E-01	C.2112E-C0	C.13CCE-C2	C.1234E-01	C.3173E-C2	C.1C32E-C1	C.7558E-02	C.2573E-03
C.2483E C3	C.1C46E C1	C.2147E-03	C.1167E-C3	C.5455E CC	C.1CCCE 01	C.7853E C3	-C.1935E 02	C.3387E-0C	C.9449E 00
C.2213E C1	C.3C01E C2	-C.3215E 01	C.2039E 02	C.3162E-CC	C.1CCCE 01	C.3005E-CC	C.2483E C3	C.2483E C3	C.3162E-00
-C.	C.1CCCE C1	C.7853E C3	C.7852E 04	C.849CE C2	-C.8148E-03	C.1368E-C1	C.48C9E-03	C.1669E-0C	C.4750E-00
C.595CE CC	C.362CE C3	C.8C00E-C3	-C.3534E-16	C.13CCE-CC	C.1417E 01	C.2535E C1	C.4681E-CC	C.8388E-03	C.9C05E 00
C.5581E CC	C.3745E C1	C.4424E-01	C.2469E-01	C.1246E C2	C.5C52E 03	C.3859E C3	-C.3816E 02	C.4252E 01	C.5486E 01
C.54C7E CC	C.8533E-C1	C.4614E-01	C.3215E-C0	C.8CCCE-C3	C.1C91E-01	C.2457E-C2	C.3456E-C1	C.7849E-02	C.3277E-03
C.2489E C3	C.1C47E C1	C.2126E-C3	C.1276E-C3	C.5694E CC	C.1CCCE 01	C.7871E C3	-C.2433E 02	C.4419E-0C	C.9558E 00
C.2745E C1	C.3916E C2	-C.3252E 01	C.2533E C2	C.3162E-CC	C.1CCCE 01	C.2309E-CC	C.2489E C3	C.2489E C3	C.3162E-00
-C.	C.1CCCE C1	C.7871E C3	C.7852E C4	C.849CE C2	-C.2243E-02	C.1421E-01	C.6124E-03	C.1519E-00	C.4500E-00

B.5d) Typical Input Data for Mean Flow Program (NTYPE 2)

```
$DATA
    1     2 5153.     402.      6.14        .762
5.          1.006                9 .537
.26  .0   .05  .1   .15  .2   .22  .26  .335
2.02 .185 .23  .37  .69  1.19 1.4  1.83 2.02
402. 359. 362. 369. 383. 399. 405. 402. 402.
$ENDJOB
```

B.5e) Typical Output Data for Mean Flow Program (NTYPE 2)

```
NCSF= 1  NTYPE= 2  PC=  0.5153E 04    TC=  0.402CE C3   MFS=  C.614CE 01  CIA=  0.762CE CC  SF= -C.            PTM -C.
RECFS=  C.7832E 04  REFS=  C.5480E C5  TFS=  0.47C7E C2  CC=  C.5551E-C2   FFS=  C.2831E C1  CFS=  C.1016E C3  CFS=  0.2792E-04
LFS=  0.8446E C5    CLFS=  C.2358E C1

XC=      C.5CCCE C1  PPG=      0.1006E 01  PIBM=       C.5370E-C3  NPTS=    9  XCL= -C.           XCT= -C.
    YC          TT          PPM          FIBM         RECM         M            C            P            PT           TTTTE
    LLE         TTE         CCE          CUCUE        KN           RE           RET          LDEF         CCEF         TTFS
    LLFS        CCFS        CLDUFS       FPP          PPC          MCEF         EDEF         CIST         MCMT         EMT
    YB          PSI1        MLT          FM           YCEL1        DEL5         YBCEL3       TOEF         LCEL         CCEL
    TCEL        LCIF        CCIF         TCIF         CEL3         DEL4         LMLDML       YBDEL4       YBDEL5       CEL2
    TTDEF       TTCIF       YBCEL2       RW2          RM2          PSI          CMCMT        EMTM         C            YBC

  C.26C0E-CC  0.4C20E C3  0.2020E-01  0.5370E-03  C.491CE C1  C.5372E 01  0.7556E 02  C.9713E C0  C.4314E-CC  0.1C00E 01
  C.1CCCE C1  C.1COCE C1  C.1C00E C1  0.1CCCE 01  C.7239E CC  C.33C2E 05  C.5928E C4 -C.3816E C2  C.4252E C1  0.1261E 01
  C.5825E CC  C.77C3E C0  0.7568E C0  C.2658E-C1  C.2CC8E-C1  C.          0.          C.          C.          C.
  C.          C.1C47E C1  0.2294E-03  0.1276E-03  C.1CCCE C1  C.1CCCE 01  C.7871E C3 -C.2433E 02  0.4419E-00  C.9558E 00
  C.2749E C1  0.3916E C2 -0.3252E 01  C.2533E C2  C.2236E C1  C.1CCCE 01  C.95C6E 0C  C.2489E 03  0.2489F 03  0.2236E C1
 -C.          C.1CCCE C1  0.7871E C3  0.7852E C4  C.849CE C2 -C.2243E-02  C.1421E-01  C.6124E-03  C.1519E-CC  C.45C0E-G0

 -C.          C.359CE C3  C.1850E-02  0.5370E-C3  C.491CE C1  C.15C9E 01  C.5959E C1  C.97C8E CC  C.1984E-02  0.8930E 00
  C.5726E CC  0.4155E C1  0.2405E-00  0.1377E-C0  C.5669E C1  C.1184E 04  C.8861E C3  C.          C.          0.5240E 01
  C.5626E CC  0.1853E-C0  C.1042E-00  0.2901E-CC  C.1839E-C2  C.5887E-01  C.1473E-C1  C.          C.          0.
  C.         -C.          C.2114E-03  0.1276E-C3 -C.          C.6819E 01  C.3676E C1  C.          0.4274E-0C  0.7595E 00
  C.3155E C1  C.1C00E C1  0.1C00E 01  C.10CCE 01  C.2236E C1  C.6256E 01  0.5028E CC  C.          0.          0.2236E 01
  C.          0.1C00E C1  0.3676E 01  0.5474E 01  C.1CC4E-CC -C.2243E-02  0.          C.          C.9237E 0C  0.

  C.5CC0E-C1  0.362CE C3  0.2300E-C2  0.5370E-C3  C.491CE C1  C.1715E 01  0.7691E 01  C.97C5E CC  0.2691E-C2  C.9C05E 00
  C.6255E CC  C.3E4CE C1  0.2602E-00  C.1627E-CC  C.5112E C1  C.1492E 04  C.1041E C4  C.1237E-C0  0.2587E-C1  0.4843E 01
  C.6145E CC  C.2C04E-CC  0.1232E-C0  C.2332E-C0  C.2286E-02  C.6095E-01  C.1619E-C1  C.4249E-01  0.2995E-C2  0.7731E-03
  C.2218E C1  0.5685E-C2  0.2126E-03  0.1276E-03  C.1923E-CC  C.6819E 01  0.9918E C0  C.9987E-01  C.3745E-0C  C.7398E 00
  C.284CE C1  C.8763E CC  C.9741E C0  C.9C01E CC  C.2236E C1  C.6256E 01  0.557CE CC  C.3545E-CC  C.3252E-0C  0.2236E 01
  C.6977E-C1  0.9302E CC  0.9918E C0  0.5474E 01  C.1CC4E-CC -0.2243E-02  0.2227E-02  C.5851E-C3  C.9368E CC  0.2146E 01

  C.1CCCE-CC  C.369CE C3  0.37C0E-02  0.5370E-03  C.491CE C1  C.2232E 01  C.1303E 02  C.97C5E 0C  0.5993E-02  0.9179E 00
  C.7331E CC  C.3114E C1  0.3208E-C0  0.2352E-CC  C.3851E C1  C.2579E 04  C.1484E C4  C.3756E-C0  0.1058E-CC  0.3927E 01
  C.72C3E CC  C.2471E-CC  0.1780E-C0  0.1450E-CC  C.3678E-C2  C.6278E-01  C.1931E-C1  C.8254E-C1  C.6088E-C2  0.1661E-02
  C.4791E C1  C.1321E-C1  0.2156E-03  0.1276E-03  C.3846E-CC  C.6819E 01  C.2143E 01  C.330CE-CC  0.2669E-0C  0.6792E 00
  C.2114E C1  0.6244E C0  0.8942E 00  0.67C0E CC  C.2236E C1  C.6256E 01  C.6735E 00  C.7658E 0C  C.7026E 0C  0.2236E 01
  C.2326E-CC  0.7674E CC  0.2143E 01  C.5474E C1  C.1CC4E-CC -C.2243E-02  C.4527E-02  C.1257E-02  C.9664E 0C  C.471CE 01

  C.15CCE-CC  C.383CE C3  0.6900E-02  0.5370E-C3  C.491CE C1  C.31C1E 01  C.2517E C2  C.9715E CC  C.2278E-01  0.9527E 00
  C.8575E CC  C.2208E C1  C.4531E-00  C.3885E-CC  C.2365E C1  C.5832E C4  C.2385E 04  C.6666E 00  0.2798E-0C  0.2784E C1
  C.8425E CC  0.349CE-C0  0.2940E-C0  0.7782E-01  C.6859E-C2  C.5536E-01  C.1836E-01  C.1169E-C0  C.9042E-02  0.2602E-02
  C.8219E C1  C.2502E-C1  0.2215E-C3  0.1276E-C3  C.5769E CC  C.6819E 01  C.3676E 01  C.6173E CC  C.1425E-0C  C.5469E 00
  C.12C8E C1  0.3334E-C0  0.7202E C0  C.3827E-CC  C.2236E C1  C.6256E 01  0.8122E CC  C.1314E 01  C.1205E 01  0.2236E 01
  C.5581E CC  0.4419E-CC  C.3676E 01  0.5474E 01  C.1CC4E-CC -C.2243E-02  C.6724E-C2  C.197CE-C2  0.9964E 00  0.82C4E 01

  C.2CCCE-CC  0.399CE C3  C.1190E-01  C.5370E-C3  C.491CE C1  C.41C5E 01  C.4412E 02  C.9714E CC  0.9312E-01  0.5925E 00
  C.9476E CC  0.1538E C1  C.6502E C0  0.6162E CC  C.1377E C1  C.1326E 05  C.3672E C4  C.8775E 0C  0.5394E CC  0.1940E 01
  C.9311E CC  C.5C08E C0  0.4663E-C0  0.4512E-01  C.1183E-C1  C.3226E-01  C.4598E-C2  C.1418E-C0  0.1123E-01  0.3176E-02
  C.1311E C2  0.4402E-C1  0.2282E-03  0.1276E-03  C.7692E CC  C.6819E 01  C.5861E 01  C.8295E 0C  0.5236E-01  0.3498E-00
  C.5381E 00  0.1225E-C0  0.4606E-00  0.1705E-00  0.2236E 01  0.6256E 01  0.8988E 00  0.2095E 01  0.1922E C1  0.2236E 01
  C.93C2E CC  0.6977E-C1  0.5861E C1  C.5474E C1  C.1CC4E-CC -C.2243E-02  C.8352E-02  C.2404E-02  0.9977E CC  0.1309E 02

  C.22CCE-CC  0.4C5CE C3  0.1400E-C1  C.537CE-C3  C.491CE C1  C.446CE 01  0.52C8E C2  C.9712E CC  C.1469E-CC  0.1C07E 01
  C.9719E CC  C.137CE C1  C.7296E C0  0.7C91E CC  C.1161E C1  C.17C9E 05  C.4181E C4  C.9342E CC  C.6440E 0C  0.1728E 01
  C.9549E CC  C.562CE C0  0.5367E 00  0.3834E-C1  0.1392E-C1  C.1993E-01 -0.5292E-02  C.1486E-C0  0.1175E-01  C.3169E-02
  C.1855E C2  0.5405E-C1  0.2306E-03  C.1276E-C3  C.8462E CC  C.6819E 01  0.6954E 01  C.8826E C0  0.2810E-C1  0.2704E-00
  C.37C4E-CC  0.6576E-C1  0.356CE-00  0.1174E-CC  C.2236E C1  C.6256E 01  C.9234E CC  C.2485E C1  C.228CE 01  0.2236E 01
  C.1C7CE C1 -C.6977E-C1  0.6954E C1  C.5474E C1  C.1CC4E-CC -C.2243E-02  0.8741E-02  C.2399E-02  0.9995E C0  C.1555E 02

  C.26CCE-CC  C.4C20E C3  0.1830E-01  C.5370E-C3  C.225CE C1  C.511CE 01  C.6836E 02  C.9715E C0  0.3206E-0C  0.1C0CE 01
  C.9923E CC  0.1C89E C1  C.9188E C0  C.9118E CC  C.8218E CC  C.2766E 05  C.5405E 04  C.982CE 0C  C.8931E CC  C.1373E 01
  C.975CE CC  C.7078E C0  0.6901E C0  0.2934E-01  C.1819E-C1  C.7C2CE-02  C.          C.1562E-CC  0.1229E-C1  C.3064E-02
```

C.2139E C2	0.7859E-C1	C.2294E-03	0.1276E-C3	C.1CCCE C1	C.6819E 01	C.9566E C1	C.9719E CC	C.7699E-C2	0.e115E-01
C.6855E-C1	0.1801E-C1	0.1069E-CO	C.28C6E-01	C.2236E C1	C.6256E 01	C.9433E CC	C.3415E 01	C.3137E 01	C.2236E 01
C.1CCCE C1	C.	0.9566E C1	C.5474E C1	C.1CC4E-CC	-C.2243E-02	C.9141E-C2	C.2319E-C2	C.1CCCE C1	C.2139E 02
C.335CE-CC	0.4C2CE C3	C.2C2CE-C1	0.537CE-C3	C.15CCE C1	C.5372E 01	C.7556E C2	C.9713E CC	C.4314E-CC	C.1CCCE 01
C.1CCCE C1	C.1CCCE C1	C.1CCCE 01	C.1CCCE 01	C.7235E CC	C.33C2E 05	C.5528E C4	C.1CCCE C1	C.1CCCE C1	C.12C1E 01
C.5825E CC	0.77C3E CC	C.7568E CO	C.2658E-C1	C.2CCEE-C1	C.	C.	C.1555E-CC	C.1256E-01	C.3C64E-02
C.3414E C2	C.1328E-CC	C.2294E-C3	C.1276E-C3	C.128EE C1	C.6819E 01	C.1527E C2	C.1CCCE C1	C.	C.
C.	C.	C.	C.	C.2236E C1	C.6256E 01	C.95C6E CC	C.5457E 01	C.5CC6E C1	C.2236E 01
C.1CCCE C1	C.	C.1527E 02	C.5474E 01	C.1CC4E-CC	-C.2243E-02	C.9337E-02	C.2319E-C2	C.1CCCE C1	C.3414E 02

B.5f) Fortran Listing of Mean Flow Program

```
$IBFTC MAI      DECK
      DIMENSION TV(200), MUV(200), YD(50), PPM(50), TT(50), REOM(50)  ,
     1FV(200),MFV(200),PPPV(200),MV(200),PPV(200),MPV(200)
      COMMON /TABLE/TV,MUV,PPPV,MV,MFV,FV,PPV,MPV
      REAL MFS,MUFS,MUO,M,MU,MV,MS,MUT,MUV,KN,MDEF,MOMT,MDEFS ,MFV,M1,M2
     1,MPV
      C1=1.36*980./2.871E06
      C2=SQRT(1.4*2.871)*1000.
      C3=1.36*.7/1.2**3.5
      C4=SQRT(3.1416*.7)
 1000 READ (5,1) NOSP, NTYPE, PO, TO, MFS, DIA,SF,PTM
    1 FORMAT (2I5,6F10.0)
      WRITE (6,6) NOSP, NTYPE, PO, TO, MFS, DIA,SF,PTM
    6 FORMAT (1H1,1X5HNOSP=,I2,2X6HNTYPE=,I2,2X3HPO=,E12.4,4X3HTO=,
     1E12.4,3X4HMFS=,E12.4,2X4HDIA=,E12.4,2X3HSF=,E12.4,4X3HPTM,E12.4)
      TEMP = 1. + MFS**2/5.
      TEMP7 = TEMP**3.5
      TFS = TO / TEMP
      DO=C1*PO/TO
      DFS = DO/TEMP**2.5
      UFS=SQRT(TFS)*MFS*C2
      QFS=DFS*UFS**2/1960.
      DUFS = DFS*UFS
      CALL TBLKP(TFS,TV,MUFS,MUV,44)
      MUFS=MUFS*1.0E-7
      CALL TBLKP(TO,TV,MUO,MUV,44)
      MUO=MUO*1.0E-7
      REFS = DFS*UFS*DIA/MUFS
      REOFS = REFS*MUFS/MUO
      PFS=PO/TEMP7
      WRITE (6,7) REOFS,REFS,TFS,DO,PFS,QFS,DFS,UFS,DUFS)
    7 FORMAT (1X6HREOFS=,E12.4,2X5HREFS=,E12.4,2X4HTFS=,E12.4,2X3HDO=,
     1E12.4,3X4HPFS=,E12.4,2X4HQFS=,E12.4,2X4HDFS=,E12.4/
     21X4HUFS=,E12.4,4X5HDUFS=,E12.4)
C     PROFILE DATA CALCULATION
      NOS=1
      GO TO (10,20), NTYPE
   10 READ (5,2) XD, PPG, NPTS,XOU,XOT,REOO
    2 FORMAT (2F10.4,I10,3F10.4)
      WRITE (6,16) XD, PPG, NPTS,XOU,XOT,REOO
   16 FORMAT (1HO,1X3HXD=,E12.4,2X4HPPG=,E12.4,2X5HNPTS=,I5,
     12X4HXOU=,E12.4,2X4HXOT=,E12.4,2X5HREOO=,E12.4/5X2HYD,
     211X2HTI,11X3HPPM,10X4HPIBM,9X4HREOM,9X1HM,12X1HQ,12X1HP,12X2HPT,
     311X5HTTTTE/5X3HUUE,10X3HTTE,10X3HDDE,10X5HDUDUE,8X2HKN,11X2HRE,
     411X3HRET,10X4HUDEF,9X4HDDEF,9X4HTTFS/5X4HUUFS,9X4HDDFS,9X6HDUDUFS,
     57X3HPPP,10X3HPPC,10X4HMDEF,9X4HEDEF,9X4HDIST,9X4HMOMT,9X3HEMT/
     65X2HYB,11X4HPSI1,9X3HMUT,10X2HFM,11X5HYDEL1,8X4HDEL5, 9X6HYBDEL3,
     77X4HTDEF,9X4HUDEL,9X4HDDEL/5X4HTDEL,9X4HUDIF,9X4HDDIF,9X4HTDIF,
     89X4HDEL3,9X4HDEL4,9X6HDMUDMU,7X6HYBDEL4,7X6HYBDEL5,7X4HDEL2/
     95X5HTTDEF,8X5HTTDIF,8X6HYBDEL2,7X3HRW2,10X3HRH2,10X3HPSI,
     110X5HQMOMI,8X4HEMIM,9X1HC,12X3HYBC)
      READ (5,3) (YD(I), I=1,NPTS)
      READ (5,3) (PPM(I), I=1,NPTS)
      READ (5,3) (TT(I), I=1,NPTS)
      READ (5,3) (REOM(I), I=1,NPTS)
    3 FORMAT (16F5.0)
      GO TO 30
   20 READ (5,2) XD, PPG, NPTS,PIBM,XOU,XOT
      PIBM = PIBM*.001
      WRITE (6,8) XD, PPG, PIBM, NPTS,XOU,XOT
    8 FORMAT (1HO,1X3HXD=,E15.4,2X4HPPG=,E15.4,2X5HPIBM=,E15.4,
```

```
     12X5HNPTS=,I5,2X4HXOU=,E12.4,2X4HXOT=,E12.4/5X2HYD,
     211X2HTT,11X3HPPM,10X4HPIBM,9X4HREOM,9X1HM,12X1HQ,12X1HP,12X2HPT,
     311X5HTTTTE/5X3HUUE,10X3HTTE,10X3HDDE,10X5HDUDUE,8X2HKN,11X2HRE,
     411X3HRET,10X4HUDEF,9X4HDDEF,9X4HTTFS/5X4HUUFS,9X4HDDFS,9X6HDUDUFS,
     57X3HPPP,10X3HPPC,10X4HMDEF,9X4HEDEF,9X4HDIST,9X4HMOMT,9X3HEMT/
     65X2HYB,11X4HPSI1,9X3HMUT,10X2HFM,11X5HYDEL1,8X4HDEL5, 9X6HYBDEL3,
     77X4HTDEF,9X4HUDEL,9X4HDDEL/5X4HTDEL,9X4HUDIF,9X4HDDIF,9X4HTDIF,
     89X4HDEL3,9X4HDEL4,9X6HDMUDMU,7X6HYBDEL4,7X6HYBDEL5,7X4HDEL2/
     99X5HTTDEF,8X5HTTDIF,8X6HYBDEL2,7X3HRW2,10X3HRH2,10X3HPSI,
     110X5HQMOMT,8X4HEMTM,9X1HC,12X3HYBC)
      READ (5,3) (YD(I), I=1,NPTS)
      READ (5,3) (PPM(I), I=1,NPTS)
      READ (5,3) (TT(I), I=1,NPTS)
   30 DIST = 0.
      MOMT = 0.
      EMT = 0.
      YB = 0.
      MDEF=0.
      EDEF=0.
      TTTTE=1.
      UUE=1.
      TTE=1.
      DDE=1.
      DUDUE=1.
      N=0
      DEL1=YD(1)
      DEL2=SQRT(XD+XOU)
      DEL3=SQRT(XD+XOT)
      DEL4=1.0
      DEL5=1.0
      I=1
   29 YDI=YD(I)
      YDEL1=YDI/DEL1
      PPM(I) = PPM(I)*.01
      IF (I .EQ. 1) GO TO 31
      IF (I .LE. N) GO TO 32
   31 GO TO (40,50), NTYPE
   32 PPM(I)=PPM(I)/.01
      GO TO 31
   40 CALL TBLKP(TT(I),TV,MUT,MUV,44)
      MUT=MUT*1.0E-7
      IF (SF-1.0) 45,43,43
   43 IF (SF - 100.) 47,47,44
   47 RME=REOM(1)
      REM=REOM(I)
      IF (REM-RE00) 45,46,46
   46 IF (REM-RME) 45,44,44
   44 PPPI=PPM(I)/PTM
      CALL TBLKP(PPPI,PPV,M,MPV,101)
      GO TO 60
   45 FM=REOM(I)*MUT*SQRT(TT(I))/PPM(I)*PPG/P0
      F=FM*1.0E04
      IF (F-.85) 41,41,42
   41 FM = .000085
      REOM(I)=(FM*PPM(I)*P0)/(MUT*SQRT(TT(I))*PPG)
      M=8.0
      GO TO 60
   42 CALL TBLKP(F,FV,M,MFV,101)
      GO TO 60
   50 PPP = PIBM / PPM(I)
      CALL TBLKP(PPP,PPPV,M,MV,111)
```

```
      CALL TBLKP(TT(I), TV,MUT,MUV,44)
      MUT=MUT*1.0E-7
   60 MS = M**2
      TEMP1 = MS/5.
      TEMP2 = 5. / (6.*MS)
      PPC = PPM(I) / PPG
      IF (M-1.) 64,64,65
   64 Q=.7*1.36*P0*PPC*(M**2.)*(5./(5.+M**2.))**3.5
      GO TO 66
   65 TEMP5 = ((7.*MS-1.) /(6.*MS))**2.5
      TEMP6 = ((7.*MS-1.)/6.)**2.5
      Q=C3*P0*PPC*TEMP5
   66 TTFS = TT(I) / TFS/(1.+TEMP1)
      GO TO (61,62), NTYPE
   61 IF (SF-1.0) 71,62,62
   71 DUDUFS = (REOM(I)*MUT)/(.000254*DUFS)
      UUFS = Q/(QFS*DUDUFS)
      GO TO 63
   62 UUFS = M / MFS*SQRT(TTFS)
      DUDUFS = Q / QFS / UUFS
   63 DDFS = DUDUFS / UUFS
      CALL TBLKP(TTFS*TFS,TV,MU,MUV,44)
      MU=MU*1.0E-7
      DMUDMU  =DUDUFS*MU/MUFS
      RET = DUDUFS*DFS*UFS*DIA/MUT
      RE = RET*MUT / MU
      IF (M-1.) 67,67,68
   67 P=PPC*TEMP7*(5./(5.+M**2.))**3.5
      PT=PPC
      GO TO 69
   68 P = PPC*TEMP7*(TEMP2)**3.5*TEMP6
      PT = PPC*(1./6.+TEMP2)**3.5*TEMP6
   69 PPP = P / PPC/TEMP7
      KN = C4*M*.762/(RE*.000254)
      IF(I .NE. 1) GO TO 70
      UE = UUFS
      TE = TTFS
      DE = DDFS
      FMUE=MU
      TTOE = TT(I)
      GO TO 90
   70 IF(I .NE. 2) GO TO 80
      UCL = UUFS
      DCL = DDFS
      TCL=TTFS
      TTCL=TT(I)
      RW2=1./(1.-(UCL/UE))**2.
      RH2=1./((TCL/TE)-1.)**2.
   80 UUE = UUFS / UE
      DDE = DDFS / DE
      DUDUE = DUDUFS / DE / UE
      C=DDE*MU/FMUE
      MDEF = DUDUE*(1.-UUE)
      TTTTE = TT(I) / TTOE
      TTE = TTFS / TE
      EDEF = DUDUE*(1.-TTTTE)
      UDEF = (UUFS-UCL) / (UE-UCL)
      DDEF = (DDFS-DCL) / (DE-DCL)
      TDEF=(TCL-TTFS)/(TCL-TE)
      TTDEF=(TT(I)-TTCL)/(TTOE-TTCL)
      UDEL=(UE-UUFS)/UE
```

```
      DDEL=(DE-DDFS)/DE
      TDEL=(TTFS-TE)/TE
      UDIF=1.-UDEF
      DDIF=1.-DDEF
      TDIF=1.-TDEF
      TTDIF=1.-TTDEF
      IF (I .EQ. 1) GO TO 100
      IF (I .EQ. 2) GO TO 98
      DELYD = YD(I) - YD(I-1)
      DIST = (2.-DUDUES-DUDUE) / 2.*DELYD + DIST
      MOMT = (MDEFS+MDEF) / 2.*DELYD + MOMT
      EMT = ((1.-TTTTES)*DUDUES+(1.-TTTTE)*DUDUE) / 2.*DELYD+EMT
      YB =((DDES+DDE) / 2.*DELYD)*DE*UE*SQRT(REFS)+ YB
      YBDEL2=YB/DEL2
      YBDEL3=YB/DEL3
      YBDEL4=YB/DEL4
      YBDEL5=YB/DEL5
   98 GO TO (100,97), NTYPE
   97 IF (UDIF-TDIF) 99,99,109
   99 IF (DEL4-1.0  ) 101,101,102
  102 IF (DEL5 .EQ. 1.0) GO TO 109
      IF (DEL4 .EQ. 1.0) GO TO 99
      GO TO 100
  101 IF (UDIF-.500) 103,104,105
  104 DEL4=YB
      IF (DEL5 .EQ. 1.0) GO TO 109
      GO TO 4
  105 DUDUES=DUDUE
      MDEFS=MDEF
      TTTTES=TTTTE
      DDES=DDE
      UDIF0=UDIF
      TDIF0=TDIF
      YB0=YB
      NI1=I+1
      IF (NI1 .NE. NPTS) GO TO 200
      I=100
      DEL4=2.
      DEL5=2.
      GO TO 4
  200 GO TO 5
  103 DEL4=YB0+(YB -YB0)*(UDIF0-.500)/(UDIF0-UDIF)
      IF (DEL5 .EQ. 1.0) GO TO 109
      GO TO 4
  109 IF (DEL5-1.0) 111,111,102
  111 IF (TDIF-.500) 113,114,105
  114 DEL5=YB
      IF (DEL4 .EQ. 1.0) GO TO 99
      GO TO 4
  113 DEL5= YB0+(YB-YB0)*(TDIF0-.5)/(TDIF0-TDIF)
      IF (DEL4 .EQ. 1.0) GO TO 99
    4 N=I
      I = 1
      YB = 0.0
      DIST =0.
      MOMT = 0.
      EMT =0.
      YBDEL4=0.0
      YBDEL5=0.0
      GO TO 5
  100 DUDUES = DUDUE
```

```
      MDEFS = MDEF
      TTTTES = TTTTE
      DDES = DDE
      QMOMT=MOMT*UE*UE*DE
      EMTM=EMT*DE*UE
      YBC=YB*SQRT(C)
      PSI1=UE*DE*(YD(I)-DIST)
      IF (SF-1.0) 90,89,89
   89 PSI=(DEL1+UE*DE*(DIST-YD(I)))
      YBC=DEL1-YDI
   90 WRITE (6,9) YD(I),TT(I),PPM(I),PIBM,REQM(I),M,Q,P,PT,TTTTE
     1,UUE,TTE,DDE,DUDUE,KN,RE,RET,UDEF,DDEF,TTFS,UUFS,
     2 DDFS,DUDUFS,PPP,PPC,MDEF,EDEF,DIST,MOMT,EMT,YB ,PSI1,MUT ,FM,
     3YDEL1,DEL5 ,YBDEL3,TDEF,UDEL,DDEL,TDEL,UDIF,DDIF,TDIF,DEL3,DEL4,
     4DMUDMU,YBDEL4,YBDEL5,DEL2,TTDEF,TTDIF,YBDEL2,RW2,RH2,PSI,QMOMT,
     5EMTM,C,YBC
    9 FORMAT (1H0,10E13.4/(1X,10E13.4))
    5 I=I+1
      NI =I-1
      IF (NI .NE. NPTS) GO TO 29
      NOS=NOS+1
      IF (NOS .GT. NOSP ) GO TO 1000
      GO TO (10,20),NTYPE
      END
```

```
$IBFTC BLO      DECK
      BLOCK DATA
      REAL MV,MUV,MFV,MPV
      DIMENSION TV(200),MUV(200),PPPV(200),MV(200),MFV(200),FV(200),
     1PPV(200),MPV(200)
      COMMON /TABLE/TV,MUV,PPPV,MV,MFV,FV,PPV,MPV
C     TABLE 1 --- MU=F(T)
      DATA (  TV(I),I = 1,44)/ 0.0,30.,40.,50.,60.,70.,80.,90.,100.,110.
     1 ,120.,130.,140.,150.,160.,170.,180.,190.,200.,210.,220.,230.,240.
     2 ,250.,260.,270.,280.,290.,300.,310.,320.,330.,340.,350.,360.,370.
     3 ,380.,390.,400.,410.,420.,430.,440.,450./
      DATA (  MUV(I),I = 1,44)/0.0,215.7,281.1,347.3,416.3,485.6,555.1,
     1622.9,692.9,763.3,831.9,899.0,964.6,1029.,1091.,1152.,1212.,1271.,
     2 1329.,1385.,1440.,1494.,1547.,1599.,1650.,1700.,1750.,1798.,1846.
     3 ,1893.,1939.,1985.,2030.,2075.,2118.,2160.,2202.,2245.,2286.,2327
     4 .,2366.,2406.,2445.,2485./
C     TABLE 2 --- M=F(P/PFS)
      DATA (PPPV(I),I=1,111)/.007739,.007896,.008057,.008224,.008394,
     1.008572,.008754,.008943,.009138,.009338,.009546,.009761,.009983,
     1.01021,.01045,.01070,.01095,.01122,.01149,.01177,
     1                    .01207, .01222,.01237,.01253,.01269,
     1 .01285,.01302,.01319,.01336,.01354,.01372,.01409,.01448,.01488,
     2 .01530,.01574,.01619,.01667,.01716,.01768,.01823,.01880,.01939,
     3 .02002,.02067,.02136,.02208,.02284,.02364,.02449,.02537,.02631,
     4 .02730,.02834,.02945,.03062,.03187,.03319,.03459,.03609,.03768,
     5 .03938,.04120,.04314,.04523,.04747,.04987,.05247,.05526,.05829,
     6 .06157,.06513,.06900,.07323,.07785,.08291,.08848,.09461,.1014,
     7 .1089,.1173,.1266,.1371,.1489,.1622,.1773,.1945,.2142,.2368,
     8 .2628,.2930,.3280,.3685,.4159,.4689,.5283,.5913,.6560,.7209,
     9 .7840,.8430,.8956,.9183,.9395,.9575,.9725,.9844,.9930,.9983,
     1 .9994,1.0/
      DATA (MV(I),I=1,111) /10.,9.9,9.8,9.7,9.6,9.5,9.4,9.3,9.2,9.1,9.0,
     18.9,8.8,8.7,8.6,8.5,8.4,8.3,8.2,8.1,
     1                    8.0,7.95,7.90,7.85,7.80,7.75,7.70,7.65,
     1 7.60,7.55,7.5,7.4,7.3,7.2,7.1,7.0,6.9,6.8,6.7,6.6,6.5,6.4,6.3,
     2 6.2,6.1,6.0,5.9,5.8,5.7,5.6,5.5,5.4,5.3,5.2,5.1,5.0,4.9,4.8,4.7,
     3 4.6,4.5,4.4,4.3,4.2,4.1,4.0,3.9,3.8,3.7,3.6,3.5,3.4,3.3,3.2,3.1,
     4 3.0,2.9,2.8,2.7,2.6,2.5,2.4,2.3,2.2,2.1,2.0,1.9,1.8,1.7,1.6,1.5,
     5 1.4,1.3,1.2,1.1,1.0,.9,.8,.7,.6,.5,.4,.35,.3,.25,.2,.15,.1,.05,
     6 .03,.0 /
C     TABLE 3 --- M=F(FM)
      DATA (FV(I), I=1,101) / .8385,.8388,.8392,.8397,.8399,.8404,.8406,
     1.8409,.8414,.8418,.8423,.8427,.8431,.8436,.8443,.8452,.8457,.8462,
     2.8467,.8473,.8480,.8485,.8491,.8497,.8504,.8513,.8521,.8530,.8539,
     3.8548,.8557,.8565,.8575,.8589,.8600,.8613,.8621,.8631,.8649,.8662,
     4.8676,.8691,.8706,.8721,.8742,.8762,.8780,.8798,.8819,.8843,.8865,
     5.8894,.8918,.8944,.8975,.9009,.9042,.9077,.9114,.9155,.9196,.9247,
     6.9299,.9343,.9403,.9464,.9523,.9596,.9667,.9753,.9837,.9933,
     71.0035,1.0149,1.0265,1.0403,1.0536,1.0695,1.0864,1.1046,1.1248,
     81.1357,1.1463,1.1583,1.1702,1.1830,1.1956,1.2090,1.2221,1.2371,
     91.2510,1.2663,1.2809,1.2961,1.3104,1.3244,1.3380,1.3494,1.3585,
     11.3664,1.3680/
      DATA (MFV(I),I=1,101)/10.,9.9,9.8,9.7,9.6,9.5,9.4,9.3,9.2,9.1,9.0,
     18.9,8.8,8.7,8.6,8.5,8.4,8.3,8.2,8.1,      8.0,7.9,7.8,7.7,7.6,
     1          7.5,7.4,7.3,7.2,7.1,7.0,6.9,6.8,6.7,6.6,6.5,6.4,6.3,
     2 6.2,6.1,6.0,5.9,5.8,5.7,5.6,5.5,5.4,5.3,5.2,5.1,5.0,4.9,4.8,4.7,
     3 4.6,4.5,4.4,4.3,4.2,4.1,4.0,3.9,3.8,3.7,3.6,3.5,3.4,3.3,3.2,3.1,
     4 3.0,2.9,2.8,2.7,2.6,2.5,2.4,2.3,2.2,2.1,2.0,1.95,1.9,1.85,1.8,
     11.75,1.7,1.65,1.6,1.55,1.5,1.45,1.4,1.35,1.3,1.25,1.2,1.15,1.1,
     11.05,1.0/
C     TABLE 4-----M=F(PPPT)
```

```
      DATA (PPV (I),I=1,101) /.003045,.003191,.003346,.003510,.003683,
     1.003866,.004061,.004267,.004486,.004718,.004964,.005226,.005504,
     1.005799,.006114,.006449,.006806,.007187,.007592,.008025,.008488,
     1.008982,.009510,.01008,.01068,.01133,.01202,.01277,.01357,
     1.01443,.01535,.01634,.01741,.01857,.01981,.02115,.02259,.02416,
     1.02584,.02767,.02965,.03180,.03412,.03664,.03938,.04236,.04560,
     1.04913,.05297,.05715,.06172,.06670,.07214,.07809,.08459,.09170,
     1.09948,.1080,.1173,.1276,.1388,.1510,.1645,.1792,.1953,.2129,
     1.2322,.2533,.2762,.3012,.3283,.3577,.3895,.4236,.4601,.4990,
     1.5401,.5833,.6281,.6742,.7209,.7442,.7674,.7902,.8127,.8346,
     1.8557,.8760,.8952,.9132,.9298,.9448,.9582,.9697,.9794,.9871,.9928,
     1.9967,.9989,.9999,1.0000/
      DATA (MPV(I),I=1,101)/10.,9.9,9.8,9.7,9.6,9.5,9.4,9.3,9.2,9.1,9.0,
     18.9,8.8,8.7,8.6,8.5,8.4,8.3,8.2,8.1,      8.0,7.9,7.8,7.7,7.6,
     1      7.5,7.4,7.3,7.2,7.1,7.0,6.9,6.8,6.7,6.6,6.5,6.4,6.3,
     2 6.2,6.1,6.0,5.9,5.8,5.7,5.6,5.5,5.4,5.3,5.2,5.1,5.0,4.9,4.8,4.7,
     3 4.6,4.5,4.4,4.3,4.2,4.1,4.0,3.9,3.8,3.7,3.6,3.5,3.4,3.3,3.2,3.1,
     4 3.0,2.9,2.8,2.7,2.6,2.5,2.4,2.3,2.2,2.1,2.0,1.95,1.9,1.85,1.8,
     11.75,1.7,1.65,1.6,1.55,1.5,1.45,1.4,1.35,1.3,1.25,1.2,1.15,1.1,
     11.05,1.0/
      END
```

```
$IBFTC TBL      DECK
       SUBROUTINE TBLKP(VO,VAR,FO,FCN,NO)
       DIMENSION VAR(100),FCN(100)
C                THIS SUBROUTINE PERFORMS TABLE LOOK-UP OPERATIONS.
       DO 100 I=1,NO
       VAR1=VAR(I)
       IF (VO-VAR1) 200,150,100
  100  CONTINUE
       WRITE (6,900)VO,NO
  900 FORMAT (34H VARIABLE EXCEEDS TABLE FOR VALUE E11.4,13H TABLE SIZE
      1=I5)
       FO =FCN(NO)
       GO TO 300
  150  FO=FCN(I)
       GO TO 300
  200  IF (I-1) 210,290,210
  210 I1=I-1
       TEMP=VO-VAR(I1)
       TEM1=VAR(I)-VAR(I1)
       RATIO=TEMP/TEM1
       FO=RATIO*(FCN(I)-FCN(I1))+FCN(I1)
       GO TO 300
  290  FO=FCN(I)
  300  RETURN
       END
```

C.1) ID Listing for Tabulated Mean Flow Data

D	D	reference length, inches
MFS	M_∞	free stream Mach number
P	p/p_∞	ratio of local static pressure to free stream static pressure
PITO	$\frac{p_{t2}}{p_o} \times 10^3$	ratio ($\times 10^3$), as corrected for tunnel gradient, of local Pitot pressure to free stream total pressure
PO	p_o	free stream total pressure, mm Hg
PPCE	$\frac{p_{t2e}}{p_o}$	ratio, as corrected for tunnel gradient, of edge Pitot pressure to free stream total pressure
PTM	$\frac{p_t}{p_o}$	ratio of local total pressure to free stream total pressure for region between shear layer edge and leading edge shock
REFS	$Re_{\infty D}$	free stream Reynolds number based on reference length
TO	T_o	free stream total temperature, ^oK
TT	T_t	local total temperature, ^oK
TTTTE	T_{t_e}/T_o	ratio of local total temperature to free stream total temperature
TW	T_W	wall temperature, ^oK
UUE	u/u_e	ratio of local velocity to edge velocity
XD	x/D	axial distance from base ratioed to reference length
YD	y/D	lateral distance from centerline ratioed to reference length

C.2) TABULATED MEAN FLOW DATA FOR FLAT PLATE MODEL (C=1,TAU=.0156)

MFS=6.04,P0=1261.,T0=403.,REFS=46490. ,D=1.

XD	=.5	.75	1.	1.5	2.	3.	4.	5.	7.	9.
P	=.998	1.02	1.03	1.06	1.07	1.08	1.07	1.05	1.04	1.06
PPCE	=26.8	27.1	27.2	27.9	28.2	28.7	28.8	29.1	28.7	28.7*.001

XD= .5			XD= .75			XD= 1.			XD= 1.5			XD= 2.		
YD	PITO	TTTTE	YD	PITO	TTTTE	YD	PITO	TTTTE	YD	PITO	TTTT	YD	PITO	TTTTE
.000	2.10	.888	.000	2.40	.901	.000	2.80	.906	.000	3.39	.913	.000	3.76	.916
.010	2.20	.896	.010	2.60	.906	.010	2.90	.908	.010	3.49	.913	.010	3.86	.918
.020	2.40	.911	.020	2.70	.913	.020	3.10	.918	.020	3.69	.923	.020	4.16	.926
.030	2.80	.928	.030	3.20	.928	.030	3.50	.933	.030	4.09	.940	.040	5.25	.963
.040	3.50	.950	.040	4.00	.945	.040	4.30	.950	.040	4.89	.958	.060	8.02	1.00
.050	4.70	.973	.050	5.10	.968	.050	5.50	.968	.050	6.08	.975	.079	13.4	1.02
.060	6.30	.993	.060	6.80	.985	.060	7.20	.988	.060	7.68	.995	.080	13.8	1.02
.070	9.00	1.01	.070	9.40	1.00	.070	9.70	1.00	.070	10.1	1.00	.100	23.0	1.01
.077	11.7	1.01	.080	13.5	1.01	.079	13.0	1.01	.080	13.9	1.02	.112	25.5	1.00
.080	13.2	1.01	.090	18.3	1.01	.080	13.7	1.01	.090	18.7	1.01	.120	26.2	1.00
.090	18.2	1.00	.100	23.0	1.00	.090	18.8	1.01	.100	23.5	1.01	.150	27.4	1.00
.105	24.0	1.00	.105	24.7	1.00	.100	23.4	1.00	.110	25.5	1.00	.200	27.9	1.00
.110	24.3	1.00	.120	25.8	1.00	.106	25.5	1.00	.120	26.3	1.00	.250	28.2	1.00
						.120	26.2	1.00	.150	27.3	1.00			
						.140	26.8	1.00	.200	27.6	1.00			
						.180	27.2	1.00	.250	27.9	1.00			

XD= 3.			4.			5.			7.			9.		
.000	4.51	.926	.000	4.99	.933	.000	5.48	.936	.000	6.34	.938	.000	7.46	.940
.010	4.70	.928	.010	5.09	.936	.010	5.48	.938	.010	6.34	.940	.010	7.46	.943
.020	4.90	.936	.020	5.28	.945	.020	5.76	.948	.020	6.52	.950	.020	7.64	.950
.040	5.88	.968	.040	6.24	.973	.040	6.61	.973	.040	7.27	.975	.040	8.20	.975
.060	8.33	.998	.060	8.16	.998	.060	8.03	1.00	.060	8.57	1.00	.060	9.32	1.00
.080	13.2	1.02	.080	12.4	1.02	.080	11.8	1.01	.080	11.7	1.01	.080	11.2	1.01
.085	15.0	1.02	.083	13.2	1.02	.087	13.9	1.02	.100	17.7	1.01	.100	14.0	1.01
.100	21.6	1.01	.100	20.1	1.01	.100	18.9	1.01	.120	23.1	1.00	.120	19.4	1.00
.122	26.3	1.00	.120	24.5	1.00	.120	24.4	1.00	.150	26.8	1.00	.150	26.6	1.00
.150	27.7	1.00	.128	25.2	1.00	.135	26.4	1.00	.200	27.7	1.00	.200	28.0	1.00
.200	28.4	1.00	.150	26.7	1.00	.150	27.2	1.00	.500	28.7	1.00	.500	28.7	1.00
.300	28.7	1.00	.200	28.3	1.00	.200	28.1	1.00						
			.400	28.8	1.00	.500	29.1	1.00						

0041 CARDS

MFS=6.07,P0=2558.,T0=404.,REFS=92760. ,D=1.

XD	=.5	.75	1.	1.5	2.	3.	4.	4.5	5.	5.5	6.	7.	8.	9.
P	=1.04	1.06	1.08	1.10	1.11	1.11	1.10	1.09	1.08	1.06	1.03	1.00	.989	.988
PPCE	=24.9	25.5	26.2	26.9	27.6	27.8	28.0	28.0	28.0	27.9	27.9	27.8	27.7	27.7*.001

XD=	.5			.75			1.			1.5			2.		
YD	PITO	TTTTE	YD	PITO	TTTTE	YD	PITO	TTTTE	YD	PITO	TTTT	YD	PITO	TTTTE
.000	1.72	.886	.000	2.12	.899	.000	2.53	.904	.000	3.11	.911	.000	3.60	.913
.010	1.93	.886	.010	2.22	.908	.010	2.63	.908	.010	3.21	.916	.010	3.70	.918
.020	2.33	.913	.020	2.73	.926	.020	3.13	.926	.020	3.71	.933	.020	4.30	.936
.030	3.35	.951	.030	3.74	.948	.030	4.25	.951	.030	4.82	.958	.030	5.20	.951
.040	5.07	.980	.040	5.56	.978	.040	6.06	.975	.040	6.62	.980	.040	7.00	.973
.050	7.81	1.00	.050	8.79	.998	.050	9.40	.995	.050	9.84	.995	.050	10.0	.988
.057	11.0	1.01	.060	14.2	1.01	.060	14.5	1.01	.060	14.3	1.01	.060	14.0	1.01
.060	13.2	1.01	.070	19.7	1.01	.070	20.2	1.01	.070	19.0	1.01	.065	16.3	1.01
.070	18.8	1.00	.080	23.5	1.00	.080	24.0	1.00	.080	23.9	1.00	.070	18.8	1.01
.077	21.5	1.00	.090	24.7	1.00	.090	25.2	1.00	.085	25.0	1.00	.080	23.5	1.01
.080	22.5	1.00	.100	25.2	1.00	.100	25.7	1.00	.090	25.5	1.00	.087	25.0	1.00
.090	23.8	1.00	.120	25.5	1.00	.120	26.2	1.00	.100	26.0	1.00	.090	25.3	1.00
.100	24.3	1.00	.140	24.8	1.00	.150	26.0	1.00	.120	26.5	1.00	.100	26.2	1.00
.110	23.7	1.00				.170	25.7	1.00	.150	26.9	1.00	.120	26.9	1.00
.118	22.8	1.00				.185	24.0	1.00	.200	26.9	1.00	.150	27.4	1.00
												.200	27.6	1.00

XD=	3.			4.			4.5			5.			5.5	
.000	4.39	.923	.000	5.28	.931	.000	6.12	.933	.000	7.15	.933	.000	8.52	.933
.010	4.49	.928	.010	5.37	.936	.010	6.41	.936	.010	7.44	.936	.010	8.81	.936
.020	5.07	.941	.020	6.24	.938	.020	7.17	.953	.020	8.20	.940	.020	9.47	.943
.030	6.05	.955	.030	7.29	.951	.040	10.0	.968	.040	10.9	.968	.040	11.6	.968
.040	7.81	.973	.040	9.31	.970	.060	14.2	.993	.060	14.6	.990	.060	14.9	.988
.050	10.5	.988	.050	11.5	.985	.080	20.0	.998	.080	19.6	1.00	.080	18.8	.998
.060	14.2	.998	.060	14.1	.993	.100	24.5	1.00	.100	23.6	1.00	.100	22.6	1.00
.069	17.6	1.01	.070	17.1	.995	.120	26.2	1.00	.120	25.9	1.00	.120	25.2	1.00
.070	17.9	1.00	.080	20.6	.998	.150	27.3	1.00	.150	27.3	1.00	.150	26.9	1.00
.080	22.3	1.00	.090	23.8	.998	.200	27.6	1.00	.200	27.7	1.00	.200	27.6	1.00
.090	24.6	1.00	.100	25.2	1.00	.400	28.0	1.00	.400	28.0	1.00	.400	27.9	1.00
.095	25.4	1.00	.120	26.4	1.00									
.100	25.9	1.00	.150	27.2	1.00									
.120	26.8	1.00	.200	27.5	1.00									
.150	27.3	1.00	.400	28.0	1.00									
.200	27.6	1.00												
.300	27.8	1.00												

XD=	6.			7.			8.			9.	
.000	10.1	.936	.000	13.2	.946	.000	15.3	.953	.000	16.6	.960
.010	10.2	.938	.010	13.3	.948	.010	15.4	.955	.010	16.7	.960
.020	10.6	.946	.020	13.5	.951	.020	15.5	.958	.020	16.7	.963
.040	12.2	.970	.040	14.4	.968	.040	16.1	.970	.040	17.1	.970
.060	15.1	.988	.060	16.0	.985	.060	17.0	.985	.060	17.8	.983
.080	18.3	.998	.080	18.2	.998	.080	18.4	.995	.080	18.6	.990
.100	21.6	1.00	.100	20.5	1.00	.100	20.0	1.00	.100	19.6	.998
.120	24.4	1.00	.120	22.7	1.00	.120	21.5	1.00	.120	20.8	1.00
.150	26.5	1.00	.150	25.3	1.00	.150	24.1	1.00	.150	22.9	1.00
.200	27.4	1.00	.200	27.1	1.00	.200	26.6	1.00	.200	25.7	1.00
.400	27.9	1.00	.500	27.8	1.00	.500	27.7	1.00	.500	27.7	1.00

0057 CARDS

MFS=6.08,P0=3857.,T0=404.,REFS=139300.,D=1.

XD	.5	.75	1.	1.5	2.	3.	3.5	4.	4.5	5.	6.	7.	9.
P	1.03	1.06	1.07	1.08	1.10	1.10	1.09	1.07	1.05	1.03	1.00	.993	1.01
PPCE	26.0	26.5	27.1	27.7	28.3	28.5	28.6	28.5	28.5	28.6	28.6	28.7	28.8*.001

XD= .5			.75			1.			1.5			2.		
YD	PITO	TTTTE	YD	PITO	TTTTE	YD	PITO	TTTTE	YD	PITO	TTTT	YD	PITO	TTTTE
.000	1.72	.876	.000	2.12	.886	.000	2.42	.896	.000	3.01	.906	.000	3.50	.911
.010	1.92	.879	.010	2.22	.896	.010	2.62	.904	.010	3.21	.913	.010	3.80	.916
.020	2.63	.908	.020	2.93	.923	.020	3.32	.928	.020	3.71	.933	.020	4.40	.938
.030	4.15	.948	.030	4.55	.955	.030	5.04	.958	.030	5.72	.960	.030	6.50	.963
.040	6.27	.985	.040	7.89	.985	.040	8.36	.985	.040	9.23	.985	.040	10.0	.985
.052	15.2	1.00	.050	14.1	1.01	.051	15.0	1.00	.050	14.9	.998	.053	16.6	1.01
.060	20.1	1.00	.060	20.5	1.00	.060	20.9	1.00	.060	20.9	1.00	.060	20.7	1.00
.070	23.5	1.00	.066	23.0	1.01	.070	24.5	1.00	.073	25.4	1.00	.070	24.5	1.00
.080	24.7	1.00	.070	24.2	1.00	.080	25.6	1.00	.080	26.5	1.00	.080	26.6	1.00
.090	25.1	1.00	.080	25.5	1.00	.090	26.4	1.00	.090	27.2	1.00	.090	27.4	1.00
.100	25.0	1.00	.090	25.9	1.00	.100	26.9	1.00	.100	27.5	1.00	.100	27.7	1.00
			.100	26.2	1.00	.120	27.1	1.00	.120	27.6	1.00	.120	28.0	1.00
			.130	26.0	1.00	.150	26.8	1.00	.150	27.7	1.00	.150	28.3	1.00
						.170	26.2	1.00						
						.180	24.3	1.00						

XD= 3.			3.5			4.			4.5			5.		
.000	4.51	.926	.000	5.72	.931	.000	7.32	.933	.000	9.40	.938	.000	12.2	.943
.010	4.80	.933	.010	6.11	.933	.010	7.80	.936	.010	9.78	.941	.010	12.3	.946
.020	5.98	.948	.020	7.36	.946	.020	8.95	.948	.020	10.8	.948	.020	12.8	.955
.040	11.3	.985	.040	12.0	.983	.040	12.9	.983	.040	13.6	.980	.040	14.8	.982
.060	19.1	1.00	.060	18.7	1.00	.060	18.2	1.00	.060	17.8	1.00	.060	17.7	1.00
.080	25.5	1.00	.080	24.5	1.00	.080	23.4	1.00	.080	22.2	1.00	.080	21.5	1.01
.090	26.6	1.00	.092	26.5	1.00	.090	25.3	1.00	.100	25.5	1.00	.100	24.5	1.01
.100	27.2	1.00	.100	27.0	1.00	.097	26.2	1.00	.110	26.5	1.00	.125	27.0	1.00
.120	28.2	1.00	.120	27.6	1.00	.100	26.5	1.00	.120	27.0	1.00	.150	28.0	1.00
.150	28.5	1.00	.150	28.2	1.00	.120	27.5	1.00	.150	28.1	1.00	.200	28.6	1.00
			.200	28.6	1.00	.150	28.2	1.00	.200	28.3	1.00			
						.200	28.4	1.00	.300	28.5	1.00			
						.250	28.5	1.00						

XD= 6.			7.			9.		
.000	15.2	.958	.000	17.3	.965	.000	19.6	.968
.010	15.2	.960	.010	17.3	.968	.010	19.6	.970
.020	15.5	.965	.020	17.4	.970	.020	19.6	.973
.040	16.5	.983	.040	18.0	.978	.040	19.8	.978
.060	18.0	.998	.060	18.9	.988	.060	20.1	.988
.080	20.2	1.01	.080	20.0	.998	.080	20.8	.995
.100	22.6	1.01	.100	21.3	1.01	.100	21.5	1.00
.120	24.4	1.01	.120	22.8	1.01	.120	22.4	1.01
.155	26.9	1.00	.150	25.3	1.01	.150	24.0	1.01
.200	28.3	1.00	.180	27.1	1.00	.180	25.8	1.01
.300	28.6	1.00	.200	27.8	1.00	.200	26.3	1.00
			.400	28.7	1.00	.500	28.8	1.00

0053 CARDS

MFS=6.10,P0=5154.,T0=404.,REFS=184500.,D=1.

XD	.5	.75	1.	1.5	2.	3.	3.5	4.	4.5	5.	7.	9.
P	1.03	1.05	1.07	1.08	1.10	1.09	1.07	1.05	1.03	1.02	1.00	1.02
PPCE	26.3	26.7	27.1	27.6	28.1	28.4	28.3	28.2	28.1	28.3	28.3	28.3*.001

XD= .5			.75			1.			1.5			2.		
YD	PITO	TTTTE	YD	PITO	TTTTE	YD	PITO	TTTTE	YD	PITO	TTTT	YD	PITO	TTTTE
.000	1.62	.884	.000	2.02	.889	.000	2.42	.896	.000	3.11	.911	.000	3.70	.916
.010	1.82	.899	.010	2.22	.896	.010	2.62	.906	.010	3.31	.921	.010	4.00	.926
.020	2.83	.928	.020	3.24	.936	.020	3.53	.938	.020	4.21	.943	.020	4.90	.951
.030	5.36	.973	.030	5.66	.980	.030	5.94	.975	.030	6.51	.973	.030	7.30	.975
.040	11.2	1.01	.040	11.6	1.01	.040	11.1	1.00	.040	11.4	1.00	.040	11.9	.998
.047	16.8	1.02	.047	17.4	1.01	.046	15.8	1.01	.050	18.8	1.01	.051	19.3	1.01
.050	19.2	1.01	.060	23.5	1.00	.050	18.9	1.01	.060	24.0	1.01	.060	23.9	1.01
.059	23.1	1.00	.070	25.1	1.00	.060	23.6	1.00	.069	25.9	1.00	.070	26.0	1.00
.070	24.4	1.00	.080	25.8	1.00	.070	25.4	1.00	.080	26.9	1.00	.080	27.2	1.00
.080	24.8	1.00	.090	26.1	1.00	.080	26.3	1.00	.090	27.4	1.00	.090	27.7	1.00
.090	24.6	1.00	.100	26.3	1.00	.090	26.6	1.00	.100	27.6	1.00	.100	27.8	1.00
.100	24.3	1.00	.120	26.3	1.00	.100	26.9	1.00	.150	27.6	1.00	.150	28.0	1.00
			.140	25.6	1.00	.120	27.1	1.00	.200	27.6	1.00	.200	28.1	1.00
						.150	26.6	1.00						
						.175	24.0	1.00						

XD= 3.			3.5			4.			4.5			5.		
.000	4.72	.933	.000	6.41	.938	.000	9.07	.943	.000	11.5	.948	.000	13.7	.955
.010	5.40	.941	.010	6.80	.946	.010	9.46	.948	.010	11.7	.953	.010	13.8	.958
.020	7.37	.955	.020	8.26	.958	.020	10.2	.963	.020	12.3	.960	.020	14.2	.963
.040	12.8	.995	.030	10.4	.973	.040	13.9	.988	.040	14.9	.988	.040	16.0	.985
.050	16.9	1.00	.040	13.2	.990	.060	19.0	1.00	.066	20.0	1.01	.060	18.2	1.00
.060	22.1	1.01	.060	20.0	1.00	.064	20.2	1.01	.080	22.3	1.01	.074	21.0	1.01
.070	24.9	1.00	.070	23.1	1.00	.080	23.9	1.00	.100	25.3	1.00	.080	21.6	1.01
.080	26.3	1.00	.080	25.3	1.00	.090	25.5	1.00	.112	26.2	1.00	.100	24.5	1.01
.100	27.5	1.00	.090	26.4	1.00	.097	26.3	1.00	.120	26.7	1.00	.125	26.7	1.00
.120	27.8	1.00	.100	27.1	1.00	.120	27.2	1.00	.150	27.7	1.00	.150	27.8	1.00
.150	28.2	1.00	.120	27.5	1.00	.150	27.8	1.00	.200	27.9	1.00	.200	28.1	1.00
.200	28.3	1.00	.150	28.0	1.00	.200	28.0	1.00	.300	28.1	1.00	.300	28.3	1.00
.250	28.4	1.00	.200	28.2	1.00	.300	28.2	1.00						
			.300	28.3	1.00									

XD= 7.			9.		
.000	18.2	.965	.000	20.1	.965
.020	18.3	.970	.020	20.2	.965
.040	18.8	.978	.040	20.4	.975
.060	19.6	.988	.060	20.6	.985
.080	20.6	1.00	.080	21.2	.995
.100	21.7	1.01	.100	22.0	1.00
.114	22.9	1.01	.120	23.0	1.01
.120	23.3	1.01	.130	23.7	1.01
.150	25.2	1.01	.150	24.7	1.01
.190	27.2	1.00	.200	26.6	1.00
.200	27.6	1.00	.240	27.8	1.00
.300	28.3	1.00	.400	28.3	1.00

0053 CARDS

C.3) TABULATED MEAN FLOW DATA FOR 20 DEGREE WEDGE (H=.15)

MFS=6.04,P0=1259.,T0=TT=402.,REFS=6987. ,D=.15

XD	3.	5.	7.	10.	15.	20.	25.	30.	35.	40.	50.	55.	60.
P	.888	.996	1.04	1.07	1.10	1.10	1.11	1.10	1.07	1.06	1.06	1.05	1.05
PPCE	19.4	21.2	22.8	24.4	25.7	26.3	26.6	26.5	26.2	26.0	26.0	26.1	26.1*.001

XD =3.		5.		7.		10.		15.		20.		25.	
YD	PITO	YD	PITO	YD	PITO	YD	PITO	YD	PITO	YD	PITO	YD	PITO
.000	1.80	.000	2.30	.000	2.80	.000	3.60	.000	4.37	.000	5.01	.000	5.55
.050	1.85	.050	2.40	.050	2.90	.050	3.70	.050	4.47	.050	5.11	.100	5.64
.100	2.00	.100	2.60	.100	3.20	.100	3.80	.100	4.67	.100	5.21	.200	6.42
.150	2.30	.150	2.90	.150	3.50	.150	4.20	.150	4.87	.200	6.00	.300	7.59
.200	2.70	.200	3.40	.200	4.00	.200	4.70	.200	5.36	.300	7.37	.400	9.73
.300	4.30	.300	5.20	.300	5.80	.300	6.50	.300	6.95	.400	9.63	.500	13.1
.400	7.01	.400	8.20	.400	9.00	.400	9.70	.400	9.63	.500	13.5	.600	17.5
.500	11.2	.500	13.1	.500	14.5	.500	14.8	.500	14.3	.600	18.7	.700	22.1
.550	13.5	.600	18.0	.600	19.7	.600	20.2	.600	19.9	.700	22.6	.800	24.1
.575	14.2	.700	20.8	.650	21.2	.700	22.9	.700	23.0	.800	24.3	1.00	25.3
		.750	21.4	.700	22.0	.800	23.8	.800	24.3	1.00	25.3	1.40	26.1
		.800	22.0	.800	22.6	1.00	24.3	1.00	25.1	1.40	26.1	2.00	26.5
				1.00	22.8	1.10	24.4	1.20	25.7	1.80	26.3	2.40	26.6

XD =30.		35.		40.		50.		55.		60.	
.000	5.84	.000	6.13	.000	6.36	.000	6.80	.000	6.99	.000	7.18
.100	6.03	.100	6.32	.100	6.45	.200	7.36	.200	7.55	.200	7.83
.200	6.60	.200	6.79	.200	7.01	.400	9.41	.400	9.41	.400	9.69
.300	7.85	.300	7.82	.300	7.95	.600	14.0	.600	13.5	.600	14.0
.400	9.57	.400	9.33	.400	9.35	.800	20.8	.800	20.0	.800	20.0
.500	12.4	.500	11.8	.500	11.7	1.00	24.1	1.00	23.9	1.00	24.0
.600	16.6	.600	14.3	.600	15.0	1.25	25.0	1.25	24.6	1.25	25.3
.700	20.8	.700	19.4	.700	18.5	1.50	25.4	1.50	25.4	1.50	25.6
.800	23.4	.800	22.6	.800	21.9	2.00	25.9	2.00	25.8	2.50	26.1
1.00	25.2	1.00	24.7	1.00	23.6	3.00	26.3	2.50	26.1	3.00	27.1
1.40	25.9	1.40	25.6	1.40	25.4	4.00	27.0	4.00	27.4	4.00	28.1
2.00	26.4	2.00	26.1	2.00	26.0	5.00	27.9	5.00	28.1	5.00	28.8
2.40	26.5	2.80	26.2	2.80	26.2	6.00	28.3	6.00	28.3	6.00	28.9

0039 CARDS

MFS=6.07,P0=2557.,T0=TT=402.,REFS=14010.,D=.15

XD	=3.	5.	7.	10.	15.	20.	25.	30.	35.	40.	45.	50.	55.	60.
P	=.787	.943	1.01	1.04	1.07	1.08	1.09	1.07	1.07	1.04	1.02	1.00	1.00	1.00
PPCE=	18.9	21.0	22.5	24.3	25.4	26.0	25.7	25.7	26.0	25.9	25.9	25.9	25.9	25.8*.001

XD =3.		5.		7.		10.		15.		20.		25.	
YD	PITO	YD	PITO	YD	PITO	YD	PITO	YD	PITO	YD	PITO	YD	PITO
.000	1.31	.000	1.91	.000	2.52	.000	3.21	.000	3.98	.000	4.82	.000	5.49
.050	1.41	.050	2.01	.050	2.62	.050	3.31	.050	4.08	.050	4.92	.100	5.97
.100	1.61	.100	2.32	.100	2.92	.100	3.71	.100	4.38	.100	5.11	.200	7.71
.150	2.12	.150	2.82	.150	3.62	.150	4.31	.150	4.97	.150	5.70	.300	10.5
.200	2.92	.200	3.83	.200	4.73	.200	5.41	.200	5.97	.200	6.69	.400	14.5
.250	4.23	.250	5.24	.250	6.24	.250	6.92	.250	7.36	.250	8.16	.500	18.6
.300	5.84	.300	7.55	.300	8.45	.300	9.52	.300	9.55	.300	10.0	.600	22.2
.350	8.36	.350	10.2	.350	11.8	.400	15.9	.400	15.3	.400	14.7	.800	24.4
.400	11.2	.400	13.5	.400	15.8	.500	21.1	.500	20.6	.500	19.5	1.00	24.9
.450	13.9	.450	16.4	.500	20.5	.600	23.2	.600	23.3	.600	22.7	2.00	25.7
.475	14.8	.500	18.6	.600	22.1	.800	24.2	.800	24.6	.800	24.6		
		.550	19.9	.700	22.5	.900	24.3	1.00	25.1	1.00	25.7		
		.600	20.5					1.50	25.4	2.00	26.0		
		.650	20.7										

XD =30.		35.		40.		45.		50.		55.		60.	
.000	6.48	.000	8.05	.000	9.95	.000	11.6	.000	13.0	.000	14.0	.000	14.9
.100	6.96	.100	8.43	.100	10.3	.200	12.4	.200	13.5	.200	14.5	.200	15.2
.200	8.68	.200	9.75	.200	11.3	.400	14.7	.400	15.0	.400	15.5	.400	15.9
.300	11.2	.300	11.8	.300	12.7	.600	18.1	.600	17.6	.600	17.4	.600	17.4
.400	14.1	.400	14.4	.400	14.7	.800	21.6	.800	20.4	.800	19.7	.800	19.4
.600	20.7	.600	19.9	.600	19.1	1.00	23.7	1.00	22.8	1.00	21.9	1.00	21.3
.800	24.1	.800	23.6	.800	22.7	1.20	24.7	1.20	24.2	1.20	23.7	1.20	23.0
1.00	24.8	1.00	24.9	1.00	24.5	2.00	25.6	2.00	25.5	1.60	25.0	1.60	24.9
2.00	25.7	1.60	25.7	1.60	25.6	3.00	25.9	3.00	25.9	2.00	25.2	2.00	25.3
		2.00	26.0	2.00	25.9			4.00	26.9	3.00	25.9	2.50	25.6
								5.00	27.5			3.00	25.8
								6.00	27.6			4.00	26.5
												5.00	27.1

0037 CARDS

MFS=6.08,P0=3855.,T0=TT=402.,REFS=21030.,D=.15

XD =	3.	5.	7.	10.	15.	20.	25.	30.	35.	40.	45.	50.	55.	60.
P =	.767	.942	.999	1.04	1.06	1.08	1.07	1.05	1.04	1.03	1.01	1.01	1.01	1.02
PPCE=	21.4	22.5	23.4	25.0	25.9	26.8	26.5	26.5	26.6	26.8	26.5	26.4	26.4	26.3*.001

XD = 3.		5.		7.		10.		15.		20.		25.	
YD	PITO	YD	PITO	YD	PITO	YD	PITO	YD	PITO	YD	PITO	YD	PITO
.000	1.22	.000	2.02	.000	2.52	.000	3.22	.000	4.21	.000	5.16	.000	6.62
.050	1.32	.050	2.12	.050	2.63	.050	3.32	.050	4.31	.050	5.36	.100	7.60
.100	1.62	.100	2.53	.100	3.23	.100	3.93	.100	4.91	.100	5.96	.200	9.93
.150	2.44	.150	3.54	.150	4.24	.150	4.83	.150	5.81	.150	6.95	.300	13.6
.200	3.55	.200	5.06	.200	5.96	.200	6.54	.200	7.51	.200	8.64	.400	17.8
.250	5.28	.250	7.79	.250	9.09	.250	9.36	.250	10.1	.250	10.9	.500	21.9
.300	7.61	.300	11.3	.300	12.8	.300	13.3	.300	13.4	.300	13.4	.600	24.0
.350	10.5	.350	15.5	.350	16.9	.350	17.6	.350	17.0	.350	16.5	.700	25.0
.400	14.4	.400	18.4	.400	20.5	.400	20.7	.400	20.5	.400	19.9	.800	25.4
.425	15.9	.450	20.2	.450	22.1	.450	22.6	.450	22.5	.500	23.5	1.00	25.8
		.500	20.8	.500	22.9	.500	23.7	.500	23.7	.600	24.8	1.40	26.2
		.550	21.0	.600	23.4	.600	24.6	.600	24.7	.700	25.3	2.00	26.5
		.575	21.2			.700	24.9	.700	25.1	.800	25.6		
						.800	25.0	.800	25.4	1.00	25.9		
								1.00	25.7	1.60	26.8		
								1.60	25.9				

XD = 30.		35.		40.		45.		50.		55.		60.	
.000	9.24	.000	11.9	.000	13.9	.000	15.1	.000	15.9	.000	16.6	.000	17.1
.100	9.81	.100	12.3	.100	14.1	.200	15.5	.200	16.2	.200	16.8	.200	17.2
.200	11.6	.200	13.1	.200	14.5	.400	16.4	.400	17.2	.400	17.4	.400	17.8
.300	14.0	.300	14.8	.400	16.7	.600	19.1	.600	18.8	.600	18.6	.600	18.8
.400	17.1	.400	16.8	.600	20.0	.800	21.9	.800	20.7	.800	20.3	.800	20.1
.500	20.2	.600	21.4	.800	23.2	1.00	24.1	1.00	23.0	1.00	22.2	1.00	21.8
.600	22.7	.800	24.3	1.00	25.0	1.20	25.2	1.20	24.7	1.20	23.9	1.20	23.5
.700	24.3	1.00	25.6	1.40	26.2	1.40	25.7	1.40	25.7	1.40	25.0	1.40	24.8
.800	25.1	1.40	26.2	2.00	26.6	2.00	26.0	2.00	25.9	2.00	25.9	2.00	25.8
1.00	25.7	2.00	26.4	3.00	26.8	3.00	26.5	3.00	26.4	3.00	26.4	3.00	26.3
1.40	26.2	3.00	26.6					4.00	27.2			4.00	26.6
2.00	26.5							5.00	27.6			5.00	26.7

0038 CARDS

MFS=6.10,P0=5154.,T0=TT=402.,REFS=27880.,D=.15

XD =	3.	5.	7.	10.	15.	20.	25.	30.	35.	40.	45.	50.	55.	60.
P =	.838	.925	.996	1.03	1.05	1.06	1.06	1.04	1.03	1.03	1.02	1.01	1.01	1.02
PPCE=	19.7	21.5	23.1	24.6	25.2	26.0	25.8	25.7	25.9	25.8	25.6	25.5	25.5	25.5*.001

XD = 3.		5.		7.		10.		15.		20.		25.	
YD	PITO	YD	PITO	YD	PITO	YD	PITO	YD	PITO	YD	PITO	YD	PITO
.000	1.11	.000	1.72	.000	2.32	.000	3.02	.000	3.91	.000	5.25	.000	7.41
.050	1.31	.050	1.92	.050	2.63	.050	3.22	.050	4.21	.050	5.55	.100	8.39
.100	1.72	.100	2.53	.100	3.23	.100	3.83	.100	4.91	.100	6.34	.200	11.1
.150	2.63	.150	3.74	.150	4.54	.150	5.34	.150	6.21	.150	7.73	.300	15.1
.200	4.25	.200	6.07	.200	7.07	.200	7.75	.200	8.62	.200	9.81	.400	19.5
.300	9.60	.300	13.7	.300	15.3	.300	15.6	.300	15.0	.300	15.0	.500	22.7
.350	12.7	.350	17.2	.400	21.0	.400	21.6	.400	21.0	.400	20.4	.600	24.0
.400	15.6	.400	19.3	.450	22.2	.450	22.9	.450	22.5	.450	22.2	.700	24.6
		.450	20.2	.500	22.7	.500	23.5	.500	23.3	.500	23.2	.800	24.8
		.500	20.3	.600	23.1	.600	24.1	.600	24.2	.600	24.3	1.00	25.2
		.550	20.4			.800	24.6	.800	24.8	.800	25.0	1.80	25.8
								1.00	25.2	1.00	25.4		
										1.60	26.0		

XD = 30.		35.		40.		45.		50.		55.		60.	
.000	10.2	.000	12.5	.000	14.2	.000	15.3	.000	15.9	.000	16.5	.000	16.8
.100	10.8	.100	12.7	.100	14.4	.200	15.7	.200	16.3	.200	16.6	.200	17.1
.200	12.2	.200	13.6	.200	14.9	.400	17.1	.400	17.1	.400	17.3	.400	17.7
.300	14.7	.300	14.9	.300	15.7	.600	19.2	.600	18.7	.600	18.6	.600	18.7
.400	18.0	.400	17.0	.400	16.9	.800	21.9	.800	20.9	.800	20.3	.800	20.1
.500	20.9	.500	19.2	.500	18.4	1.00	23.8	1.00	22.9	1.00	22.2	1.00	21.9
.600	22.8	.600	21.3	.600	20.0	1.20	25.2	1.20	24.2	1.20	23.7	1.20	23.4
.700	24.0	.700	22.8	.700	21.8	2.00	25.4	2.00	25.2	2.00	25.1	2.00	25.1
.800	24.6	.800	23.8	.800	23.1	3.00	25.6	3.00	25.5	3.00	25.5	3.00	25.5
1.00	25.1	1.00	24.7	1.00	24.5			4.00	25.6				
1.80	25.7	2.00	25.5	1.20	25.1			5.00	27.1				
		3.00	25.9	2.00	25.7								
				3.00	25.8								

0036 CARDS

C.4) TABULATED MEAN FLOW DATA FOR 20 DEGREE WEDGE (H=.3,ADIABATIC WALL)

MFS=6.05,P0=1261.,T0=400.,REFS=14040.,D=.3

XD	=.1	.25	.5	.75	1.	1.25	1.5	2.	3.	5.	7.	10.	15.	20.
P	=.408	.436	.548	.648	.709	.739	.769	.796	.856	1.00	1.08	1.13	1.14	1.13
PPCE=	7.15	7.86	11.6	13.0	13.5	14.2	14.8	15.8	17.7	20.9	23.1	24.8	26.5	26.6*.001

XD =25.
P =1.12
PPCE=27.0*.001

XD=	.1			.25			.5			.75			1.		
YD	PITO	TTTTE	YD	PITO	TTTTE	YD	PITO	TTTTE	YD	PITO	TTTTE	YD	PITO	TTTTE
.000	.247	.870	.000	.264	.870	.000	.331	.870	.000	.390	.870	.000	.514	.873
.380	.247	.870	.270	.264	.870	.120	.331	.870	.050	.420	.875	.050	.570	.880
.400	.293	.880	.275	.273	.893	.130	.331	.870	.100	.550	.893	.100	.770	.903
.425	.546	.893	.300	.344	.900	.150	.404	.888	.150	.780	.913	.150	1.08	.923
.450	.909	.900	.325	.435	.910	.175	.485	.893	.200	1.15	.933	.200	1.60	.945
.475	1.36	.918	.350	.556	.920	.200	.607	.900	.250	1.55	.955	.250	2.30	.970
.500	2.12	.930	.375	.728	.930	.225	.708	.905	.300	1.90	.980	.290	2.55	.993
.525	3.13	.943	.400	.960	.938	.250	.860	.918						
.550	4.55	.958	.425	1.21	.948	.275	.991	.923						
			.450	1.57	.958	.300	1.16	.933						

XD=	1.25			1.5			2.			3.			5.	
.000	.632	.878	.000	.746	.880	.000	1.10	.885	.000	1.55	.893	.000	2.19	.905
.050	.700	.885	.050	.840	.885	.050	1.12	.888	.050	1.60	.898	.050	2.30	.913
.100	.950	.905	.100	1.15	.900	.075	1.20	.898	.100	1.75	.918	.100	2.60	.930
.150	1.33	.925	.150	1.62	.920	.100	1.35	.908	.150	2.25	.945	.150	3.20	.958
.200	2.00	.948	.200	2.35	.953	.125	1.60	.920	.200	3.00	.970	.200	4.20	.980
.250	2.90	.970	.250	3.35	.980	.150	1.87	.935	.250	4.25	.993	.250	5.85	1.00
.300	3.50	.993	.300	4.45	1.01	.175	2.19	.950	.300	6.20	1.01	.300	8.40	1.02
			.320	4.65	1.02	.200	2.55	.968	.350	8.40	1.02	.350	11.7	1.03
						.225	3.03	.980	.375	10.0	1.03	.400	15.8	1.02
						.250	3.65	.993	.390	10.9	1.03	.450	19.0	1.01
						.275	4.30	1.00	.450	15.0	1.02	.475	19.9	1.00
						.300	5.10	1.01	.480	16.4	1.01	.500	20.4	1.00
						.325	6.00	1.02				.550	20.8	1.00
						.350	6.90	1.02				.600	20.9	1.00
						.375	7.70	1.03				.650	20.9	1.00
						.385	7.75	1.03				.660	20.9	1.00

XD=	7.			10.			15.			20.			25.	
.000	2.69	.913	.000	3.26	.928	.000	4.11	.940	.000	4.62	.945	.000	5.12	.950
.050	2.74	.920	.050	3.36	.933	.050	4.21	.940	.050	4.71	.945	.050	5.21	.950
.100	3.09	.943	.100	3.65	.945	.100	4.51	.945	.100	4.91	.950	.100	5.40	.953
.150	3.74	.963	.150	4.29	.965	.150	5.05	.960	.150	5.39	.958	.150	5.88	.958
.200	4.74	.985	.200	5.23	.985	.200	5.88	.973	.200	6.16	.970	.200	6.54	.968
.250	6.48	1.01	.250	6.91	1.01	.250	7.25	.990	.250	7.41	.983	.250	7.77	.975
.300	9.37	1.02	.300	9.38	1.02	.300	9.21	1.01	.300	9.04	.995	.300	9.19	.985
.330	11.7	1.03	.330	11.6	1.02	.350	12.1	1.01	.350	11.4	1.01	.350	11.1	1.00
.350	13.3	1.03	.350	13.1	1.02	.380	14.2	1.02	.400	14.6	1.01	.400	13.6	1.01
.400	17.7	1.02	.400	17.7	1.01	.400	15.9	1.02	.430	16.8	1.02	.470	18.5	1.02
.450	20.9	1.01	.450	21.1	1.01	.450	20.2	1.01	.450	18.3	1.01	.500	20.4	1.01
.475	21.8	1.00	.490	22.7	1.00	.500	22.8	1.00	.500	21.6	1.01	.550	22.7	1.01
.500	22.3	1.00	.500	23.1	1.00	.535	23.7	1.00	.550	23.5	1.00	.595	24.0	1.00
.550	22.9	1.00	.550	24.0	1.00	.550	24.0	1.00	.575	24.0	1.00	.600	24.1	1.00
.600	23.1	1.00	.600	24.4	1.00	.600	24.8	1.00	.600	24.4	1.00	.650	24.7	1.00
.700	23.1	1.00	.700	24.7	1.00	.650	25.3	1.00	.650	25.0	1.00	.700	25.1	1.00
.800	22.6	1.00	.800	24.8	1.00	.700	25.6	1.00	.700	25.3	1.00	.800	25.8	1.00
.850	22.3	1.00	.900	24.8	1.00	.800	25.9	1.00	.800	25.7	1.00	1.00	26.4	1.00
			1.00	24.7	1.00	1.00	26.3	1.00	1.00	26.2	1.00	1.20	26.8	1.00
						1.20	26.5	1.00	1.20	26.5	1.00	1.40	27.0	1.00

0061 CARDS

MFS=6.11,P0=2556.,T0=402.,REFS=27530.,D=.3

XD	.1	.25	.5	1.	1.5	2.	3.	5.	7.	10.	15.	20.	25.	30.
P	.323	.335	.426	.588	.637	.672	.781	.959	1.04	1.10	1.09	1.08	1.04	1.00
PPCE	5.50	5.86	8.74	9.50	11.2	12.9	15.8	19.5	22.0	23.5	24.9	24.8	25.0	25.1*.001

XD= .1			.25			.5			1.			1.5		
YD	PITO	TTTTE	YD	PITO	TTTTE	YD	PITO	TTTTE	YD	PITO	TTTTE	YD	PITO	TTTTE
.000	.184	.871	.000	.191	.871	.000	.243	.871	.000	.387	.871	.000	.588	.871
.370	.184	.871	.225	.191	.871	.100	.243	.871	.050	.430	.876	.050	.660	.871
.375	.230	.871	.250	.191	.871	.130	.243	.871	.100	.600	.901	.100	.900	.898
.400	.320	.871	.275	.270	.876	.150	.270	.898	.150	.950	.925	.150	1.45	.938
.425	.470	.876	.300	.350	.888	.175	.349	.906	.200	1.70	.953	.200	2.55	.968
.450	.700	.888	.325	.460	.901	.200	.449	.915	.260	2.40	.978	.250	3.95	.995
.475	1.15	.901	.350	.599	.910	.225	.569	.925				.283	4.70	1.01
.500	1.90	.918	.375	.779	.923	.250	.749	.933						
.525	3.20	.938	.400	.999	.933	.275	.948	.940						
.550	5.30	.958	.425	1.28	.943	.300	1.15	.950						

XD= 2.			3.			5.			7.			10.		
.000	.791	.871	.000	1.16	.876	.000	1.78	.883	.000	2.42	.891	.000	3.08	.901
.050	.831	.873	.050	1.19	.883	.050	1.98	.891	.050	2.72	.896	.050	3.23	.903
.075	.940	.883	.100	1.58	.901	.100	2.67	.910	.100	3.26	.913	.100	4.01	.913
.100	1.09	.898	.150	2.47	.938	.150	3.96	.943	.150	4.45	.938	.150	5.67	.935
.125	1.38	.918	.200	3.96	.978	.200	6.33	.980	.200	7.41	.970	.200	8.11	.963
.150	1.78	.935	.250	6.63	1.00	.250	10.1	1.00	.250	11.9	.990	.250	12.0	.988
.175	2.27	.953	.300	9.79	1.02	.280	13.1	1.01	.300	16.6	1.01	.305	17.3	1.00
.200	2.87	.973	.310	10.6	1.02	.300	14.5	1.01	.350	20.1	1.00	.330	19.4	1.00
.225	3.76	.988	.350	13.8	1.01	.355	18.5	1.00	.360	20.4	1.00	.350	20.7	1.00
.250	4.60	1.00				.400	19.4	1.00	.400	21.3	1.00	.385	21.9	1.00
.275	5.59	1.01				.450	19.5	1.00	.450	21.6	1.00	.450	22.9	1.00
.300	6.63	1.02				.500	19.4	1.00	.500	21.9	1.00	.500	23.2	1.00
.325	7.72	1.02				.560	18.8	1.00	.550	22.0	1.00	.550	23.3	1.00
.337	8.06	1.02							.650	21.7	1.00	.600	23.4	1.00
									.700	21.5	1.00	.700	23.5	1.00

XD= 15.			20.			25.			30.		
.000	3.87	.920	.000	5.05	.935	.000	7.73	.943	.000	10.6	.948
.050	4.07	.923	.050	5.33	.938	.050	7.87	.945	.050	10.7	.948
.100	4.83	.928	.100	6.13	.940	.100	8.01	.948	.100	11.0	.950
.150	6.65	.945	.150	7.02	.950	.150	9.35	.955	.150	11.5	.958
.200	8.37	.963	.200	9.36	.963	.200	10.7	.963	.200	12.3	.965
.250	11.3	.978	.250	11.7	.978	.250	12.4	.978	.250	13.3	.978
.300	15.0	.993	.300	14.0	.993	.300	14.1	.993	.300	14.4	.993
.350	18.7	1.00	.350	16.8	1.00	.350	16.0	.998	.350	15.6	.995
.400	21.1	1.01	.400	19.4	1.01	.400	18.1	1.00	.400	16.9	.998
.440	22.4	1.00	.450	21.3	1.00	.450	19.9	1.00	.450	18.3	1.00
.500	23.1	1.00	.500	22.4	1.00	.500	21.3	1.00	.500	19.6	1.00
.600	23.7	1.00	.600	23.4	1.00	.590	23.0	1.00	.600	21.7	1.00
.700	24.0	1.00	.800	24.0	1.00	.700	24.0	1.00	.710	23.2	1.00
.800	24.3	1.00	1.00	24.3	1.00	.800	24.3	1.00	.800	23.9	1.00
1.00	24.5	1.00	1.20	24.8	1.00	1.00	24.8	1.00	1.00	24.6	1.00
1.20	24.9	1.00				1.20	25.0	1.00	1.20	25.1	1.00

0053 CARDS

MFS=6.12,P0=3855.,T0=402.,REFS=41340.,D=.3

XD	.1	.25	.5	1.	1.5	2.	3.	5.	7.	10.	15.	20.	25.	30.
P	.287	.294	.369	.528	.579	.625	.771	.972	1.06	1.09	1.08	1.02	1.01	1.03
PPCE	4.86	5.08	8.14	13.5	14.5	15.6	17.2	20.0	22.3	23.9	25.1	24.9	25.1	24.8*.001

XD= .1			.25			.5			1.			1.5		
YD	PITO	TTTTE	YD	PITO	TTTTE	YD	PITO	TTTTE	YD	PITO	TTTTE	YD	PITO	TTTTE
.000	.162	.873	.000	.166	.873	.000	.208	.873	.000	.348	.873	.000	.533	.873
.360	.162	.873	.235	.166	.873	.100	.208	.873	.025	.348	.873	.025	.540	.874
.400	.290	.873	.250	.200	.883	.125	.270	.873	.050	.370	.876	.050	.670	.876
.425	.450	.878	.275	.270	.888	.150	.330	.873	.075	.460	.878	.075	.850	.883
.450	.650	.891	.300	.370	.896	.175	.430	.878	.100	.620	.883	.100	1.10	.891
.475	1.05	.906	.325	.500	.901	.200	.540	.883	.125	.850	.891	.125	1.45	.906
.500	1.75	.925	.350	.640	.906	.225	.710	.891	.150	1.15	.903	.150	2.00	.925
.525	2.65	.950	.375	.780	.913	.250	.900	.901	.175	1.57	.917	.175	2.60	.940
.550	4.28	.970	.400	.930	.923	.275	1.08	.910	.200	2.18	.930	.200	3.35	.958

XD= 2.			3.			5.			7.			10.		
.000	.739	.873	.000	1.09	.876	.000	1.85	.883	.000	2.50	.898	.000	3.19	.913
.025	.743	.876	.050	1.28	.886	.050	2.13	.896	.050	2.90	.903	.050	3.68	.923
.050	.842	.881	.100	1.97	.910	.100	3.22	.935	.100	4.23	.925	.100	5.15	.943
.075	1.14	.891	.150	3.45	.950	.150	5.44	.965	.150	6.88	.958	.150	7.36	.965
.100	1.39	.908	.200	5.81	.983	.200	9.55	.995	.200	11.0	.990	.200	11.8	.990
.125	1.78	.925	.250	9.46	1.00	.250	15.2	1.01	.240	15.2	1.01	.250	16.6	1.01
.150	2.48	.940	.280	11.8	1.01	.300	18.9	1.00	.300	20.5	1.00	.300	20.4	1.00
.175	3.22	.953	.345	15.0	1.00	.350	19.8	1.00	.350	21.5	1.00	.340	22.0	1.00
.200	4.01	.965				.390	20.0	1.00	.400	22.0	1.00	.400	23.1	1.00
.225	4.95	.983							.500	22.3	1.00	.500	23.6	1.00
.250	6.24	.995										.600	23.9	1.00
.275	7.43	1.00										.700	23.9	1.00
.292	8.02	1.01												

XD= 15.			20.			25.			30.		
.000	5.31	.933	.000	9.27	.940	.000	12.7	.948	.000	14.6	.950
.050	5.84	.938	.050	9.46	.943	.050	12.8	.950	.050	14.7	.953
.100	6.95	.948	.100	10.2	.950	.100	13.1	.953	.100	14.7	.955
.150	9.21	.965	.150	11.4	.960	.150	13.5	.958	.150	14.9	.958
.200	12.0	.983	.200	12.9	.970	.200	14.2	.965	.200	15.3	.963
.250	15.0	.995	.250	14.7	.980	.250	15.1	.975	.250	15.7	.970
.300	18.2	1.00	.300	16.5	.990	.300	16.1	.983	.300	16.2	.978
.330	19.7	1.00	.350	18.3	.998	.350	17.1	.990	.350	16.8	.985
.410	22.5	1.00	.400	19.9	1.00	.400	18.3	.995	.400	17.6	.990
.500	23.7	1.00	.450	21.3	1.00	.500	20.5	1.00	.500	19.1	1.00
.600	24.1	1.00	.530	22.8	1.00	.600	22.3	1.00	.600	20.8	1.00
.800	24.6	1.00	.600	23.4	1.00	.690	23.3	1.00	.700	22.1	1.00
1.00	24.8	1.00	.800	24.2	1.00	.800	24.1	1.00	.840	23.4	1.00
1.20	25.1	1.00	1.00	24.6	1.00	1.00	24.7	1.00	1.00	24.2	1.00
			1.20	24.9	1.00	1.20	25.1	1.00	1.20	24.8	1.00

0049 CARDS

MFS=6.14,P0=5153.,T0=402.,REFS=54800.,D=.3

XD	=.1	.25	.5	1.	1.5	2.	3.	5.	7.	10.	15.	20.	25.	30.
P	=.260	.264	.333	.485	.535	.600	.770	.971	1.05	1.08	1.06	1.02	1.03	1.03
PPCE	=4.52	4.79	7.28	14.5	15.8	16.4	17.8	20.1	22.0	23.6	24.7	24.6	24.6	24.8*.001

XD=	.1			.25			.5			1.			1.5	
YD	PITO	TTTTE	YD	PITO	TTTTE	YD	PITO	TTTTE	YD	PITO	TTTTE	YD	PITO	TTTTE
.000	.144	.873	.000	.146	.873	.000	.184	.873	.000	.308	.873	.000	.484	.873
.360	.144	.873	.230	.146	.873	.100	.184	.873	.025	.308	.873	.025	.495	.876
.375	.190	.873	.250	.195	.873	.125	.215	.873	.050	.340	.876	.050	.570	.878
.400	.290	.878	.275	.275	.878	.150	.270	.873	.075	.460	.876	.075	.800	.886
.425	.480	.891	.300	.390	.883	.175	.375	.873	.100	.650	.878	.100	1.08	.896
.450	.800	.901	.325	.540	.891	.200	.520	.873	.125	.920	.883	.125	1.53	.908
.475	1.30	.913	.350	.710	.896	.225	.720	.883	.150	1.34	.891	.150	2.09	.928
.500	2.18	.925	.375	.830	.903	.250	.900	.891	.175	1.85	.903	.175	2.70	.945

XD=	2.			3.			5.			7.			10.	
.000	.680	.873	.000	1.05	.876	.000	1.84	.893	.000	2.52	.908	.000	3.54	.920
.025	.695	.876	.050	1.24	.881	.050	2.29	.901	.050	3.07	.915	.050	4.33	.928
.050	.794	.878	.100	2.18	.901	.100	3.68	.918	.100	4.75	.933	.100	6.10	.948
.075	1.14	.883	.150	4.01	.945	.150	6.86	.953	.150	8.42	.963	.150	9.44	.970
.100	1.49	.891	.200	6.68	.985	.200	11.8	.993	.200	13.8	.990	.200	13.9	.988
.125	2.09	.903	.250	11.0	1.00	.220	13.9	1.01	.230	16.8	1.01	.260	19.5	1.01
.150	2.73	.920	.270	12.6	1.01	.260	18.2	1.00	.275	20.3	1.00	.305	21.4	1.00
.175	3.48	.933	.315	15.0	1.00	.335	20.1	1.00	.350	21.6	1.00	.350	22.4	1.00
.200	4.47	.950	.340	14.9	1.00	.400	20.0	1.00	.400	21.9	1.00	.400	23.0	1.00
.225	5.56	.965				.430	19.4	1.00	.500	22.0	1.00	.500	23.4	1.00
.250	6.95	.985							.600	21.9	1.00	.600	23.6	1.00
.290	8.34	1.00							.622	21.3	1.00	.700	23.6	1.00

XD=	15.			20.			25.			30.	
.000	6.68	.938	.000	10.2	.953	.000	13.6	.960	.000	15.1	.963
.050	7.16	.945	.050	10.4	.958	.050	13.7	.963	.050	15.1	.965
.100	8.66	.953	.100	11.1	.963	.100	14.0	.968	.100	15.3	.968
.150	10.8	.965	.150	12.3	.973	.150	14.4	.975	.150	15.4	.975
.200	13.6	.980	.200	13.7	.983	.200	14.9	.983	.200	15.8	.983
.250	16.3	.995	.250	15.3	.990	.250	15.7	.990	.250	16.2	.988
.300	19.4	1.00	.300	16.9	.998	.300	16.6	.995	.300	16.7	.993
.320	20.2	1.01	.370	19.3	1.00	.350	17.6	.998	.350	17.3	.995
.380	22.0	1.00	.400	20.1	1.00	.400	18.7	1.00	.400	18.0	.996
.500	23.5	1.00	.450	21.4	1.00	.450	19.8	1.00	.450	18.7	.998
.600	24.1	1.00	.500	22.3	1.00	.500	20.8	1.00	.500	19.5	1.00
.800	24.4	1.00	.530	22.6	1.00	.550	21.7	1.00	.550	20.3	1.00
.900	24.6	1.00	.600	23.4	1.00	.600	22.4	1.00	.600	21.2	1.00
1.00	24.7	1.00	.700	23.9	1.00	.685	23.4	1.00	.700	22.6	1.00
			.800	24.0	1.00	.800	24.0	1.00	.840	23.7	1.00
			1.10	24.6	1.00	1.00	24.4	1.00	1.00	24.3	1.00
						1.20	24.6	1.00	1.20	24.8	1.00

0049 CARDS

MFS=6.05,P0=1261.,T0=400.,REFS=14040.,D=.3,PTM=.7115

XD=	0.0			.1				.25			
YD	PITO	TTTTE	UUE	YD	PITO	TTTTE	UUE	YD	PITO	TTTTE	UUE
1.075	71.62	1.000	.9914	1.105	70.71	1.000	.9869	1.165	70.74	1.000	.9847
1.000	70.51	1.000	.9923	1.055	70.71	1.000	.9869	1.100	69.73	1.000	.9855
.9000	68.69	1.000	.9938	1.000	68.69	1.000	.9886	1.000	67.71	1.000	.9871
.8500	67.68	1.000	.9946	.9000	66.67	1.000	.9902	.9000	65.29	1.000	.9891
.8000	66.57	1.000	.9955	.8000	60.61	1.000	.9952	.8000	61.45	1.000	.9923
.7500	64.95	1.000	.9968	.7200	55.05	1.000	1.000	.7400	52.55	1.000	1.000
.7050	61.11	1.000	1.000	.6900	47.47	1.010	1.001	.7000	39.92	1.010	.9934
.6900	58.59	1.007	.9934	.6550	32.32	1.017	.9783	.6500	19.71	1.017	.9706
.6750	54.55	1.012	1.006	.6250	17.17	1.005	.9488	.6000	8.388	1.010	.9147
.6500	34.85	1.017	.9670	.6000	10.10	.9825	.8792	.5750	6.064	1.005	.9124
.6250	20.40	1.010	.9328	.5500	4.545	.9575	.7870	.5500	4.346	.9950	.8892
.6000	12.32	.9850	.8544	.5250	3.131	.9425	.7632	.5250	3.234	.9825	.8606
.5750	7.576	.9575	.8217	.5000	2.121	.9300	.7405	.5000	2.527	.9725	.8253
.5500	4.899	.9300	.7555	.4750	1.364	.9175	.5518	.4750	2.001	.9675	.7691
.5250	2.980	.9050	.6800					.4400	1.425	.9550	.6468

XD=	.5			.75				1.			
1.250	71.18	1.000	.9710	1.335	70.81	1.000	.9628	1.420	71.36	1.000	.9508
1.200	70.68	1.000	.9714	1.300	70.81	1.000	.9628	1.400	71.36	1.000	.9508
1.100	69.46	1.000	.9724	1.200	68.79	1.000	.9644	1.300	69.64	1.000	.9521
1.000	67.64	1.000	.9738	1.100	65.76	1.000	.9668	1.200	67.71	1.000	.9536
.9000	63.70	1.000	.9770	1.000	59.69	1.000	.9717	1.100	63.77	1.000	.9567
.8500	59.15	1.000	.9808	.9000	51.59	1.000	.9787	1.000	53.34	1.000	.9654
.8000	49.54	1.000	.9892	.8000	36.92	1.000	.9928	.9000	39.57	1.000	.9781
.7600	38.42	1.000	1.000	.7700	30.35	1.000	1.000	.8000	26.82	1.000	.9921
.7000	21.84	1.012	.9689	.7500	26.30	1.005	.9865	.7500	20.75	1.000	1.000
.6500	11.93	1.020	.9616	.7000	17.70	1.012	.9812	.7000	15.18	1.007	1.003
.6000	6.977	1.025	.9401	.6500	11.13	1.017	.9649	.6500	10.32	1.020	.9662
.5500	4.449	1.017	.9121	.6000	7.081	1.030	.9581	.6000	7.287	1.030	.9670
.5000	3.134	1.002	.8850	.5500	4.957	1.035	.9264	.5500	5.263	1.040	.9252
.4750	2.679	.9925	.8603	.5100	3.794	1.037	.9105	.5000	3.897	1.045	.8770
.4500	2.326	.9825	.8230	.5000	3.571	1.037	.9021	.4800	3.492	1.045	.8598
.4250	2.022	.9725	.7822	.4500	2.701	1.032	.8557	.4500	3.036	1.042	.8497
.4000	1.820	.9650	.7496	.4000	2.175	1.020	.8109	.4000	2.530	1.035	.8183
.3750	1.638	.9556	.7248	.3750	2.074	1.007	.7878	.3750	2.419	1.025	.8101
.3500	1.517	.9475	.6916	.3500	2.023	.9975	.7705	.3500	2.379	1.015	.8168
.3250	1.345	.9400	.6356	.3250	1.993	.9900	.7614	.3250	2.480	1.005	.8073
.3000	1.163	.9325	.5786	.3000	1.922	.9800	.7317	.3000	2.581	.9950	.7572
				.2750	1.770	.9675	.6747	.2800	2.581	.9850	.7392
				.2500	1.568	.9550	.6124	.2500	2.328	.9700	.6856

0044 CARDS

XD=		1.25				1.5	
1.510	70.89	1.000	.9448	1.600	69.91	1.000	.9405
1.500	70.89	1.000	.9448	1.500	68.90	1.000	.9413
1.400	69.87	1.000	.9456	1.400	67.78	1.000	.9421
1.300	66.84	1.000	.9479	1.300	63.32	1.000	.9456
1.200	61.77	1.000	.9519	1.200	55.42	1.000	.9520
1.100	53.67	1.000	.9587	1.100	45.39	1.000	.9608
1.000	43.54	1.000	.9678	1.000	36.17	1.000	.9698
.9000	32.91	1.000	.9785	.9000	27.66	1.000	.9792
.8000	23.29	1.000	.9899	.8000	20.47	1.000	.9884
.7200	16.20	1.000	1.000	.7000	13.58	1.000	.9989
.7000	14.38	1.007	.9825	.6900	12.97	1.000	1.000
.6500	10.63	1.020	.9395	.6500	10.54	1.007	.9762
.6000	7.696	1.032	.9267	.6000	8.105	1.020	.9444
.5500	5.722	1.042	.9115	.5500	6.180	1.032	.9484
.5000	4.354	1.050	.8949	.5000	4.813	1.045	.9286
.4600	3.565	1.052	.8704	.4400	3.749	1.052	.9229
.4500	3.443	1.050	.8843	.3900	3.293	1.045	.9000
.4000	2.886	1.042	.8593	.3500	4.002	1.030	.8758
.3750	2.734	1.030	.8553	.3200	4.711	1.017	.8277
.3500	2.856	1.017	.8546	.3000	4.509	1.007	.7897
.3250	3.241	1.005	.8439	.2500	3.394	.9775	.6968
.3000	3.544	.9925	.8466				
.2750	3.342	.9800	.8284				
.2500	2.937	.9700	.7706				

0025 CARDS

MFS=6.11,P0=2556.,T0=402.,REFS=27530.,D=.3,PTM=.7255

XD=	0.0				.1				.25			
YD	PITO	TTTTE	UUE	YD	PITO	TTTTE	UUE	YD	PITO	TTTTE	UUE
1.025	68.00	1.000	.9921	1.050	68.00	1.000	.9874	1.110	67.93	1.000	.9847
1.000	68.00	1.000	.9921	1.000	67.00	1.000	.9881	1.100	67.93	1.000	.9847
.9000	66.80	1.000	.9931	.9000	66.00	1.000	.9889	1.000	65.93	1.000	.9862
.8000	65.30	1.000	.9943	.8000	62.00	1.000	.9922	.9000	63.94	1.000	.9879
.7500	64.50	1.000	.9950	.7000	56.00	1.000	.9973	.8000	60.94	1.000	.9903
.7000	62.50	1.000	.9966	.6750	53.00	1.000	1.000	.7500	58.94	1.000	.9921
.6750	61.00	1.000	.9978	.6500	47.00	1.007	.9724	.7000	49.95	1.000	1.000
.6500	58.50	1.000	1.000	.6250	33.00	1.017	.9593	.6750	41.96	1.002	.9836
.6250	49.00	1.015	.9661	.6150	26.00	1.017	.9279	.6500	29.97	1.012	.9739
.6150	44.00	1.017	.9774	.5750	9.800	.9826	.8517	.6250	20.98	1.017	.9805
.5750	12.50	.9776	.9161	.5500	5.300	.9577	.8150	.6100	15.98	1.020	.9817
.5500	6.000	.9453	.8086	.5250	3.200	.9378	.7705	.5750	7.992	1.010	.9466
.5250	3.150	.9204	.6997	.5000	1.900	.9179	.6805	.5500	4.895	1.000	.9157
.5000	1.600	.8930	.5638	.4700	1.050	.9005	.5554	.5250	3.546	.9876	.8881
								.5000	2.597	.9751	.8827
								.4750	1.998	.9652	.8114
								.4500	1.548	.9527	.7450
								.4250	1.279	.9428	.6994

XD=	.5				1.				1.5			
1.190	68.06	1.000	.9716	1.375	67.70	1.000	.9484	1.550	66.04	1.000	.9393
1.100	67.07	1.000	.9723	1.300	66.80	1.000	.9491	1.500	65.84	1.000	.9395
1.000	66.17	1.000	.9730	1.200	65.90	1.000	.9498	1.400	65.64	1.000	.9397
.9000	63.77	1.000	.9750	1.100	63.91	1.000	.9514	1.300	63.46	1.000	.9414
.8500	61.18	1.000	.9771	1.050	61.22	1.000	.9535	1.200	56.90	1.000	.9466
.8000	54.59	1.000	.9827	1.000	56.45	1.000	.9574	1.100	47.17	1.000	.9550
.7600	46.41	1.000	.9901	.9000	43.11	1.000	.9693	1.000	37.44	1.000	.9643
.7200	36.43	1.000	1.000	.8000	30.16	1.000	.9827	.9000	29.20	1.000	.9732
.6500	17.17	1.012	.9738	.7000	19.11	1.000	.9967	.8000	21.85	1.000	.9822
.5900	8.084	1.022	.9082	.6800	16.92	1.000	1.000	.7000	15.69	1.000	.9911
.5500	4.990	1.017	.8878	.6000	9.557	1.007	.9385	.6100	10.63	1.000	1.000
.5000	3.094	1.007	.8455	.5500	6.272	1.015	.9134	.5000	5.809	1.015	.8906
.4500	2.146	.9925	.8081	.5000	4.231	1.025	.8831	.4500	4.320	1.025	.8769
.4000	1.597	.9776	.7871	.4500	3.036	1.027	.8663	.4000	3.327	1.032	.8544
.3750	1.417	.9726	.7331	.4000	2.339	1.030	.8487	.3600	2.781	1.032	.8644
.3500	1.347	.9652	.6987	.3750	2.111	1.027	.8388	.3400	2.632	1.030	.8443
.3250	1.277	.9577	.6616	.3300	1.891	1.017	.8283	.3000	3.972	1.017	.7877
.3000	1.148	.9502	.6159	.3000	2.041	1.005	.7756	.2850	4.667	1.012	.7896
.2750	.9481	.9403	.5554	.2750	2.320	.9925	.7138	.2750	4.618	1.007	.7868
				.2600	2.389	.9851	.6749	.2500	3.923	.9950	.7482

0044 CARDS

MFS=6.12,P0=3855.,T0=402.,REFS=41340.,D=.3,PTM=.7488

XD=	0.0			.1				.25			
YD	PITO	TTTTE	UUE	YD	PITO	TTTTE	UUE	YD	PITO	TTTTE	UUE
1.020	64.20	1.000	.9915	1.055	64.20	1.000	.9915	1.110	64.20	1.000	.9897
1.000	64.20	1.000	.9915	1.000	64.20	1.000	.9915	1.100	64.20	1.000	.9897
.9000	63.40	1.000	.9921	.9000	63.40	1.000	.9921	1.000	63.60	1.000	.9902
.8000	62.40	1.000	.9929	.8000	62.40	1.000	.9929	.9000	62.60	1.000	.9910
.7000	60.30	1.000	.9947	.7000	60.30	1.000	.9947	.8000	61.10	1.000	.9922
.6500	57.70	1.000	.9968	.6500	54.00	1.000	1.000	.7500	59.50	1.000	.9936
.6300	54.00	1.000	1.000	.6250	22.00	1.007	.9887	.7000	54.90	1.000	.9974
.6000	38.40	1.012	.9754	.6100	15.50	1.012	.9459	.6800	52.00	1.000	1.000
.5750	16.00	.9876	.9131	.5750	6.900	.9900	.8530	.6500	37.00	1.002	.9809
.5500	6.000	.9552	.7158	.5500	4.280	.9701	.7468	.6250	20.50	1.010	.9373
.5250	2.350	.9279	.5484	.5250	2.650	.9502	.6616	.6000	11.50	1.012	.9056
				.5000	1.750	.9254	.6302	.5750	7.500	1.007	.8916
								.5500	4.850	.9876	.8664
								.5250	3.400	.9751	.8682
								.5000	2.440	.9602	.8213
								.4750	1.800	.9502	.7806
								.4500	1.400	.9403	.7294
								.4250	1.120	.9303	.6840
								.4000	.9300	.9229	.6492

XD=	.5			1.				1.5			
1.190	64.20	1.000	.9705	1.355	64.20	1.000	.9484	1.520	64.20	1.000	.9393
1.100	63.60	1.000	.9710	1.300	64.00	1.000	.9486	1.500	64.20	1.000	.9393
1.000	62.80	1.000	.9716	1.200	62.90	1.000	.9494	1.400	63.50	1.000	.9398
.9000	61.50	1.000	.9727	1.100	61.30	1.000	.9507	1.300	61.20	1.000	.9416
.8500	59.80	1.000	.9740	1.000	55.50	1.000	.9554	1.200	56.20	1.000	.9456
.8000	55.40	1.000	.9777	.9000	46.00	1.000	.9635	1.100	47.70	1.000	.9527
.7500	47.10	1.000	.9849	.8000	33.00	1.000	.9762	1.000	38.50	1.000	.9612
.7000	34.90	1.000	.9969	.7000	20.00	1.000	.9918	.9000	30.00	1.000	.9700
.6900	32.00	1.000	1.000	.6500	14.50	1.000	1.000	.8000	22.70	1.000	.9787
.6500	22.50	1.007	.9589	.6000	10.60	1.007	.9676	.7000	16.50	1.000	.9872
.6000	12.50	1.015	.9574	.5500	7.700	1.015	.9539	.6000	11.00	1.000	.9965
.5750	9.000	1.015	.9517	.5000	5.400	1.020	.9485	.5600	9.200	1.000	1.000
.5500	6.000	1.010	.9149	.4500	3.750	1.012	.9060	.5000	6.700	1.007	.9654
.5000	3.020	.9925	.8684	.4000	2.550	1.000	.9014	.4500	5.200	1.015	.9596
.4500	1.980	.9751	.8441	.3500	1.790	.9876	.8766	.4250	4.400	1.017	.9626
.4000	1.480	.9577	.8197	.3250	1.580	.9776	.8279	.4000	3.850	1.015	.9651
.3750	1.340	.9478	.7816	.2950	1.420	.9677	.8054	.3500	2.750	1.010	.9139
.3500	1.230	.9378	.7437	.2750	1.530	.9602	.8098	.3250	2.350	1.005	.9146
.3250	1.210	.9279	.7363	.2500	1.950	.9502	.7723	.2950	2.200	1.000	.9096
.3000	1.190	.9179	.7287	.2200	2.350	.9378	.6801	.2750	2.700	.9925	.9088
.2750	1.080	.9104	.6534	.2000	2.180	.9303	.6766	.2400	4.350	.9801	.9149
.2500	.9000	.9005	.5944	.1750	1.580	.9179	.6171	.2250	4.050	.9751	.8410

0047 CARDS

MFS=6.14,P0=5153.,T0=402.,REFS=54800.,D=.3,PTM=.7442

XD=		0.0				.1				.25	
YD	PITO	TTTTE	UUE	YD	PITO	TTTTE	UUE	YD	PITO	TTTTE	UUE
1.010	62.10	1.000	.9905	1.045	62.10	1.000	.9887	1.090	62.10	1.000	.9850
1.000	62.10	1.000	.9905	1.000	62.10	1.000	.9887	1.000	62.00	1.000	.9851
.9000	61.85	1.000	.9907	.9000	61.85	1.000	.9889	.9000	61.40	1.000	.9856
.8000	60.85	1.000	.9915	.8000	60.85	1.000	.9898	.8000	60.10	1.000	.9867
.7000	59.40	1.000	.9927	.7000	59.40	1.000	.9910	.7500	58.90	1.000	.9877
.6500	57.20	1.000	.9946	.6300	49.00	1.000	1.000	.7000	55.90	1.000	.9902
.6150	51.00	1.000	1.000	.5900	22.00	1.010	.9585	.6750	51.00	1.000	.9945
.6000	44.80	1.002	.9754	.5750	14.00	1.000	.9132	.6600	45.00	1.000	1.000
.5750	23.00	1.007	.9633	.5500	6.300	.9652	.8578	.6250	28.00	1.007	.9626
.5500	10.20	.9577	.8499	.5250	3.700	.9502	.7959	.5900	14.00	1.015	.9353
.5250	4.400	.9204	.7279	.5000	2.180	.9254	.7479	.5750	9.700	1.012	.9194
.5000	1.640	.8955	.5939	.4750	1.300	.9129	.6613	.5500	5.800	.9900	.8857
				.4500	.8000	.9005	.5581	.5250	3.700	.9726	.8973
								.5000	2.520	.9552	.8721
								.4750	1.850	.9453	.7978
								.4500	1.420	.9328	.7596
								.4250	1.150	.9229	.7678
								.4000	.9800	.9129	.6828
								.3750	.8300	.9030	.6547
								.3500	.7100	.8955	.6156

XD=		.5				1.				1.5	
1.180	62.10	1.000	.9710	1.340	62.10	1.000	.9467	1.510	62.00	1.000	.9379
1.100	62.05	1.000	.9710	1.300	62.10	1.000	.9467	1.500	62.00	1.000	.9379
1.000	61.30	1.000	.9716	1.200	62.00	1.000	.9467	1.400	61.50	1.000	.9383
.9000	60.25	1.000	.9725	1.100	60.40	1.000	.9480	1.300	60.20	1.000	.9393
.8500	59.00	1.000	.9735	1.000	56.05	1.000	.9515	1.200	57.10	1.000	.9418
.8000	55.60	1.000	.9763	.9000	44.65	1.000	.9614	1.100	48.50	1.000	.9490
.7500	47.00	1.000	.9839	.8000	32.00	1.000	.9739	1.000	39.00	1.000	.9577
.7000	35.50	1.000	.9951	.7000	21.20	1.000	.9868	.9000	30.60	1.000	.9663
.6800	31.00	1.000	1.000	.6500	16.60	1.000	.9933	.8000	23.00	1.000	.9752
.6500	24.30	1.002	.9893	.6100	12.50	1.000	1.000	.7000	16.60	1.000	.9840
.6000	14.00	1.015	.9795	.5500	8.200	1.010	.9572	.6000	11.20	1.000	.9930
.5750	9.800	1.017	.9602	.5000	5.500	1.015	.9597	.5200	7.800	1.000	1.000
.5500	6.700	1.010	.9499	.4500	3.500	1.012	.9409	.5000	7.030	1.002	.9798
.5000	3.260	.9876	.9394	.4000	2.350	1.000	.9055	.4500	5.270	1.005	.9768
.4500	2.000	.9652	.9003	.3500	1.740	.9826	.8996	.4000	3.920	1.007	.9423
.4000	1.410	.9453	.8990	.3250	1.540	.9751	.8776	.3500	2.860	1.005	.9231
.3750	1.240	.9378	.8741	.3000	1.370	.9627	.8491	.3250	2.400	1.002	.8953
.3500	1.110	.9279	.8262	.2750	1.270	.9502	.8513	.3000	2.150	.9975	.8949
.3200	1.080	.9154	.8330	.2500	1.500	.9378	.8400	.2800	2.050	.9900	.8738
.3000	1.200	.9104	.7793	.2250	2.050	.9279	.8455	.2500	3.700	.9776	.8239
.2750	1.100	.9005	.7683	.2100	2.270	.9204	.7979	.2350	4.200	.9726	.7997
.2500	.9000	.8905	.7242	.1750	1.880	.9030	.7376	.2000	3.360	.9577	.7670

0048 CARDS

C.5) TABULATED MEAN FLOW DATA FOR 20 DEGREE WEDGE (H=.3,COLD WALL)

MFS=6.04,P0=1265.,T0=402.,REFS=14040.,D=.3

XD	=.1	.25	.5	1.	1.5	2.	3.	5.	7.	10.	15.	20.	25.	30.
P	=.311	.311	.423	.635	.699	.738	.832	1.01	1.07	1.10	1.13	1.14	1.13	1.09
PPCE	=5.75	5.95	9.10	21.0	28.6	15.5	17.5	19.9	22.3	23.7	24.5	25.3	25.3	25.3*.001

XD=	.1			.25			.5			1.			1.5		
YD	PITO	TTTTE	YD	PITO	TTTTE	YD	PITO	TTTTE	YD	PITO	TTTTE	YD	PITO	TTTTE
.000	.190	.216	.000	.190	.249	.000	.258	.304	.000	.492	.373	.000	.810	.435
.275	.190	.216	.175	.190	.249	.090	.258	.304	.025	.520	.378	.025	.840	.443
.300	.250	.216	.200	.200	.249	.100	.300	.313	.050	.640	.391	.050	1.00	.460
.325	.310	.261	.225	.255	.286	.125	.370	.348	.075	.830	.423	.075	1.35	.493
.350	.400	.306	.250	.340	.336	.150	.480	.378	.100	1.20	.473	.100	1.90	.555
.375	.520	.361	.275	.470	.383	.175	.630	.418	.125	1.70	.515	.125	2.65	.622
.400	.700	.410	.300	.680	.423	.200	.900	.458	.150	2.65	.580	.150	3.53	.684
.425	.960	.460	.325	.900	.465	.225	1.10	.495	.170	2.88	.634	.175	4.40	.739
.450	1.35	.508	.345	.980	.498	.250	1.27	.537				.190	4.56	.766

XD=	2.			3.			5.			7.			10.	
.000	1.04	.460	.000	1.58	.493	.000	2.49	.567	.000	3.27	.624	.000	4.07	.672
.025	1.20	.465	.025	1.70	.498	.050	2.89	.605	.050	3.67	.647	.050	4.36	.692
.050	1.40	.485	.050	1.90	.522	.100	4.09	.682	.100	4.76	.721	.100	5.34	.734
.075	1.90	.532	.075	2.30	.567	.150	5.98	.784	.150	6.75	.813	.150	7.05	.804
.100	2.45	.587	.100	2.90	.627	.200	9.17	.881	.200	10.1	.888	.200	10.1	.883
.125	3.10	.639	.125	3.50	.684	.250	13.1	.958	.250	14.6	.958	.250	14.3	.948
.150	3.80	.697	.150	4.50	.741	.300	17.0	.990	.300	18.9	.998	.300	18.5	.985
.175	4.70	.741	.175	5.50	.794	.335	18.9	1.00	.335	20.4	1.00	.365	21.7	1.00
.200	5.50	.796	.200	6.70	.843	.350	19.3	1.00	.350	20.9	1.00	.400	22.3	1.00
.225	6.40	.846	.225	8.20	.883	.400	19.8	1.00	.400	21.8	1.00	.450	22.8	1.00
.250	7.30	.891	.250	9.60	.920	.450	19.9	1.00	.450	22.1	1.00	.500	23.1	1.00
.265	7.40	.920	.275	11.2	.953				.500	22.2	1.00	.550	23.3	1.00
			.300	12.9	.973				.600	22.3	1.00	.600	23.4	1.00
			.325	14.4	.988							.700	23.6	1.00
			.350	15.3	.995							.800	23.7	1.00

XD=	15.			20.			25.			30.		
.000	4.72	.709	.000	5.24	.719	.000	5.52	.726	.000	5.78	.734	
.050	5.01	.724	.050	5.38	.736	.050	5.70	.739	.050	5.91	.741	
.100	5.77	.759	.100	5.99	.764	.100	6.16	.764	.100	6.41	.764	
.150	7.11	.809	.150	6.93	.799	.150	6.99	.796	.150	7.22	.796	
.200	9.35	.866	.200	8.43	.843	.200	8.18	.833	.200	8.48	.831	
.250	12.5	.925	.250	11.0	.893	.250	10.1	.883	.250	10.4	.866	
.300	16.4	.970	.300	13.8	.933	.300	12.6	.928	.300	12.6	.903	
.350	19.9	.995	.350	17.3	.975	.350	15.6	.960	.350	15.3	.933	
.405	22.2	1.00	.400	20.6	.995	.400	18.8	.983	.400	18.2	.958	
.450	23.2	1.00	.465	22.9	1.00	.450	21.3	.995	.450	20.3	.983	
.500	23.6	1.00	.500	23.4	1.00	.505	22.8	1.00	.500	21.7	.995	
.550	23.8	1.00	.550	23.9	1.00	.550	23.4	1.00	.540	22.2	1.00	
.600	24.1	1.00	.600	24.1	1.00	.600	23.9	1.00	.600	22.6	1.00	
.700	24.2	1.00	.700	24.5	1.00	.700	24.4	1.00	.700	23.3	1.00	
.800	24.3	1.00	.800	24.8	1.00	.800	24.7	1.00	.800	23.9	1.00	
.900	24.4	1.00	.900	25.0	1.00	.900	25.0	1.00	.900	24.5	1.00	
1.00	24.5	1.00	1.00	25.1	1.00	1.00	25.2	1.00	1.00	24.8	1.00	
			1.20	25.3	1.00	1.20	25.3	1.00	1.20	25.3	1.00	

0056 CARDS

MFS=6.11,P0=2556.,T0=402.,REFS=27530.,D=.3

XD=	.1	.25	.5	1.	1.5	2.	3.	5.	7.	10.	15.	20.	25.	30.
P	=.254	.254	.333	.526	.594	.635	.773	.957	1.01	1.03	1.04	.971	1.00	.995
PPCE	=4.41	4.53	7.29	15.7	21.8	16.4	17.8	20.2	22.3	23.5	24.6	25.5	25.9	26.0*.001

XD= .1			.25			.5			1.			1.5		
YD	PITO	TTTTE	YD	PITO	TTTTE	YD	PITO	TTTTE	YD	PITO	TTTTE	YD	PITO	TTTTE
.000	.144	.216	.000	.144	.249	.000	.189	.304	.000	.383	.373	.000	.667	.440
.300	.144	.216	.215	.144	.249	.100	.189	.304	.025	.398	.381	.025	.740	.455
.325	.270	.323	.225	.170	.286	.125	.309	.348	.050	.518	.406	.050	1.09	.490
.350	.400	.423	.250	.300	.373	.150	.469	.406	.075	.906	.460	.075	1.84	.542
.375	.520	.473	.275	.500	.448	.175	.689	.468	.100	1.67	.547	.100	2.78	.614
.400	.700	.535	.300	.829	.510	.200	.958	.515	.125	2.49	.639	.125	3.58	.697
			.325	.939	.560	.225	1.15	.570	.145	2.75	.692	.150	4.17	.771
						.250	1.23	.617				.175	4.43	.806

XD= 2.			3.			5.			7.			10.		
.000	.967	.468	.000	1.57	.522	.000	2.47	.607	.000	3.34	.639	.000	4.38	.692
.025	1.09	.478	.025	1.69	.535	.050	3.46	.654	.050	4.03	.687	.050	5.06	.726
.050	1.49	.535	.050	2.08	.587	.100	5.53	.754	.100	6.29	.784	.100	7.11	.796
.075	2.18	.602	.075	2.87	.642	.150	9.18	.866	.150	9.92	.876	.150	10.9	.883
.100	2.78	.672	.100	3.77	.709	.200	14.1	.958	.200	15.0	.958	.200	15.4	.950
.125	3.67	.734	.125	4.96	.771	.250	18.4	.998	.250	19.5	.995	.250	19.7	.990
.150	4.56	.796	.150	6.74	.841	.260	18.6	1.00	.270	20.3	1.00	.285	21.1	1.00
.175	5.55	.846	.175	7.63	.883	.300	19.9	1.00	.300	21.1	1.00	.300	21.5	1.00
.200	6.74	.886	.200	9.32	.929	.350	20.2	1.00	.350	21.8	1.00	.350	22.2	1.00
.230	7.93	.901	.225	11.3	.958	.400	20.1	1.00	.400	22.1	1.00	.400	22.6	1.00
			.250	13.4	.978				.500	22.3	1.00	.500	23.1	1.00
			.275	15.2	.993				.600	22.1	1.00	.600	23.3	1.00
			.290	15.3	.998							.700	23.5	1.00

XD= 15.			20.			25.			30.		
.000	6.89	.751	.000	11.9	.845	.000	15.5	.908	.000	17.0	.945
.050	7.37	.766	.050	12.1	.851	.050	15.6	.908	.050	17.0	.945
.100	9.09	.809	.100	12.6	.866	.100	15.8	.913	.100	17.1	.950
.150	11.4	.866	.150	13.6	.886	.150	16.0	.925	.150	17.2	.960
.200	14.4	.915	.200	14.7	.915	.200	16.4	.943	.200	17.4	.968
.250	17.5	.955	.250	16.2	.938	.250	17.0	.953	.250	17.6	.975
.300	20.4	.985	.300	17.9	.960	.300	17.6	.963	.300	18.0	.983
.355	22.3	1.00	.350	19.5	.980	.400	19.1	.978	.400	19.0	.990
.400	23.1	1.00	.400	20.9	.990	.500	20.8	.990	.500	20.1	.993
.500	23.8	1.00	.450	21.9	.995	.600	22.6	.995	.600	21.4	.995
.600	24.1	1.00	.500	22.9	.998	.700	23.9	.998	.700	22.7	.998
.700	24.3	1.00	.550	23.6	1.00	.775	24.5	1.00	.800	23.9	.998
.800	24.4	1.00	.600	24.1	1.00	.800	24.7	1.00	.900	24.8	.998
.900	24.5	1.00	.700	24.6	1.00	.900	25.3	1.00	.940	25.0	1.00
1.00	24.6	1.00	.900	25.1	1.00	1.00	25.7	1.00	1.00	25.4	1.00
			1.10	25.5	1.00	1.20	25.9	1.00	1.20	26.0	1.00

0049 CARDS

MFS=6.12,P0=3854.,T0=403.,REFS=41190.,D=.3

XD	.1	.25	.5	1.	1.5	2.	3.	5.	7.	10.	15.	20.	25.	30.
P	.218	.218	.277	.505	.540	.616	.785	.974	1.02	1.03	1.02	1.01	1.06	1.07
PPCE	3.85	4.14	6.13	15.6	19.9	16.4	17.8	20.3	22.4	23.5	24.6	25.6	25.9	26.0*.001

XD= .1			.25			.5			1.			1.5		
YD	PITO	TTTTE	YD	PITO	TTTTE	YD	PITO	TTTTE	YD	PITO	TTTTE	YD	PITO	TTTTE
.000	.123	.216	.000	.123	.248	.000	.155	.303	.000	.292	.372	.000	.524	.434
.320	.123	.216	.230	.123	.248	.100	.155	.303	.025	.328	.385	.025	.675	.447
.325	.154	.223	.250	.199	.335	.125	.269	.335	.050	.497	.434	.050	1.24	.484
.350	.319	.360	.275	.398	.397	.150	.428	.372	.075	.954	.496	.075	2.11	.546
.375	.618	.422	.300	.796	.447	.175	.687	.429	.100	1.73	.558	.100	3.02	.633
.400	.697	.484	.325	.946	.509	.200	.965	.484	.125	2.49	.620	.125	3.97	.769
						.225	1.17	.546	.140	2.64	.663	.150	4.92	.794
						.250	1.22	.593				.175	5.31	.836

XD= 2.			3.			5.			7.			10.		
.000	.831	.467	.000	1.55	.521	.000	2.92	.620	.000	4.13	.663	.000	5.58	.754
.025	1.19	.491	.025	1.69	.534	.050	4.11	.680	.050	5.41	.720	.050	6.07	.774
.050	1.79	.546	.050	2.48	.601	.100	7.32	.799	.100	8.71	.824	.100	9.39	.839
.075	2.58	.608	.075	3.47	.670	.150	11.9	.913	.150	13.2	.923	.150	13.2	.931
.100	3.48	.682	.100	4.91	.740	.200	17.5	.993	.200	18.1	.988	.200	17.5	.978
.125	4.37	.744	.125	6.44	.807	.225	19.1	1.00	.240	20.8	1.00	.250	20.3	.993
.150	5.46	.831	.150	8.08	.876	.250	19.7	1.00	.300	21.5	1.00	.270	20.8	1.00
.175	6.55	.893	.175	10.1	.918	.300	20.2	1.00	.350	21.9	1.00	.300	21.6	1.00
.205	7.99	.943	.200	12.4	.960	.350	20.3	1.00	.400	22.2	1.00	.350	22.3	1.00
			.225	14.4	.980	.410	19.8	1.00	.500	22.4	1.00	.400	22.6	1.00
			.260	15.1	.995							.450	22.9	1.00
												.500	23.1	1.00
												.600	23.5	1.00

XD= 15.			20.			25.			30.		
.000	10.4	.876	.000	14.7	.926	.000	17.1	.943	.000	17.7	.953
.050	10.9	.883	.050	14.8	.928	.050	17.2	.945	.050	17.7	.955
.100	12.1	.898	.100	15.2	.936	.100	17.4	.950	.100	17.8	.960
.150	13.7	.918	.150	15.8	.943	.150	17.6	.955	.150	18.0	.968
.200	15.8	.945	.200	16.6	.953	.200	17.9	.958	.200	18.2	.975
.250	18.1	.963	.250	17.5	.960	.250	18.4	.963	.250	18.6	.980
.300	20.2	.980	.300	18.5	.973	.300	18.9	.968	.300	18.9	.983
.350	21.6	.990	.350	19.5	.980	.350	19.5	.975	.350	19.4	.985
.410	22.7	1.00	.400	20.4	.988	.400	20.2	.980	.400	19.8	.990
.450	23.2	1.00	.450	21.5	.990	.450	20.9	.985	.450	20.3	.993
.500	23.6	1.00	.500	22.3	.995	.500	21.7	.990	.500	20.9	.993
.600	24.1	1.00	.600	23.6	.998	.600	23.1	.995	.600	22.1	.995
.700	24.3	1.00	.630	23.9	1.00	.700	24.2	.998	.700	23.2	.995
.800	24.4	1.00	.700	24.4	1.00	.785	24.9	1.00	.800	24.0	.998
.900	24.6	1.00	.800	24.7	1.00	.800	25.0	1.00	.900	24.7	.998
1.00	24.5	1.00	.900	25.1	1.00	.900	25.4	1.00	.960	25.0	1.00
			1.00	25.3	1.00	1.00	25.8	1.00	1.00	25.3	1.00
			1.10	25.6	1.00	1.10	25.9	1.00	1.30	26.0	1.00

0051 CARDS

MFS=6.14,P0=5151.,T0=403.,REFS=54580.,D=.3

XD	=.1	.25	.5	1.	1.5	2.	3.	5.	7.	10.	15.	20.	25.	30.
P	=.202	.202	.240	.448	.508	.592	.795	.972	1.01	1.01	1.01	1.05	1.09	1.06
PPCE=	3.43	3.53	5.16	13.9	19.4	16.4	17.9	20.3	22.1	23.3	24.2	25.3	26.0	26.4*.001

XD= .1			.25			.5			1.			1.5		
YD	PITO	TTTTE	YD	PITO	TTTTE	YD	PITO	TTTTE	YD	PITO	TTTTE	YD	PITO	TTTTE
.000	.111	.216	.000	.111	.248	.000	.132	.303	.000	.250	.372	.000	.503	.422
.330	.111	.216	.240	.111	.248	.130	.132	.303	.025	.289	.377	.025	.666	.427
.350	.200	.248	.250	.145	.273	.150	.200	.340	.050	.498	.397	.050	1.59	.439
.375	.460	.323	.275	.300	.335	.175	.419	.392	.075	.917	.434	.075	2.64	.484
.400	.600	.397	.300	.599	.397	.200	.798	.442	.100	1.79	.472	.100	3.68	.558
			.330	.899	.472	.225	1.12	.491	.125	2.39	.521	.125	4.28	.720
						.260	1.20	.558	.135	2.39	.551	.150	4.28	.856

XD= 2.			3.			5.			7.			10.		
.000	.908	.459	.000	1.89	.529	.000	3.72	.633	.000	5.13	.695	.000	7.07	.789
.025	1.19	.484	.025	2.38	.541	.050	4.96	.665	.050	6.32	.730	.050	7.95	.807
.050	2.04	.539	.050	3.57	.591	.100	8.59	.749	.100	9.67	.794	.100	10.6	.856
.075	2.78	.596	.075	4.67	.645	.150	14.1	.888	.150	14.8	.888	.150	14.6	.921
.100	3.77	.645	.100	5.96	.707	.200	18.9	1.00	.210	19.6	1.00	.200	18.4	.968
.125	4.77	.720	.125	7.54	.794	.250	19.9	1.00	.250	20.8	1.00	.250	20.7	1.00
.150	5.96	.807	.150	9.43	.888	.300	20.3	1.00	.300	21.3	1.00	.300	21.6	1.00
.175	7.35	.869	.175	11.2	.950	.350	20.1	1.00	.350	21.7	1.00	.350	22.1	1.00
.190	7.94	.918	.200	13.8	.978				.400	22.0	1.00	.400	22.5	1.00
			.235	14.9	.995				.450	22.1	1.00	.450	22.7	1.00
									.500	22.1	1.00	.500	22.9	1.00
												.600	23.1	1.00
												.700	23.3	1.00

XD= 15.			20.			25.			30.		
.000	12.1	.918	.000	15.3	.936	.000	16.8	.943	.000	17.4	.950
.050	12.3	.923	.050	15.3	.938	.050	16.8	.948	.050	17.5	.953
.100	13.3	.933	.100	15.7	.945	.100	17.0	.958	.100	17.6	.955
.150	14.7	.945	.150	16.2	.950	.150	17.4	.963	.150	17.9	.960
.200	16.4	.960	.200	16.9	.963	.200	17.8	.970	.200	18.2	.968
.250	18.1	.978	.250	17.8	.973	.250	18.4	.978	.250	18.6	.975
.300	19.6	.985	.300	18.8	.980	.300	18.9	.980	.300	19.1	.980
.350	21.0	.995	.350	19.9	.988	.350	19.7	.983	.350	19.6	.983
.400	22.0	.998	.400	21.0	.993	.400	20.5	.988	.400	20.2	.985
.420	22.2	1.00	.450	21.9	.995	.450	21.3	.990	.450	20.8	.988
.450	22.5	1.00	.500	22.7	.998	.500	22.1	.993	.500	21.5	.990
.500	23.0	1.00	.585	23.6	1.00	.600	23.4	.995	.600	22.7	.993
.600	23.4	1.00	.600	23.7	1.00	.700	24.4	.998	.700	23.7	.995
.700	23.7	1.00	.700	24.2	1.00	.735	24.6	1.00	.800	24.5	.998
.800	23.9	1.00	.800	24.5	1.00	.800	25.0	1.00	.900	25.0	1.00
.900	24.0	1.00	.900	24.8	1.00	.900	25.3	1.00	1.00	25.3	1.00
1.00	24.2	1.00	1.00	25.0	1.00	1.00	25.5	1.00	1.30	26.4	1.00
			1.20	25.3	1.00	1.30	26.0	1.00			

0050 CARDS

MFS=6.04,P0=1265.,T0=402.,REFS=14040.,D=.3,PTM=.7581

XD=	0.0			.1				.25			
YD	PITO	TTTTE	UUE	YD	PITO	TTTTE	UUE	YD	PITO	TTTTE	UUE
1.040	65.20	1.000	.9924	1.070	65.20	1.000	.9907	1.125	65.20	1.000	.9873
1.000	65.20	1.000	.9924	1.000	64.80	1.000	.9910	1.100	65.00	1.000	.9874
.9000	64.30	1.000	.9931	.9000	64.00	1.000	.9917	1.000	64.30	1.000	.9879
.8000	63.20	1.000	.9940	.8000	62.90	1.000	.9926	.9000	63.70	1.000	.9884
.7000	61.80	1.000	.9952	.7000	59.00	1.000	.9957	.8000	62.50	1.000	.9894
.6500	60.00	1.000	.9966	.6550	54.00	1.000	1.000	.7500	61.50	1.000	.9902
.6300	56.00	1.000	1.000	.6500	52.00	.9975	.9976	.7000	55.00	1.000	.9956
.6250	54.00	.9975	.9897	.6250	40.00	.9627	.9780	.6850	50.00	1.000	1.000
.6000	35.00	.9900	.9035	.6000	25.50	.8831	.9062	.6500	33.00	1.007	.9590
.5750	18.50	.8706	.7634	.5750	15.00	.8085	.8730	.6000	15.20	.9279	.8757
.5500	9.400	.7040	.6614	.5500	8.000	.7338	.8165	.5500	7.000	.8159	.8106
.5250	4.500	.5721	.5649	.5250	4.600	.6592	.7176	.5000	3.650	.7164	.7630
.5000	2.100	.4602	.5080	.5000	2.900	.6045	.6767	.4500	1.940	.6418	.6459
.4750	1.100	.3731	.4191	.4750	1.950	.5597	.5909	.4000	1.270	.5672	.5798
.4500	.5800	.2488	.5154	.4500	1.350	.5075	.4817	.3450	.9800	.4975	.4678
.4250	.3200	.2239	.3488	.4250	.9700	.4602	.3565	.3250	.9000	.4652	.3656
.4000	.1900	.1915	.1973								

XD=	.5			1.				1.5			
1.200	65.20	1.000	.9780	1.370	65.20	1.000	.9505	1.530	65.20	1.000	.9408
1.100	65.00	1.000	.9782	1.300	65.00	1.000	.9507	1.500	65.20	1.000	.9408
1.000	64.20	1.000	.9788	1.200	64.20	1.000	.9513	1.400	65.10	1.000	.9409
.9500	63.80	1.000	.9791	1.100	63.50	1.000	.9518	1.300	65.00	1.000	.9409
.9000	63.20	1.000	.9796	1.050	62.00	1.000	.9530	1.200	60.20	1.000	.9446
.8500	62.20	1.000	.9804	1.000	58.00	1.000	.9562	1.100	49.30	1.000	.9536
.8000	57.50	1.000	.9842	.9000	45.00	1.000	.9673	1.000	39.30	1.000	.9626
.7600	49.50	1.000	.9911	.8000	32.00	1.000	.9800	.9000	30.40	1.000	.9717
.7200	40.00	1.000	1.000	.7000	20.70	1.000	.9935	.8000	22.90	1.000	.9805
.7000	35.00	1.007	.9776	.6600	16.20	1.000	1.000	.7000	16.50	1.000	.9893
.6500	22.50	1.005	.9646	.6500	15.00	.9975	.9868	.6000	11.10	1.000	.9983
.6000	12.80	.9453	.9146	.6000	10.60	.9851	.9734	.5850	10.20	1.000	1.000
.5500	7.000	.8905	.8656	.5500	7.600	.9602	.9450	.5500	8.600	.9975	.9846
.5000	4.200	.8333	.7987	.5000	5.400	.9279	.9025	.5000	6.600	.9876	.9744
.4500	2.720	.7861	.7461	.4500	3.950	.8930	.8706	.4500	5.100	.9701	.9329
.4000	1.870	.7363	.6756	.4000	2.950	.8582	.8217	.4000	4.000	.9453	.8731
.3500	1.450	.6915	.5555	.3500	2.280	.8284	.7827	.3500	3.200	.9204	.8491
.3250	1.350	.6592	.5214	.3000	1.850	.8109	.7039	.3000	2.650	.8831	.7710
.3000	1.300	.6244	.4907	.2500	1.600	.7886	.6324	.2750	2.500	.8607	.7350
.2750	1.300	.5796	.4845	.2250	1.630	.7662	.6196	.2500	2.600	.8408	.7378
.2500	1.250	.5373	.4534	.2000	2.100	.7189	.6167	.2250	3.600	.8134	.7249
.2250	1.080	.4950	.3732	.1750	2.880	.6219	.5671	.2000	4.560	.7662	.6908
				.1500	2.650	.5796	.5550	.1750	4.400	.7388	.6879

0046 CARDS

MFS=6.11,P0=2556.,T0=402.,REFS=27530.,D=.3,PTM=.7488

XD=	0.0			.1				.25			
YD	PITO	TTTTE	UUE	YD	PITO	TTTTE	UUE	YD	PITO	TTTTE	UUE
1.000	62.50	1.000	.9937	1.030	62.50	1.000	.9929	1.080	62.44	1.000	.9902
.9000	61.90	1.000	.9942	1.000	62.00	1.000	.9933	1.000	61.94	1.000	.9906
.8000	61.10	1.000	.9949	.9000	61.70	1.000	.9935	.9000	61.34	1.000	.9911
.7000	60.00	1.000	.9958	.8000	60.80	1.000	.9943	.8000	60.44	1.000	.9919
.6500	59.00	1.000	.9966	.7000	59.00	1.000	.9957	.7000	58.44	1.000	.9935
.6000	55.70	1.000	.9994	.6500	56.00	1.000	.9983	.6800	55.94	1.000	.9956
.5950	55.00	1.000	1.000	.6200	54.00	1.000	1.000	.6600	50.95	1.000	1.000
.5750	43.00	.9826	.9580	.6000	38.00	1.007	.9820	.6300	37.46	1.020	.9822
.5500	18.00	.8955	.8939	.5750	22.00	.9328	.9730	.6000	23.48	.9950	.9650
.5250	7.400	.7711	.7744	.5500	12.50	.8458	.9364	.5500	9.491	.9030	.9117
.5000	3.000	.6418	.6100	.5250	6.600	.7836	.8445	.5000	4.096	.8159	.8254
.4750	1.300	.4975	.5149	.5000	3.600	.7214	.7699	.4500	2.048	.7537	.7916
.4500	.5600	.3731	.4643	.4750	2.100	.6791	.6633	.4000	1.239	.6841	.7376
				.4500	1.380	.6294	.6094	.3500	.9291	.6070	.6726
				.4250	.9500	.5846	.5566	.3300	.9291	.5597	.5932

XD=	.5			1.				1.5			
1.160	62.38	1.000	.9729	1.330	62.22	1.000	.9538	1.490	62.07	1.000	.9439
1.100	61.88	1.000	.9733	1.300	62.12	1.000	.9538	1.400	61.57	1.000	.9443
1.000	61.48	1.000	.9736	1.200	61.62	1.000	.9542	1.300	60.77	1.000	.9450
.9000	60.68	1.000	.9743	1.100	60.73	1.000	.9550	1.200	57.89	1.000	.9472
.8000	58.88	1.000	.9757	1.050	60.03	1.000	.9555	1.100	48.96	1.000	.9547
.7500	49.40	1.000	.9838	1.000	58.54	1.000	.9567	1.000	39.72	1.000	.9632
.7000	37.43	1.000	.9953	.9500	53.76	1.000	.9606	.9000	31.28	1.000	.9718
.6800	32.93	1.000	1.000	.9000	45.89	1.000	.9675	.8000	23.83	1.000	.9805
.6400	23.45	1.020	.9837	.8000	32.75	1.000	.9804	.7000	17.38	1.000	.9893
.6000	15.47	.9950	.9950	.7000	21.80	1.000	.9934	.6200	12.12	1.000	.9978
.5500	8.084	.9378	.9582	.6500	17.12	1.000	1.000	.5700	10.92	1.000	1.000
.5000	4.591	.8881	.9153	.6000	12.74	.9900	.9917	.5500	9.930	.9950	.9844
.4500	2.844	.8408	.8648	.5500	9.159	.9701	.9862	.5000	7.845	.9826	.9937
.4000	1.896	.7960	.7912	.5000	6.471	.9527	.9906	.4500	6.058	.9677	.9627
.3500	1.347	.7463	.7394	.4500	4.530	.9279	.9303	.4000	4.667	.9552	.9512
.3000	1.118	.6915	.6918	.4000	3.186	.9080	.9012	.3500	3.525	.9378	.9148
.2500	1.228	.6169	.6695	.3500	2.290	.8856	.8382	.3000	2.731	.9254	.9060
.2250	1.148	.5697	.6420	.3000	1.762	.8632	.8199	.2500	2.185	.9005	.8855
.2000	.9681	.5149	.6134	.2500	1.414	.8259	.8017	.2300	1.986	.8706	.8747
.1750	.6986	.4677	.5691	.2100	1.254	.7910	.7733	.2000	2.681	.8383	.8398
.1500	.4691	.4055	.5136	.1750	1.842	.7463	.7665	.1750	4.369	.8060	.7609

0042 CARDS

MFS=6.12,P0=3854.,T0=403.,REFS=41190.,D=.3,PTM=.7674

XD=	0.0			.1				.25			
YD	PITO	TTTTE	UUE	YD	PITO	TTTTE	UUE	YD	PITO	TTTTE	UUE
.9950	61.75	1.000	.9934	1.030	61.75	1.000	.9916	1.075	61.72	1.000	.9854
.9000	61.55	1.000	.9935	1.000	61.55	1.000	.9918	1.000	61.42	1.000	.9856
.8000	60.96	1.000	.9940	.9000	61.25	1.000	.9920	.9000	60.93	1.000	.9860
.7000	59.96	1.000	.9948	.8000	60.56	1.000	.9926	.8000	60.23	1.000	.9866
.6500	59.06	1.000	.9955	.7000	59.16	1.000	.9937	.7000	58.34	1.000	.9881
.6000	56.77	1.000	.9975	.6500	55.78	1.000	.9966	.6750	55.75	1.000	.9903
.5850	53.78	1.000	1.000	.6100	51.79	1.000	1.000	.6500	48.78	1.000	.9964
.5750	49.80	.9926	.9773	.5900	41.83	1.005	.9794	.6400	44.80	1.000	1.000
.5500	23.90	.8685	.9133	.5750	31.87	.9677	.9672	.6250	36.83	1.002	.9856
.5250	9.163	.7444	.7078	.5500	17.93	.8511	.9684	.5900	20.91	1.017	.9420
.5000	3.187	.6203	.5267	.5250	9.163	.7816	.9125	.5500	10.45	.9429	.8794
.4750	1.195	.4963	.3938	.5000	3.586	.7196	.7572	.5000	4.480	.8313	.8043
				.4750	2.141	.6700	.6629	.4500	2.041	.7395	.7699
				.4500	1.295	.6005	.5745	.4000	1.145	.6576	.7061
				.4250	.8566	.5459	.4454	.3500	.8960	.5583	.6515
				.4000	.6972	.4839	.5170	.3250	.9457	.5087	.6021
				.3750	.6175	.4218	.6117	.3000	.7964	.4467	.5887

XD=	.5			1.				1.5			
1.150	61.69	1.000	.9732	1.315	61.63	1.000	.9533	1.480	61.57	1.000	.9450
1.100	61.49	1.000	.9733	1.300	61.43	1.000	.9535	1.400	61.07	1.000	.9454
1.000	60.80	1.000	.9739	1.200	60.74	1.000	.9540	1.300	60.58	1.000	.9458
.9000	60.10	1.000	.9744	1.100	60.14	1.000	.9545	1.200	57.60	1.000	.9482
.8000	58.61	1.000	.9756	1.000	58.05	1.000	.9561	1.100	49.26	1.000	.9550
.7500	52.24	1.000	.9810	.9000	47.71	1.000	.9648	1.000	40.02	1.000	.9634
.7000	38.81	1.000	.9933	.8000	33.80	1.000	.9781	.9000	31.58	1.000	.9719
.6700	32.34	1.000	1.000	.7000	22.37	1.000	.9912	.8000	23.93	1.000	.9806
.6500	27.36	1.002	.9695	.6300	16.10	1.000	1.000	.7000	17.87	1.000	.9887
.6100	18.91	1.017	.9692	.6000	13.82	.9926	.9878	.6000	12.71	1.000	.9968
.5500	9.652	.9752	.8791	.5500	10.14	.9777	.9882	.5600	10.92	1.000	1.000
.5000	5.373	.9057	.8647	.5000	7.058	.9529	.9310	.5000	8.739	.9851	.9844
.4500	2.985	.8437	.8387	.4500	4.970	.9256	.9143	.4500	7.100	.9727	.9845
.4000	1.841	.7816	.7910	.4000	3.479	.8983	.8923	.4000	5.660	.9479	.9511
.3500	1.294	.7295	.7238	.3500	2.416	.8610	.8476	.3500	4.419	.9256	.9517
.3000	1.045	.6650	.6945	.3000	1.759	.8313	.8103	.3000	3.426	.9057	.8972
.2750	1.154	.6328	.6818	.2500	1.352	.8065	.7814	.2500	2.632	.8784	.8894
.2500	1.224	.5931	.6438	.2100	1.223	.7866	.7537	.2100	2.383	.8586	.8516
.2250	1.144	.5459	.6523	.2000	1.243	.7816	.7749	.1750	5.313	.8362	.8759
.2000	.9453	.4839	.6324	.1750	1.690	.7370	.7418	.1500	4.916	.8065	.8481
.1750	.6667	.4293	.5424	.1500	2.535	.6824	.7164	.1250	3.972	.7196	.7972

0044 CARDS

MFS=6.14,P0=5151.,T0=403.,REFS=54580.,D=.3,PTM=.7720

XD=	0.0			.1				.25			
YD	PITO	TTTTF	UUE	YD	PITO	TTTTE	UUE	YD	PITO	TTTTE	UUE
.9700	61.00	1.000	.9950	1.000	61.00	1.000	.9942	1.050	60.94	1.000	.9916
.9000	60.50	1.000	.9954	.9000	60.40	1.000	.9946	1.000	60.74	1.000	.9917
.8000	60.00	1.000	.9958	.8000	59.90	1.000	.9950	.9000	60.29	1.000	.9921
.7000	59.30	1.000	.9964	.7000	58.90	1.000	.9959	.8000	59.64	1.000	.9926
.6500	58.50	1.000	.9971	.6000	54.00	1.000	1.000	.7000	58.44	1.000	.9936
.6000	57.10	1.000	.9982	.5750	30.00	.9677	.9858	.6500	54.75	1.000	.9967
.5750	55.00	1.000	1.000	.5500	13.00	.8883	.9380	.6350	50.95	1.000	1.000
.5500	33.00	.9677	.9395	.5250	6.700	.7940	.8747	.6250	46.95	1.007	.9949
.5250	11.50	.7940	.8518	.5000	3.600	.7072	.8165	.6000	32.97	1.017	.9727
.5000	3.500	.6203	.6370	.4750	1.970	.6328	.7263	.5500	10.99	.9553	.9314
.4750	.9600	.4218	.3398	.4500	1.100	.5583	.6221	.5000	4.196	.8313	.8373
				.4250	.7700	.4715	.5489	.4500	1.898	.7320	.7945
				.4000	.6000	.3970	.4963	.4000	1.049	.6377	.7163
				.3750	.4500	.3226	.4534	.3700	.7992	.5658	.6907
				.3500	.2000	.2481	.2927	.3500	.8492	.5211	.6151
								.3300	.8991	.4715	.5903

XD=	.5			1.				1.5			
1.125	60.88	1.000	.9750	1.295	60.79	1.000	.9529	1.450	60.67	1.000	.9436
1.100	60.58	1.000	.9753	1.200	59.99	1.000	.9535	1.400	60.17	1.000	.9440
1.000	60.18	1.000	.9756	1.100	59.39	1.000	.9540	1.300	59.67	1.000	.9444
.9000	59.68	1.000	.9760	1.000	58.00	1.000	.9551	1.200	58.28	1.000	.9455
.8000	58.88	1.000	.9767	.9500	53.81	1.000	.9585	1.100	50.42	1.000	.9519
.7500	54.39	1.000	.9804	.9000	47.63	1.000	.9637	1.000	40.48	1.000	.9607
.7000	42.91	1.000	.9905	.8000	34.08	1.000	.9766	.9000	31.82	1.000	.9693
.6600	33.43	1.000	1.000	.7000	23.12	1.000	.9890	.8000	24.66	1.000	.9774
.6500	30.94	1.005	.9865	.6100	15.25	1.000	1.000	.7000	18.30	1.000	.9857
.6000	18.96	1.017	.9869	.6000	14.35	.9975	1.000	.6000	12.93	1.000	.9940
.5500	10.38	.9926	.9351	.5500	10.76	.9926	.9880	.5200	9.647	1.000	1.000
.5000	5.140	.9305	.9053	.5000	7.573	.9801	.9823	.5000	8.851	.9975	.9919
.4500	2.944	.8561	.8612	.4500	5.132	.9578	.9335	.4500	7.011	.9926	.9856
.4000	1.747	.7940	.7923	.4000	3.438	.9256	.9251	.4000	5.370	.9851	.9503
.3500	1.148	.7320	.7203	.3500	2.392	.8933	.8786	.3500	4.078	.9677	.9255
.3300	1.018	.7072	.6875	.3000	1.724	.8561	.8254	.3000	3.133	.9479	.8999
.3000	.9780	.6576	.7115	.2500	1.295	.8189	.7775	.2500	2.287	.9256	.8305
.2600	1.198	.5583	.6348	.2000	1.196	.7692	.7798	.2000	1.790	.8983	.8139
.2400	1.148	.5211	.6533	.1750	1.365	.6824	.7065	.1800	1.740	.8834	.7996
.2250	1.048	.4913	.6399	.1500	2.093	.5831	.7149	.1500	4.674	.8437	.8071
.2000	.7984	.4417	.5839	.1350	2.392	.5509	.6753	.1250	4.177	.7816	.7769

0043 CARDS

TABLE I

Test Summary

Model	p_o, psig	Re_∞/in.	M_∞	T_{t_∞} °K	T_{model}, °K	Measured data	$\frac{x}{H}$
Flat Plate c=1.0 in., τ= .016 in. (FP)	10	$.47\times10^5$	6.04	403	Ad. Wall	$\frac{p_{t_2}}{p_o}$, $p_{\text{¢}}$, T_t	.1→9 ($\frac{x}{L}$)
	35	.94	6.07	404			
	60	1.40	6.08	404			
	85	1.90×10^5	6.10	404			
20° Wedge H = .15 in. (.15w)	10	$.47\times10^5$	6.04	402	Ad. Wall	$\frac{p_{t_2}}{p_o}$, $p_{\text{¢}}$	5→60
	35	.94	6.07	402			
	60	1.40	6.08	402			
	85	1.90×10^5	6.10	402			
20° Wedge H = .15 in. (.15w)	10*	$.47\times10^5$	6.05	400	Ad. Wall	p_b	0
	20	.67	6.10	402			
	35*	.94	6.11	402			
	50	1.22	6.11	402			
20° Wedge H= .3 in. (3w-1)	60*	1.42	6.12	402		p_b	0
	70	1.60	6.13	402		p^*_{ws}	-.15, -.45, -.65
	85*	1.90	6.14	402			
	100	2.18×10^5	6.15	402			
20° Wedge H = .3 in. (.3w-2A)	10	$.47\times10^5$	6.05	400	348	$\frac{p_{t_2}}{p_o}$, $p_{\text{¢}}$, T_t, Nu_t	0→30
	35	.94	6.11	402	350		
	60	1.40	6.12	402	351		
	85	1.90×10^5	6.14	402	351		
20° Wedge H = .3 in. (.3w-2C)	10	$.47\times10^5$	6.04	402	77	$\frac{p_{t_2}}{p_o}$, $p_{\text{¢}}$, T_t, Nu_t	0→30
	35	.94	6.11	402	77		
	60	1.40	6.12	403	77		
	85	1.90×10^5	6.14	403	77		

TABLE II

Accuracy Summary

Quantity	Overall Uncertainty	
	Shear Layer	Wake
Measured Data		
p_{t_2}/P_o	± 2%	± 2%
p_{ℓ}/p_∞	---	± 2%
p_e/p_∞ (Far Wake)	---	± 5%
T_{awm}	± .5%	± .5%
Nu_t	± 3%	---
p_b/p_∞ (Base Tap)	± 4%	---
p_b/p_∞ (ℓ Probe-Low Re)	+ 7%	---
p_{ws}/p_∞ (Ad. Wall)	± 2%	---
$x/H)_{sp}$	± .1H	---
Derived Result		
T_t/T_o (Min.-Edge)	± 1%	± 1%
T_t/T_o (Max.-Ad. Wall)	± 2%	± 1%
T_t/T_o (Max.-Cold Wall)	± 15°K	± 10°K
$\rho u/\rho_\infty u_\infty$	± 5%	---
u/u_e	± 7%	± 2%
M	± 15%	± 3%
p/p_∞	± 20%	---
p_t/p_o	± 20%	± 4%
T/T_e	± 15%	± 3%
x, y	± .002 in.	± .002 in.
$\psi/\rho_\infty u_\infty H$		
$\left(\frac{T_t}{T_o}\right)_C$	$0 \leq \frac{x}{H} \leq .25$	± .01H	---
	$\frac{x}{H} > .25$	± .02H	---
$\left(\frac{P_t}{P_o}\right)_C$			

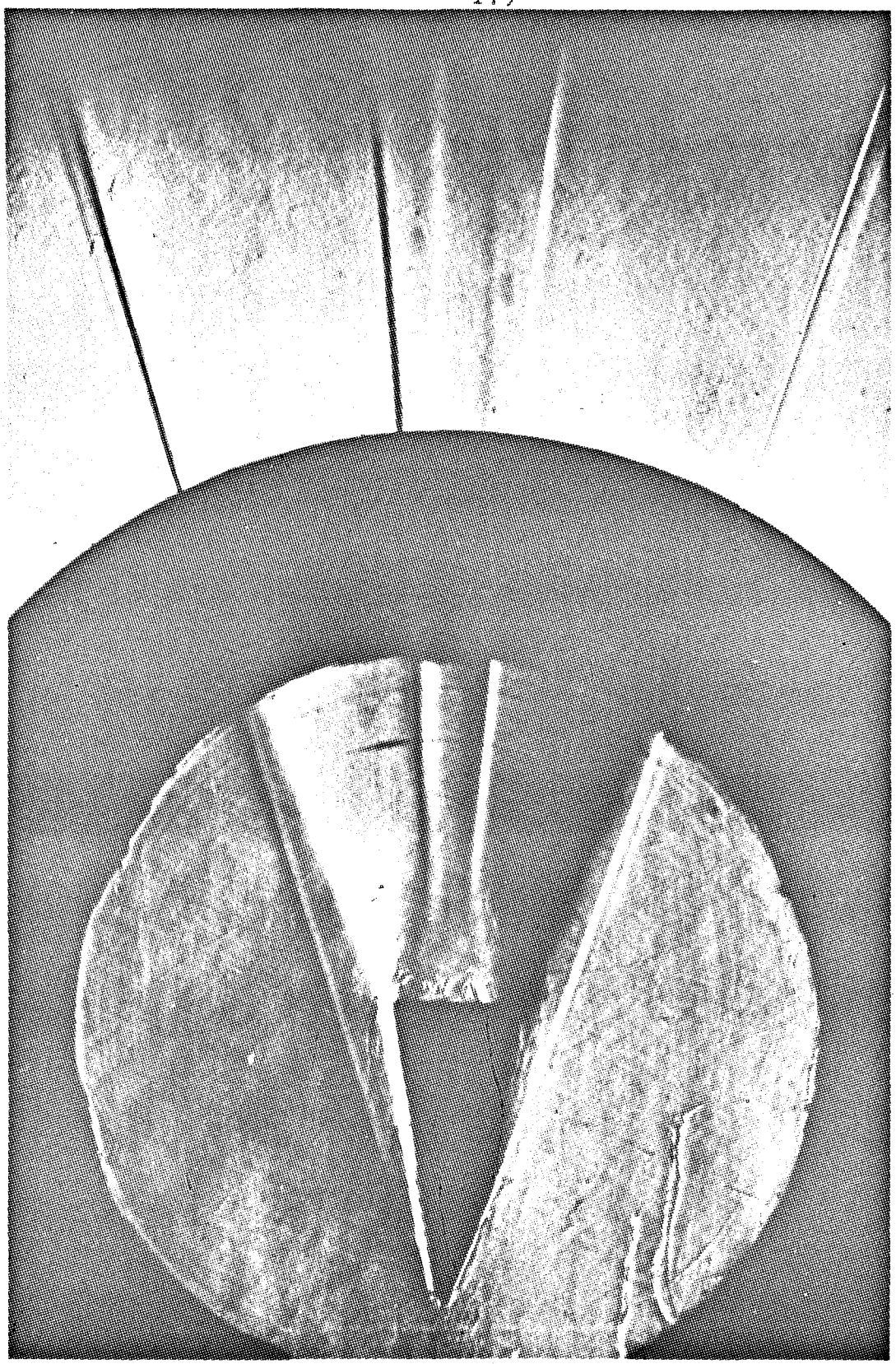

Fig. 1 Schlieren Photograph of Wake behind 20°, Adiabatic Wall Wedge ($H = .3$) at $M_\infty = 6$ and $Re_{\infty H} = 5.2 \times 10^4$

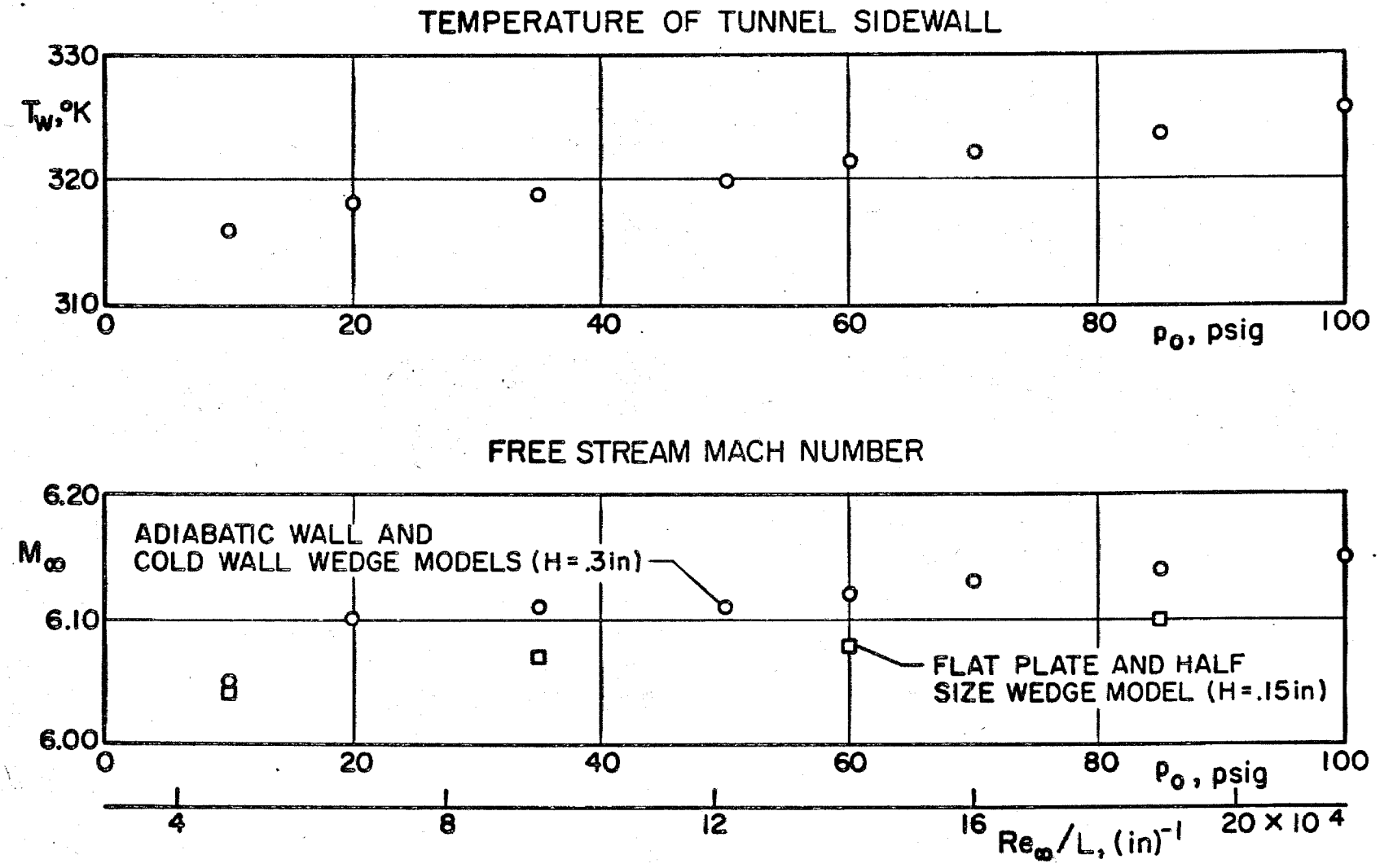

FIG.2 VARIATION OF FREE STREAM MACH NUMBER AND TEMPERATURE OF TUNNEL SIDEWALL WITH FREE STREAM STAGNATION PRESSURE - THIRD PORT CENTERLINE

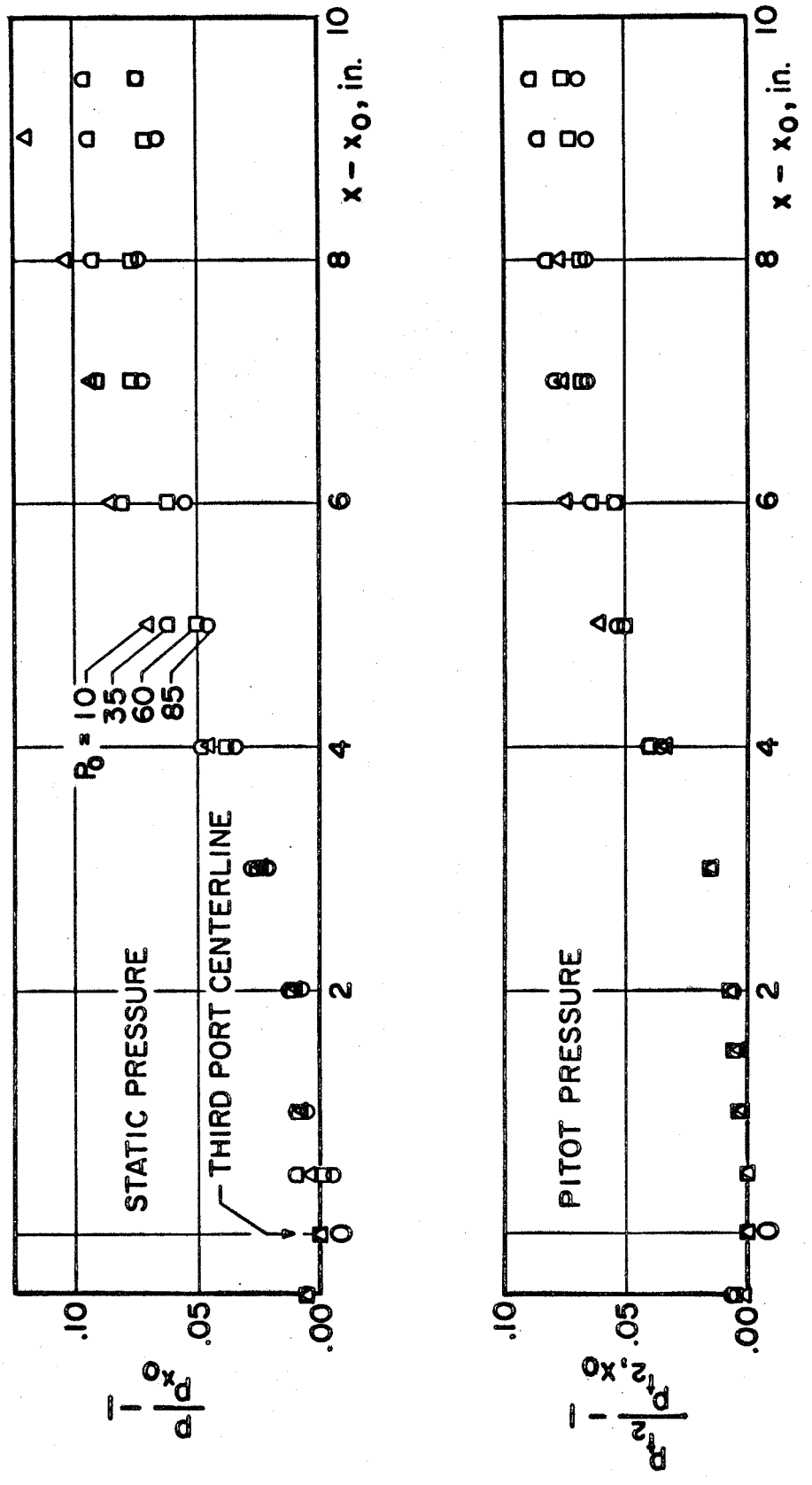

FIG.3 VARIATION OF FREE STREAM CONDITIONS ALONG TUNNEL CENTERLINE

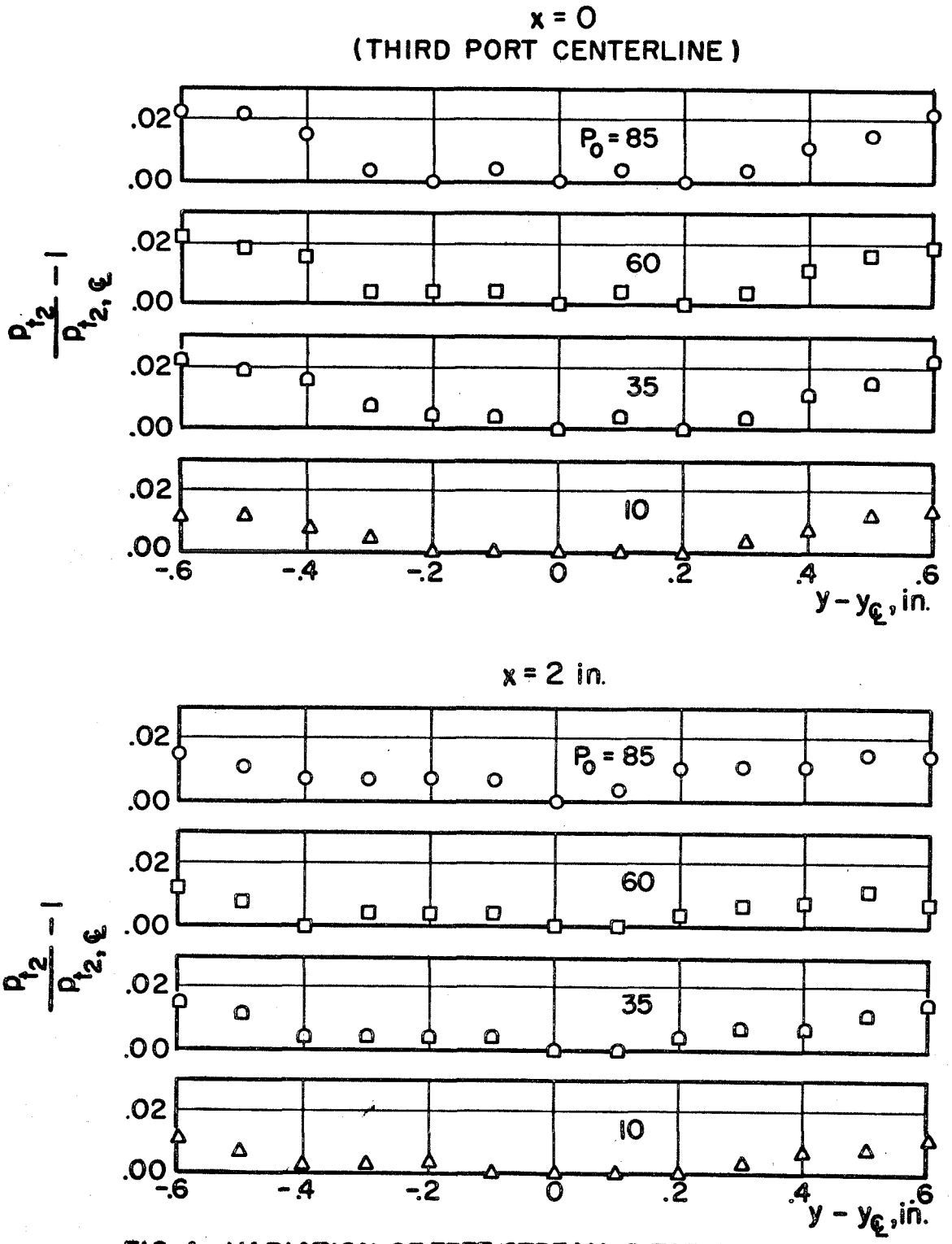

FIG. 4 VARIATION OF FREE STREAM PITOT PRESSURE IN VERTICAL CENTERPLANE OF TUNNEL

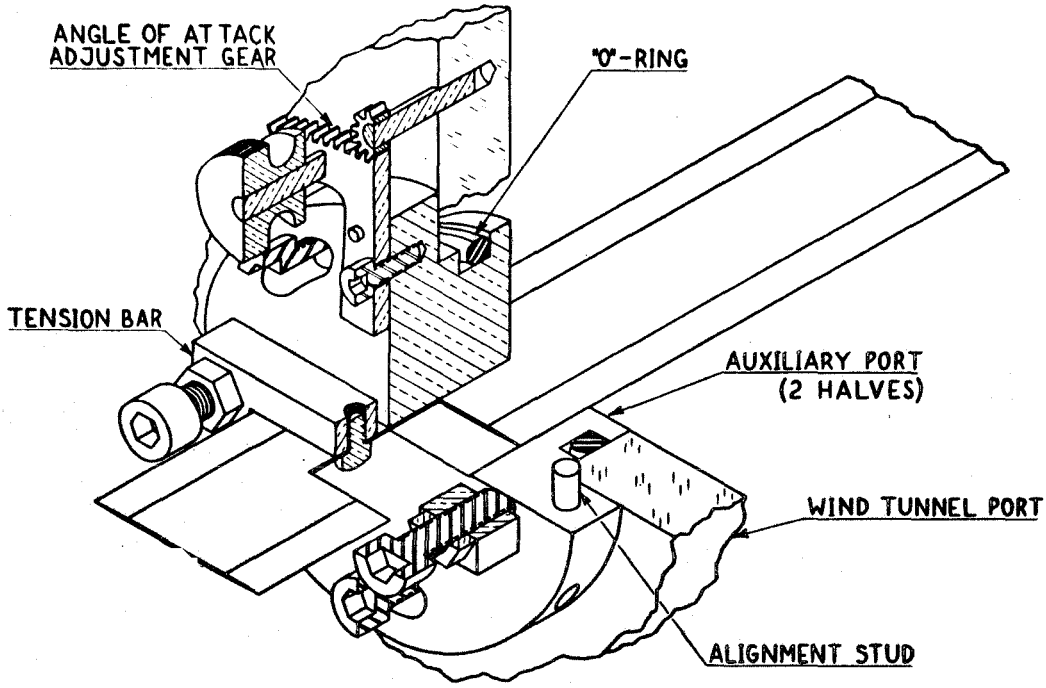

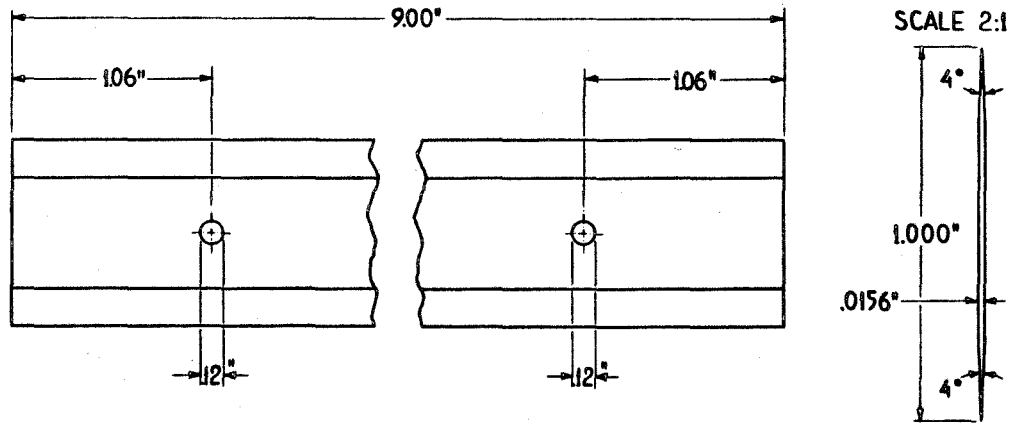

FIG. 5 a. FLAT PLATE MODEL (FP)

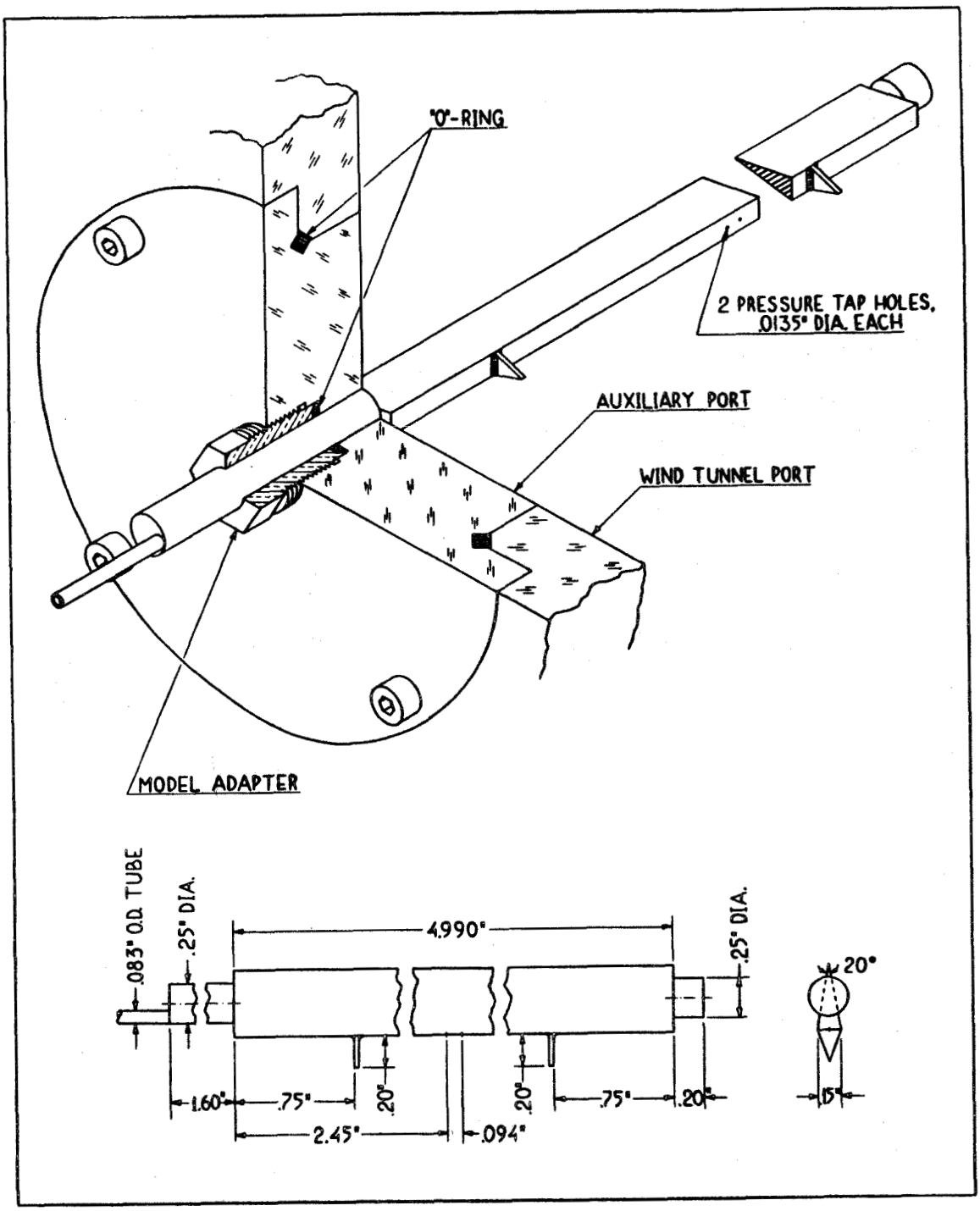

FIG. 5 b. 20° WEDGE MODEL-H=.15" (.15 W)

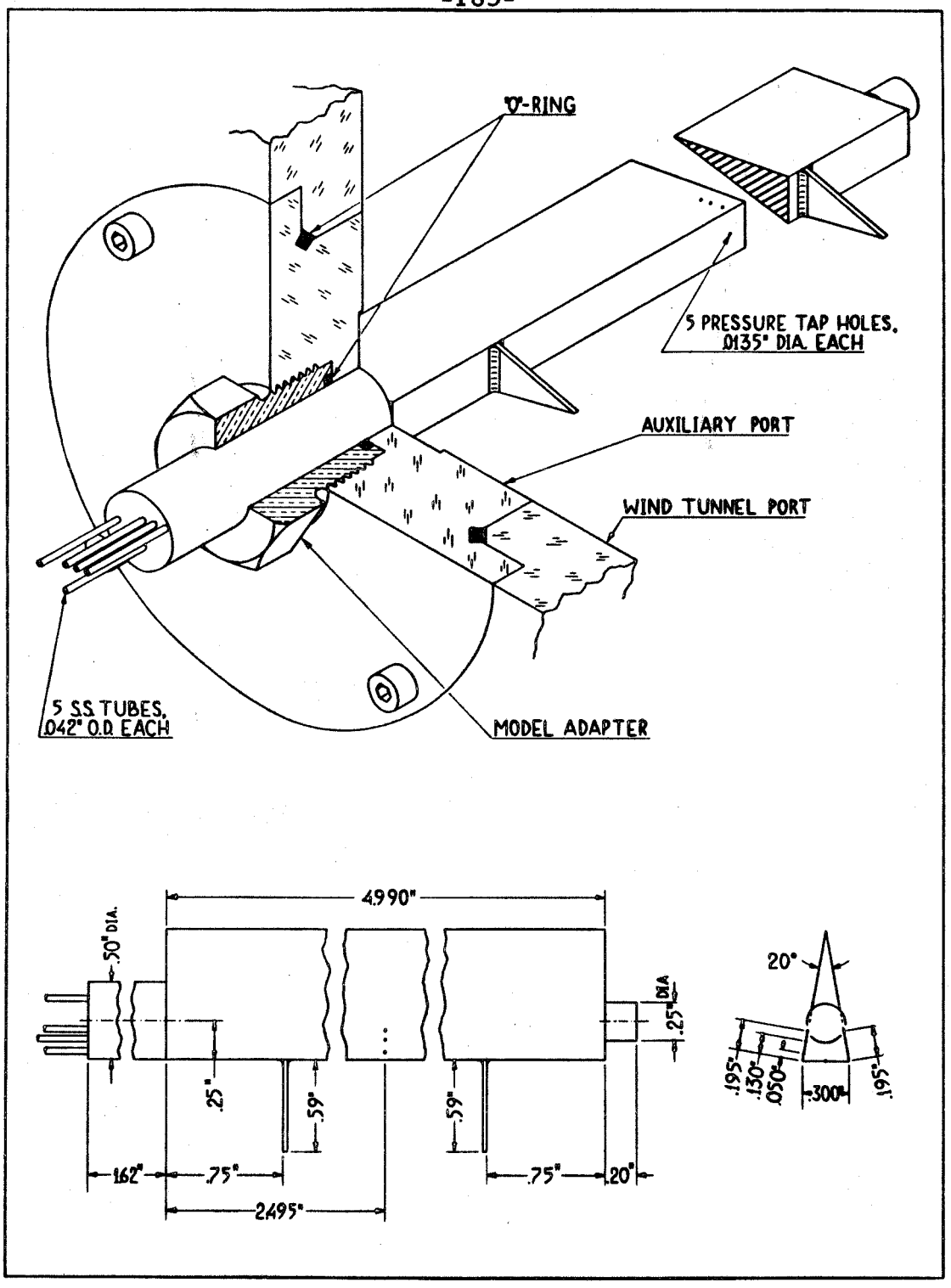

FIG. 5 c. 20° WEDGE MODEL - H = .3" (3W-1)

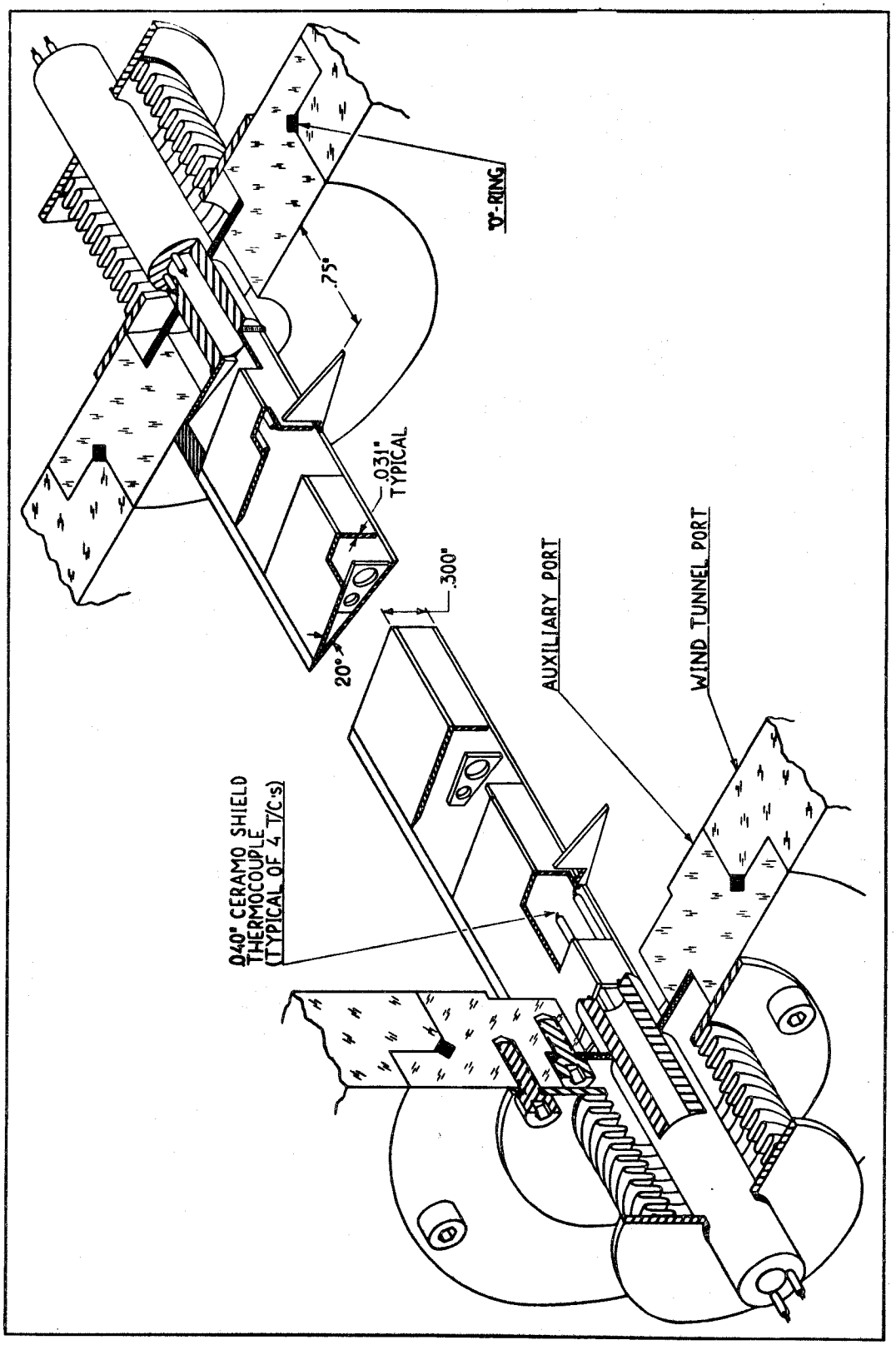

FIG. 5d. 20° WEDGE MODEL - H=.3" (3W-2)

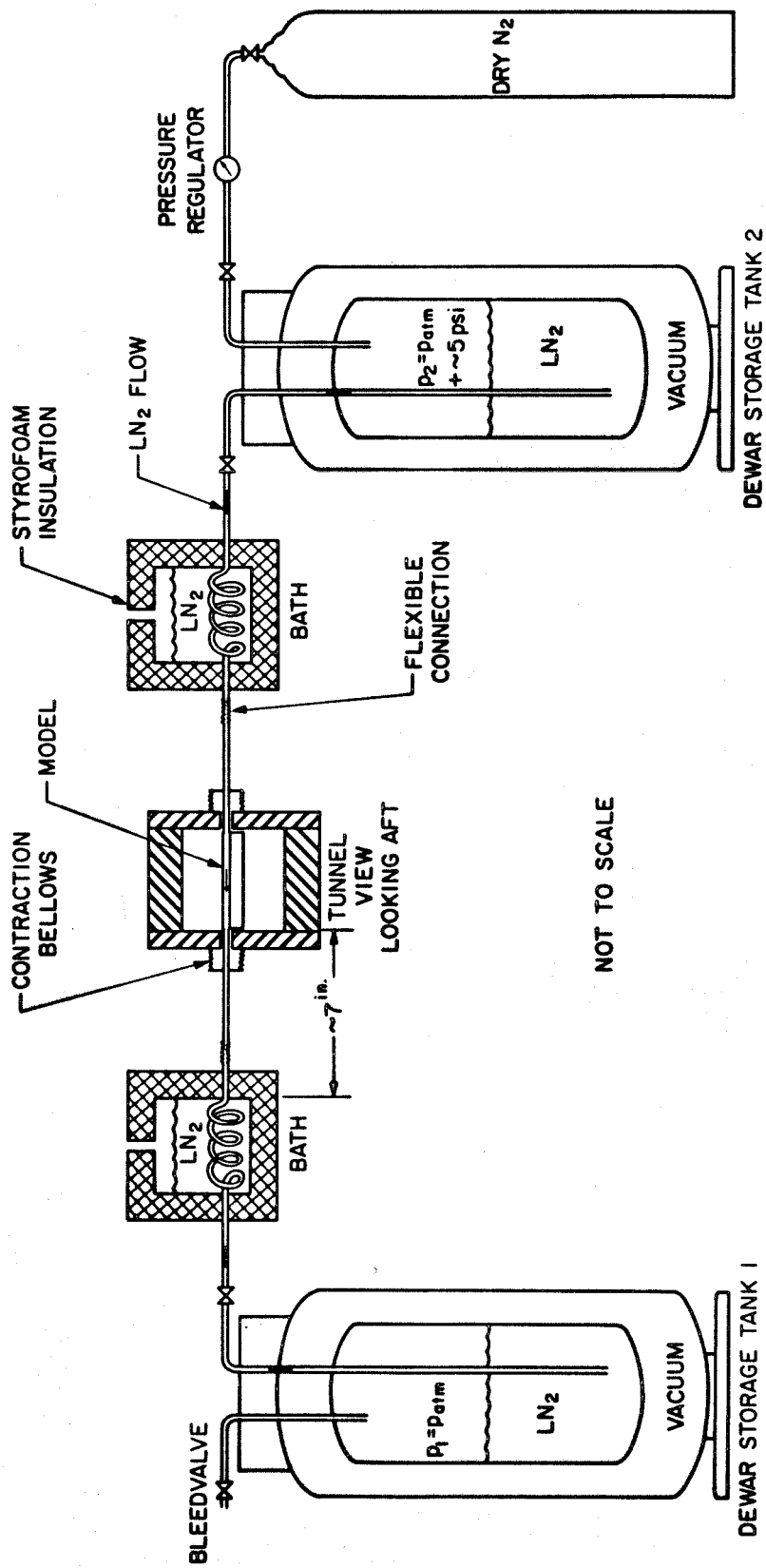

Figure 6. Liquid Nitrogen Cooling System.

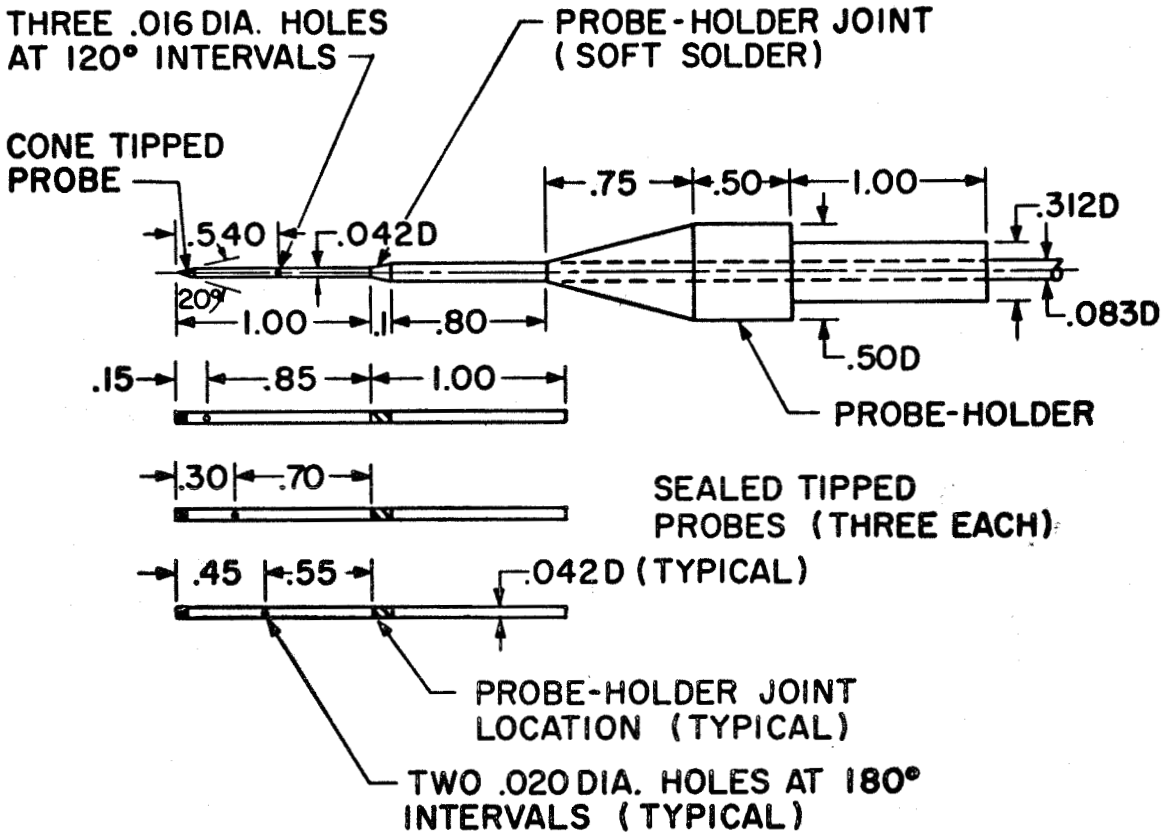

STATIC PRESSURE PROBES

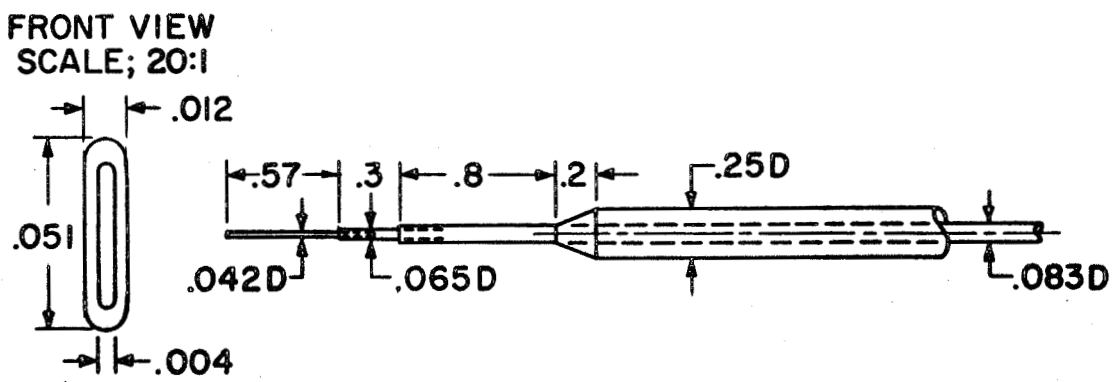

PITOT PRESSURE PROBE

SCALE: FULL
DIMENSIONS: INCHES

FIG.7 STATIC AND PITOT PRESSURE PROBES

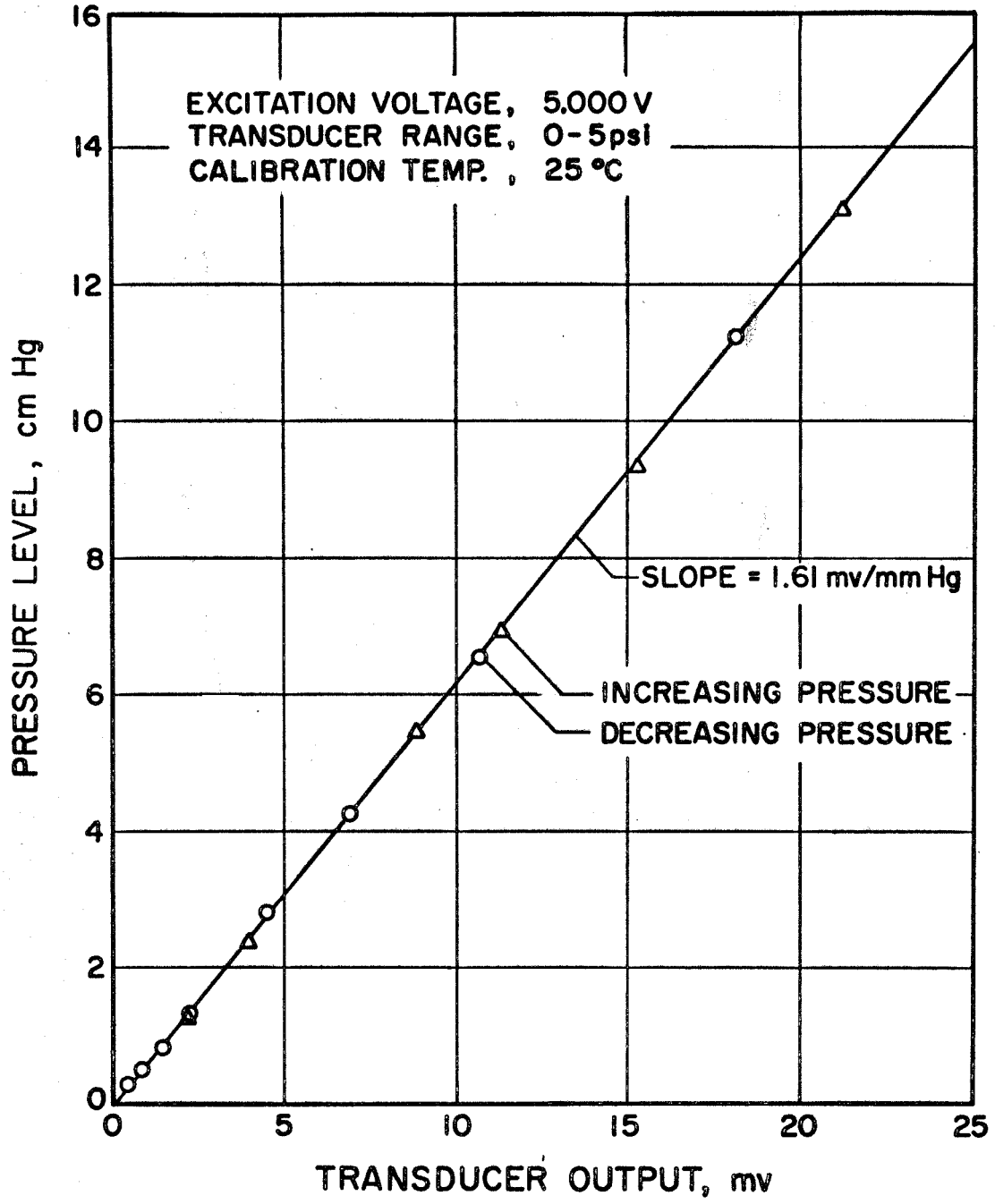

FIG. 8 CALIBRATION OF STATHAM PRESSURE TRANSDUCER

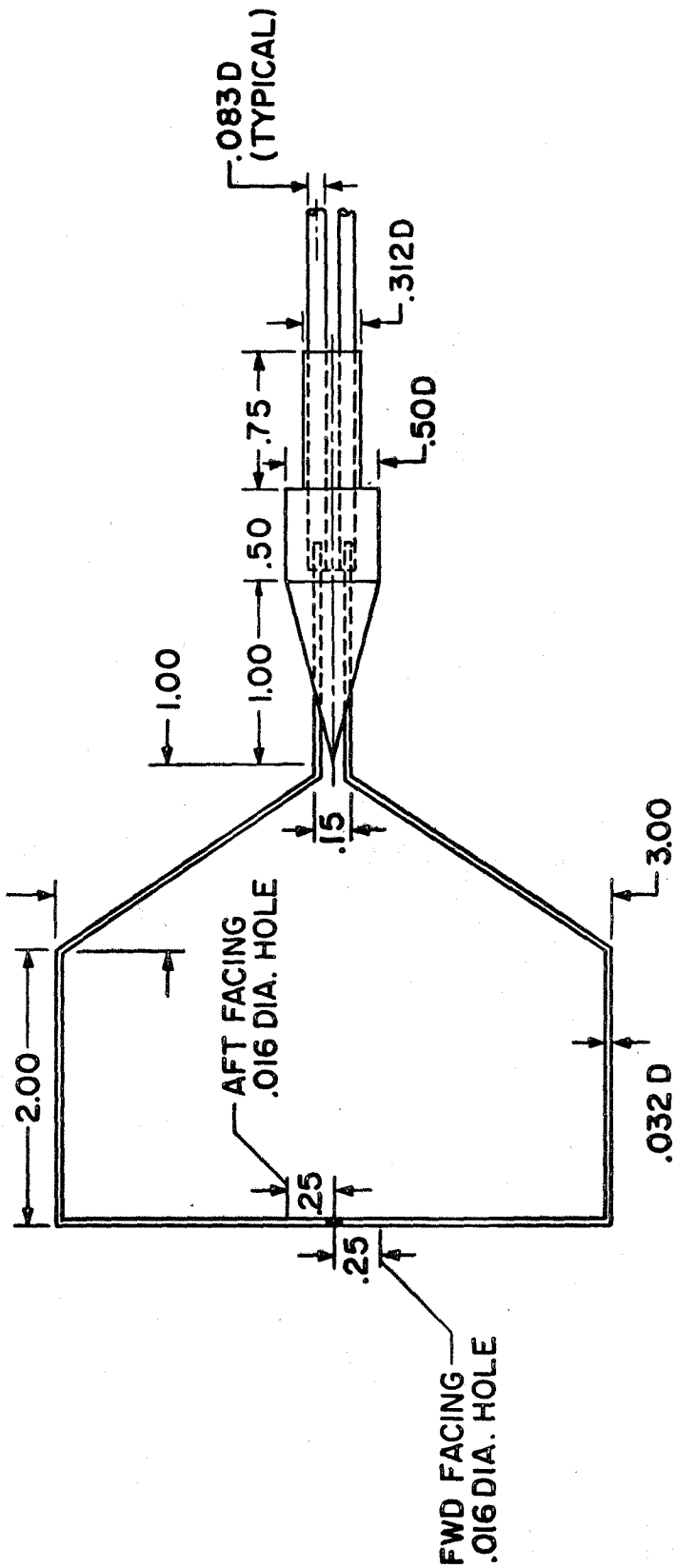

SCALE: FULL
DIMENSIONS: INCHES

FIG.9 BASE REGION STAGNATION POINT PROBE

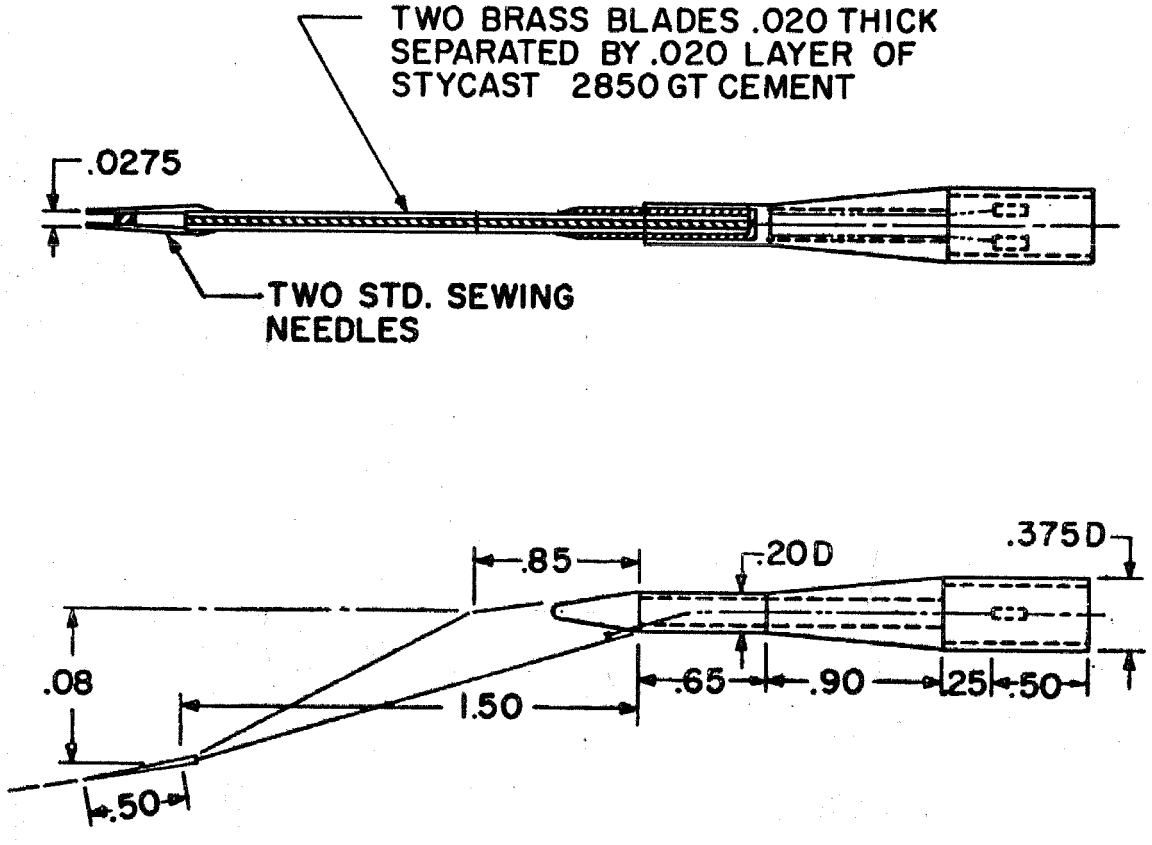

SCALE: FULL
DIMENSIONS: INCHES

FIG.10 HOT WIRE PROBE

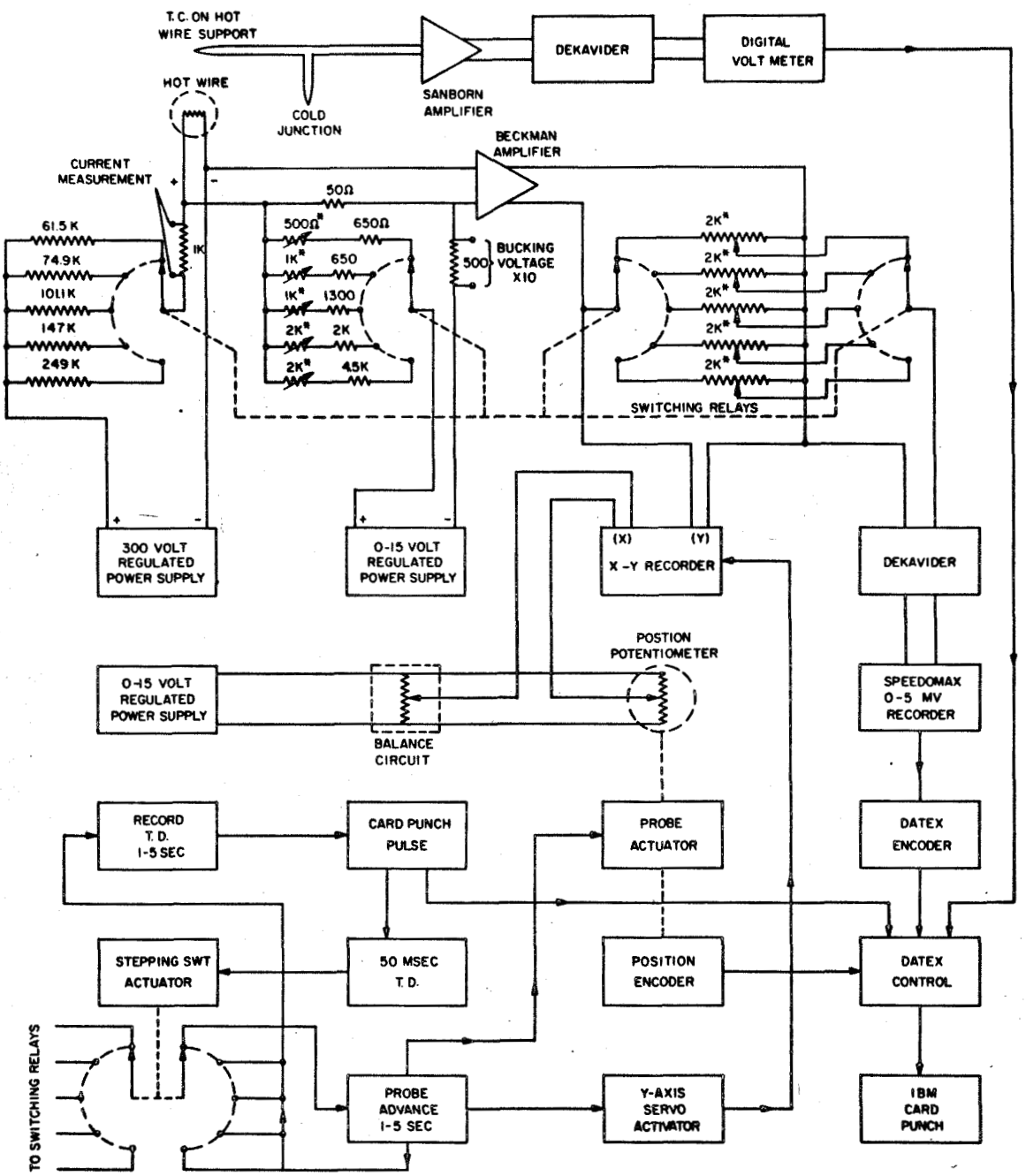

*10-TURN PRECISION POTENTIOMETERS

SWITCHING RELAYS SHOWN IN HIGH CURRENT POSITION

Fig. 11. Simplified Schematic for Hot Wire Recording System

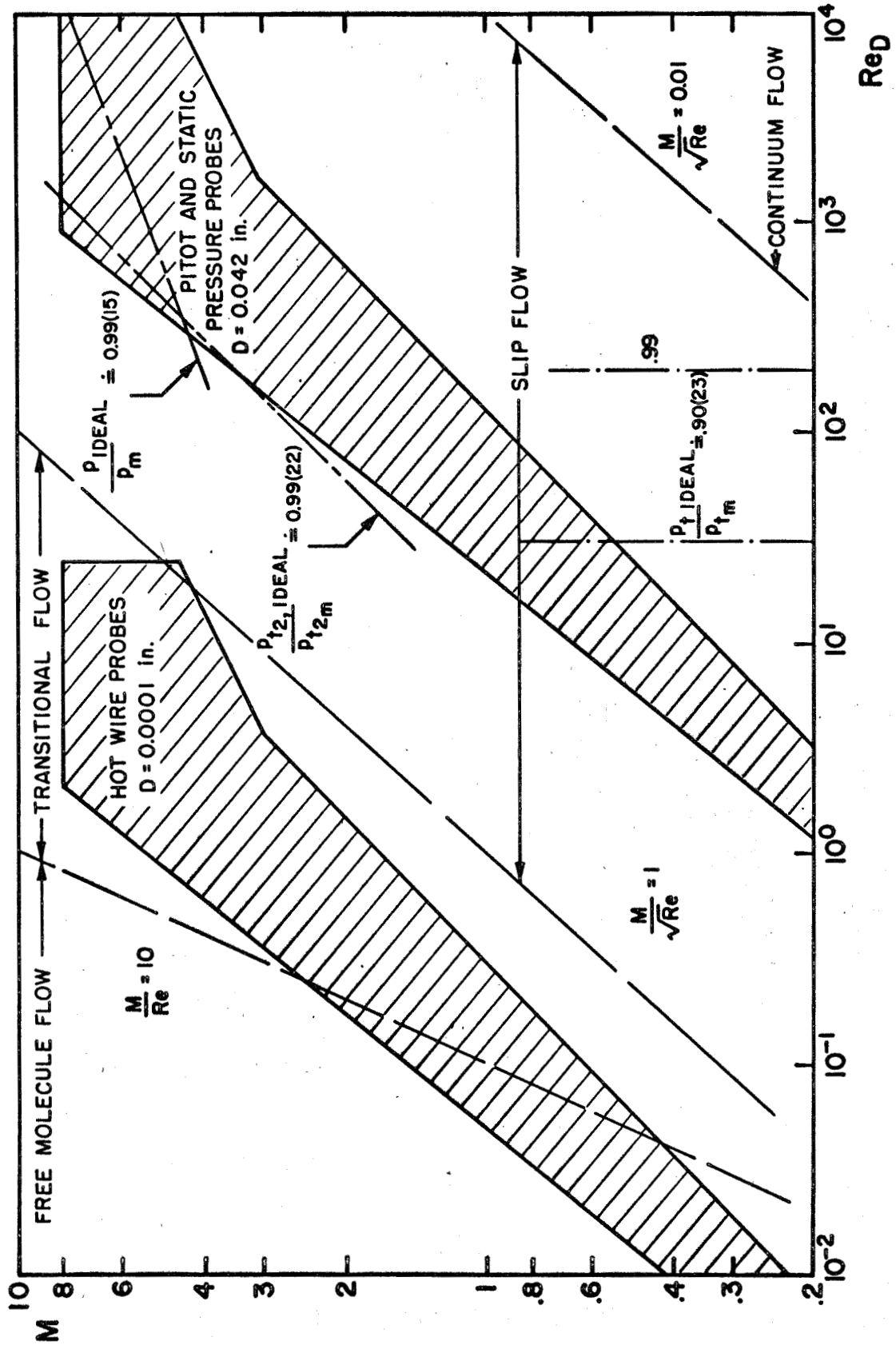

FIG.12 PROBE FLOW REGIMES IN THE M - RE PLANE

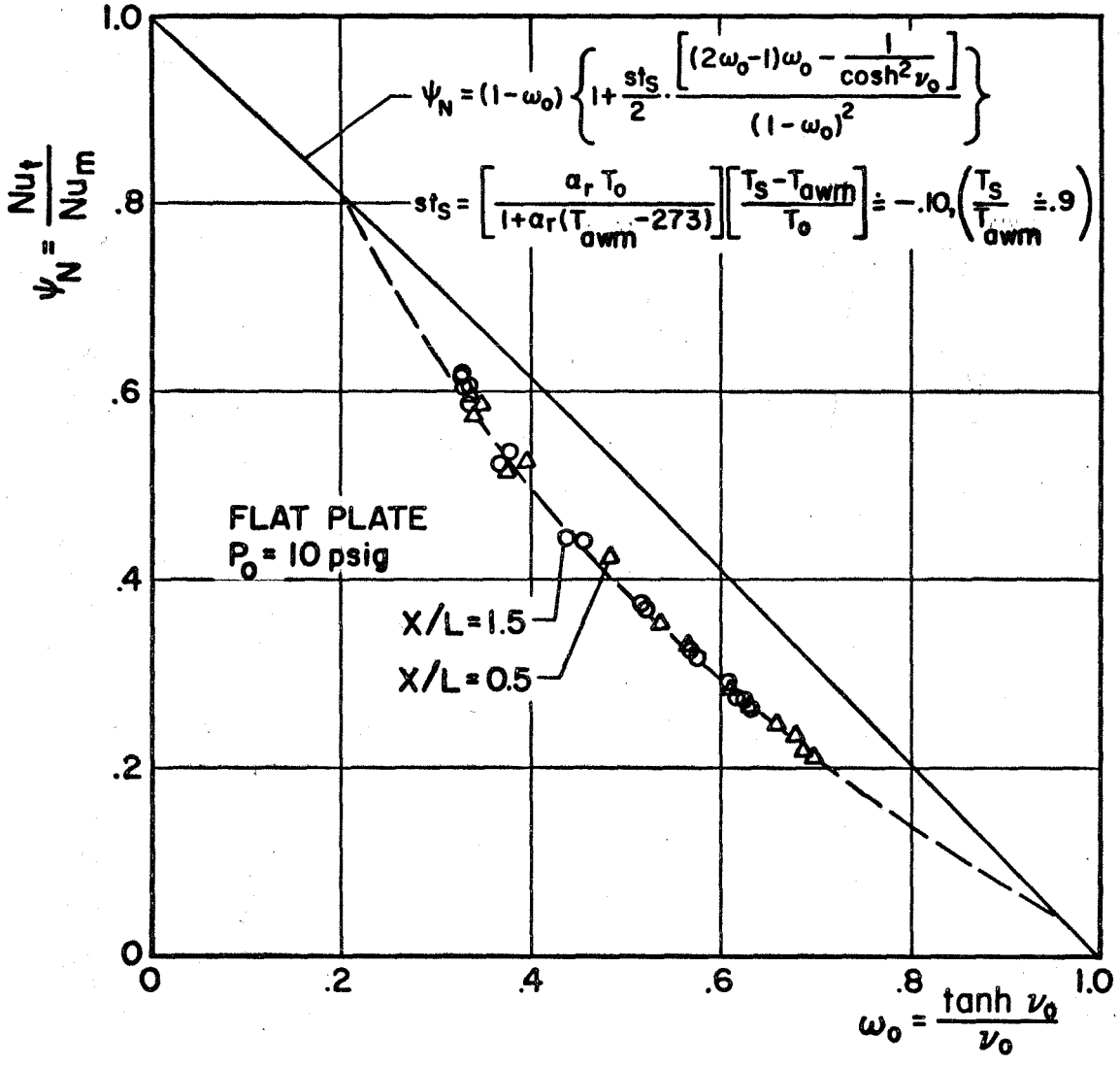

FIG.13 NUSSELT NUMBER END LOSS CORRECTION FACTOR

CORRELATION OF MEASURED RESULTS FOR FLAT PLATE WITH THEORETICAL VARIATION FROM DEWEY'S END LOSS ANALYSIS

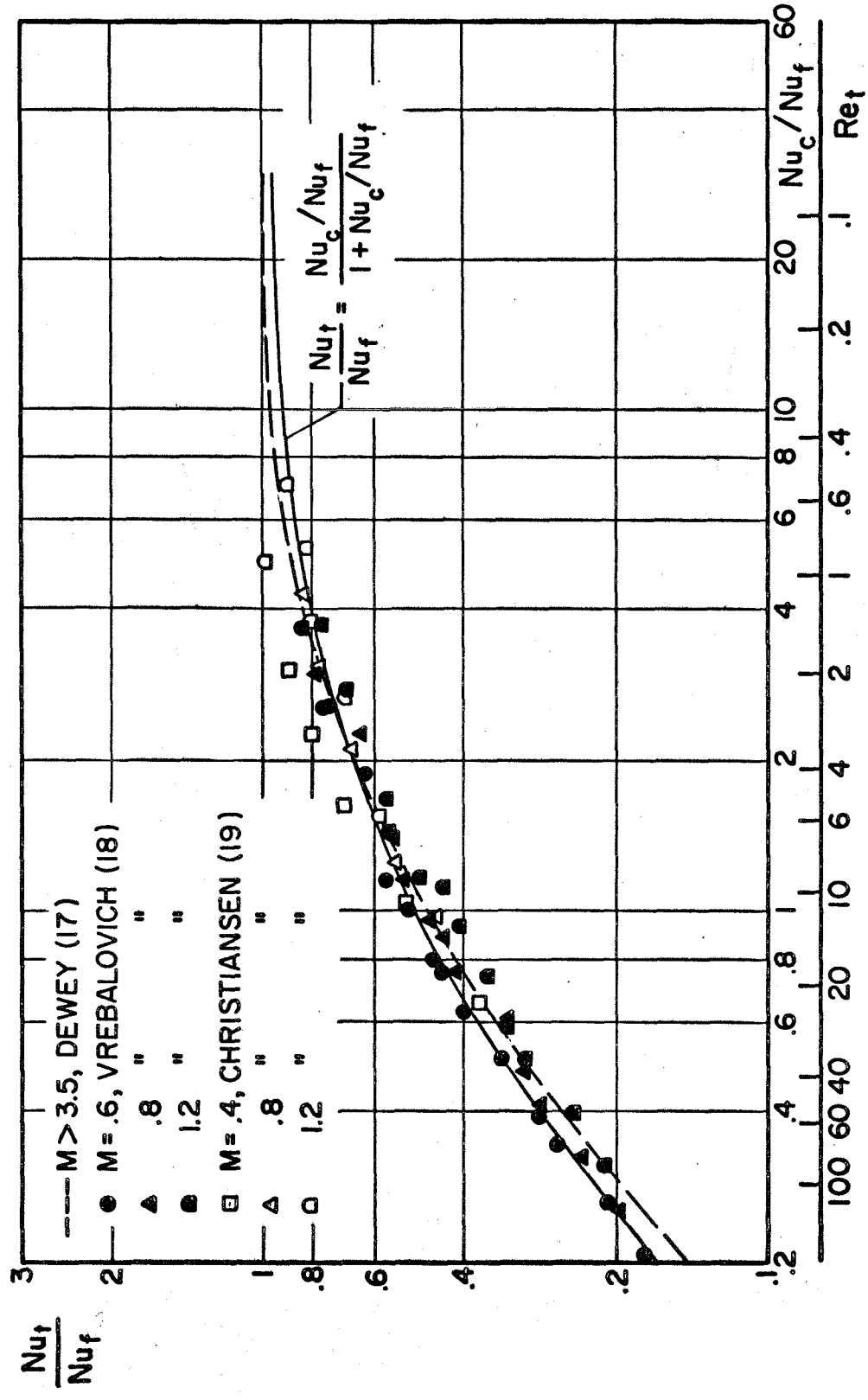

FIG.14 CORRELATION OF CYLINDER HEAT TRANSFER DATA

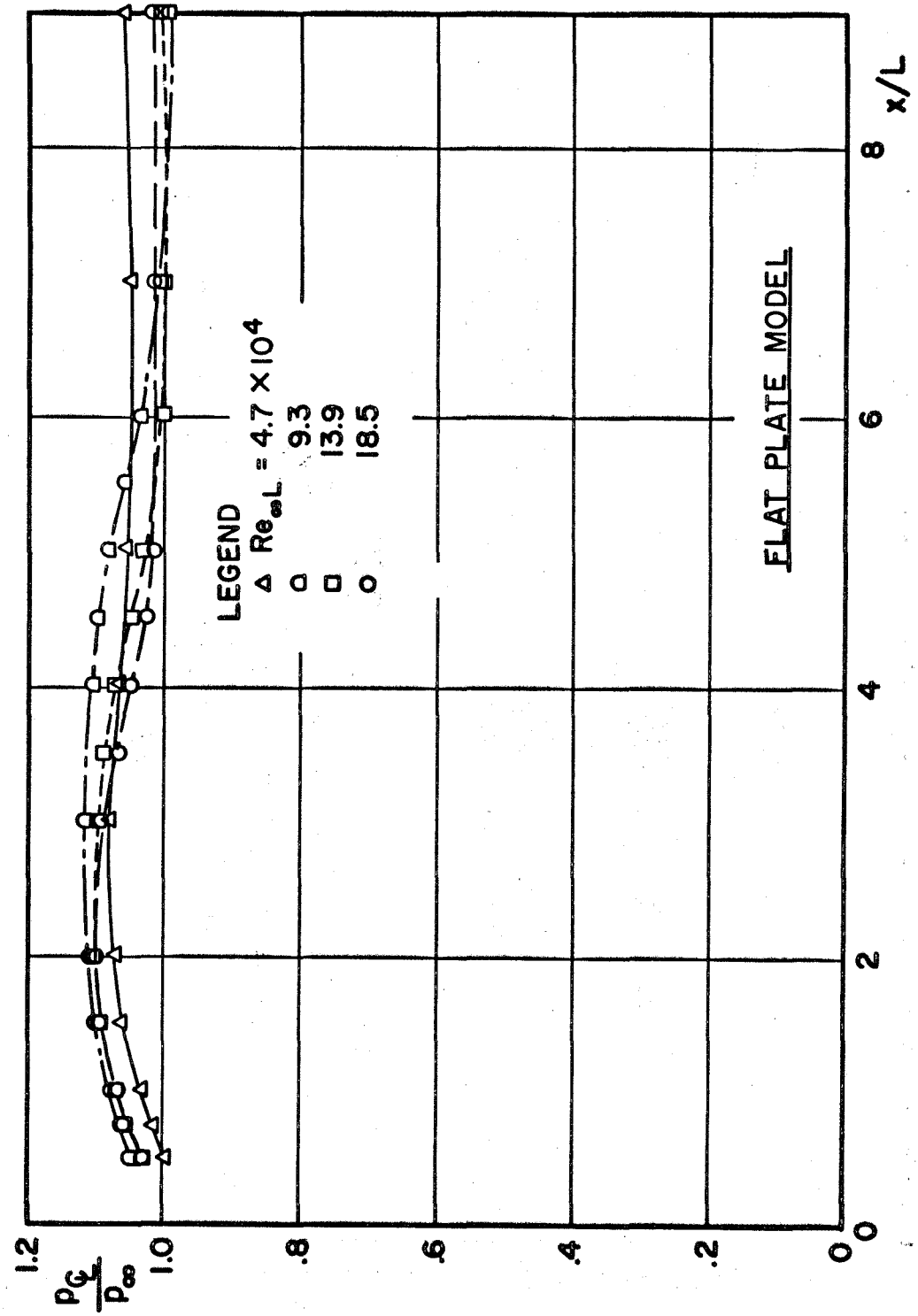

FIG.15a VARIATION OF STATIC PRESSURE ALONG WAKE CENTERLINE AT $M_\infty = 6$

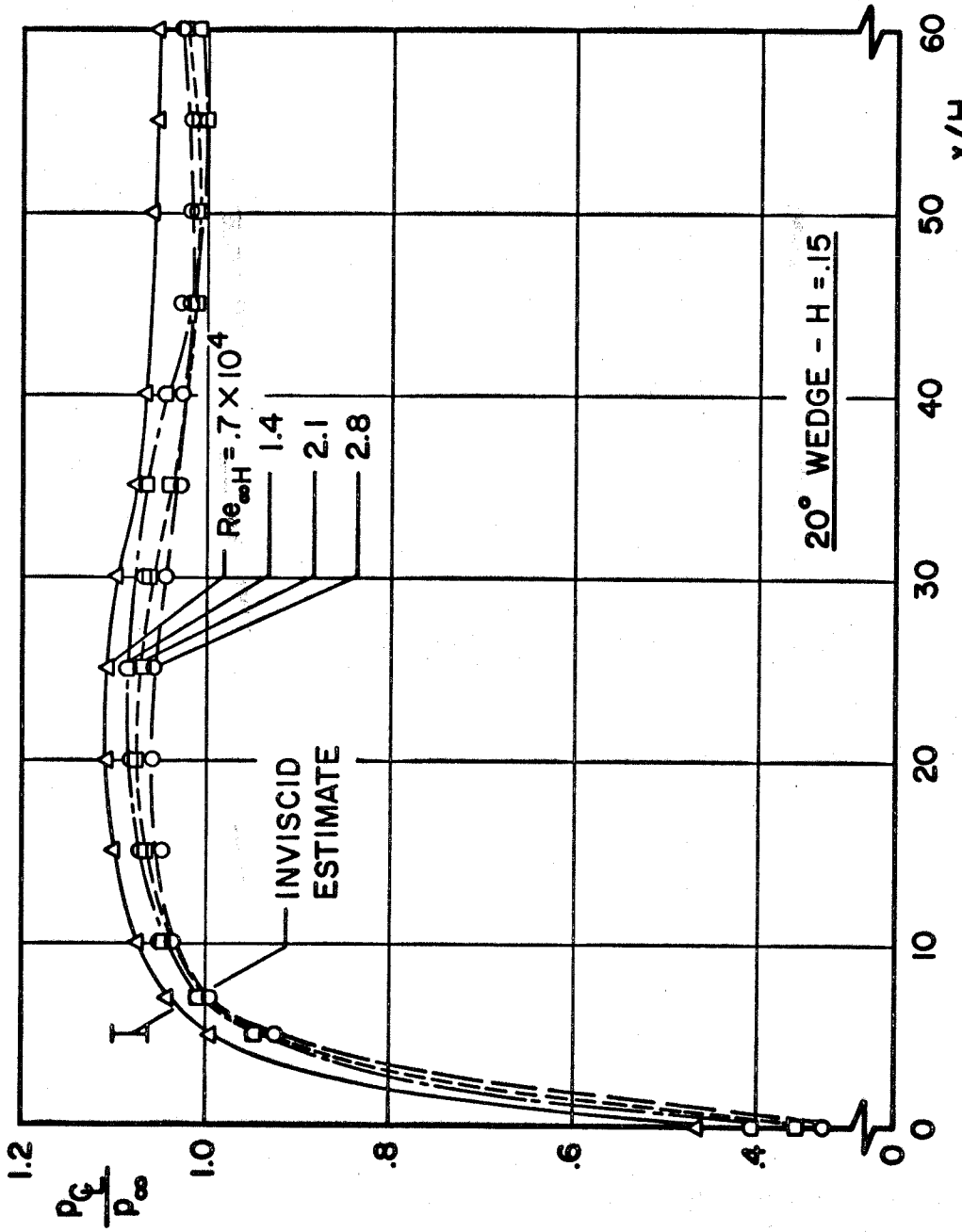

FIG.15b VARIATION OF STATIC PRESSURE ALONG WAKE CENTERLINE AT $M_\infty = 6$

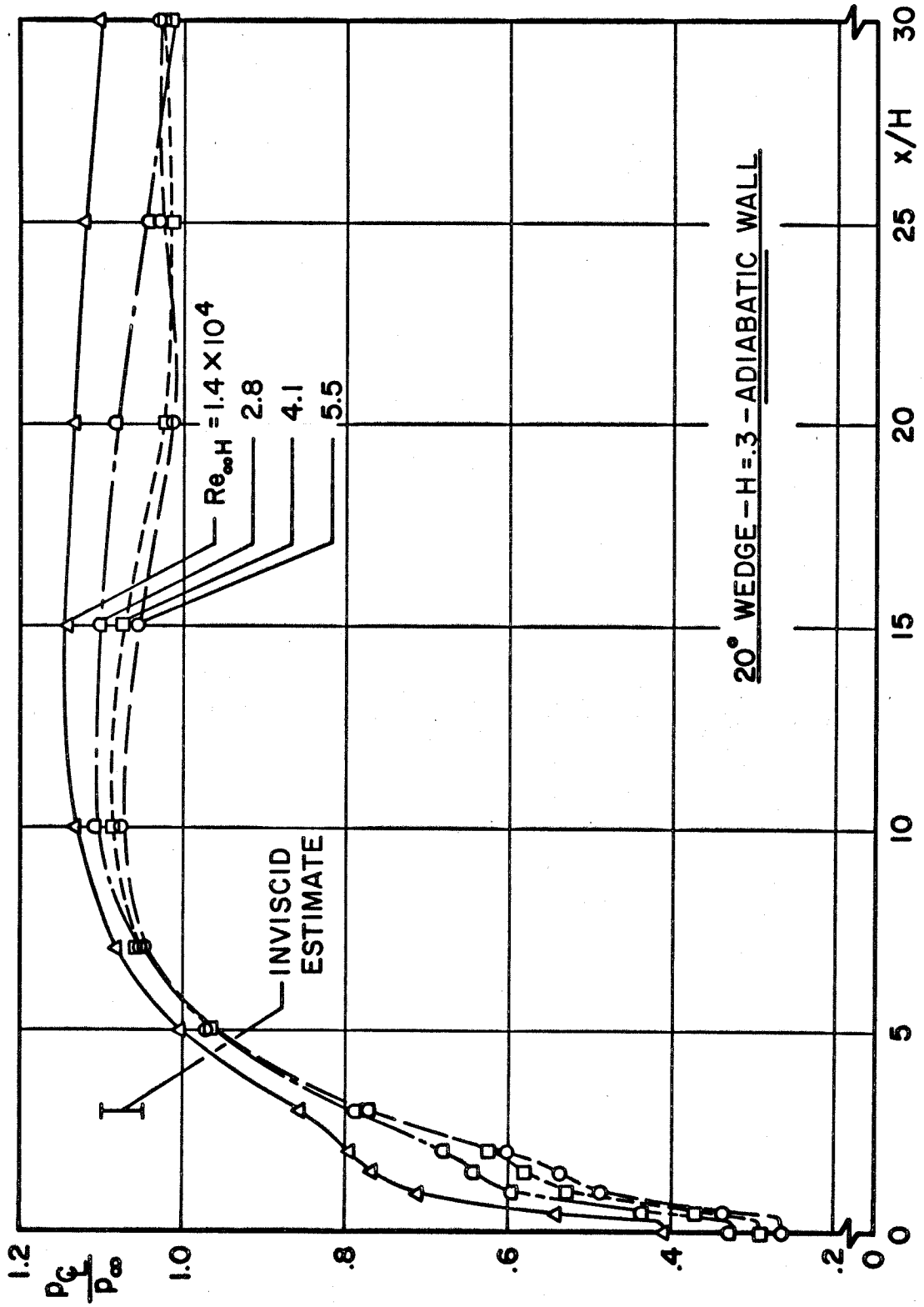

FIG.15c-I VARIATION OF STATIC PRESSURE ALONG WAKE CENTERLINE AT $M_\infty = 6$

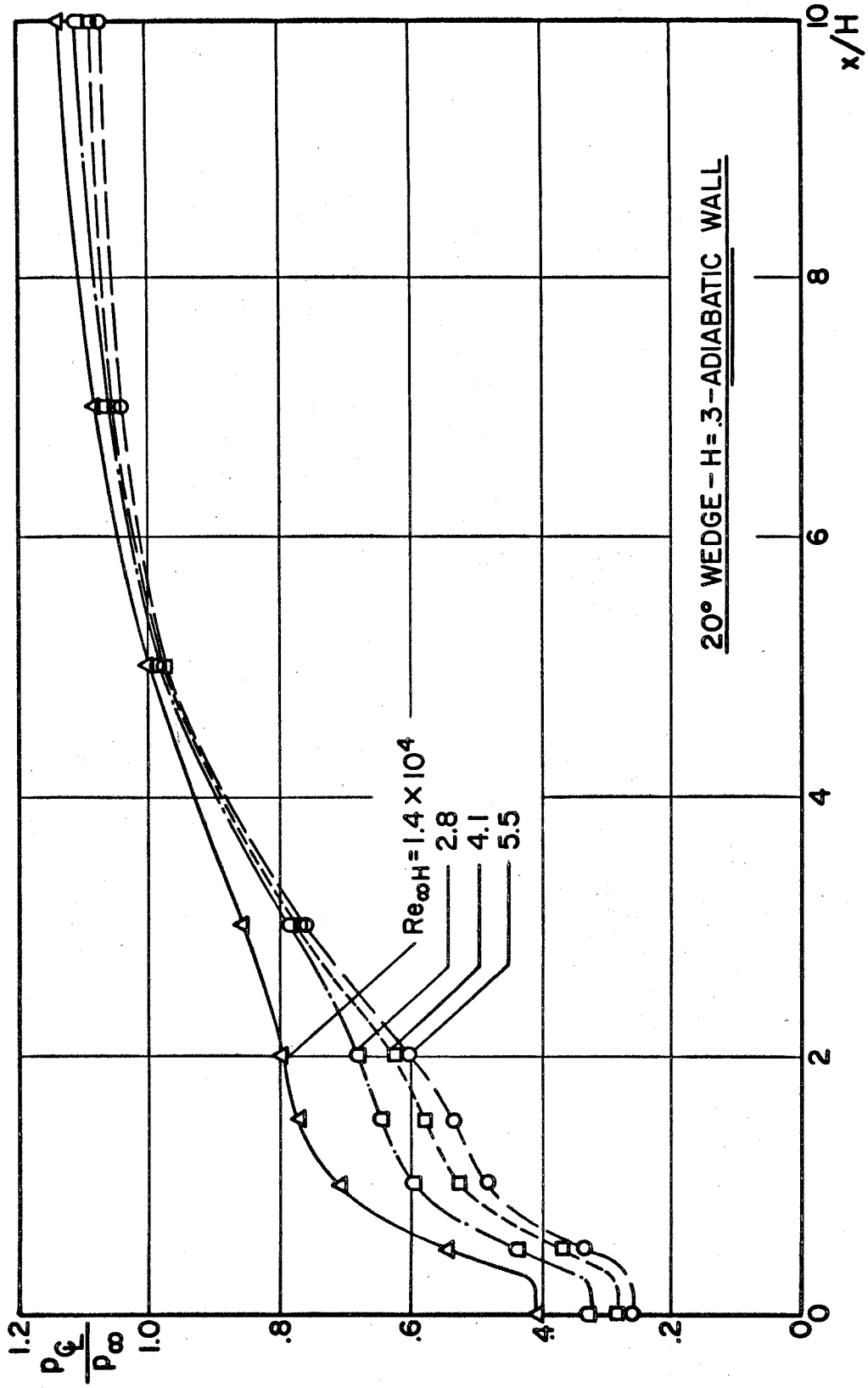

FIG. 15c-2 VARIATION OF STATIC PRESSURE ALONG WAKE CENTERLINE AT $M_\infty = 6$

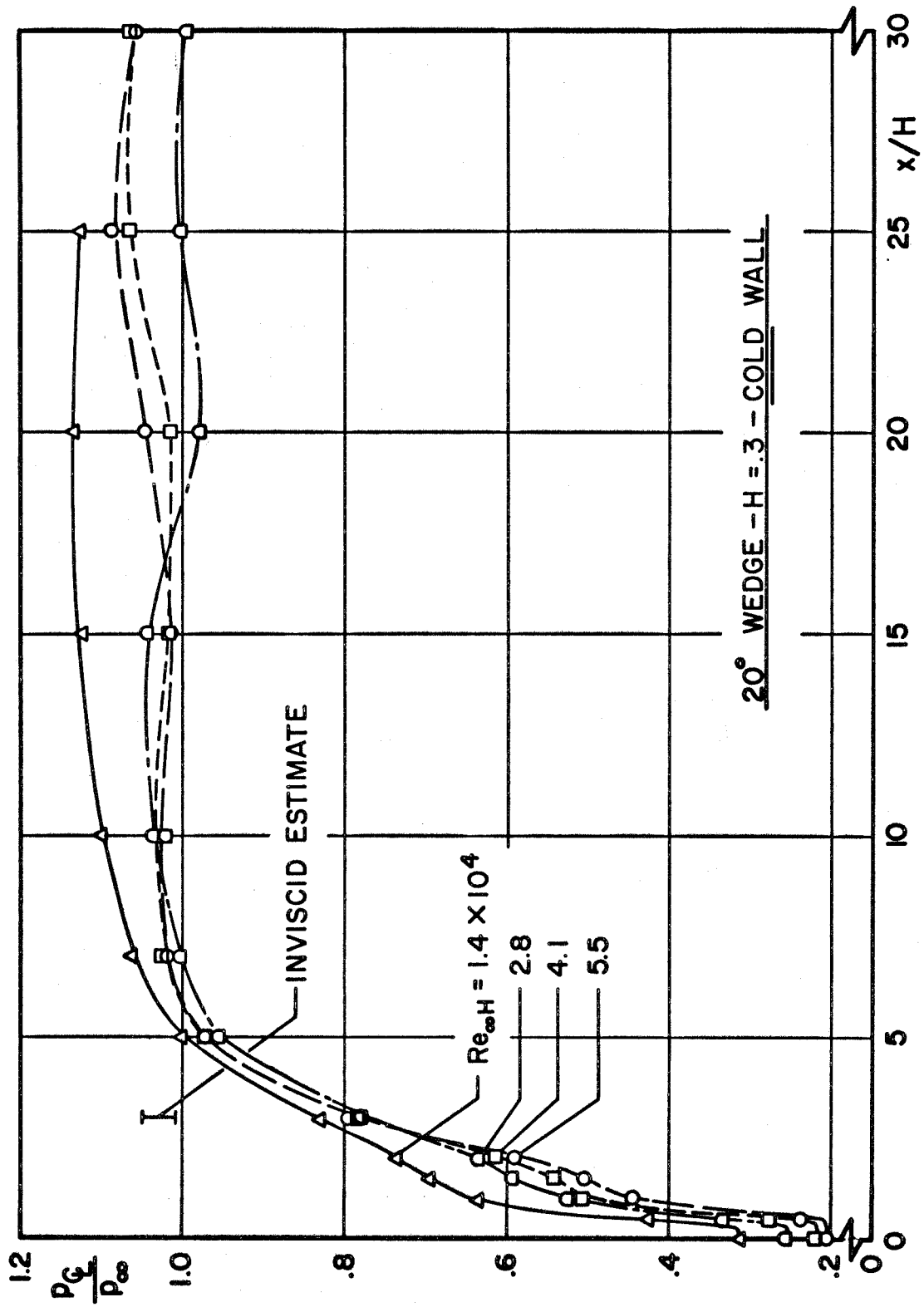

FIG.15d-1 VARIATION OF STATIC PRESSURE ALONG WAKE CENTERLINE AT $M_\infty = 6$

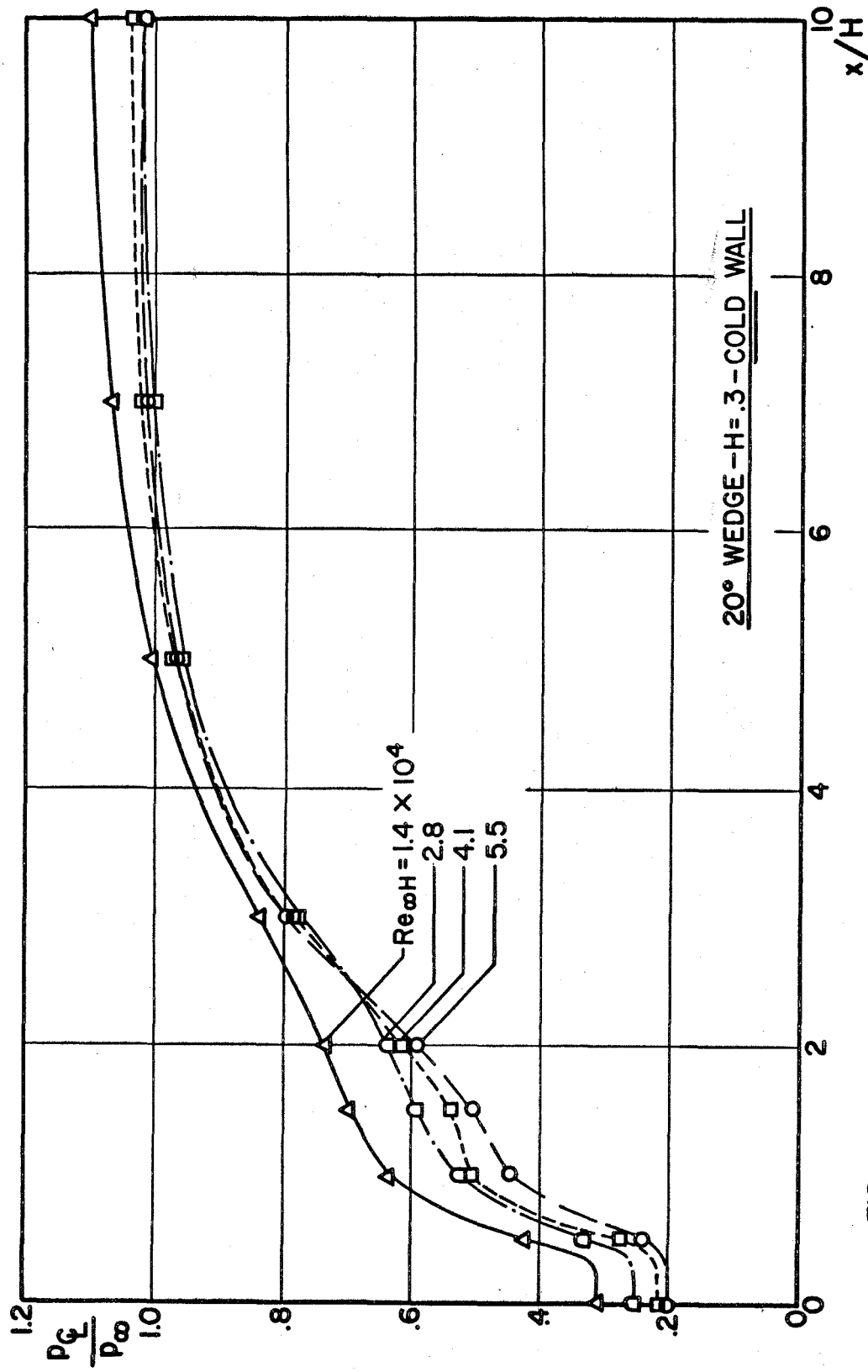

FIG. 15d-2 VARIATION OF STATIC PRESSURE ALONG WAKE CENTERLINE AT $M_\infty = 6$

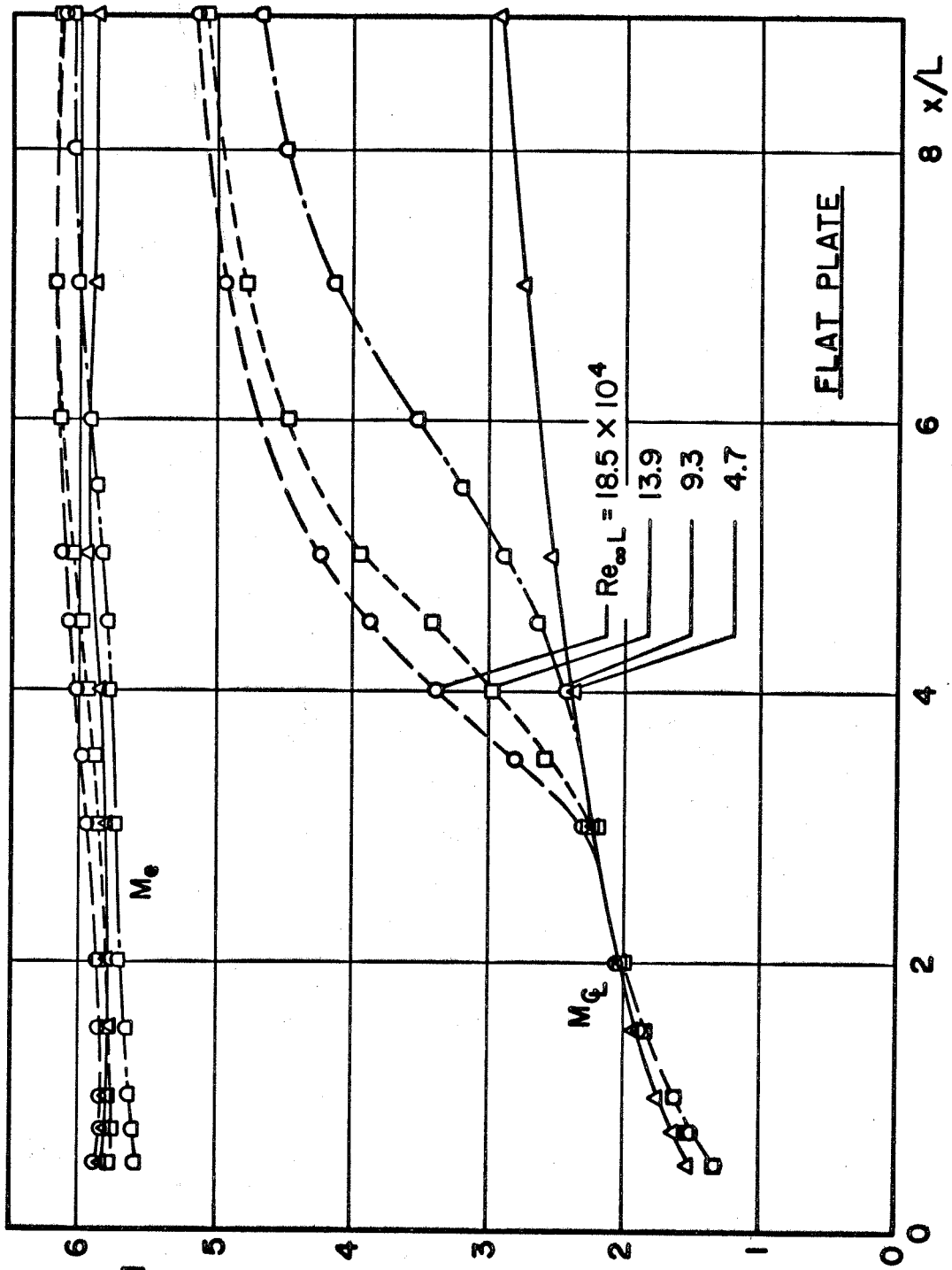

FIG. 16a VARIATION OF CENTERLINE MACH NUMBER WITH AXIAL DISTANCE AT $M_\infty = 6$

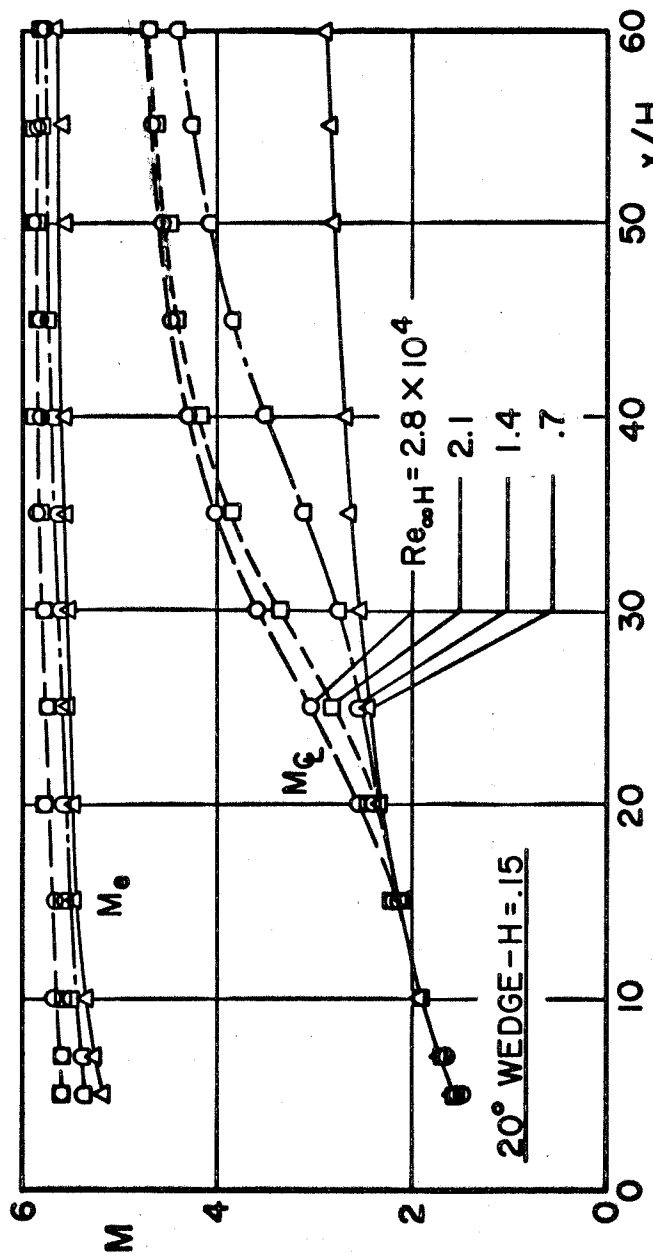

FIG.16b VARIATION OF CENTERLINE AND EDGE MACH NUMBER WITH AXIAL DISTANCE AT $M_\infty = 6$

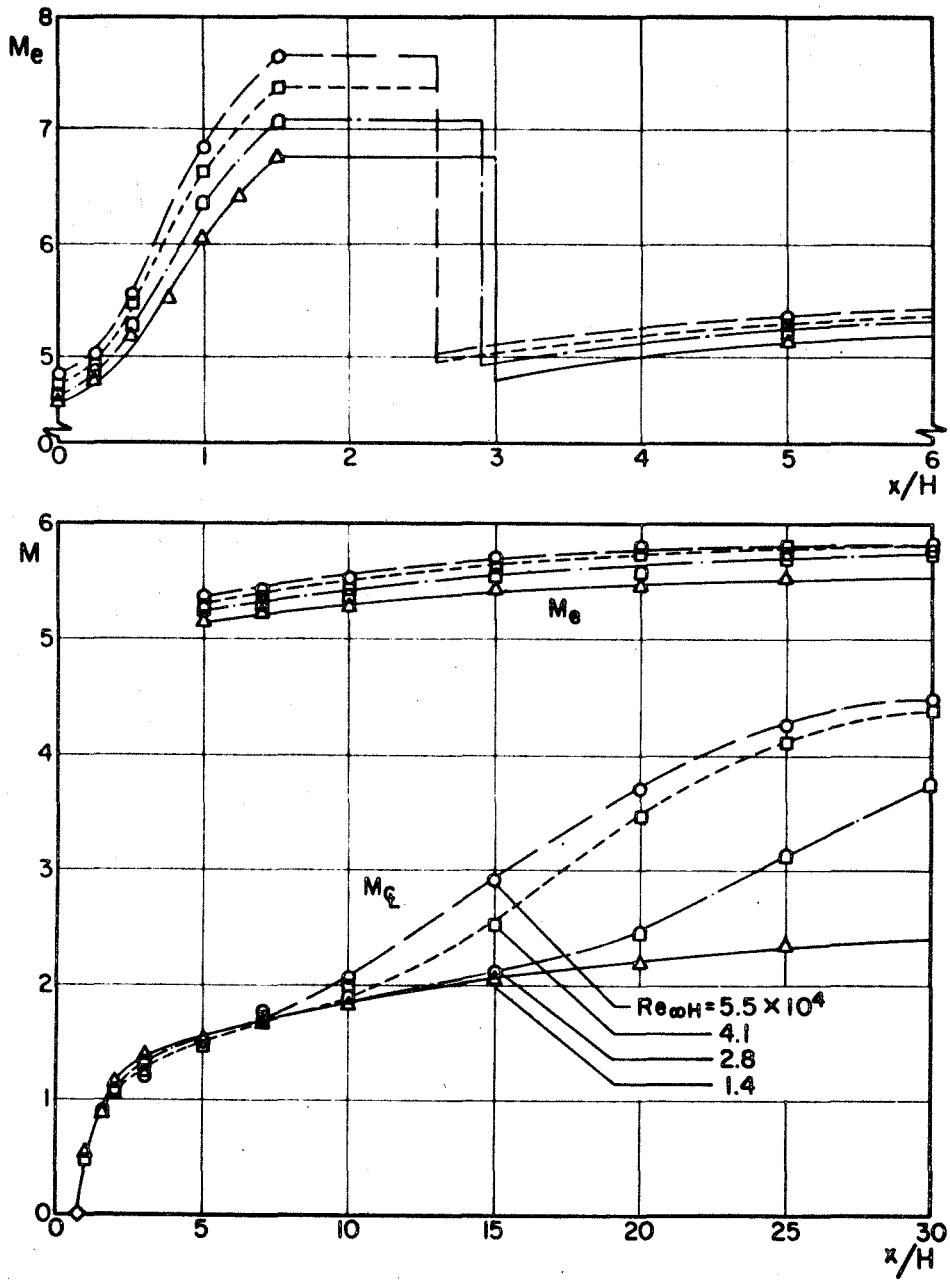

FIG. 16c VARIATION OF CENTERLINE AND EDGE MACH NUMBER WITH AXIAL DISTANCE AT $M_\infty = 6$
20° WEDGE MODEL - H = .3 - ADIABATIC WALL

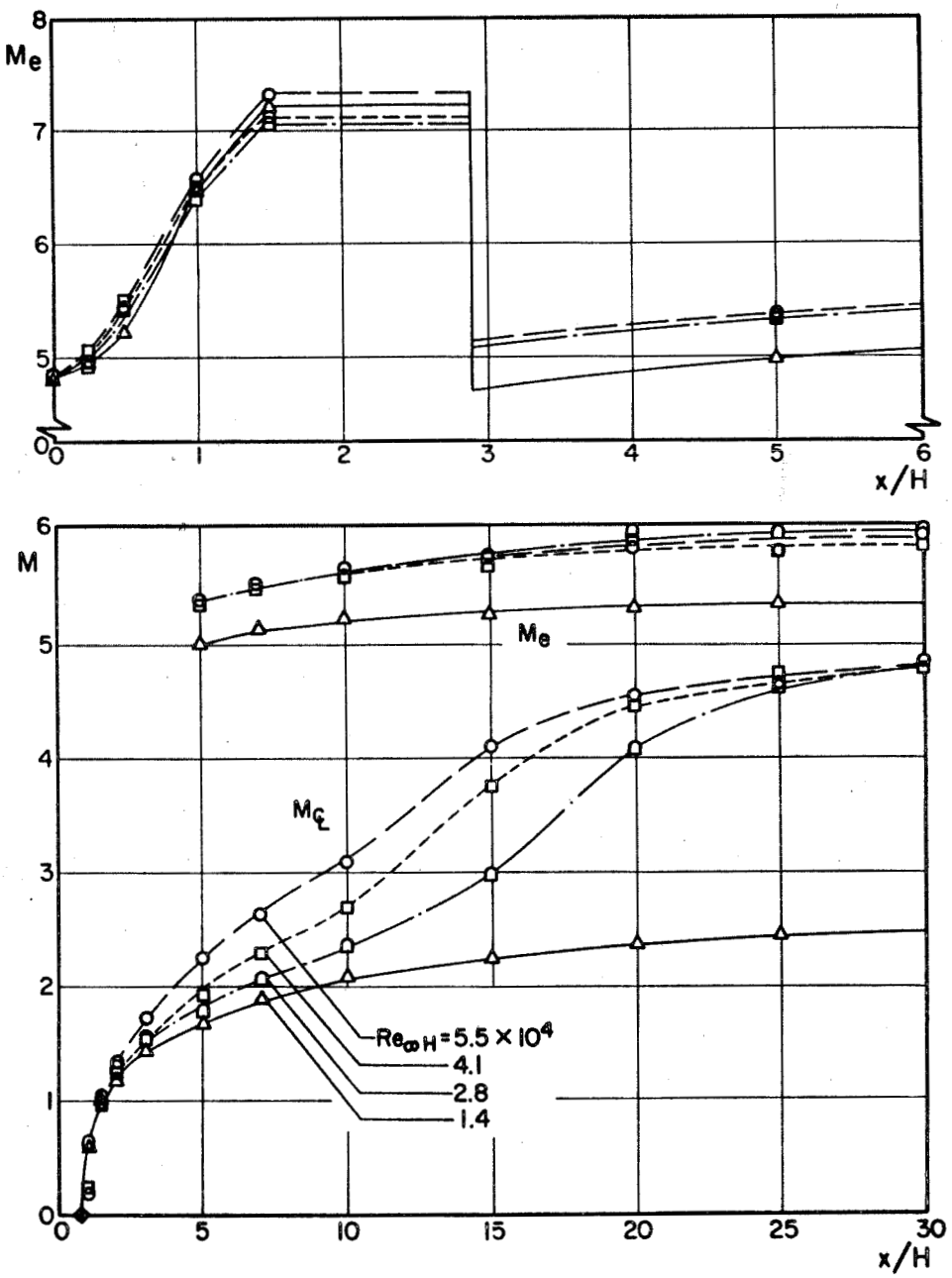

FIG. 16 d VARIATION OF CENTERLINE AND EDGE MACH NUMBER WITH AXIAL DISTANCE AT $M_\infty = 6$
20° WEDGE MODEL – H = .3 COLD WALL

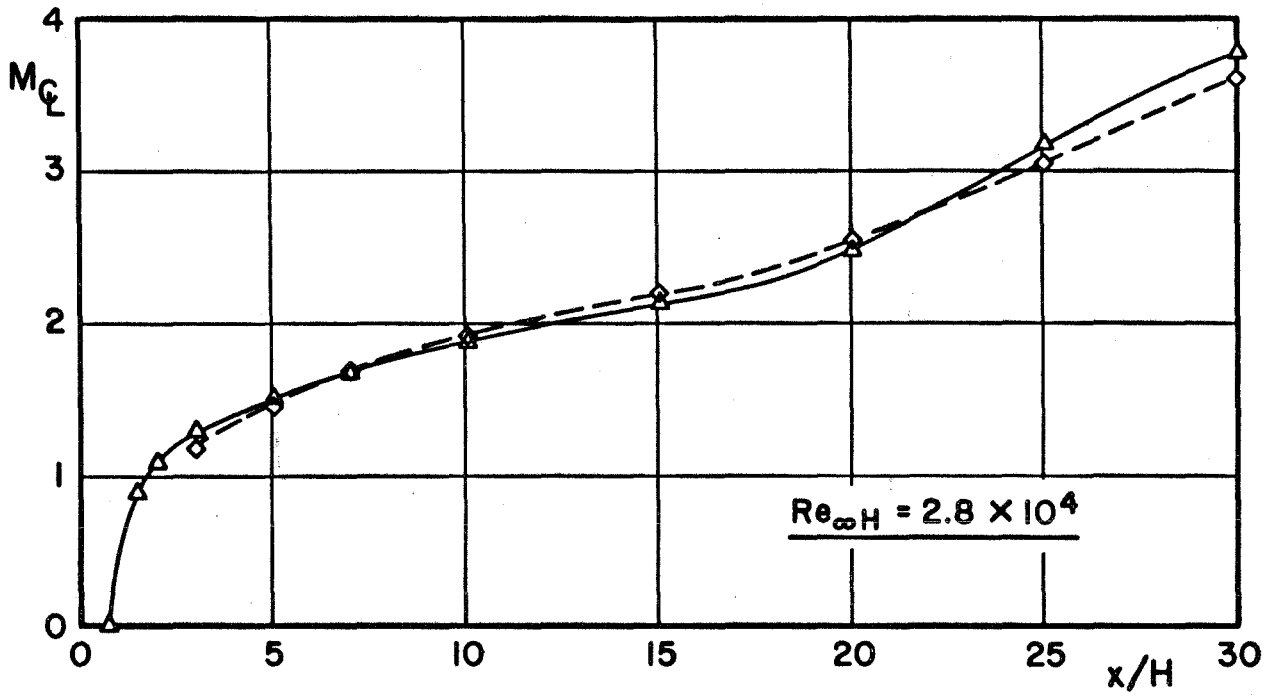

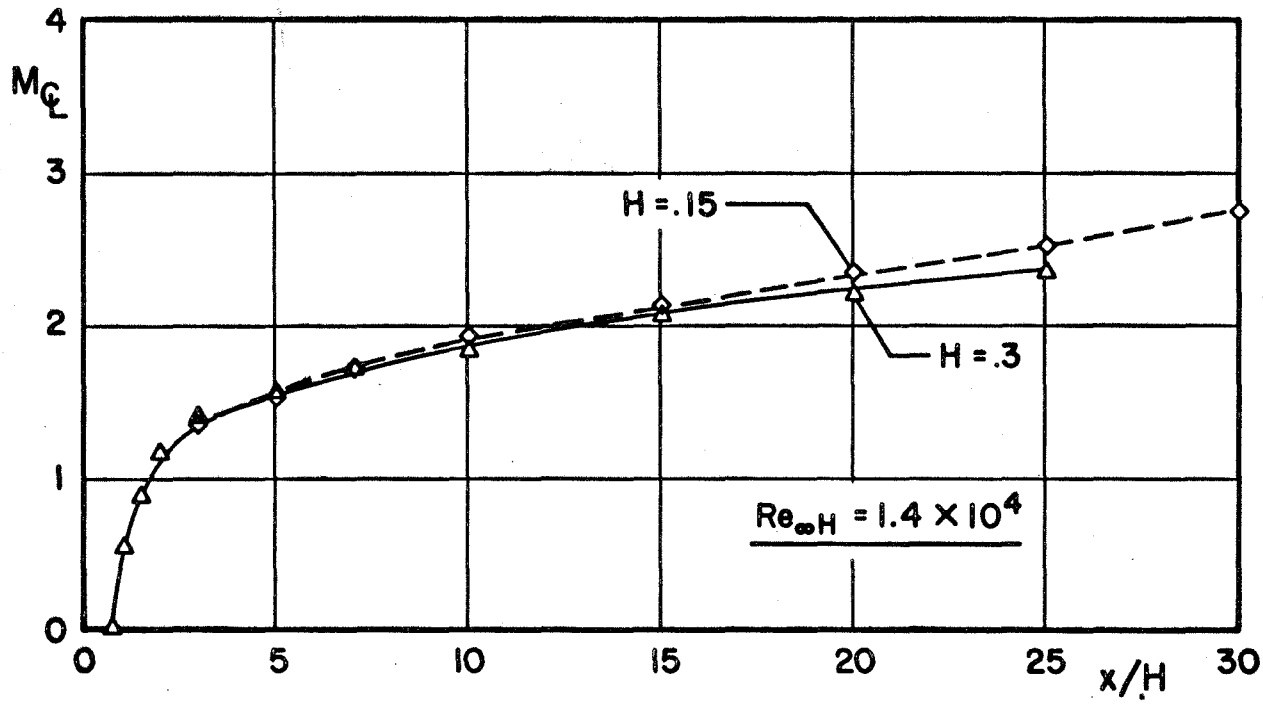

FIG.17 CORRELATION OF CENTERLINE MACH NUMBER FOR 20° ADIABATIC WALL WEDGE AT $M_\infty = 6$

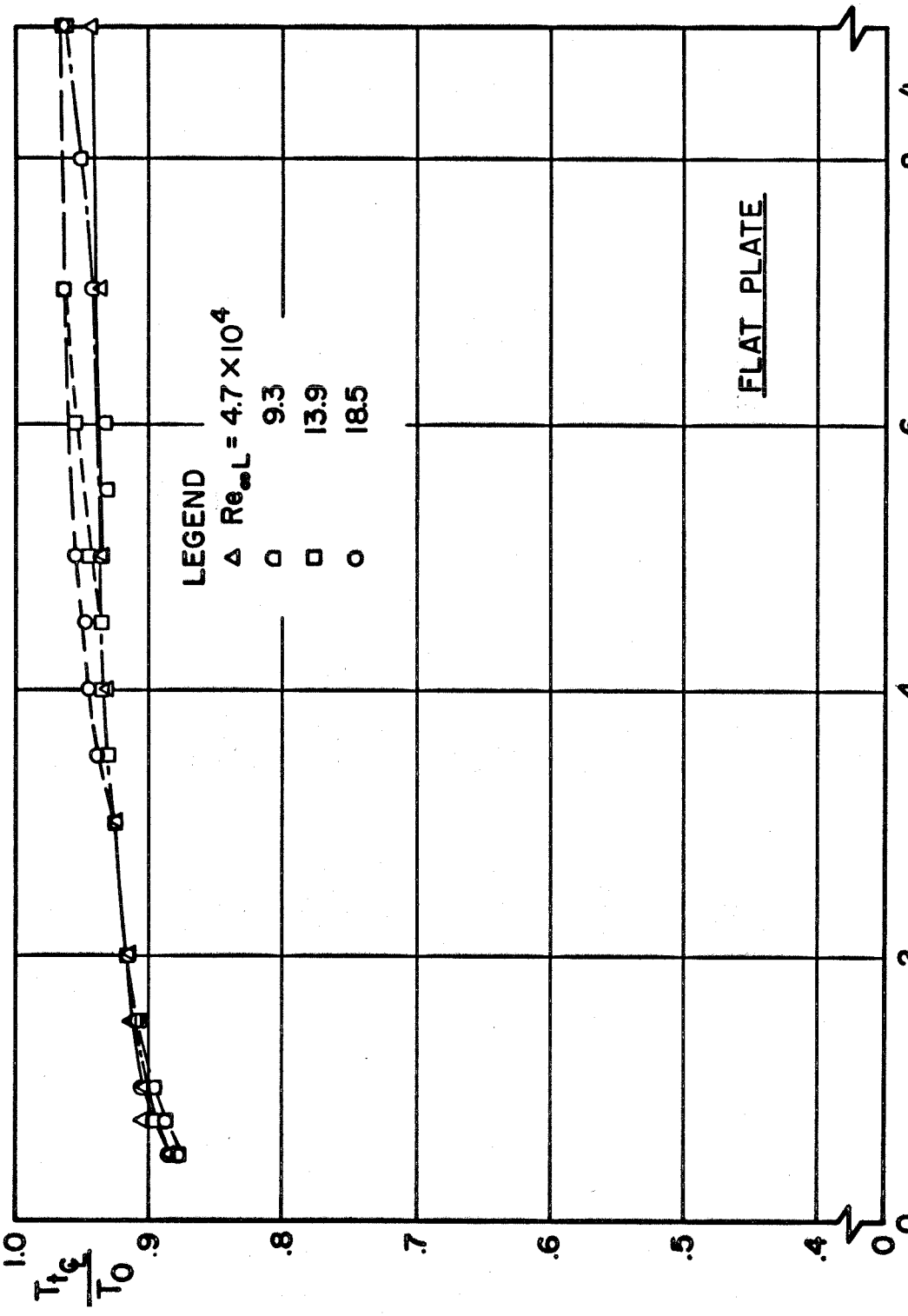

FIG. 18a VARIATION OF CENTERLINE TOTAL TEMPERATURE WITH AXIAL DISTANCE AT $M_\infty = 6$

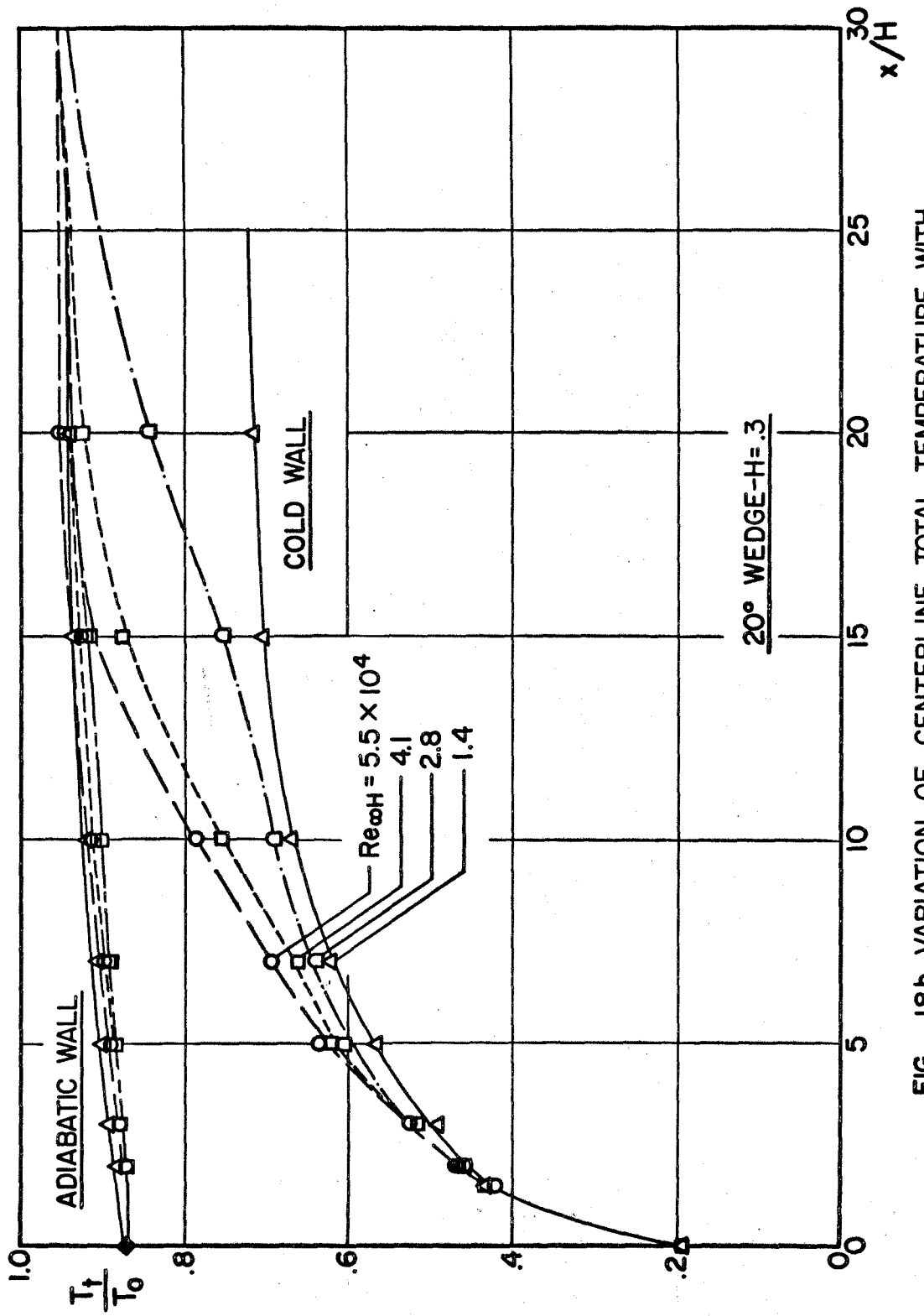

FIG. 18b VARIATION OF CENTERLINE TOTAL TEMPERATURE WITH AXIAL DISTANCE AT $M_\infty = 6$

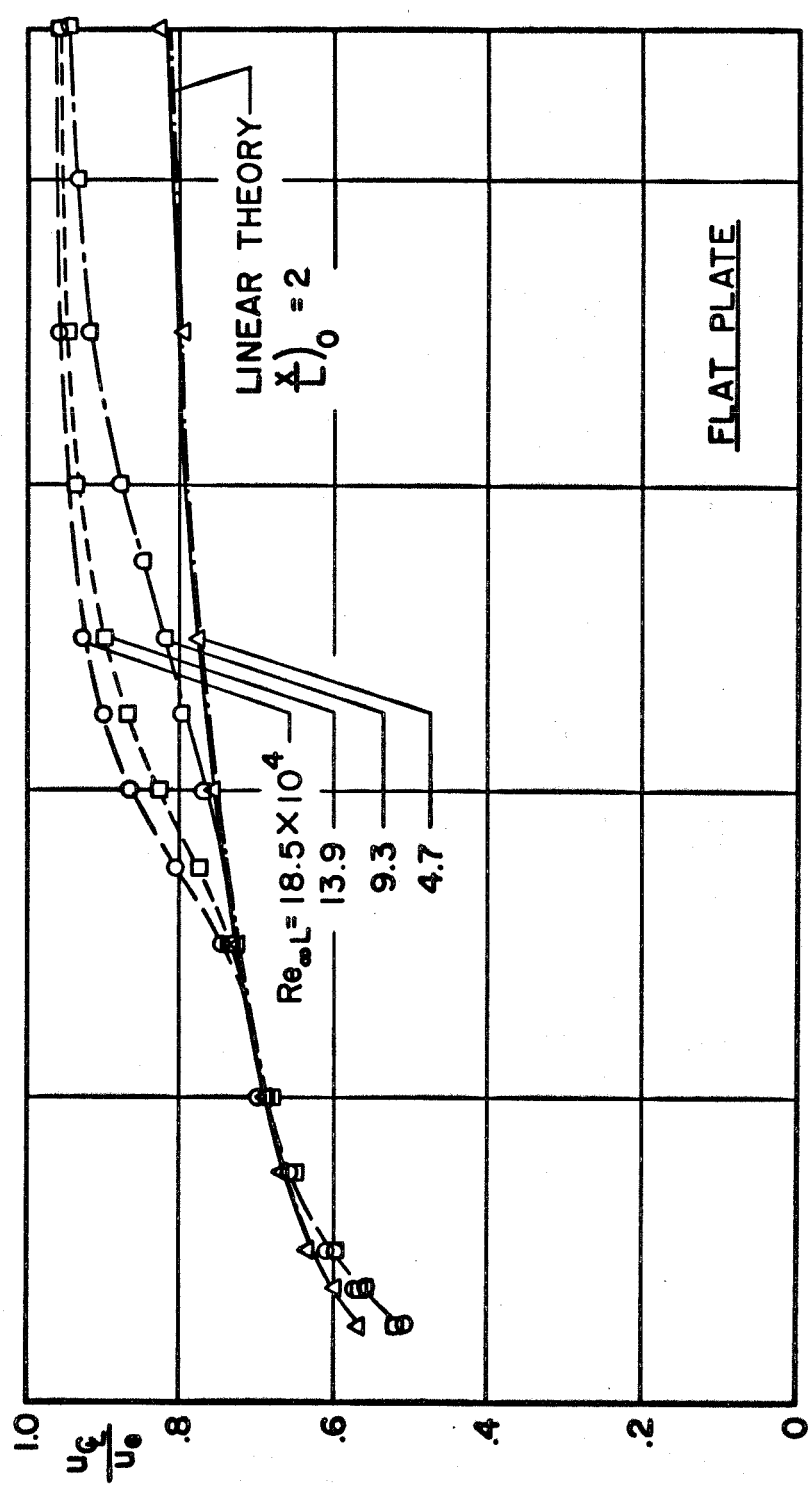

FIG. 19a VARIATION OF CENTERLINE VELOCITY WITH AXIAL DISTANCE AT $M_\infty = 6$

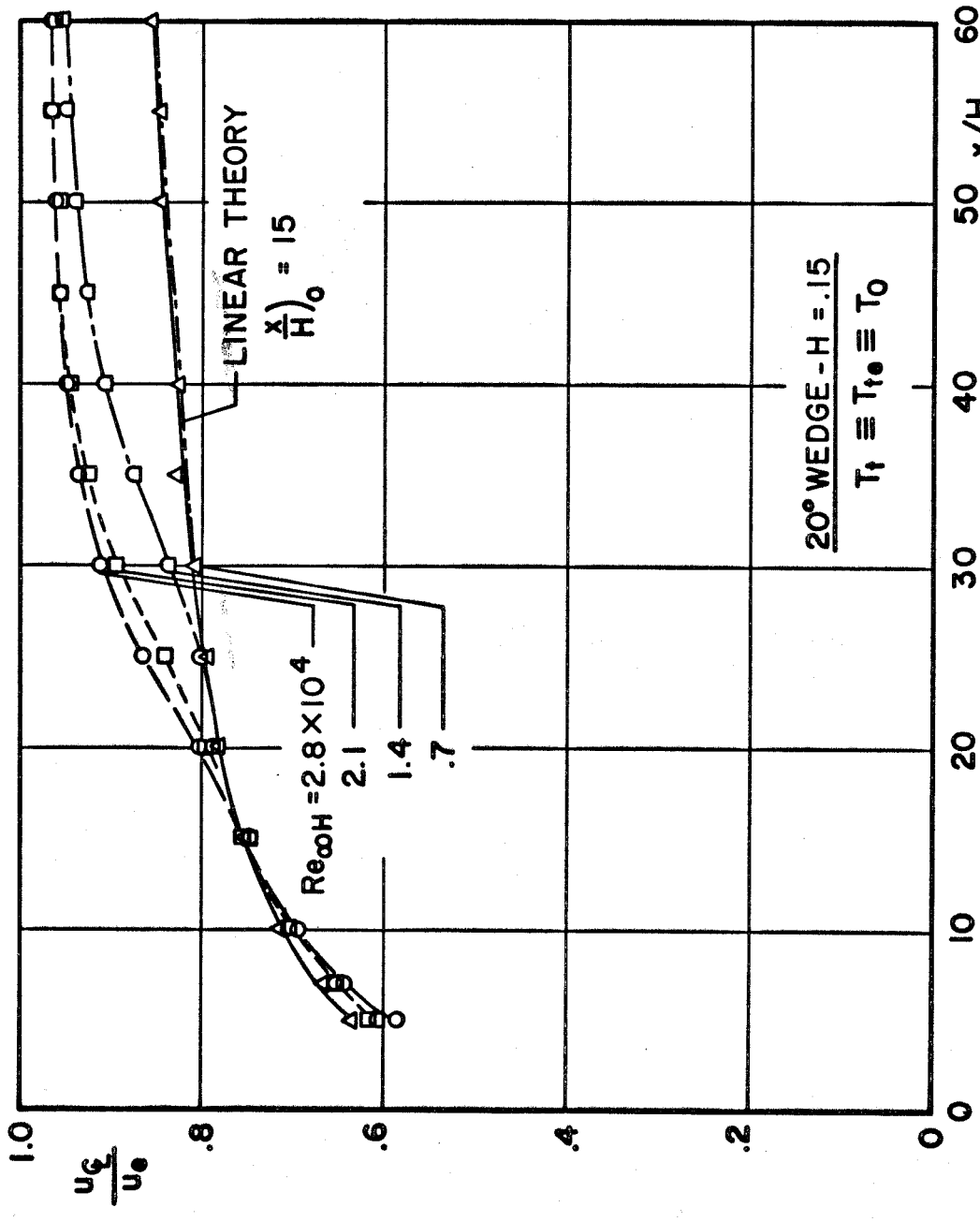

FIG.19b VARIATION OF CENTERLINE VELOCITY WITH AXIAL DISTANCE AT $M_\infty = 6$

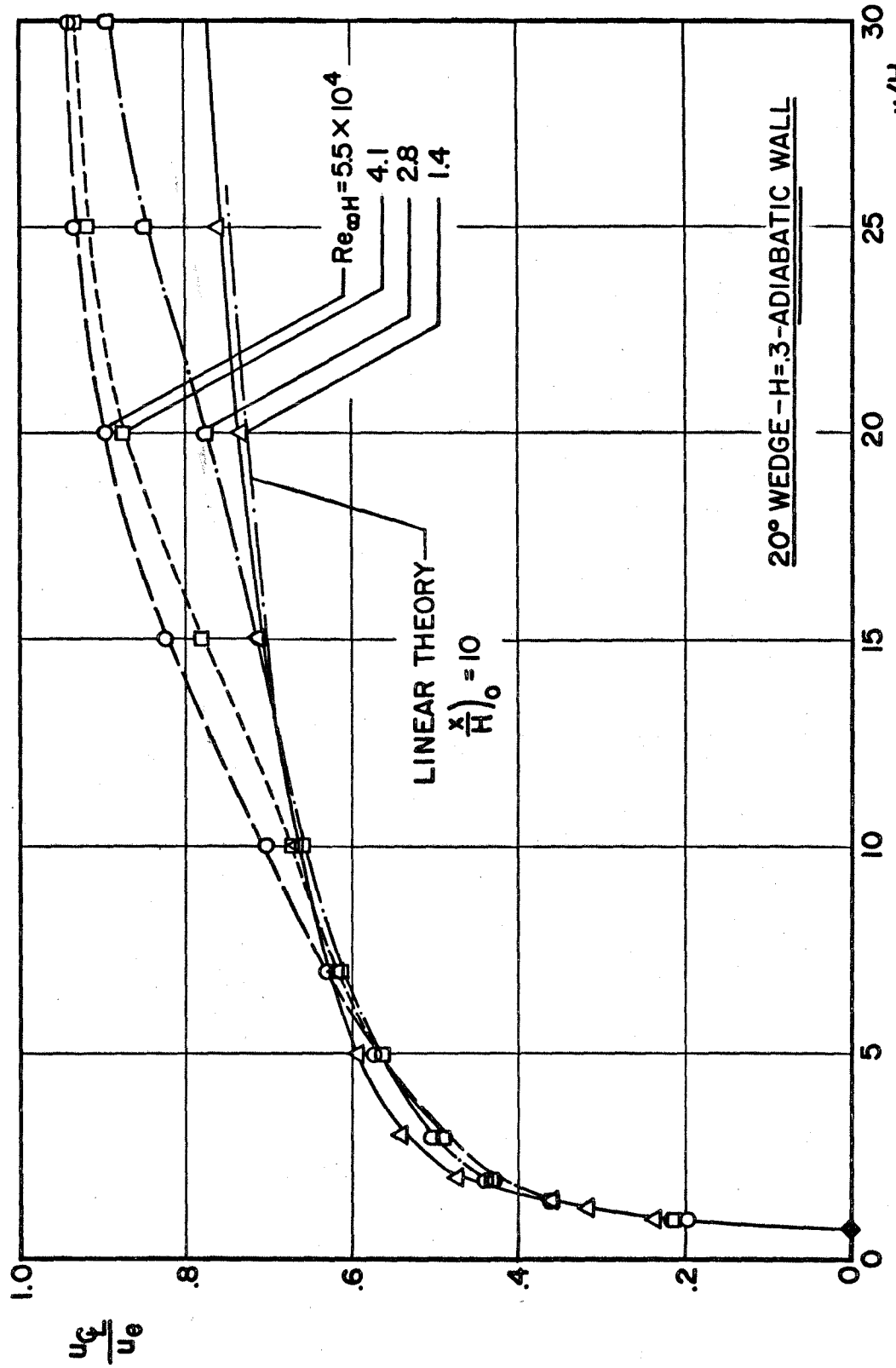

FIG. 19c VARIATION OF CENTERLINE VELOCITY WITH AXIAL DISTANCE AT $M_\infty = 6$

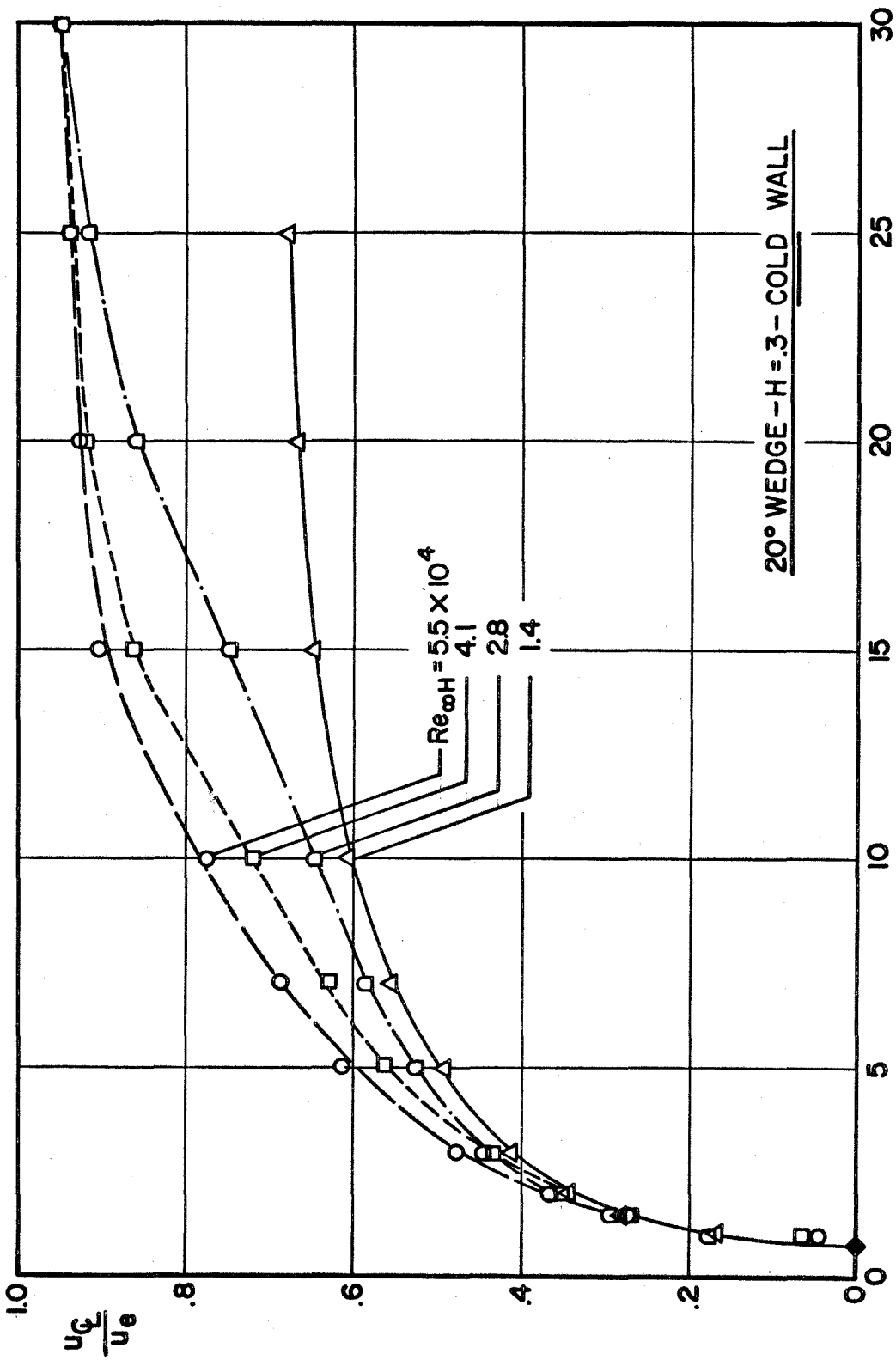

FIG. 19d VARIATION OF CENTERLINE VELOCITY WITH AXIAL DISTANCE AT $M_\infty = 6$

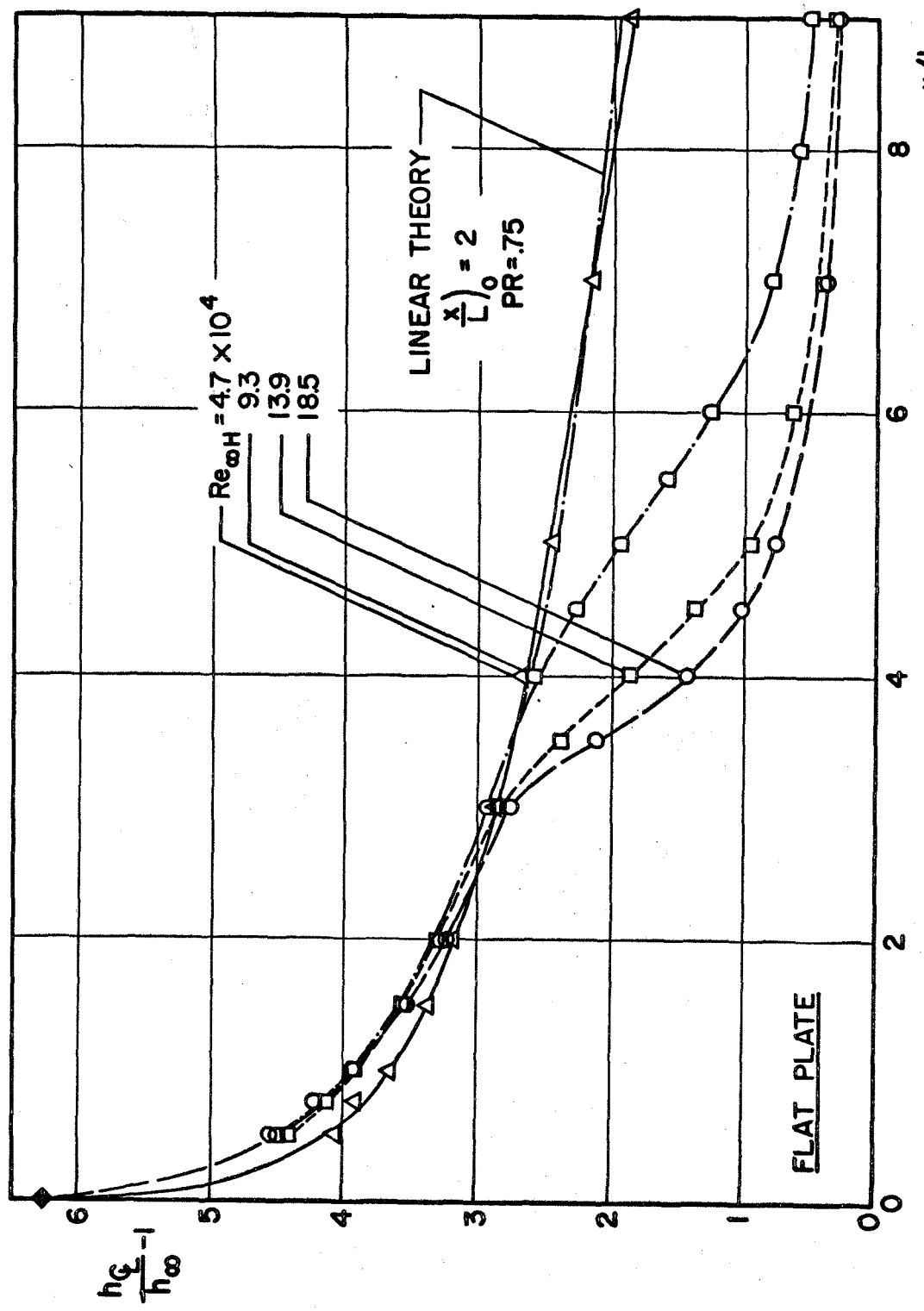

FIG. 20a VARIATION OF CENTERLINE ENTHALPY WITH AXIAL DISTANCE AT $M_\infty = 6$

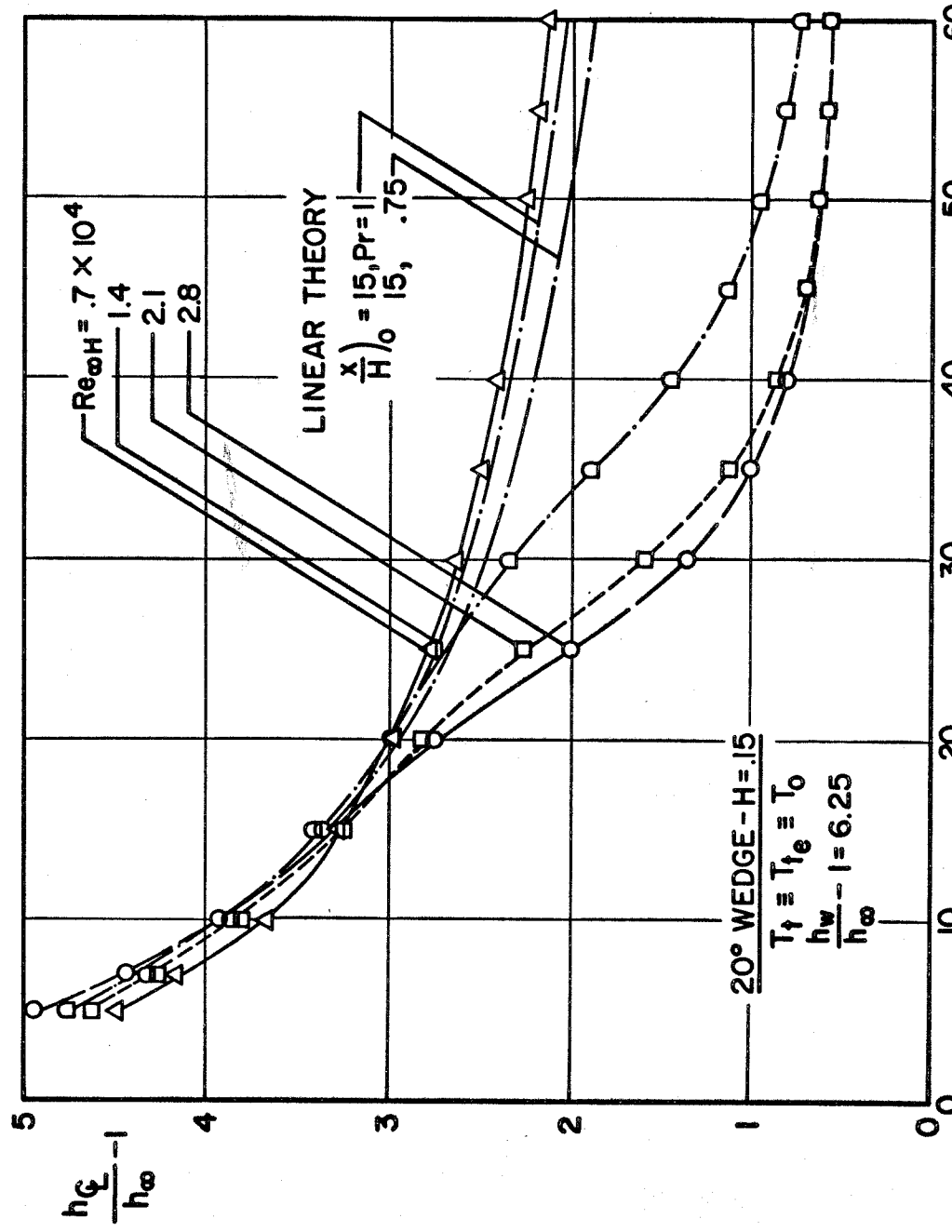

FIG. 20b VARIATION OF CENTERLINE ENTHALPY WITH AXIAL DISTANCE AT $M_\infty = 6$

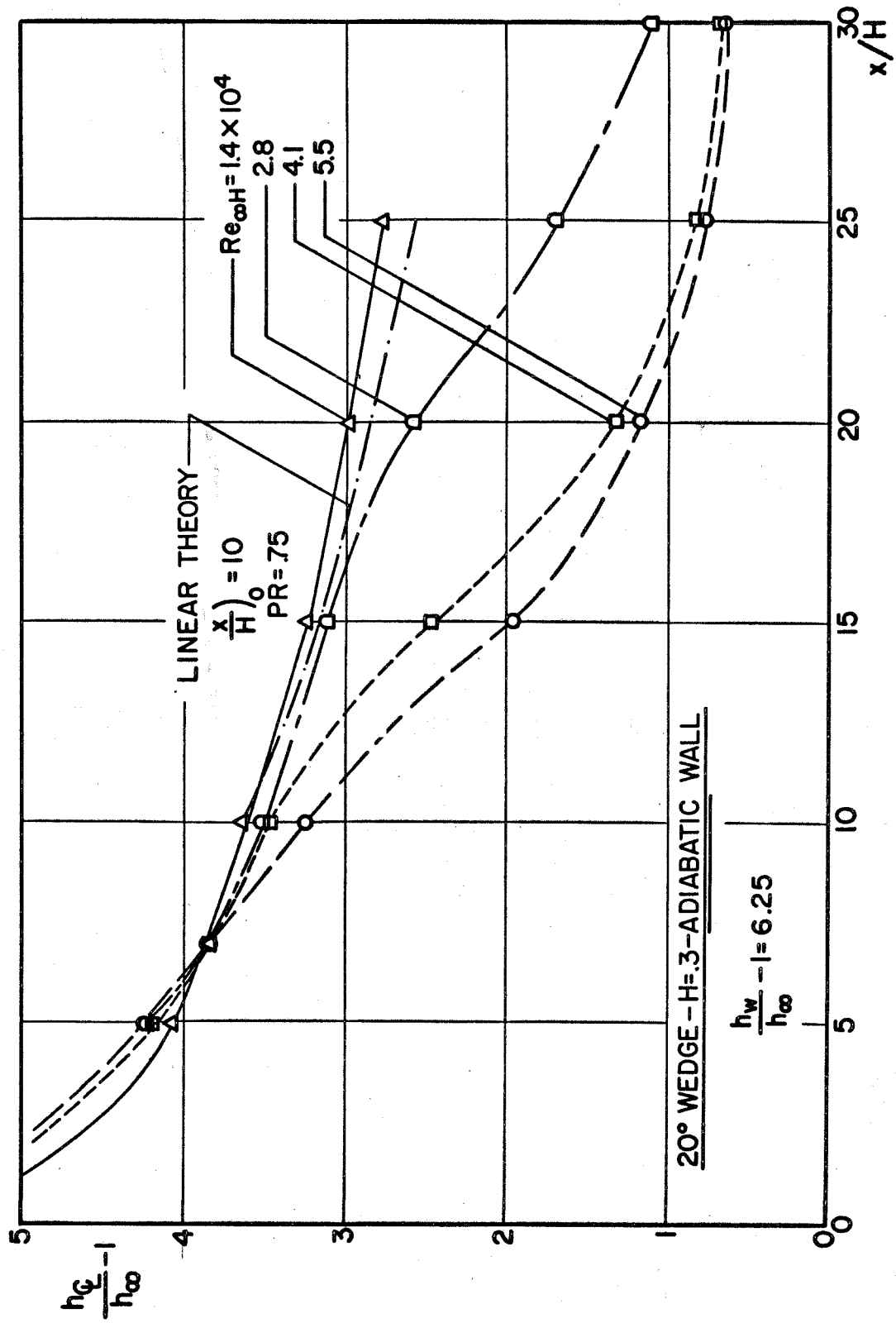

FIG. 20c VARIATION OF CENTERLINE ENTHALPY WITH AXIAL DISTANCE AT $M_\infty = 6$

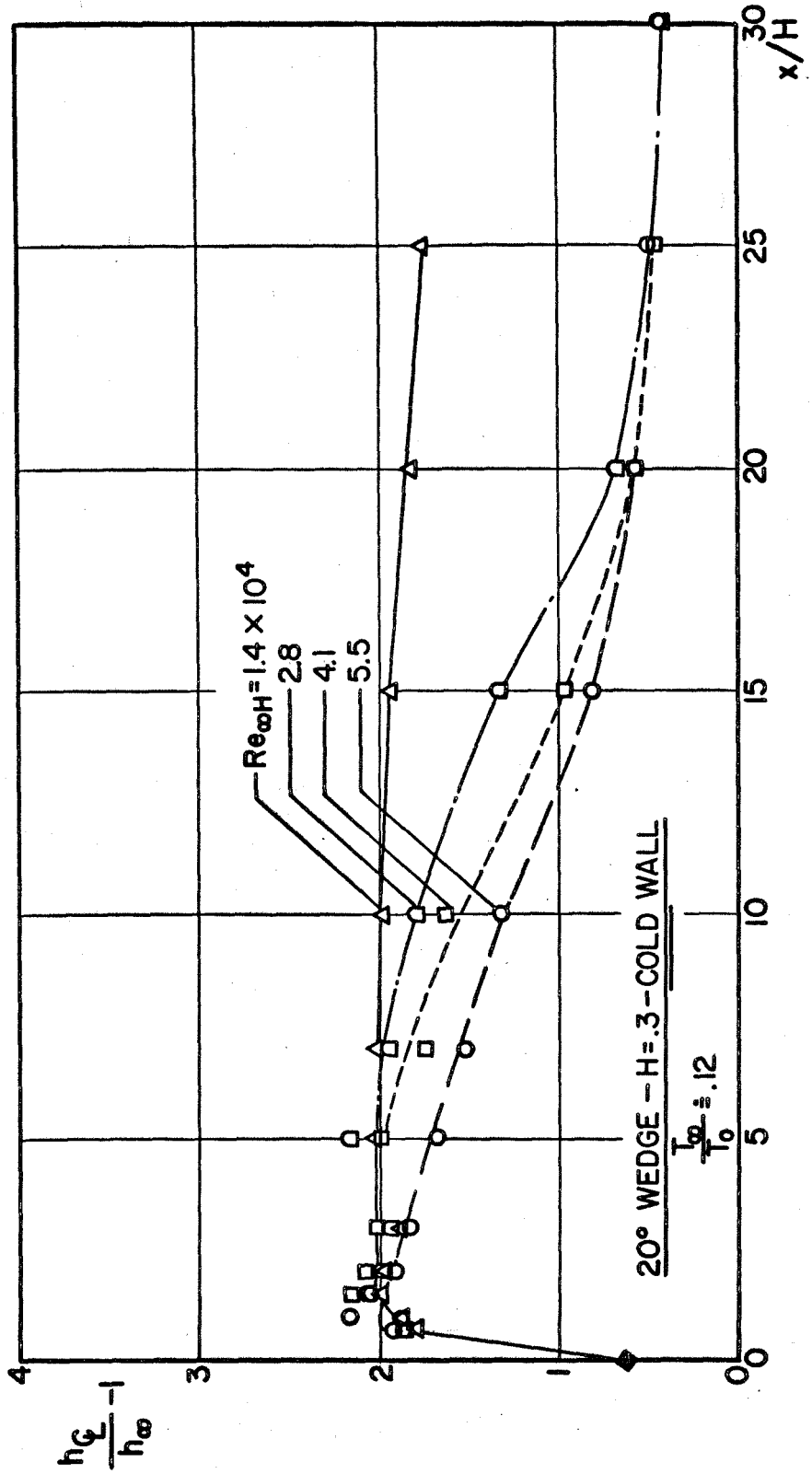

FIG. 20d VARIATION OF CENTERLINE ENTHALPY WITH AXIAL DISTANCE AT $M_\infty = 6$

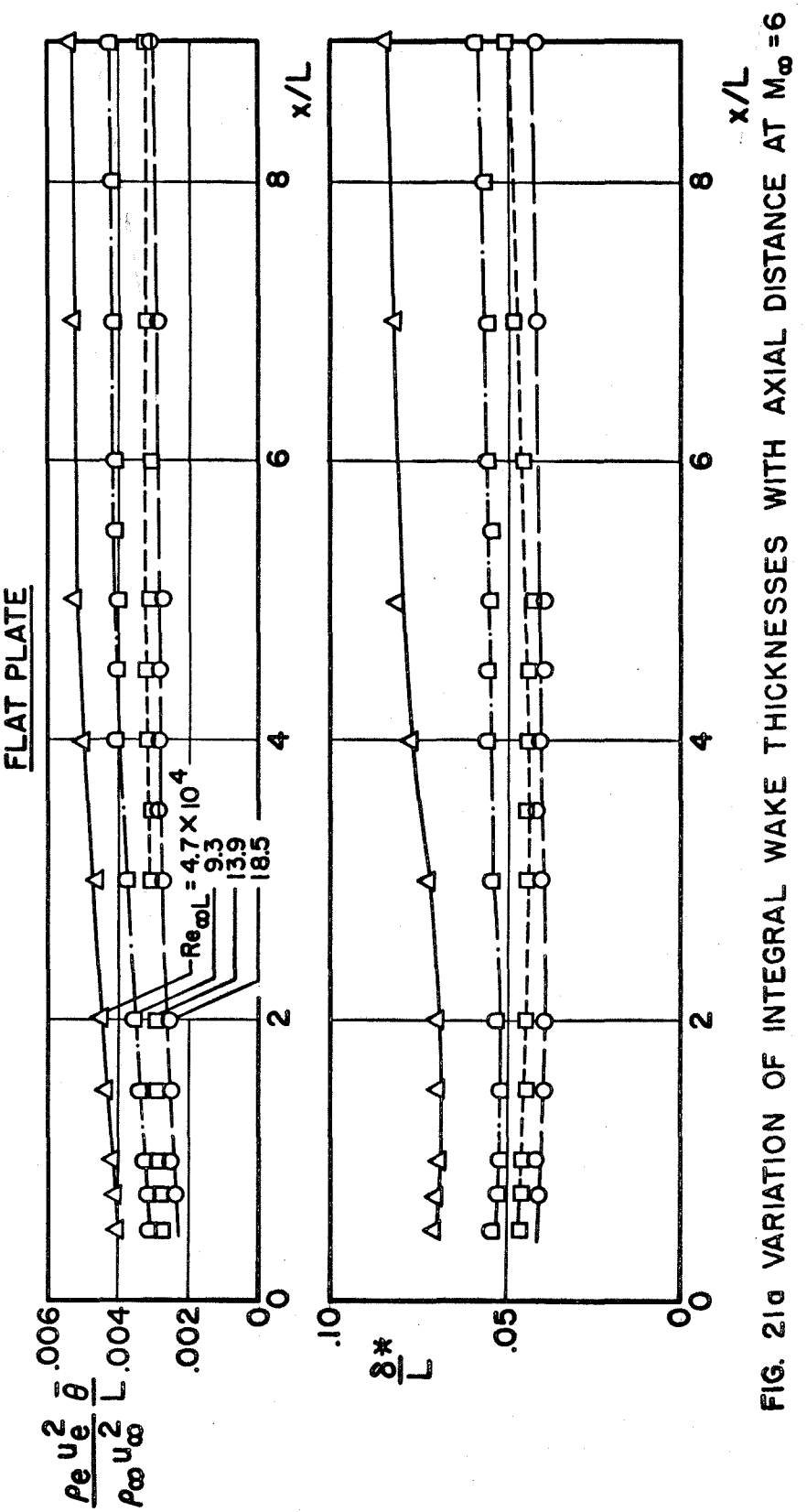

FIG. 21a VARIATION OF INTEGRAL WAKE THICKNESSES WITH AXIAL DISTANCE AT $M_\infty = 6$

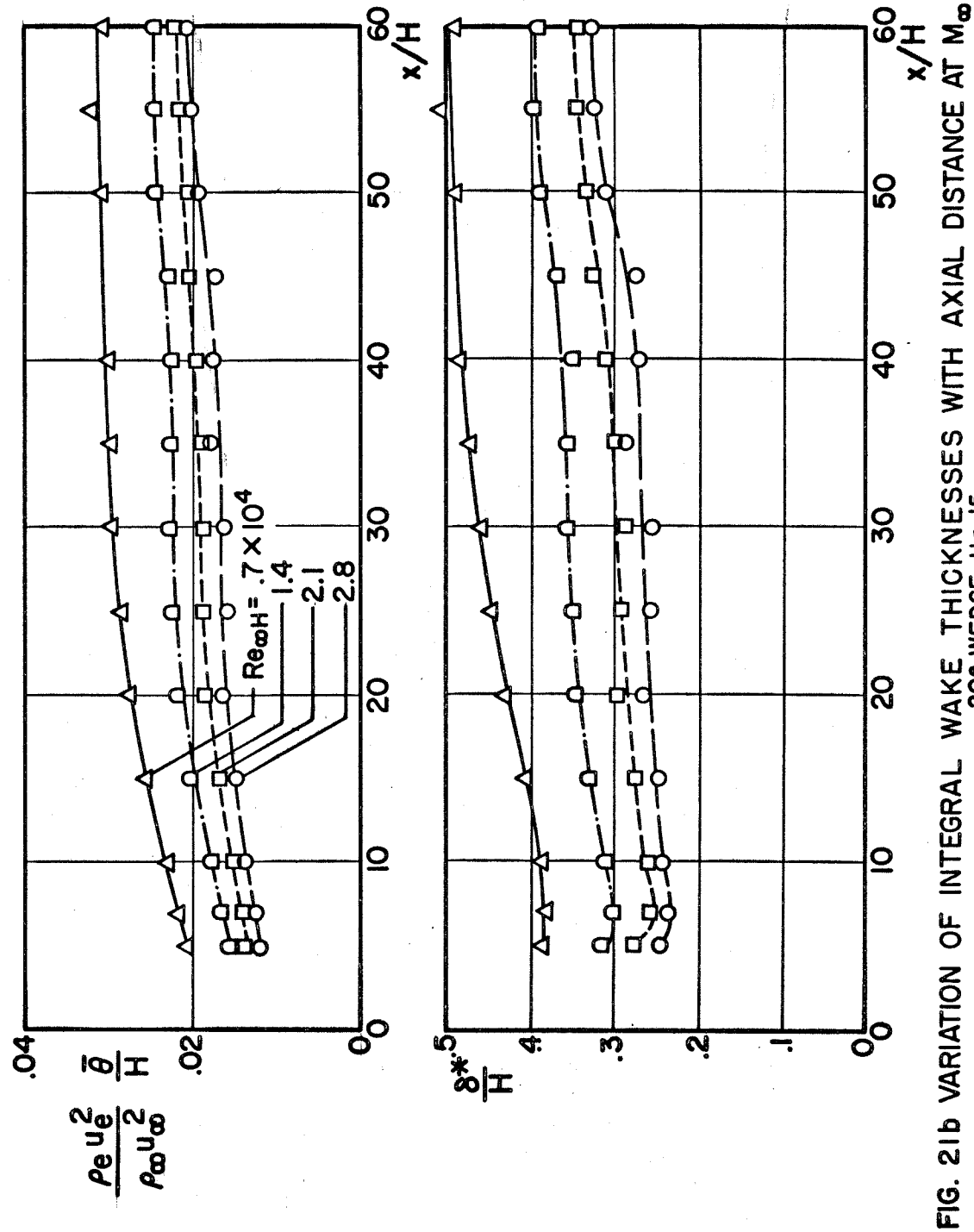

FIG. 21b VARIATION OF INTEGRAL WAKE THICKNESSES WITH AXIAL DISTANCE AT $M_\infty = 6$
20° WEDGE-H=.15

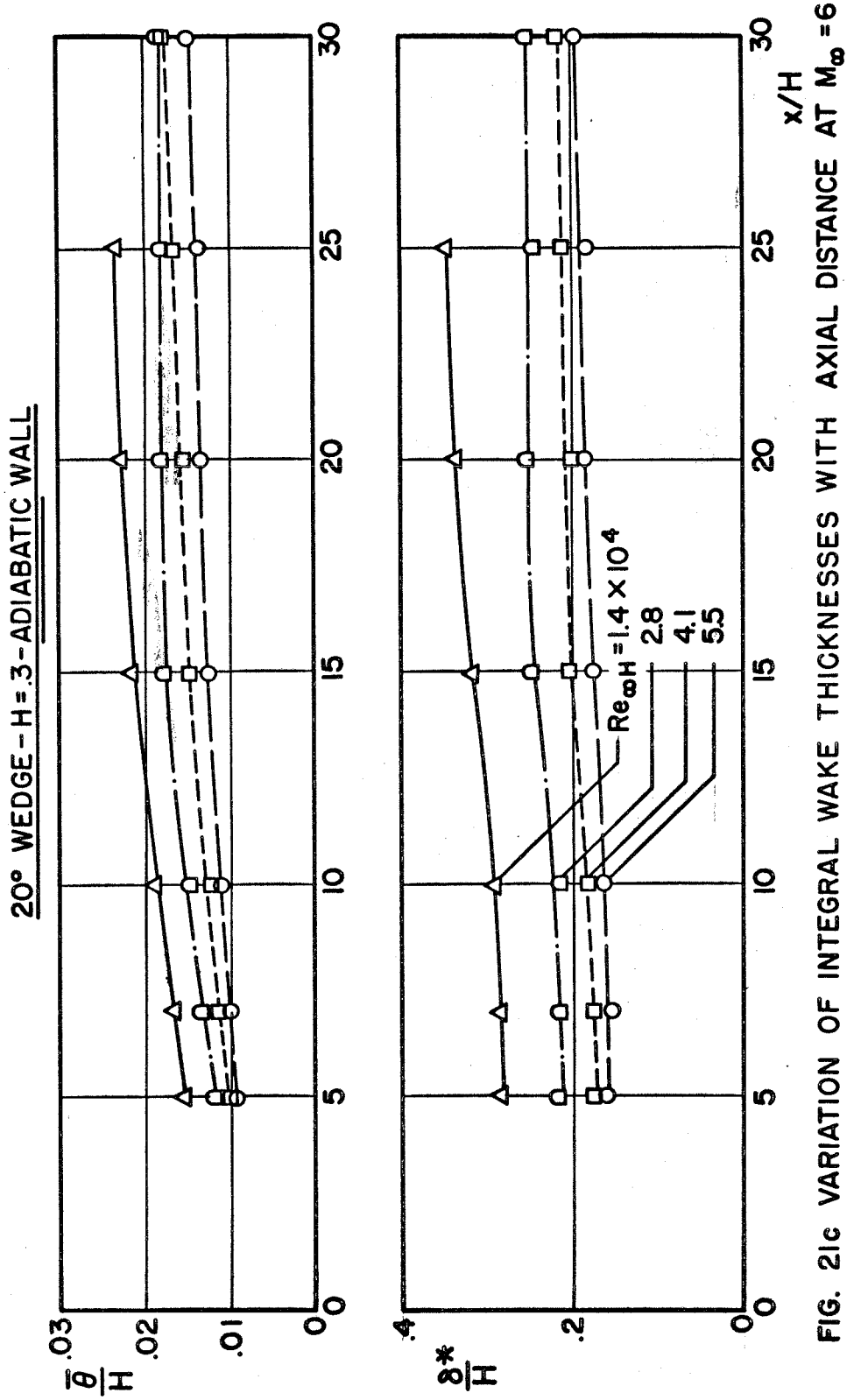

FIG. 21c VARIATION OF INTEGRAL WAKE THICKNESSES WITH AXIAL DISTANCE AT $M_\infty = 6$

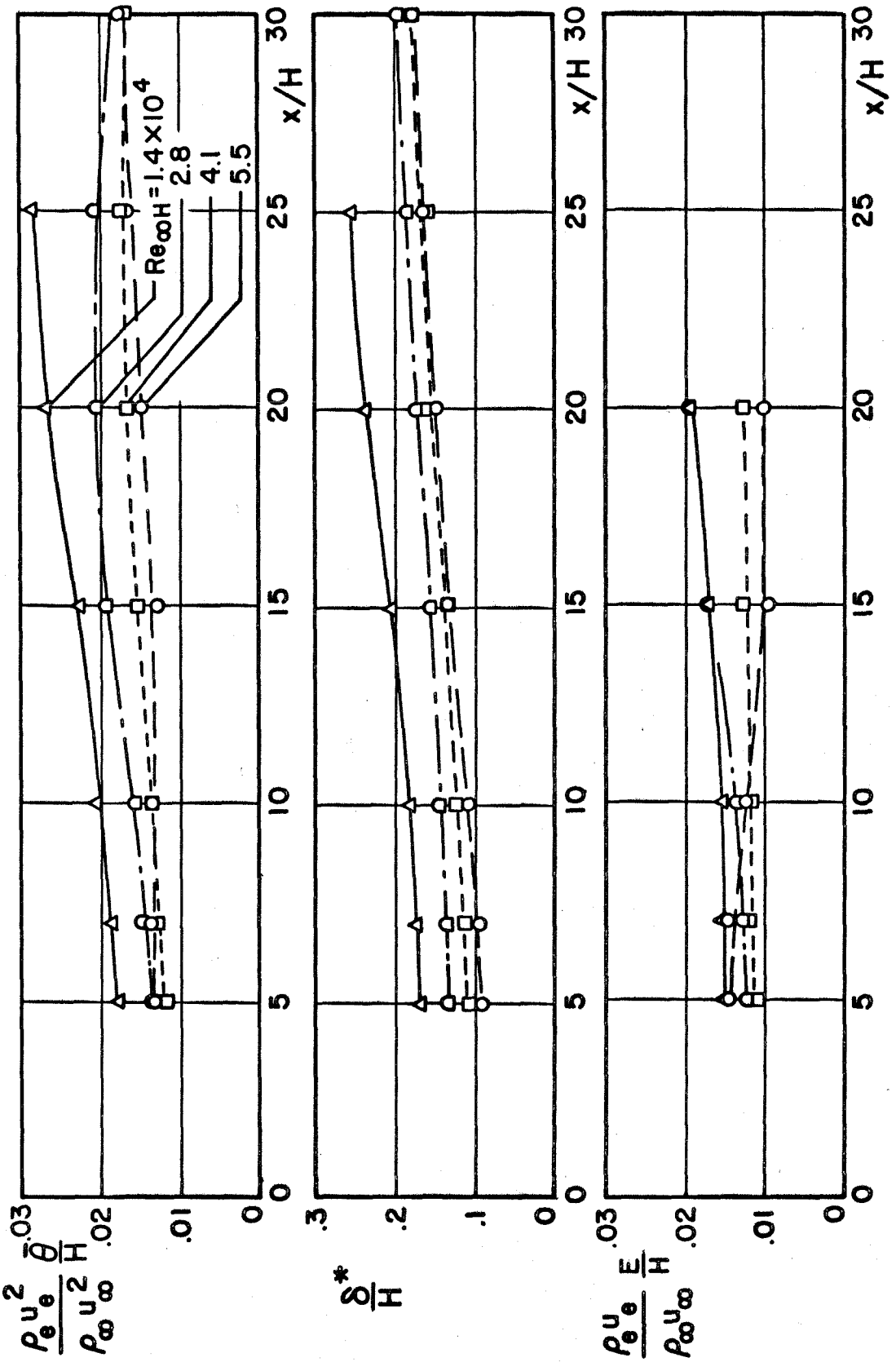

FIG. 21d VARIATION OF INTEGRAL WAKE THICKNESSES WITH AXIAL DISTANCE AT $M_\infty=6$
20° WEDGE - H=.3 - COLD WALL

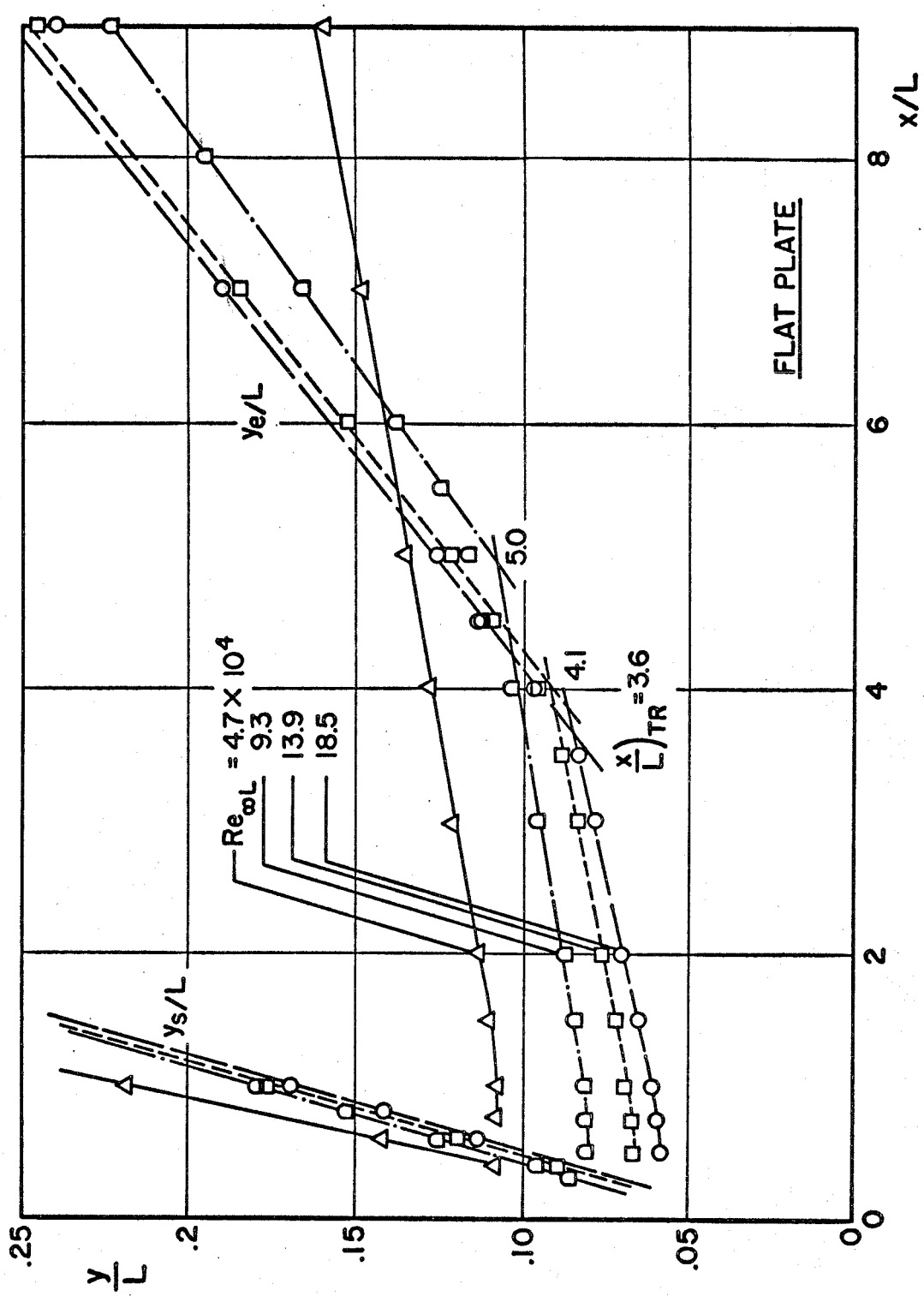

FIG. 22a VARIATION OF WAKE THICKNESS AND WAKE SHOCK POSITION WITH AXIAL DISTANCE AT $M_\infty = 6$

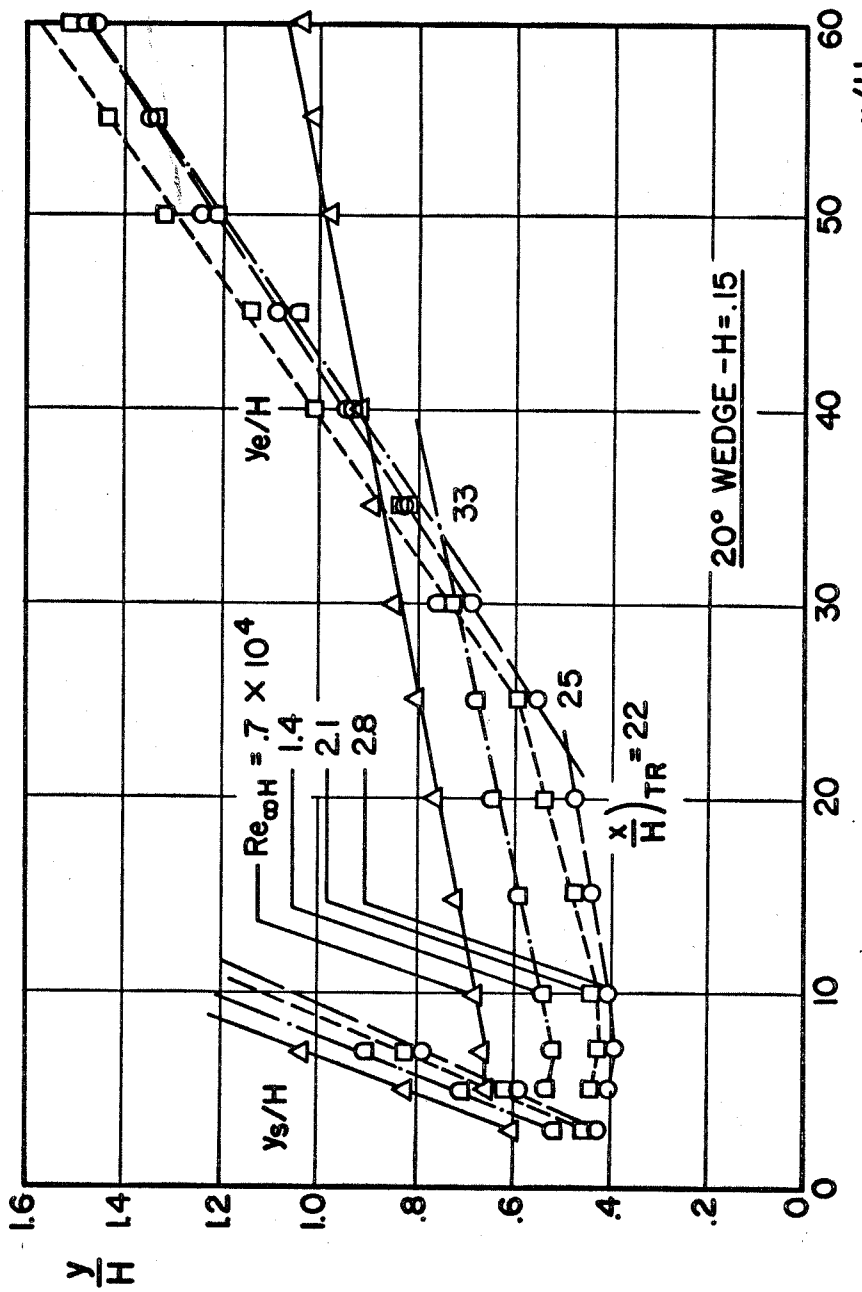

FIG. 22b VARIATION OF WAKE THICKNESS AND WAKE SHOCK POSITION WITH AXIAL DISTANCE AT $M_\infty = 6$

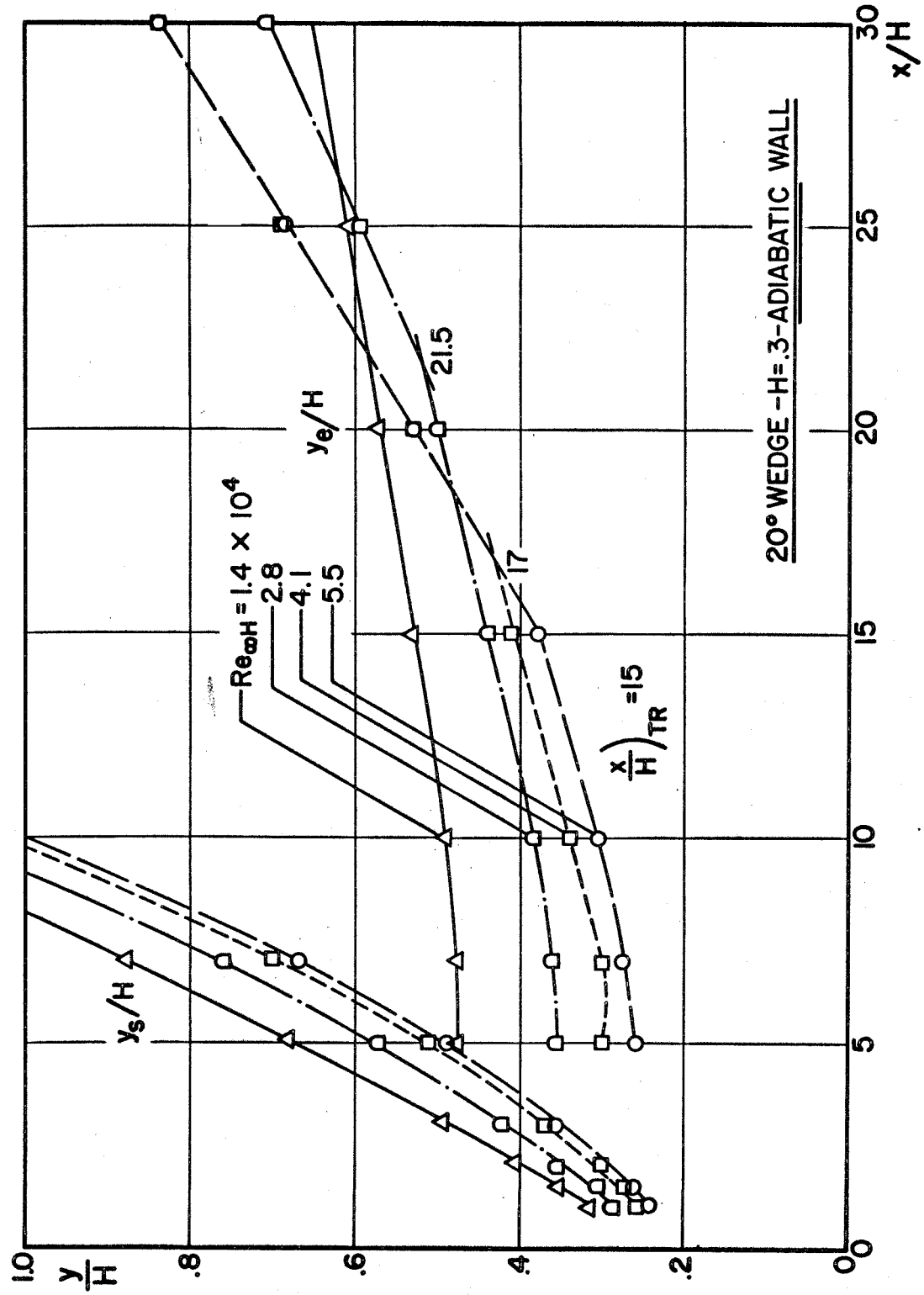

FIG. 22c VARIATION OF WAKE THICKNESS AND WAKE SHOCK POSITION WITH AXIAL DISTANCE AT $M_\infty = 6$

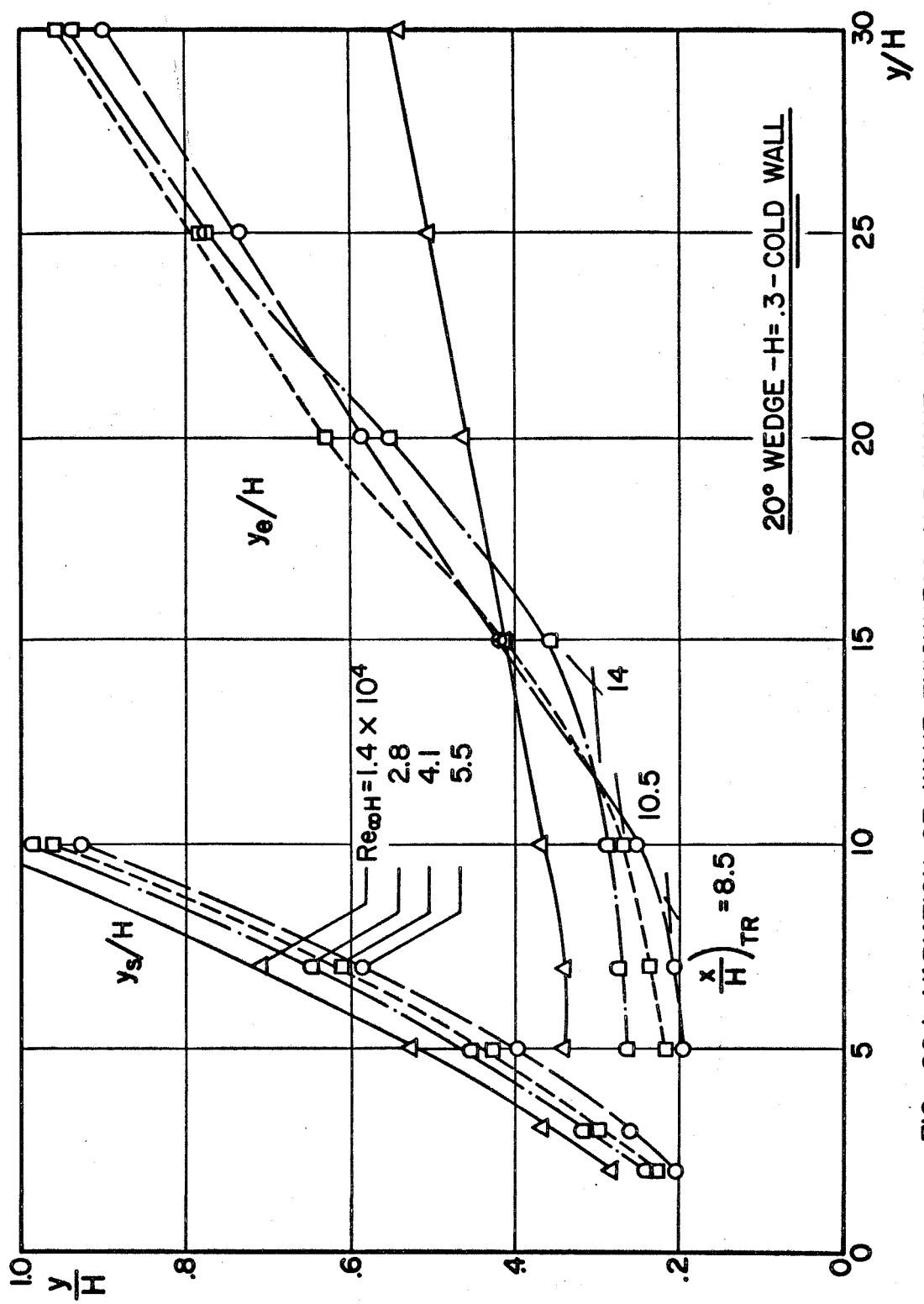

FIG. 22d VARIATION OF WAKE THICKNESS AND WAKE SHOCK POSITION WITH AXIAL DISTANCE AT $M_\infty = 6$

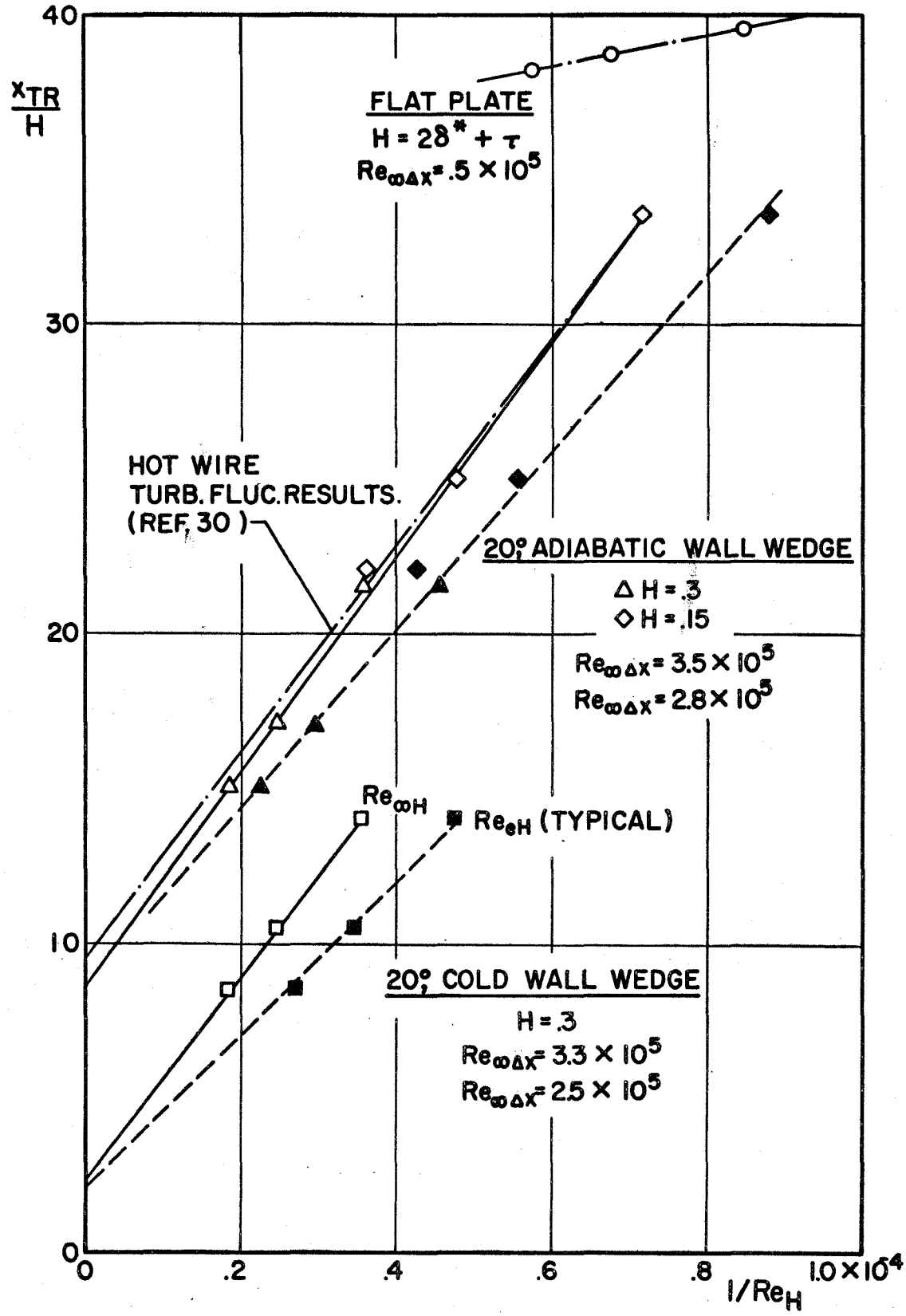

FIG. 23 WAKE TRANSITION CORRELATION AT $M_\infty = 6$

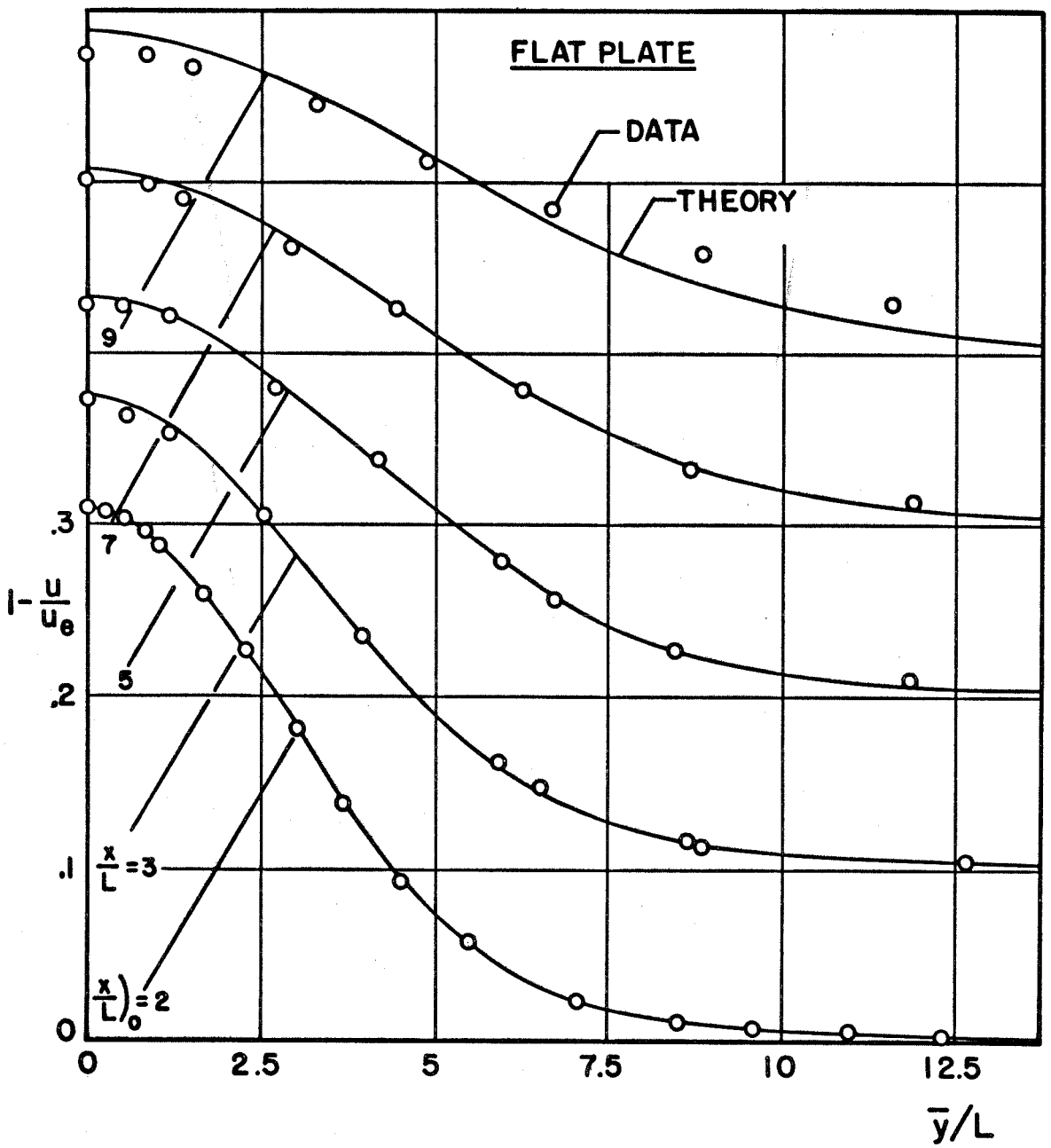

FIG.24a COMPARISON OF VELOCITY DEFECT DATA WITH LINEAR THEORY FOR $M_\infty = 6$ AND $Re_{\infty L} = 4.7 \times 10^4$

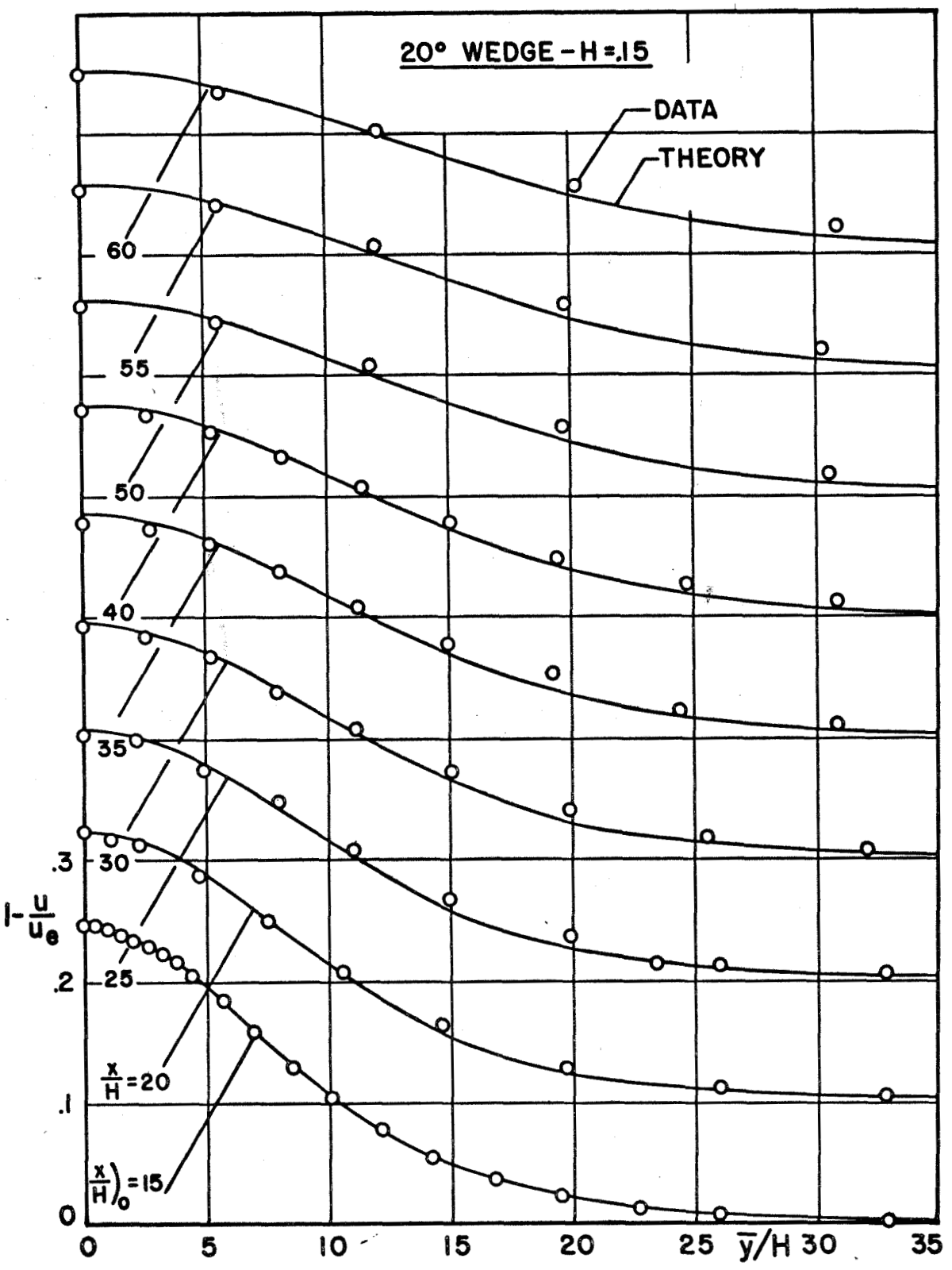

FIG.24b COMPARISON OF VELOCITY DEFECT DATA WITH LINEAR THEORY FOR $M_\infty = 6$ AND $Re_{\infty H} = .7 \times 10^4$

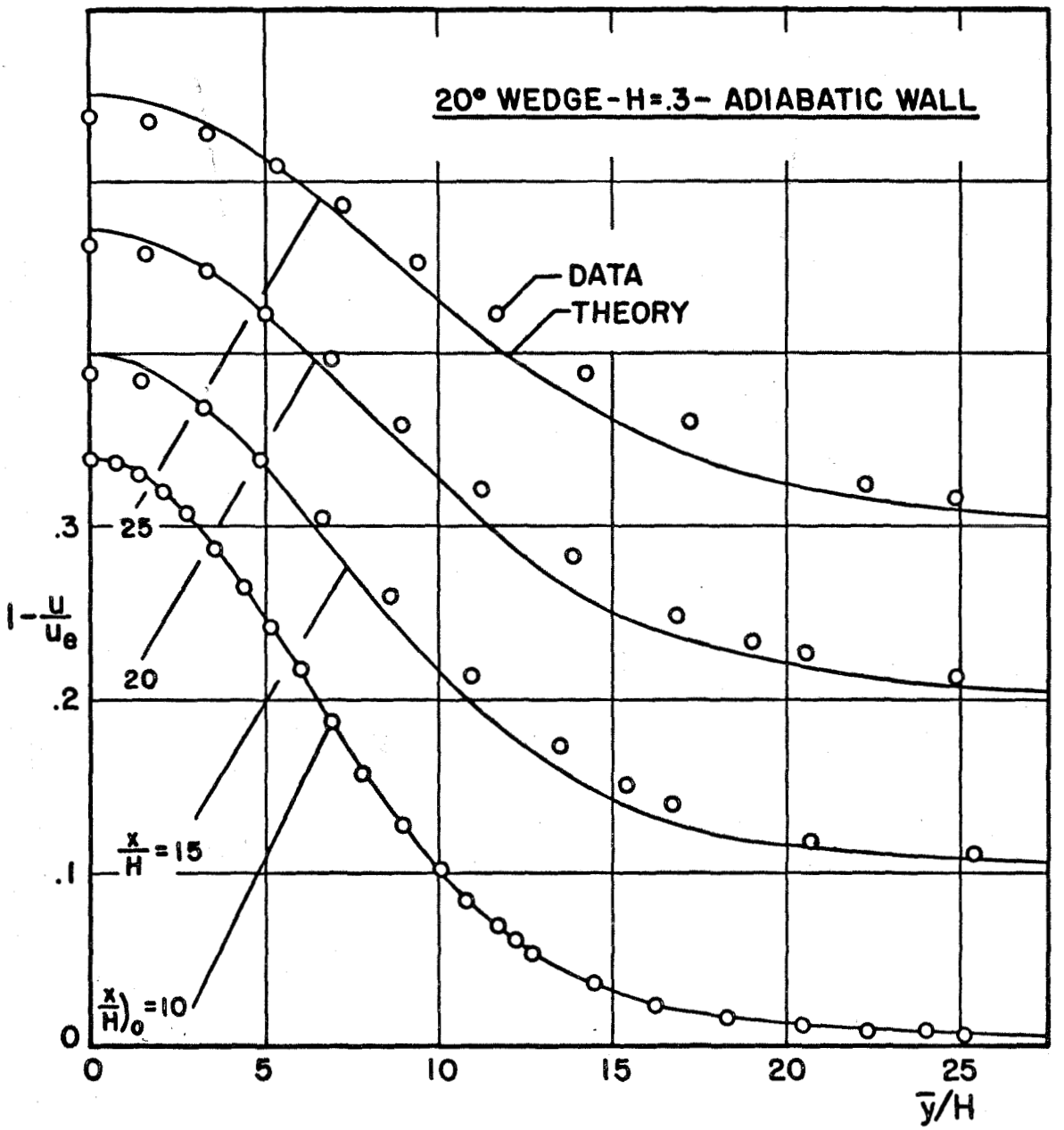

FIG.24c COMPARISON OF VELOCITY DEFECT DATA WITH LINEAR THEORY FOR $M_\infty = 6$ AND $Re_{\infty H} = 1.4 \times 10^4$

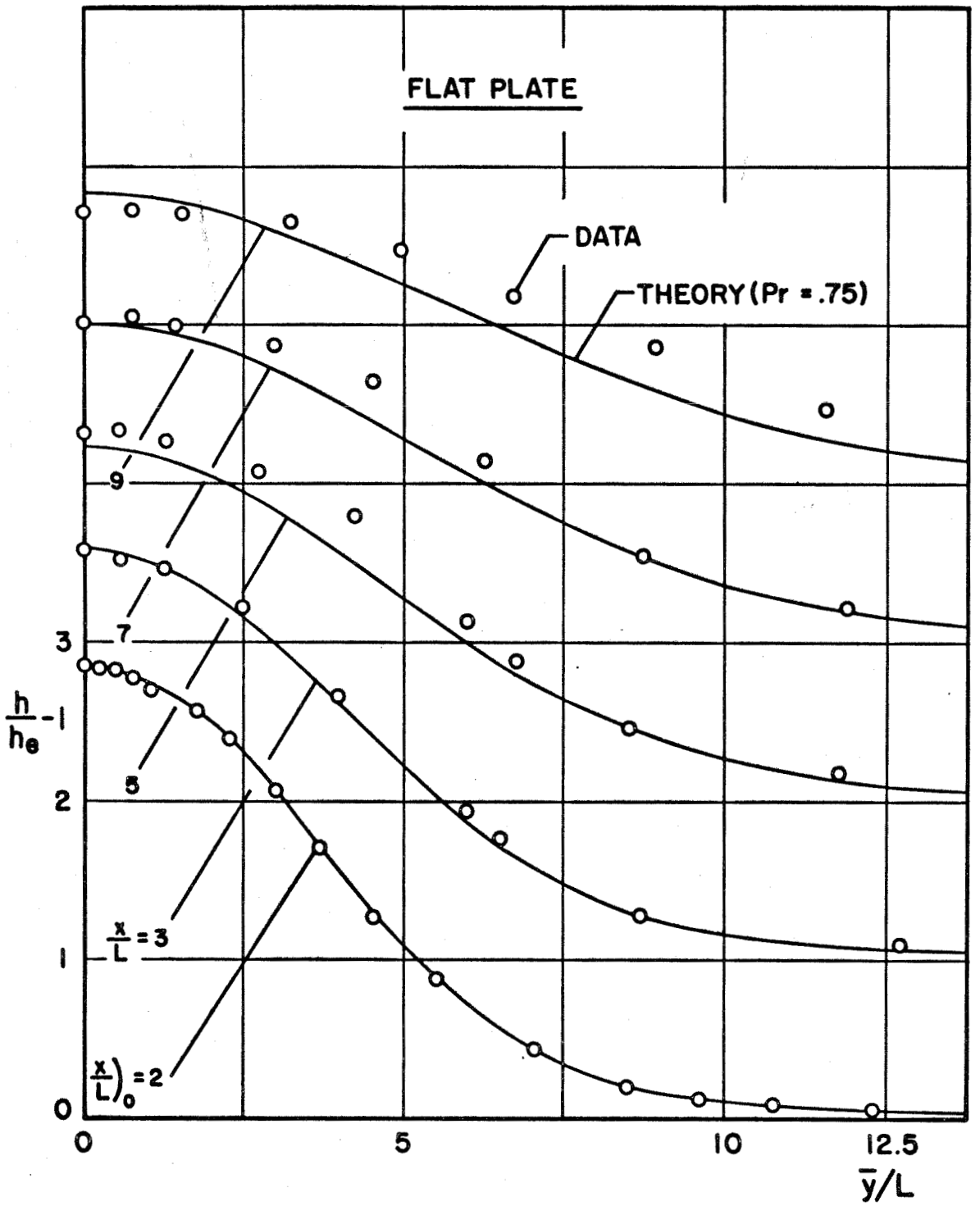

FIG.25a COMPARISON OF ENTHALPY EXCESS DATA WITH LINEAR THEORY FOR $M_\infty = 6$ AND $Re_{\infty L} = 4.7 \times 10^4$

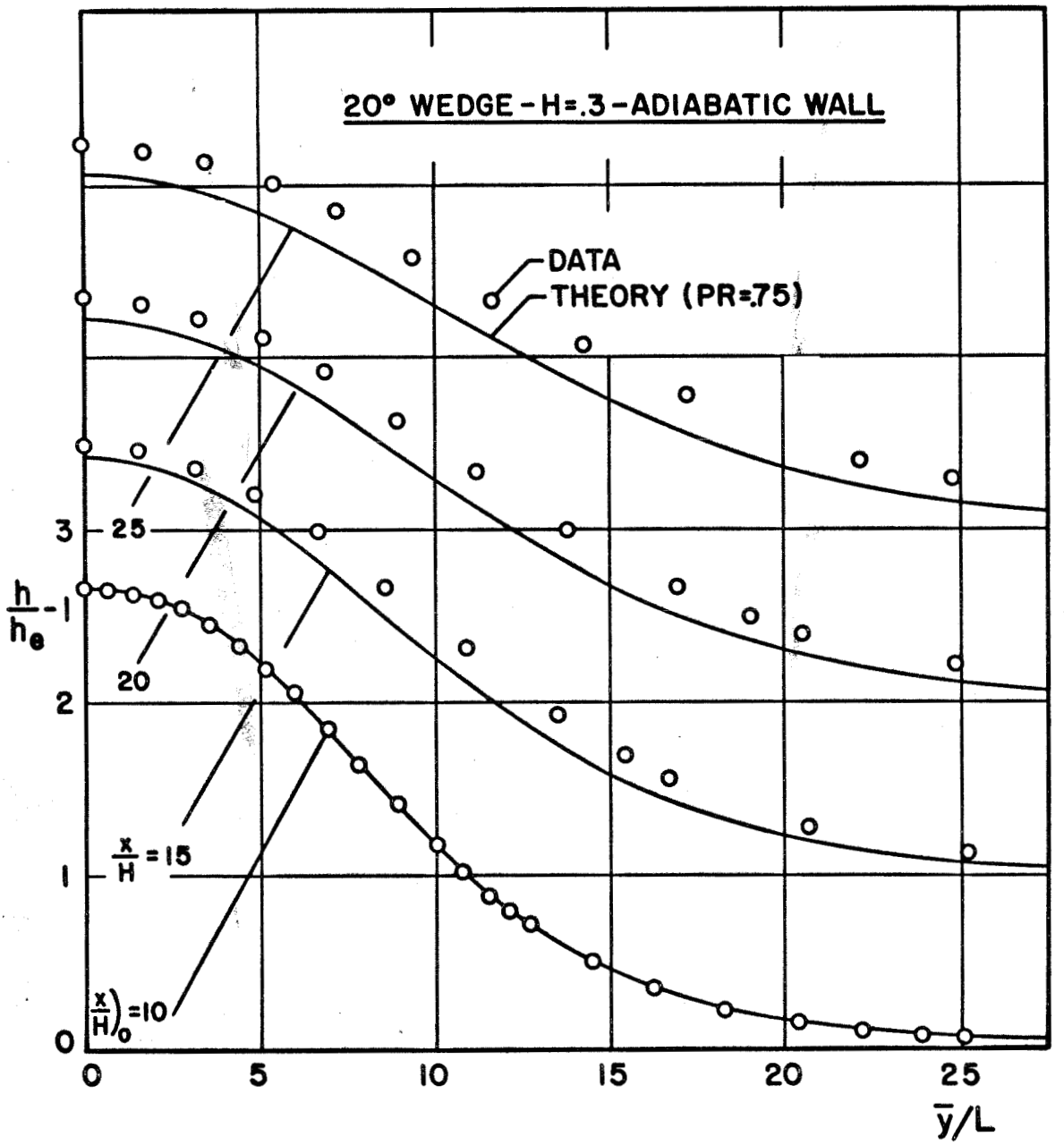

FIG.25b COMPARISON OF ENTHALPY EXCESS DATA WITH LINEAR THEORY FOR $M_\infty = 6$ AND $Re_{\infty H} = 1.4 \times 10^4$

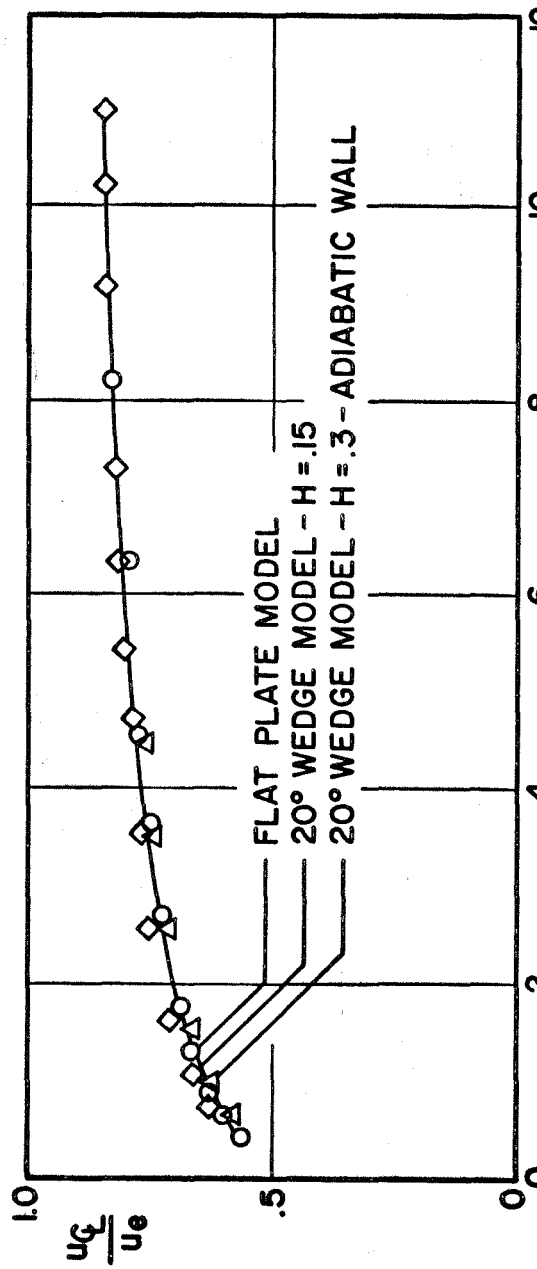

FIG. 26 CORRELATION OF CENTERLINE VELOCITY DATA WITH LINEAR THEORY

$Re_{\infty/IN} = 4.7 \times 10^4$

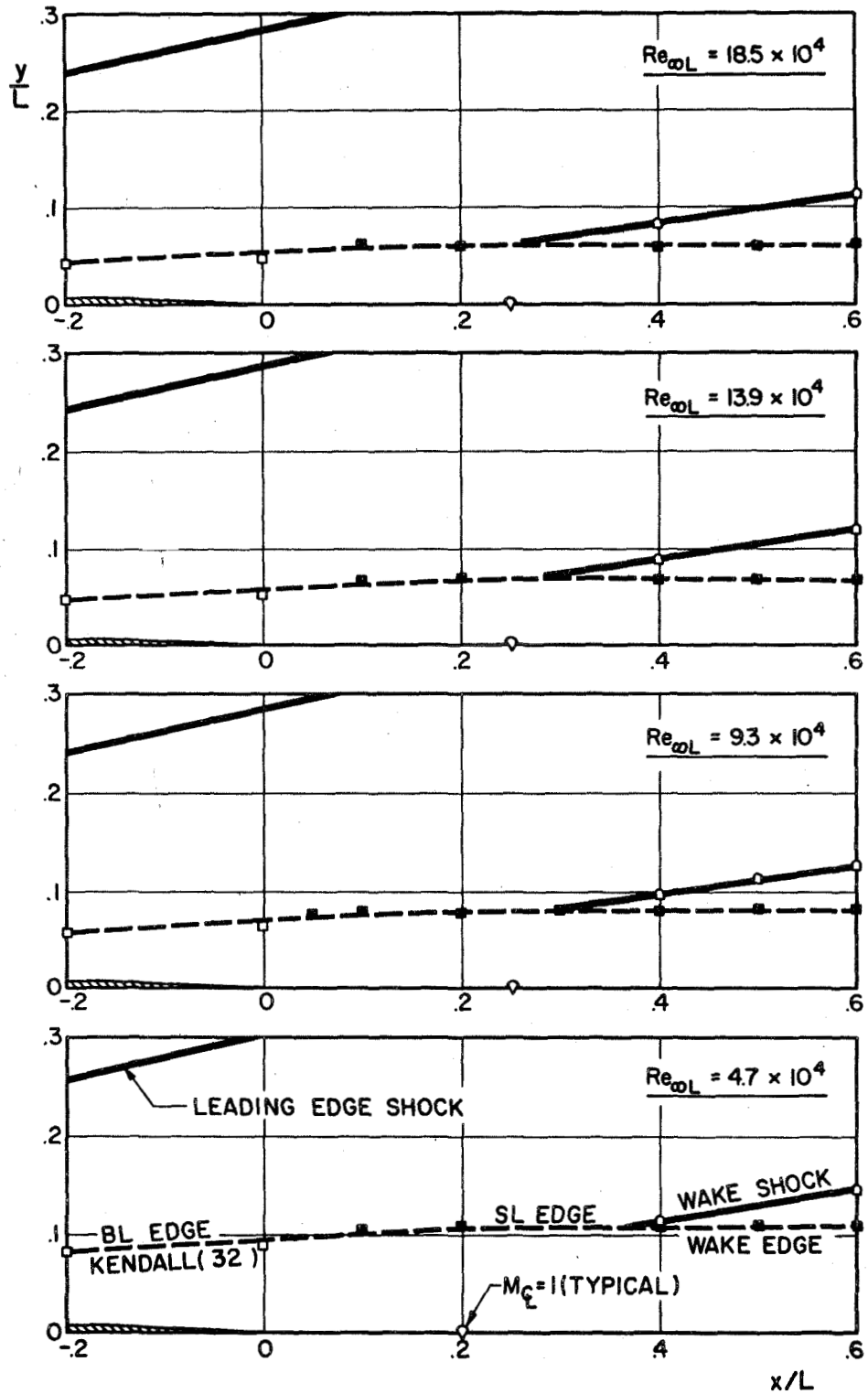

FIG. 27 FLOW FIELD MAPPING OF NEAR WAKE BEHIND FLAT PLATE AT $M_\infty = 6$

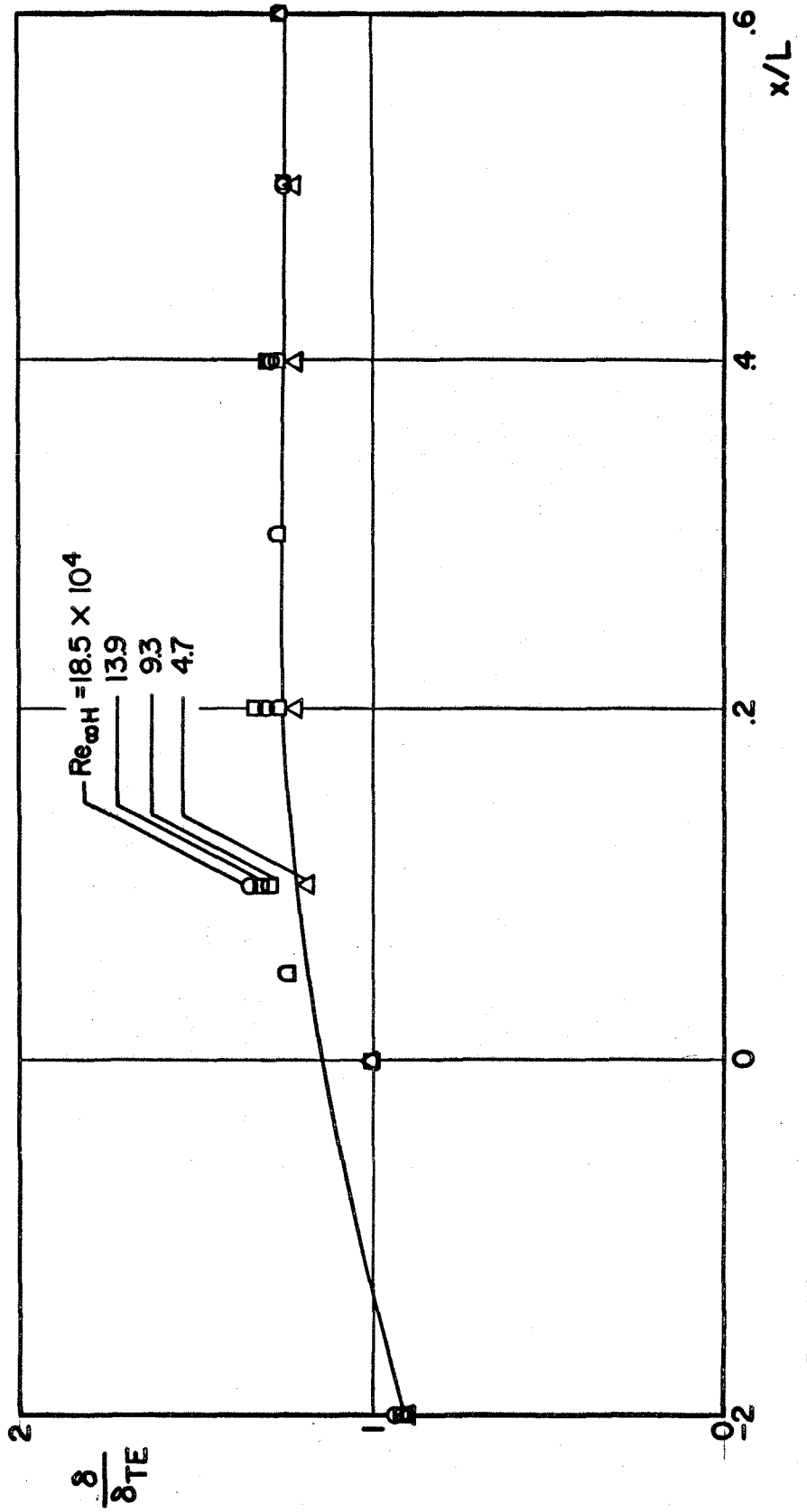

FIG. 28 CORRELATION OF NEAR WAKE THICKNESS BEHIND FLAT PLATE AT $M_\infty = 6$

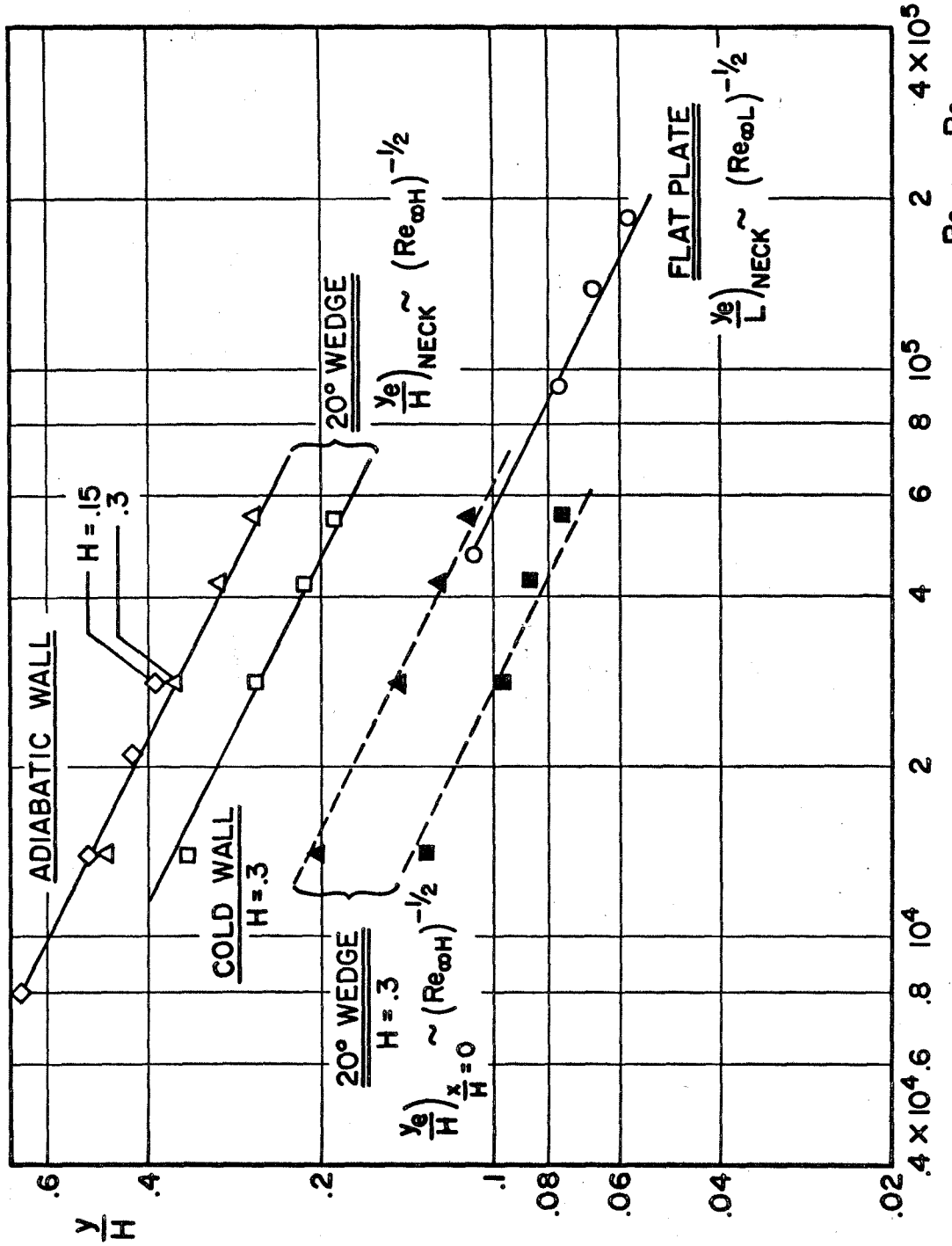

FIG.29 VARIATION OF TRAILING EDGE AND NECK THICKNESS WITH FREE STREAM REYNOLDS NUMBER AT $M_\infty = 6$

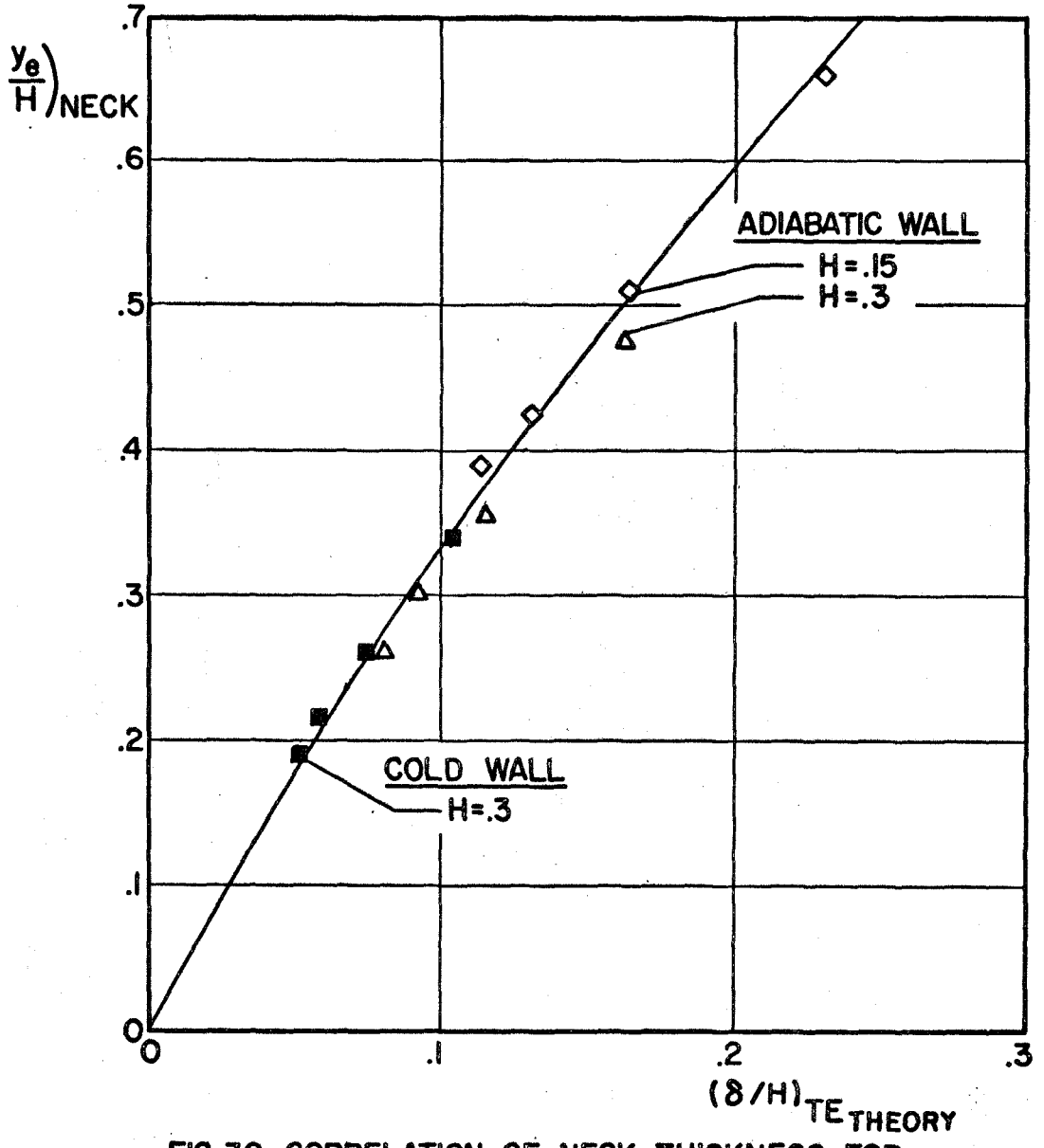

FIG. 30 CORRELATION OF NECK THICKNESS FOR 20° WEDGES AT $M_\infty = 6$.

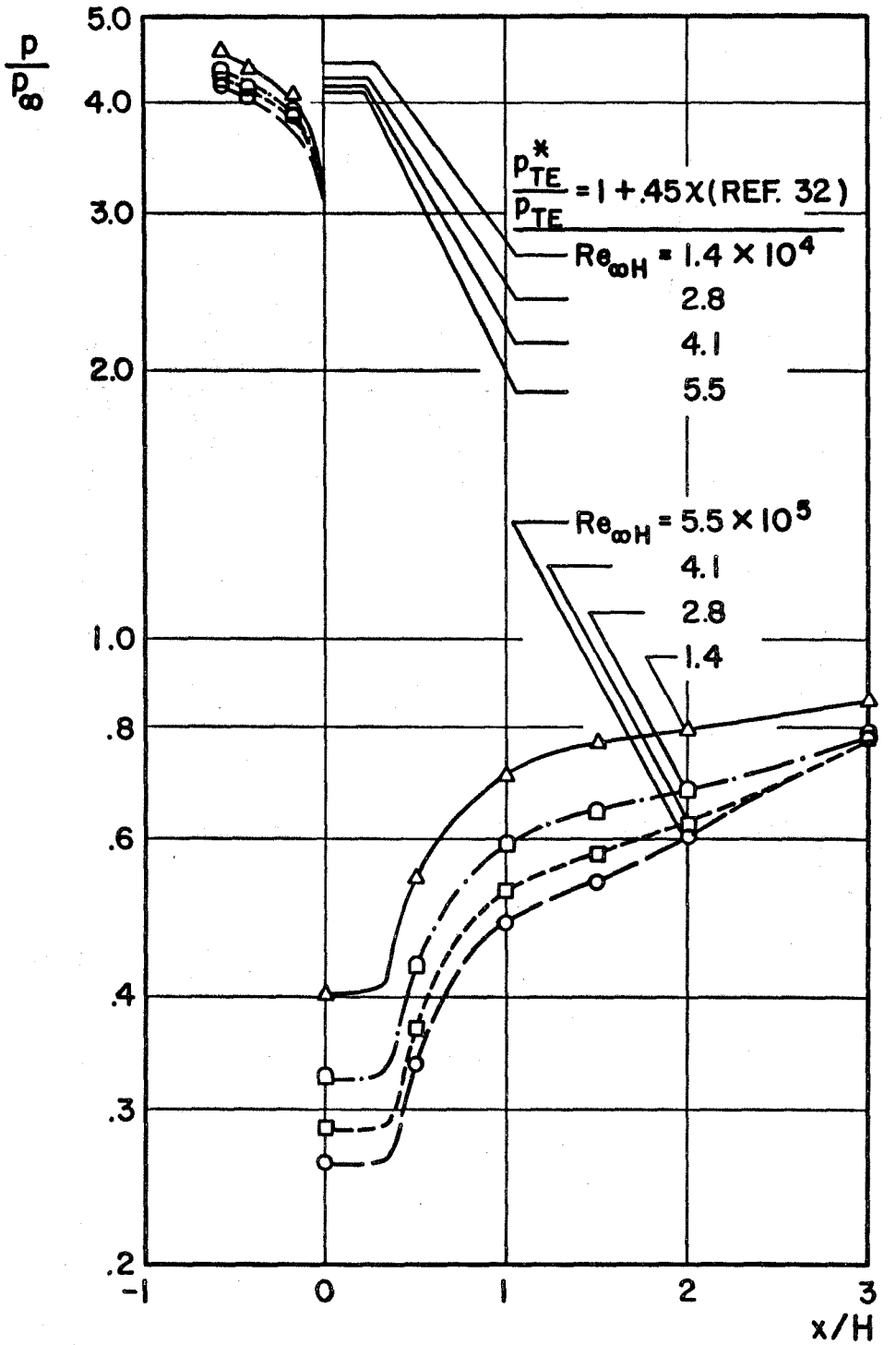

FIG.31 SURFACE PRESSURE DISTRIBUTION NEAR TRAILING EDGE OF 20°, ADIABATIC WALL WEDGE AT $M_\infty = 6$

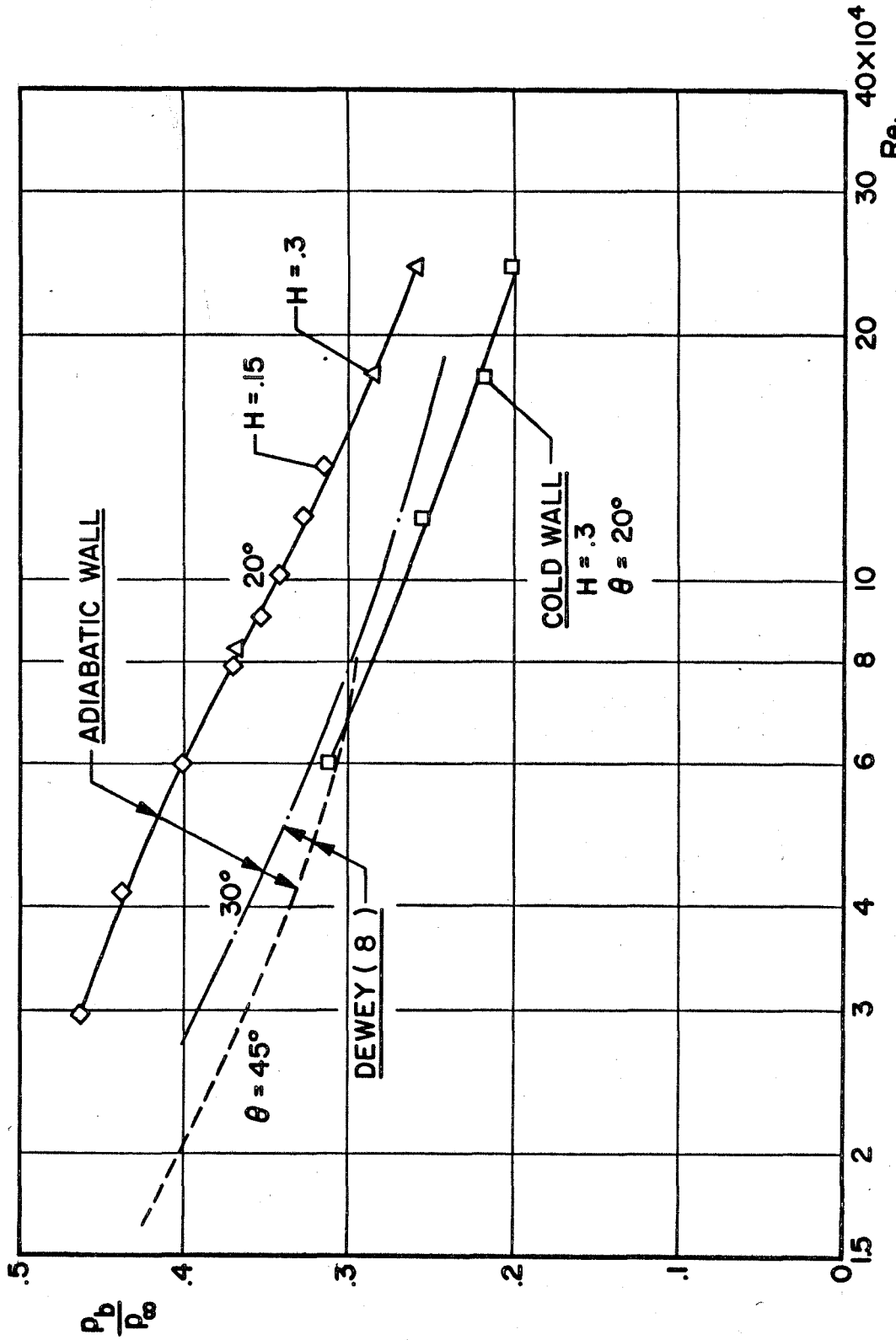

FIG.32 WEDGE BASE PRESSURE AT $M_\infty = 6$

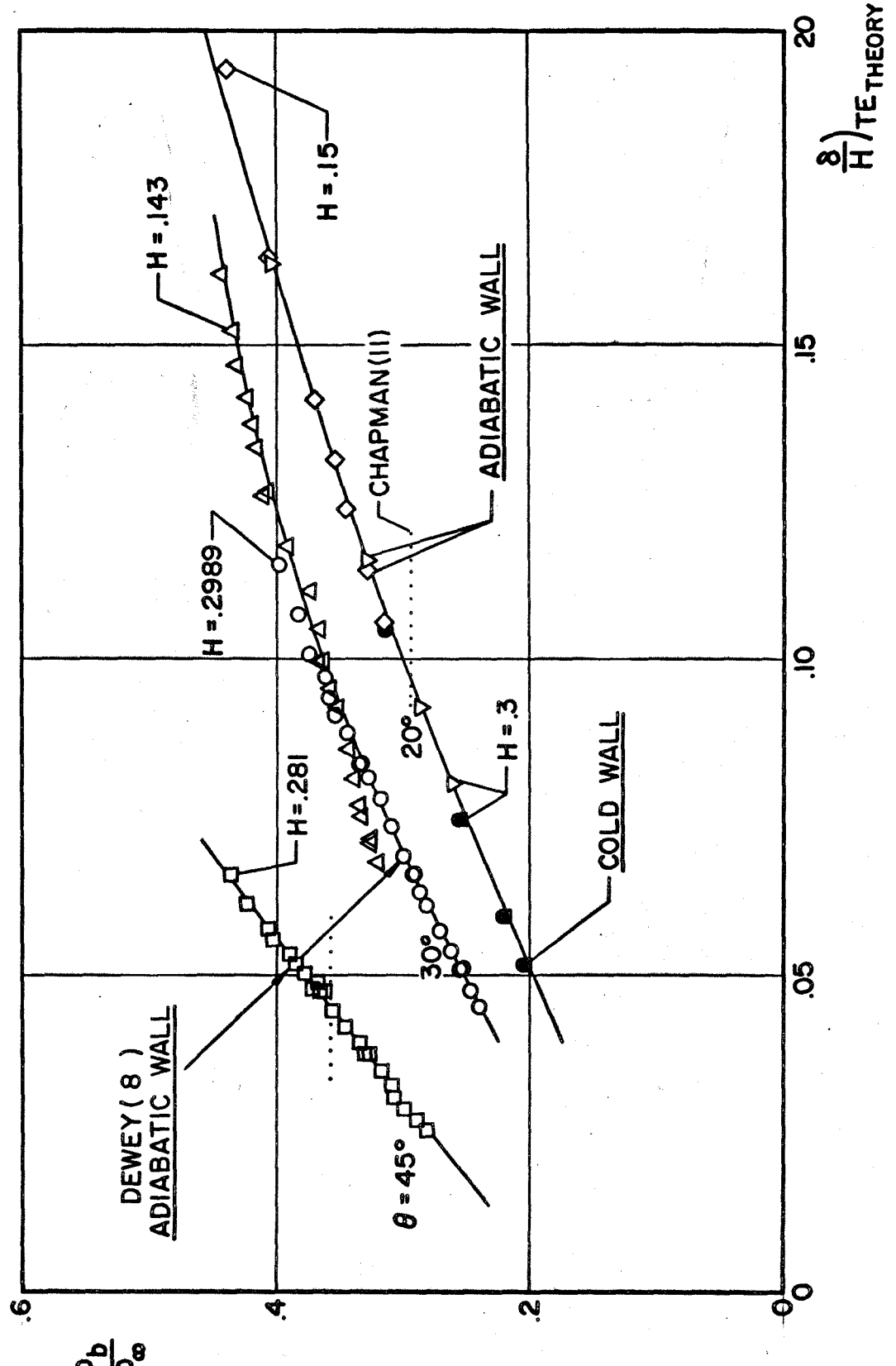

FIG. 33 CORRELATION OF WEDGE BASE PRESSURE DATA AT $M_\infty = 6$

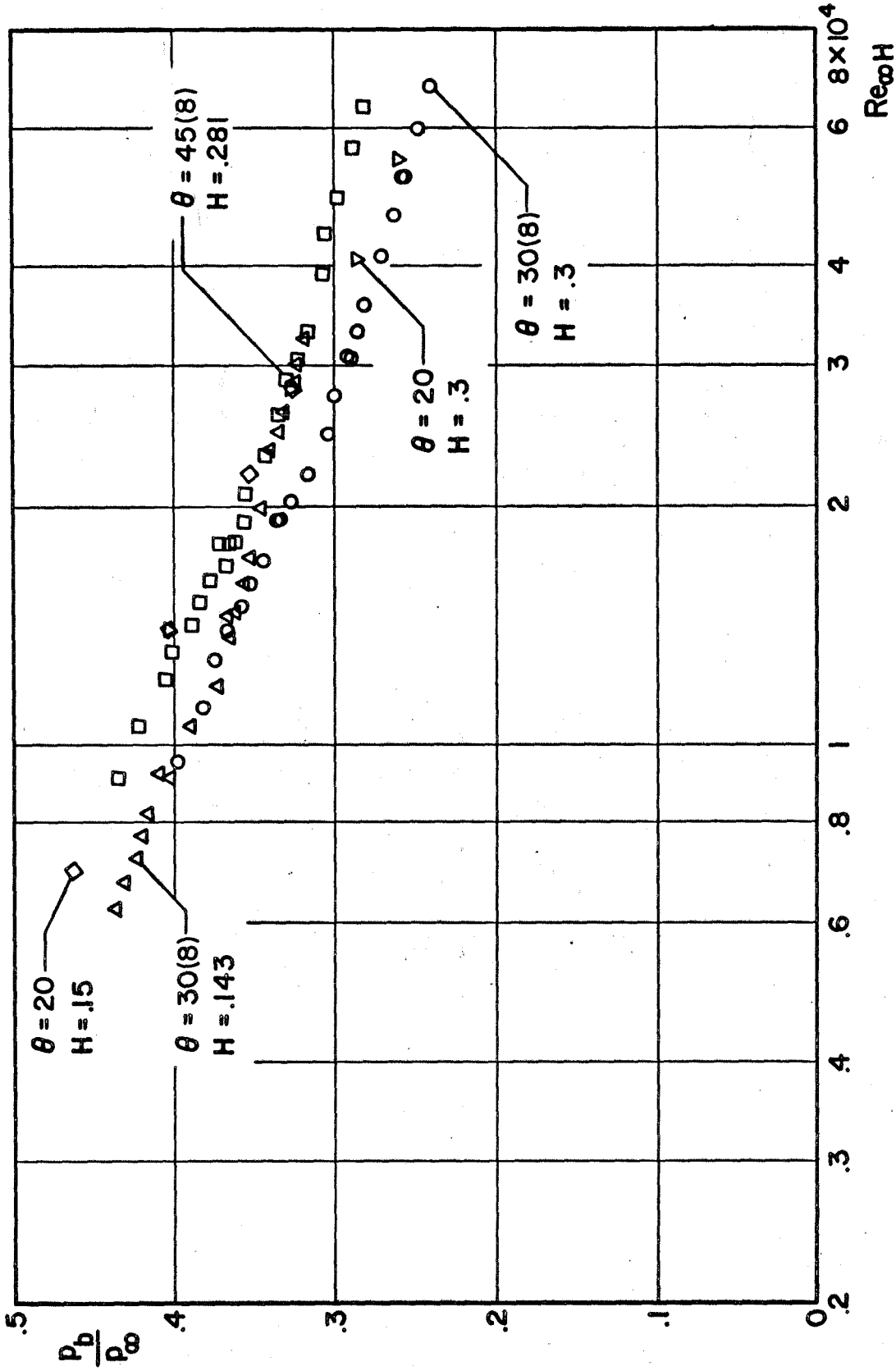

FIG.34 CORRELATION OF BASE PRESSURE DATA FOR ADIABATIC WALL WEDGES

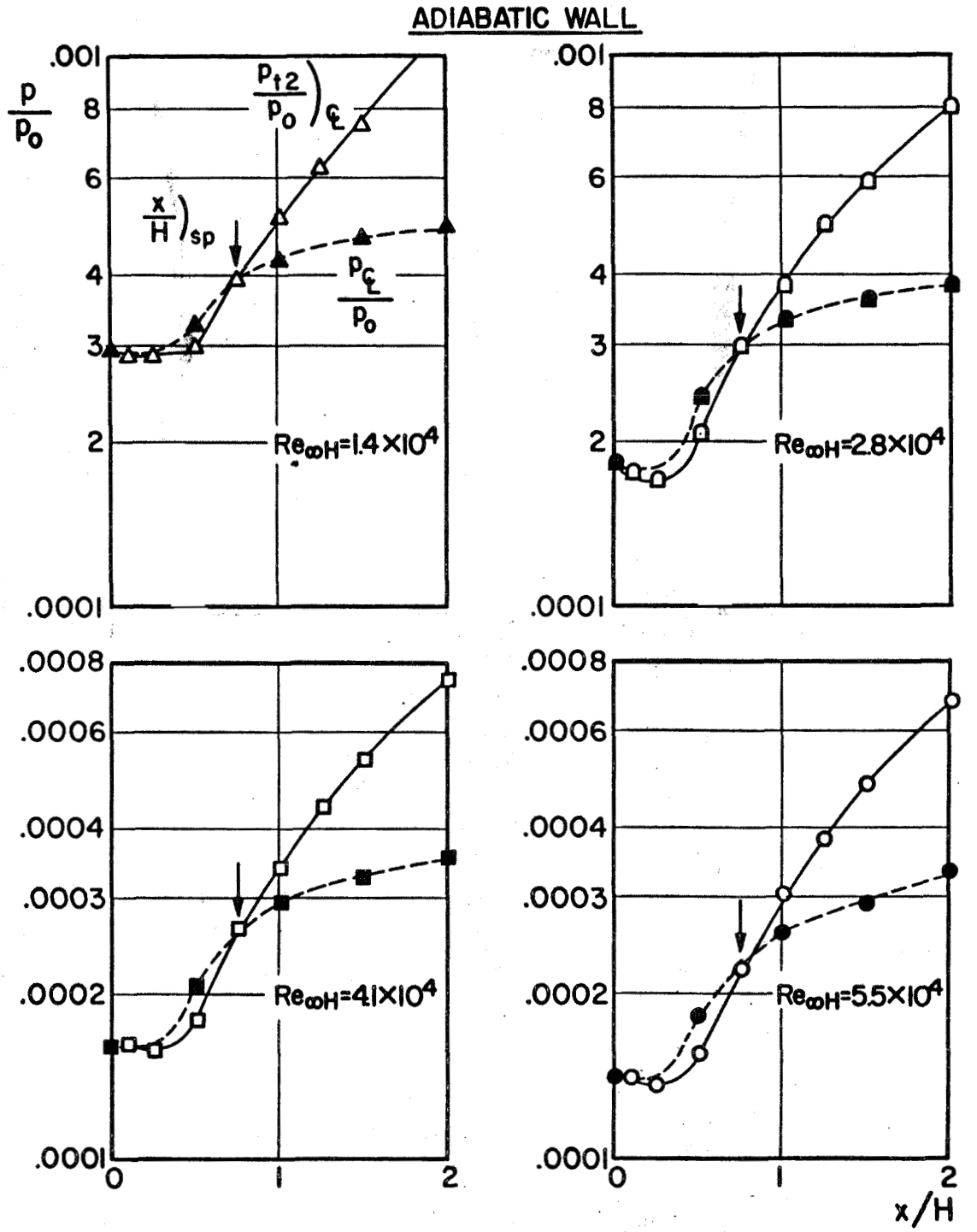

FIG. 35a REAR STAGNATION POINT LOCATION FOR NEAR WAKE BEHIND 20° WEDGE AT M_∞=6 (H=.3)

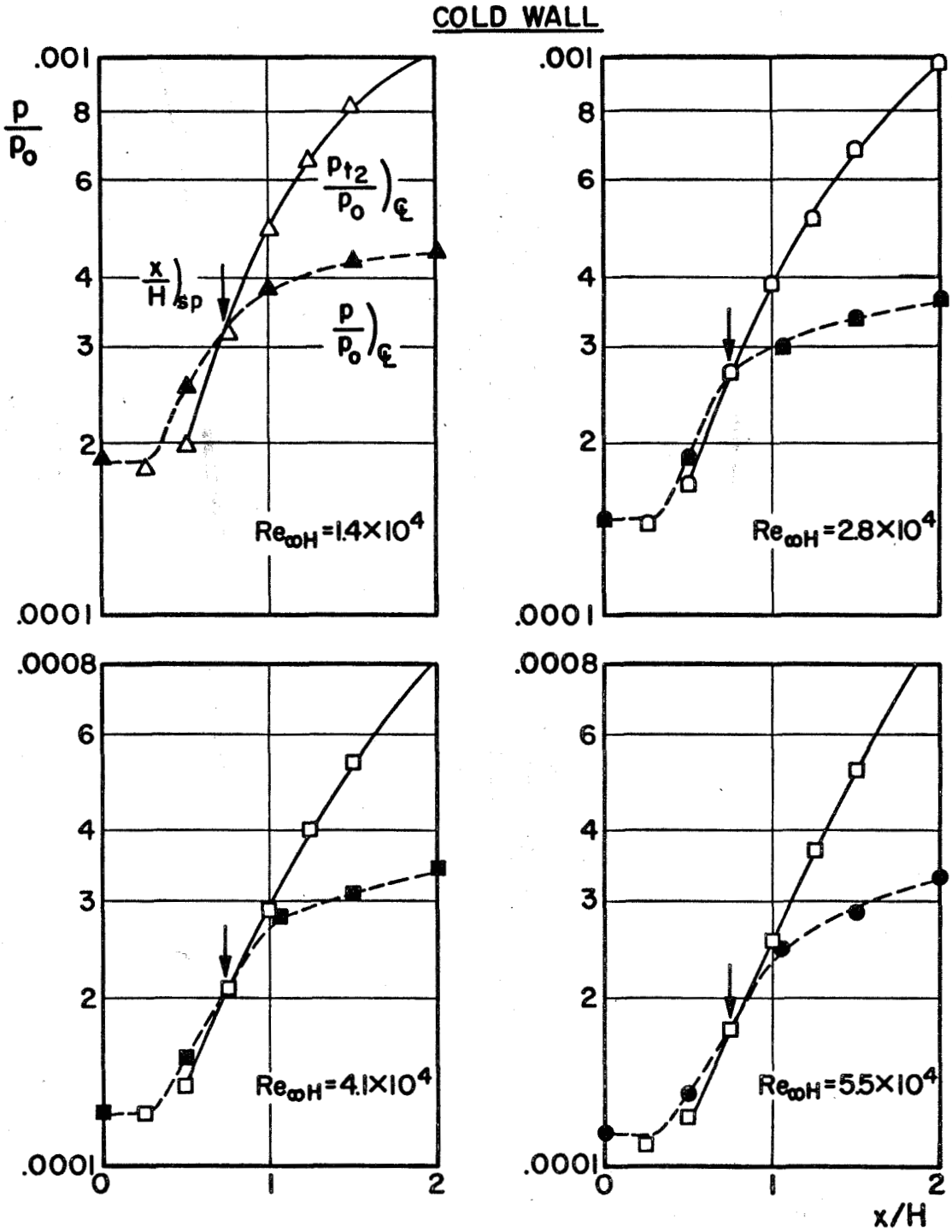

FIG.35 b REAR STAGNATION POINT LOCATION FOR NEAR WAKE BEHIND 20° WEDGE AT M_∞=6 (H=.3)

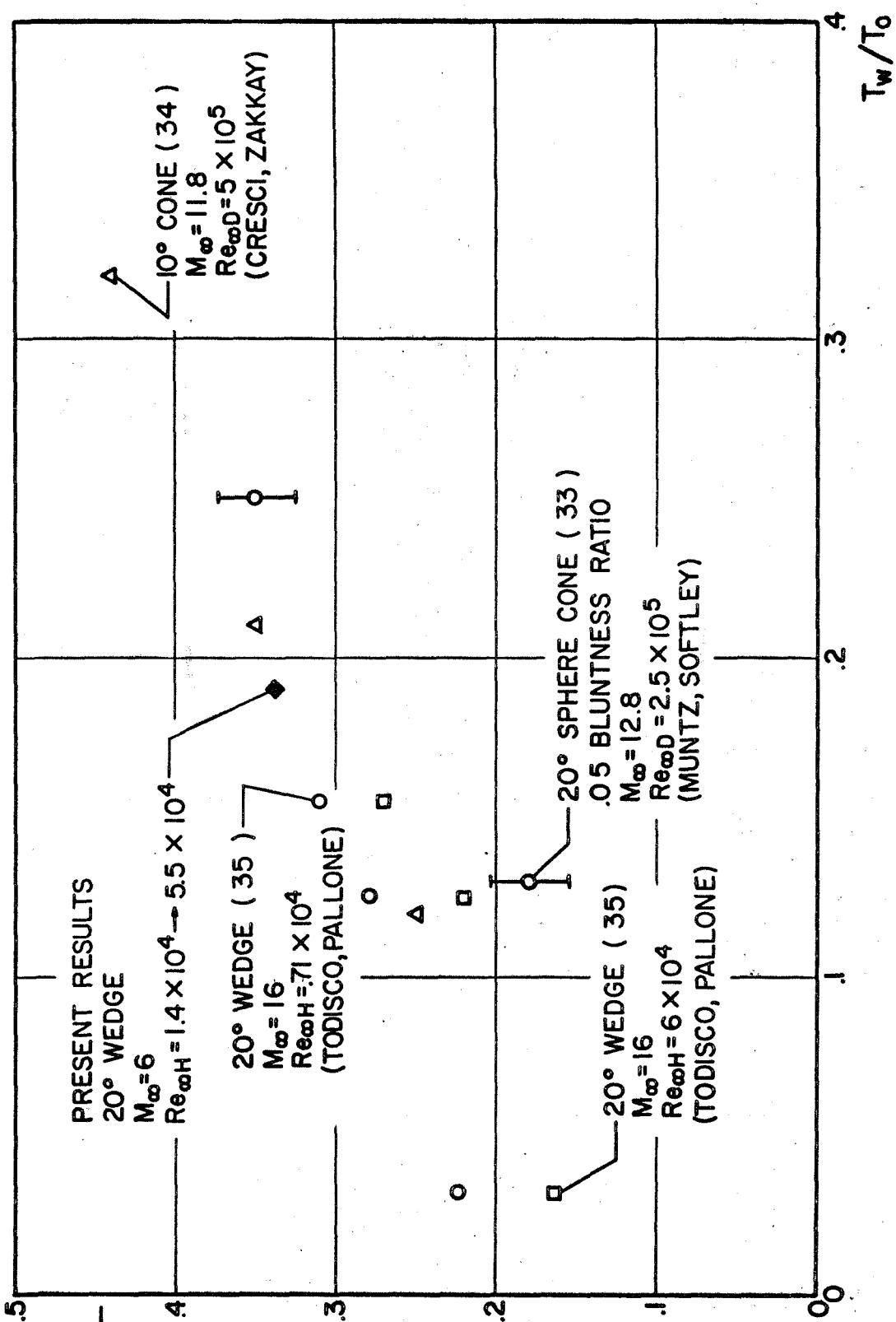

FIG.36 VARIATION OF REAR STAGNATION POINT TEMPERATURE WITH WALL TEMPERATURE RATIO

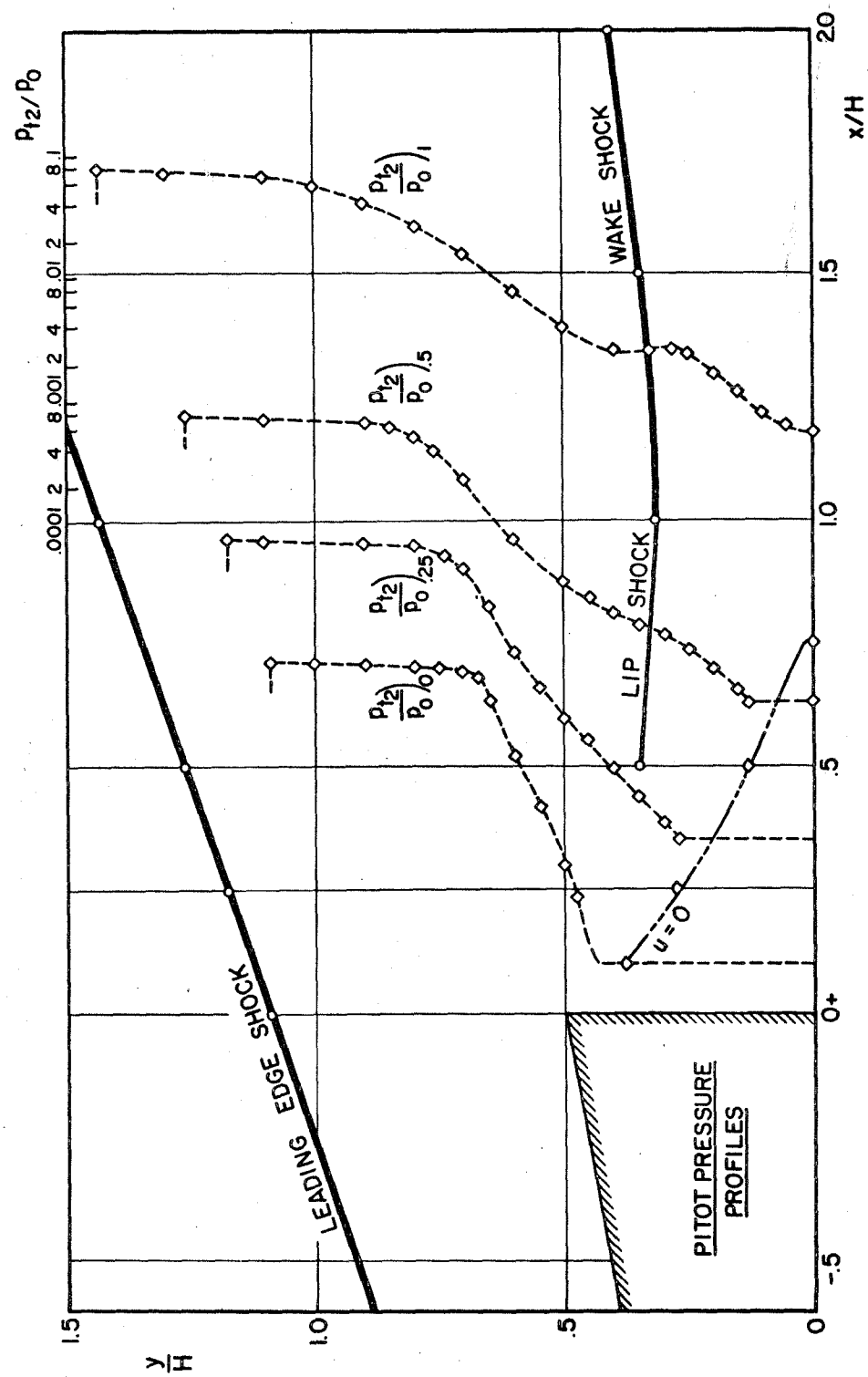

FIG. 37a TYPICAL SHEAR LAYER PROFILES FOR NEAR WAKE BEHIND 20°, ADIABATIC WALL WEDGE AT $M_\infty = 6$ AND $Re_{\infty H} = 1.4 \times 10^4 (H = .3)$

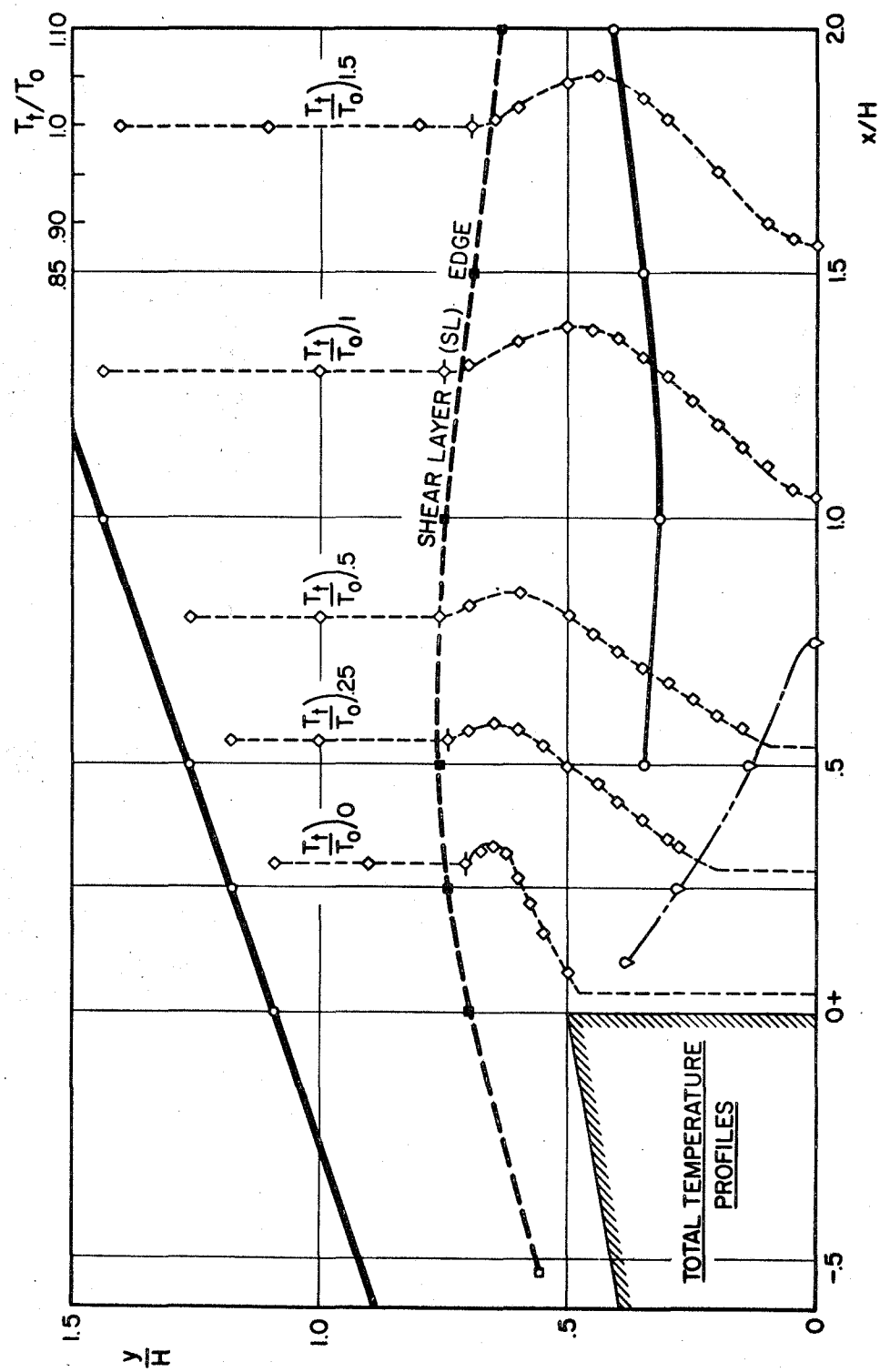

FIG. 37b TYPICAL SHEAR LAYER PROFILES FOR NEAR WAKE BEHIND 20°; ADIABATIC WALL WEDGE AT $M_\infty = 6$ & $Re_{\infty H} = 1.4 \times 10^4$ (H = .3)

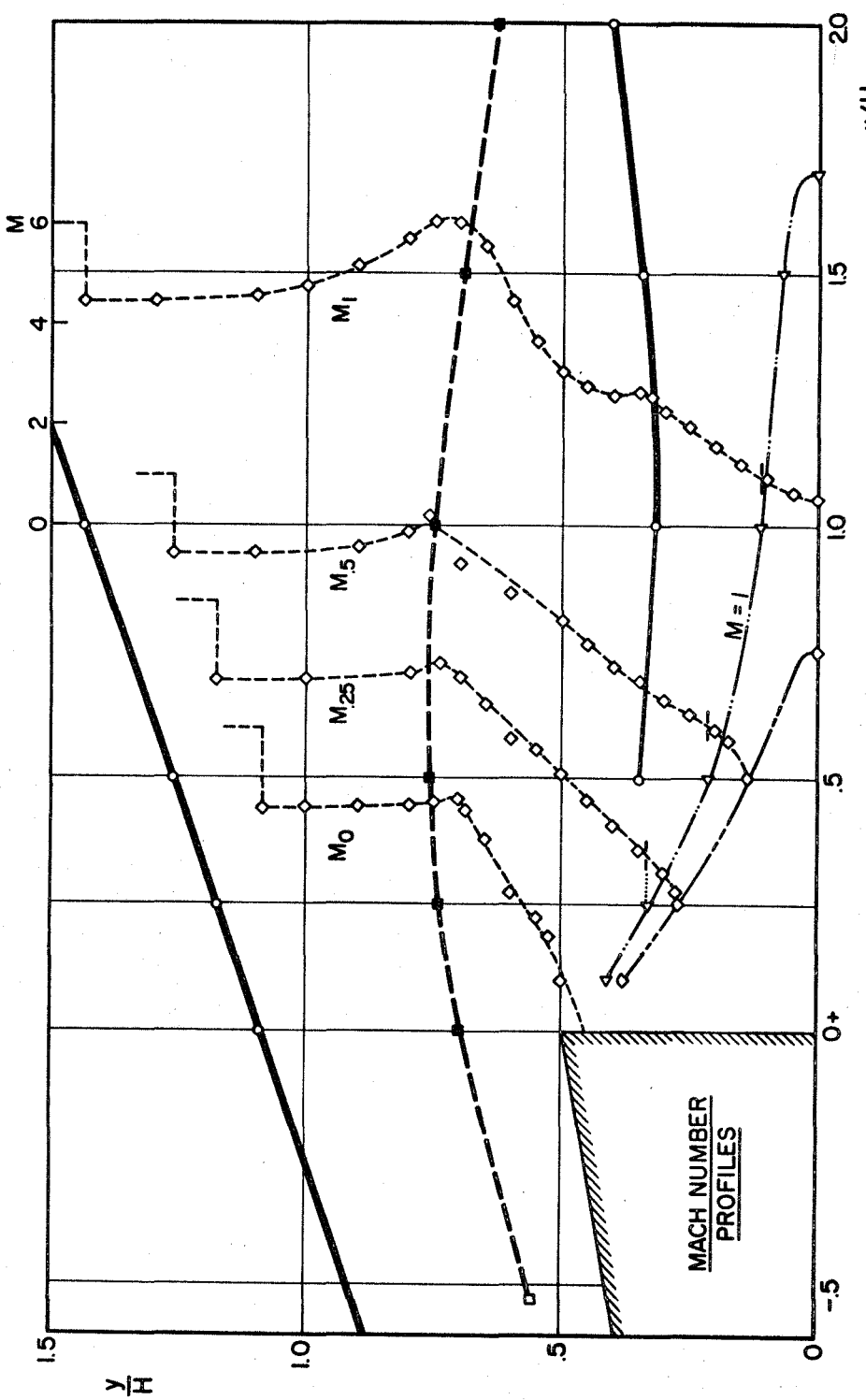

FIG. 37c TYPICAL SHEAR LAYER PROFILES FOR NEAR WAKE BEHIND 20°; ADIABATIC WALL WEDGE AT $M_\infty = 6$ AND $Re_{\infty H} = 1.4 \times 10^4 (H = .3)$

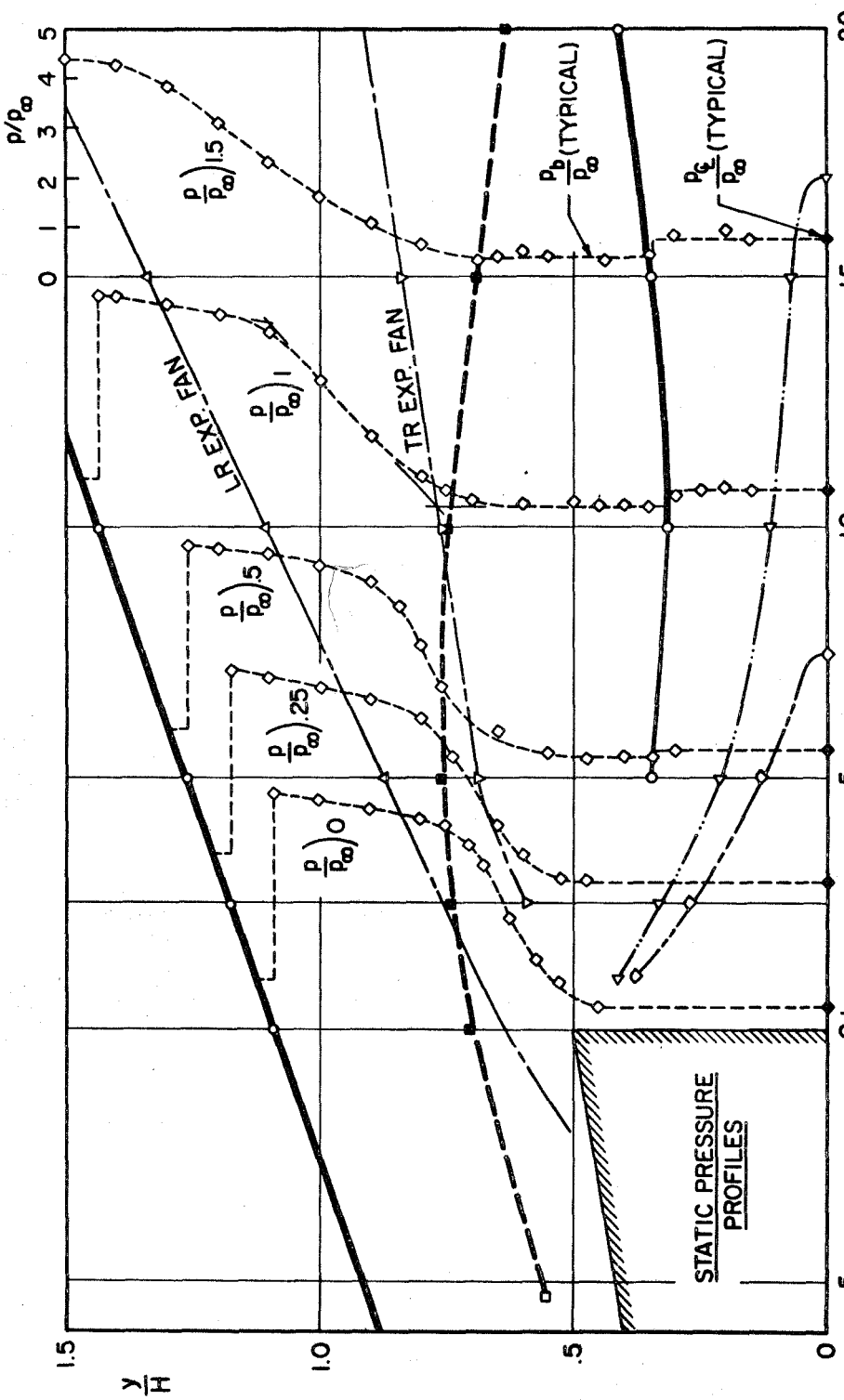

FIG. 37d TYPICAL SHEAR LAYER PROFILES FOR NEAR WAKE BEHIND 20°; ADIABATIC WALL WEDGE AT $M_\infty = 6$ & $Re_{\infty H} = 1.4 \times 10^4$ (H = .3)

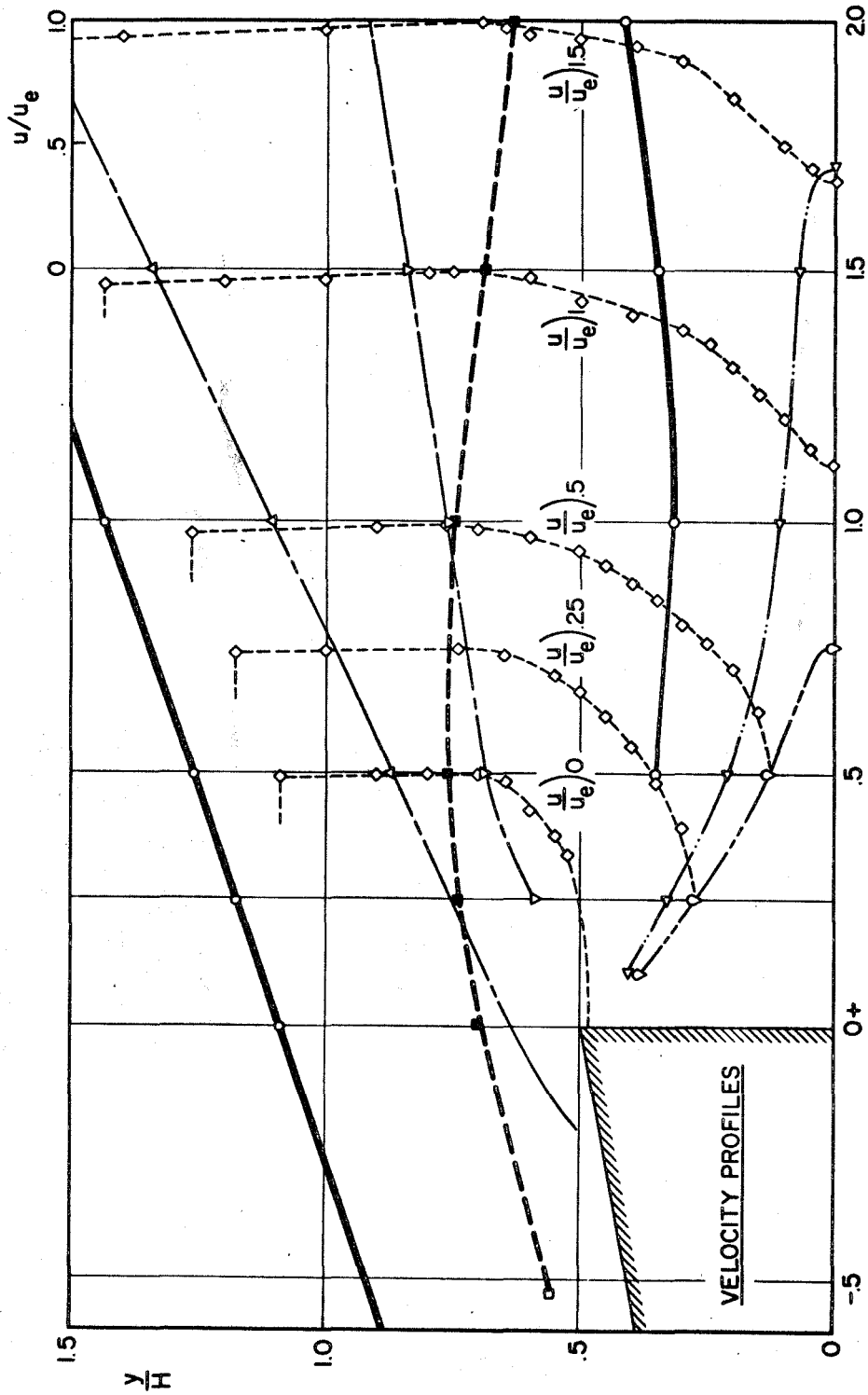

FIG. 37e TYPICAL SHEAR LAYER PROFILES FOR NEAR WAKE BEHIND 20°; ADIABATIC WALL WEDGE AT $M_\infty = 6$ & $Re_{\infty H} = 1.4 \times 10^4$ (H = .3)

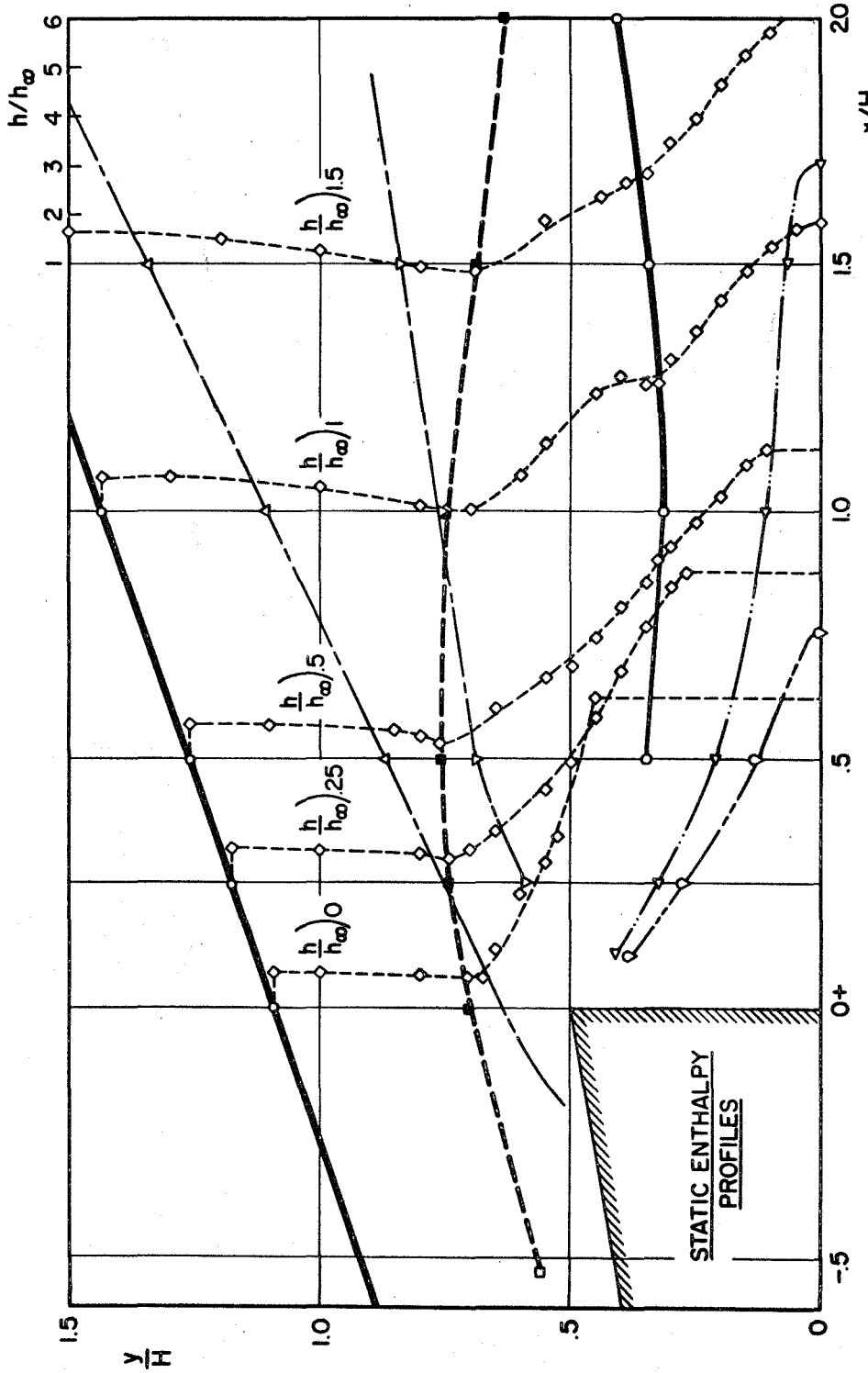

FIG. 37f TYPICAL SHEAR LAYER PROFILES FOR NEAR WAKE BEHIND 20°, ADIABATIC WALL WEDGE AT $M_\infty = 6$ & $Re_{\infty H} = 1.4 \times 10^4$ (H = .3)

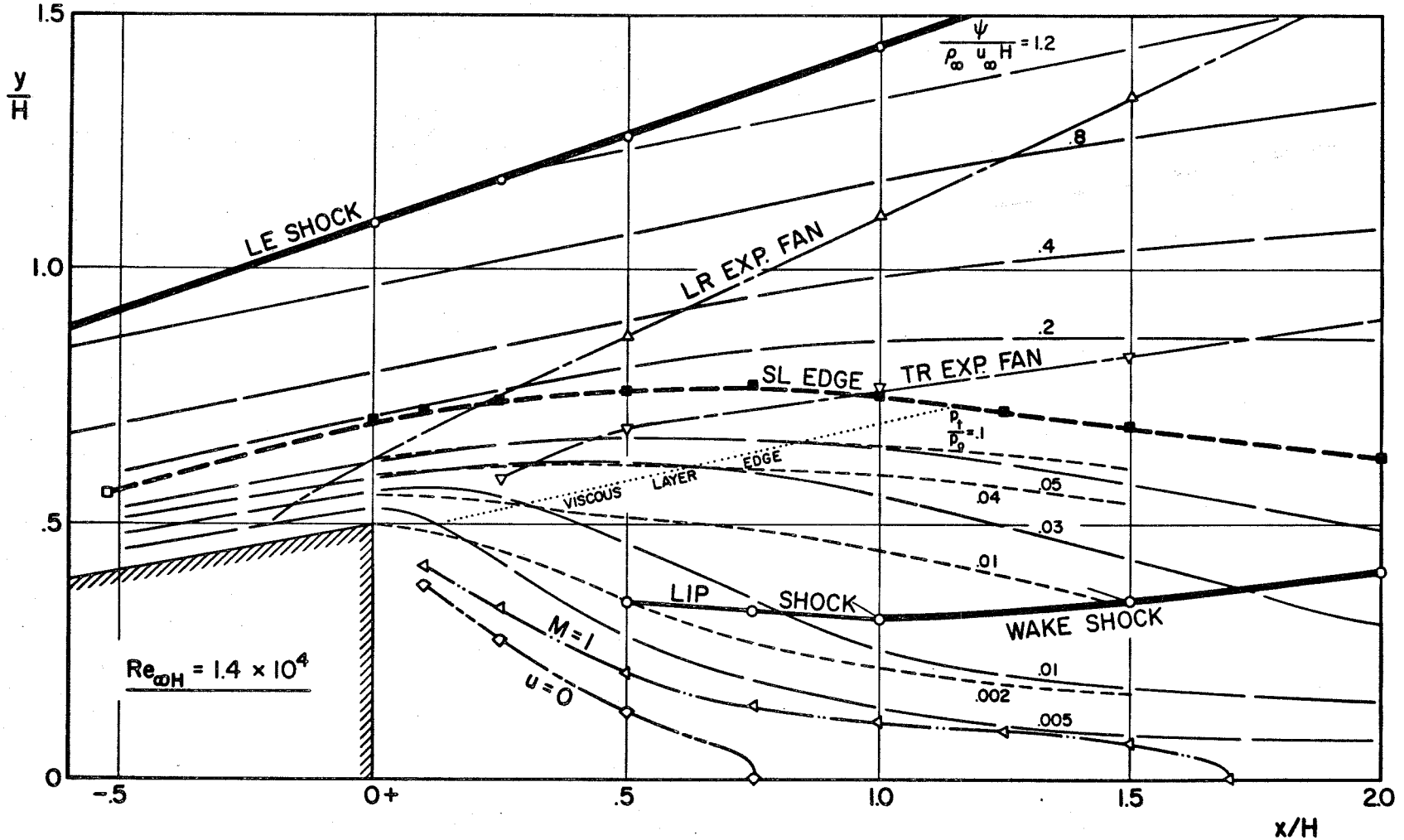

FIG. 38a FLOW FIELD MAPPING OF NEAR WAKE BEHIND 20°, ADIABATIC WALL WEDGE AT $M_\infty = 6$ (H = .3)

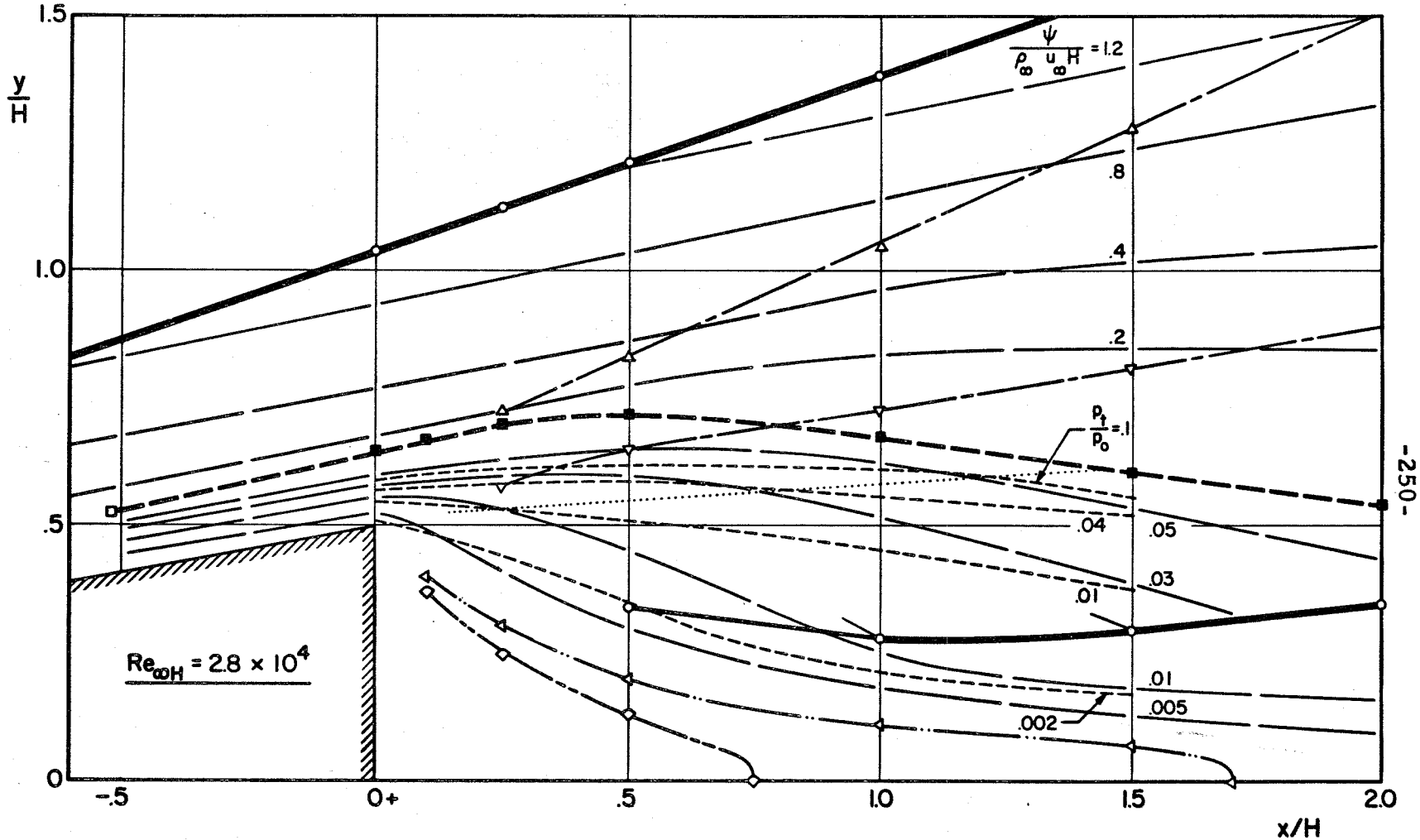

FIG.38 b FLOW FIELD MAPPING OF NEAR WAKE BEHIND 20°, ADIABATIC WALL WEDGE AT $M_\infty = 6$ (H = .3)

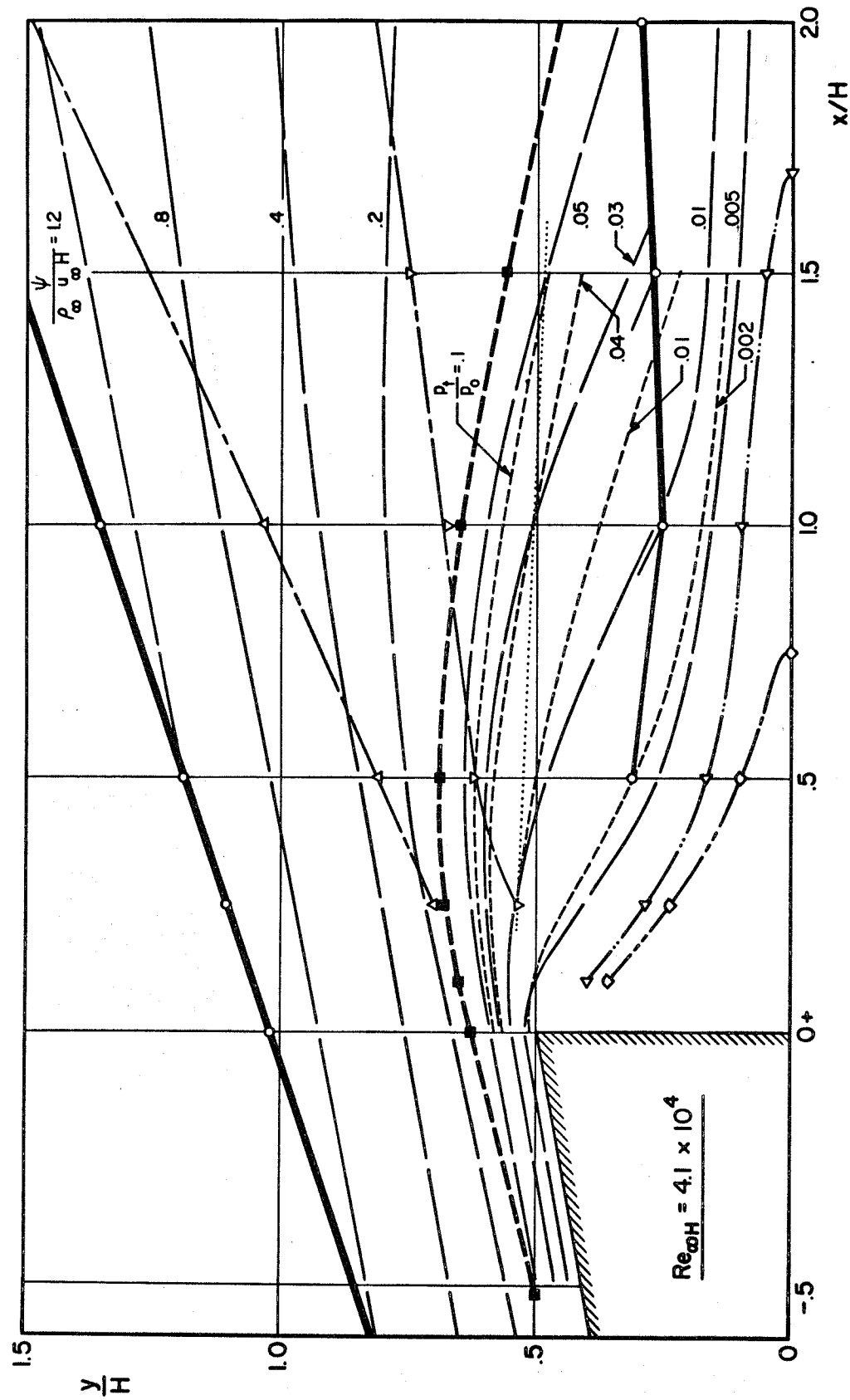

FIG. 38c FLOW FIELD MAPPING OF NEAR WAKE BEHIND 20°; ADIABATIC WALL WEDGE AT $M_\infty = 6$ (H = .3)

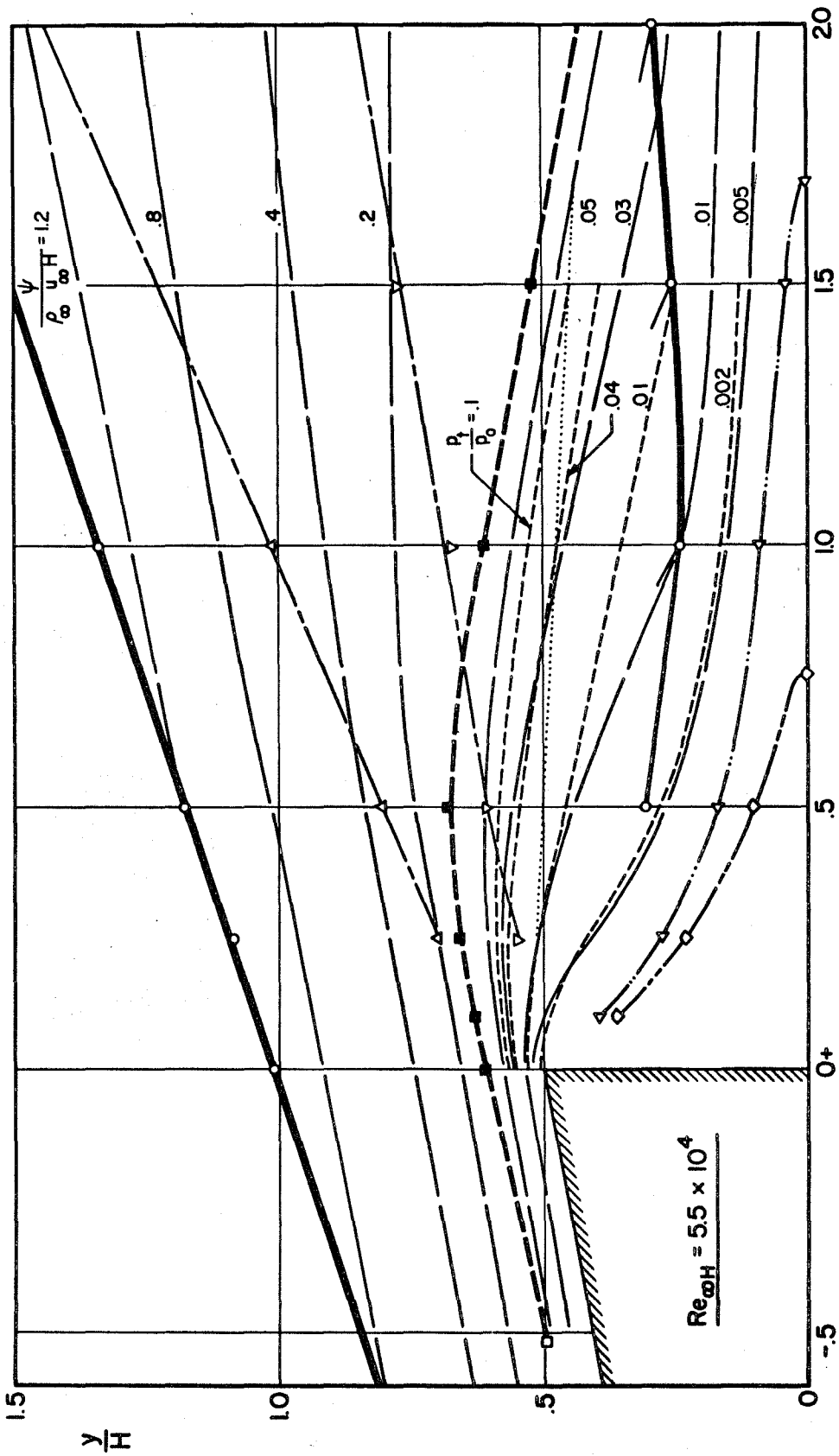

FIG.38d-1 FLOW FIELD MAPPING OF NEAR WAKE BEHIND 20°, ADIABATIC WALL WEDGE AT $M_\infty = 6$ (H=3)

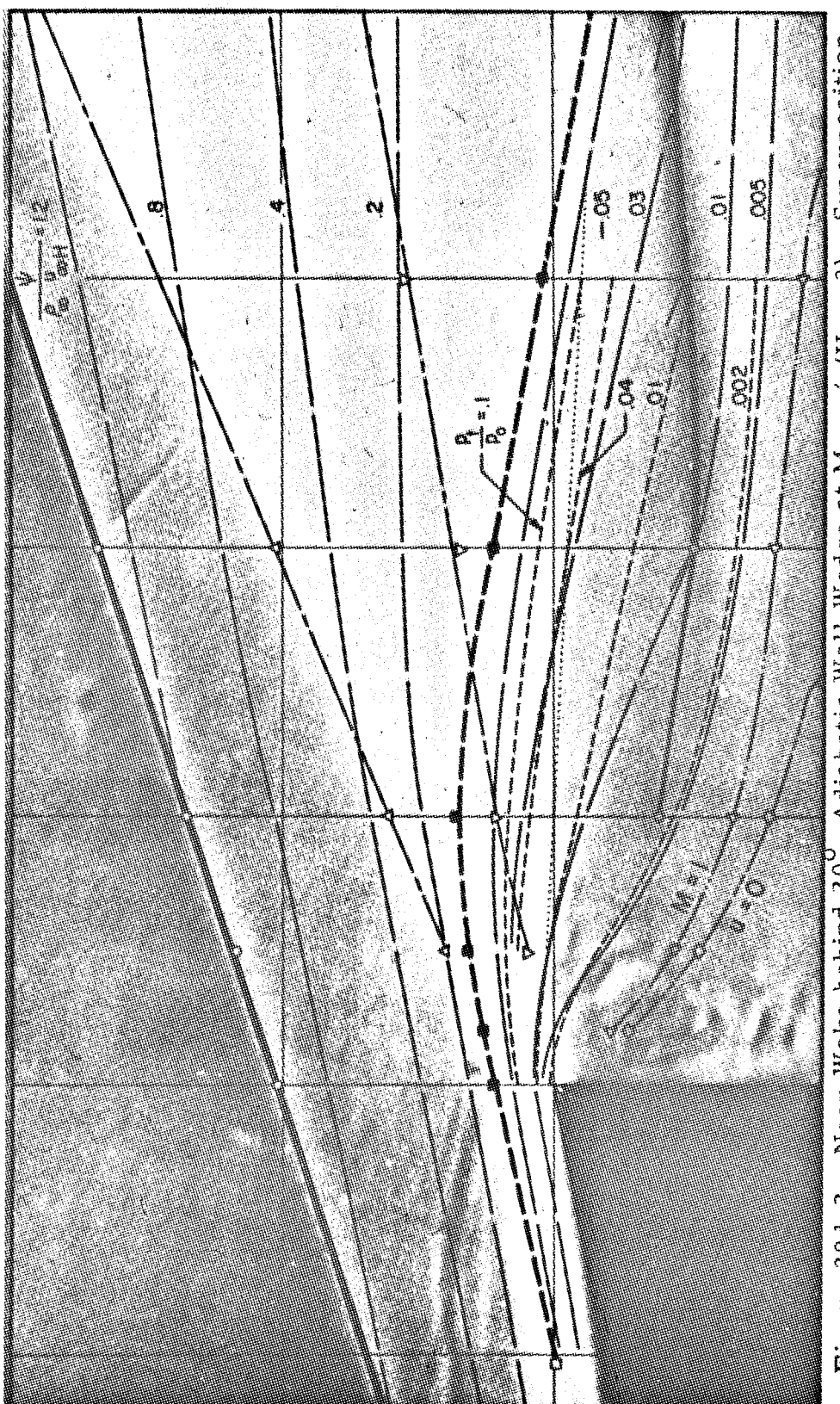

Figure 38d-2. Near Wake behind 20°, Adiabatic Wall Wedge at $M_\infty = 6$ (H = .3) - Superposition of Flow Field Mapping ($Re_{\infty H} = 5.5 \times 10^4$) and Schlieren Photograph ($Re_{\infty H} = 5.2 \times 10^4$)

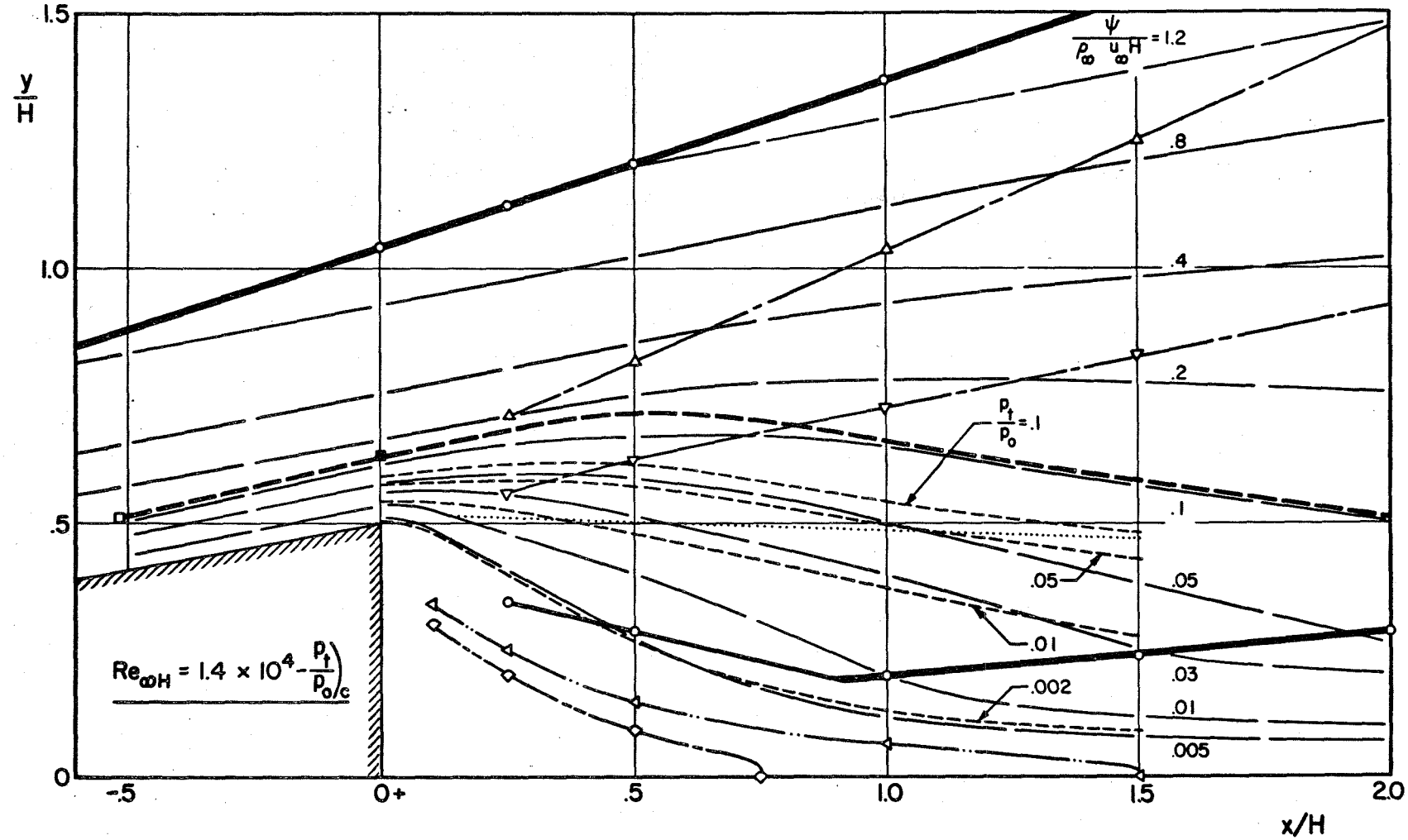

FIG. 39a-1 FLOW FIELD MAPPING OF NEAR WAKE BEHIND 20°, COLD WALL WEDGE AT $M_\infty = 6$ ($H = .3$, $T_w/T_o = .19$)

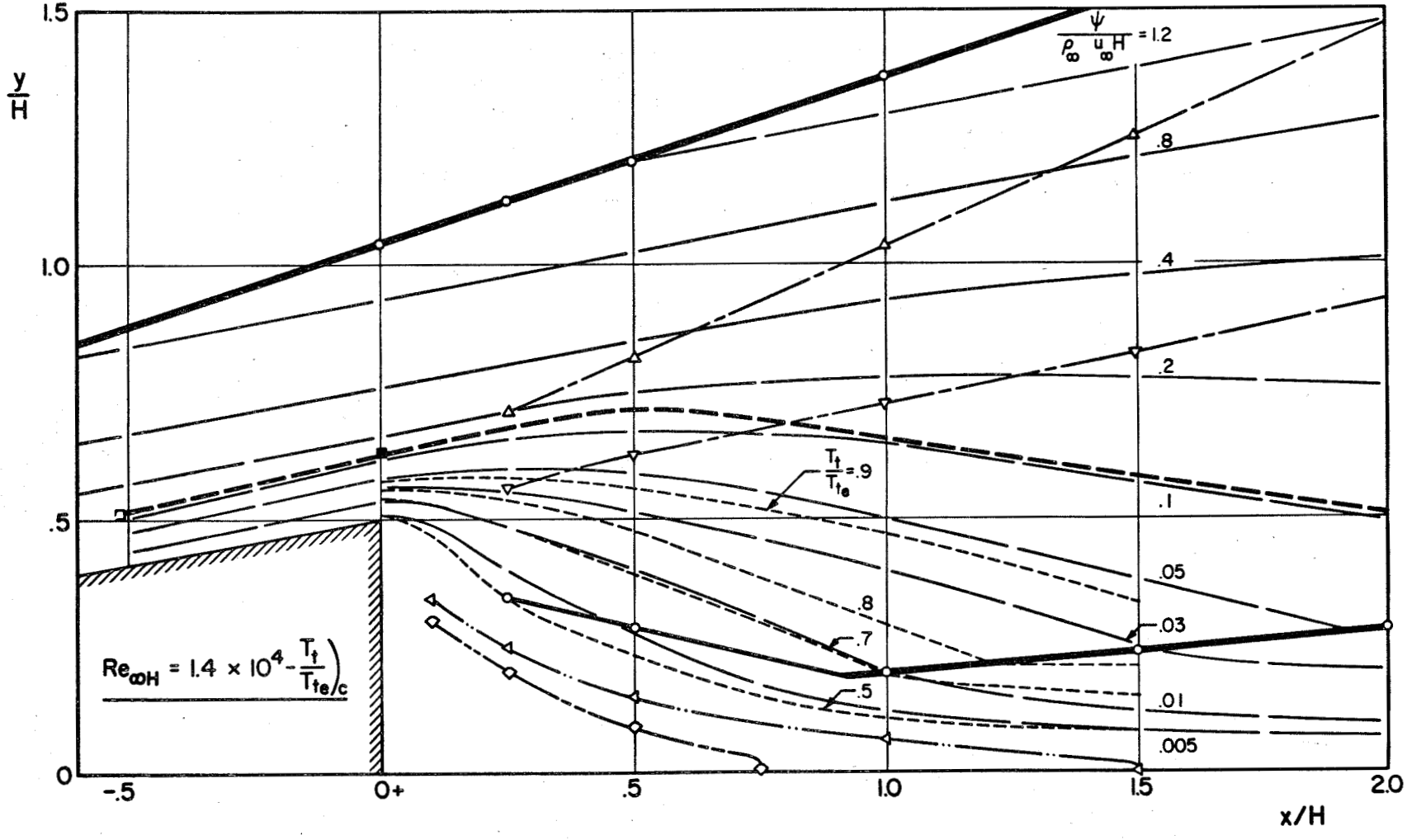

FIG. 39a-2 FLOW FIELD MAPPING OF NEAR WAKE BEHIND 20°, COLD WALL WEDGE AT $M_\infty = 6$ ($H = .3$, $T_w / T_0 = .19$)

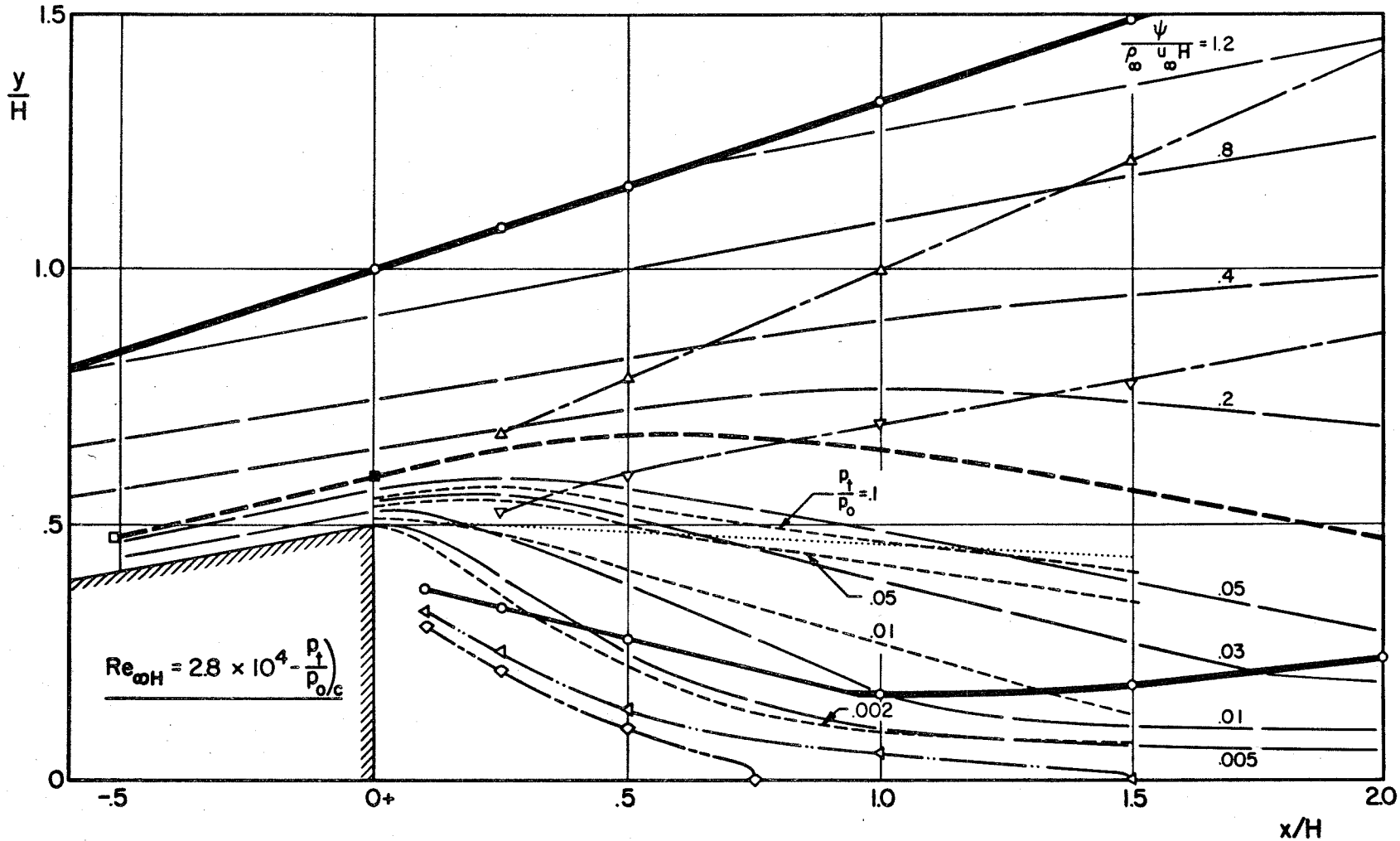

FIG.39b-1 FLOW FIELD MAPPING OF NEAR WAKE BEHIND 20°, COLD WALL WEDGE AT $M_\infty = 6$ ($H = .3$, $T_w/T_0 = .19$)

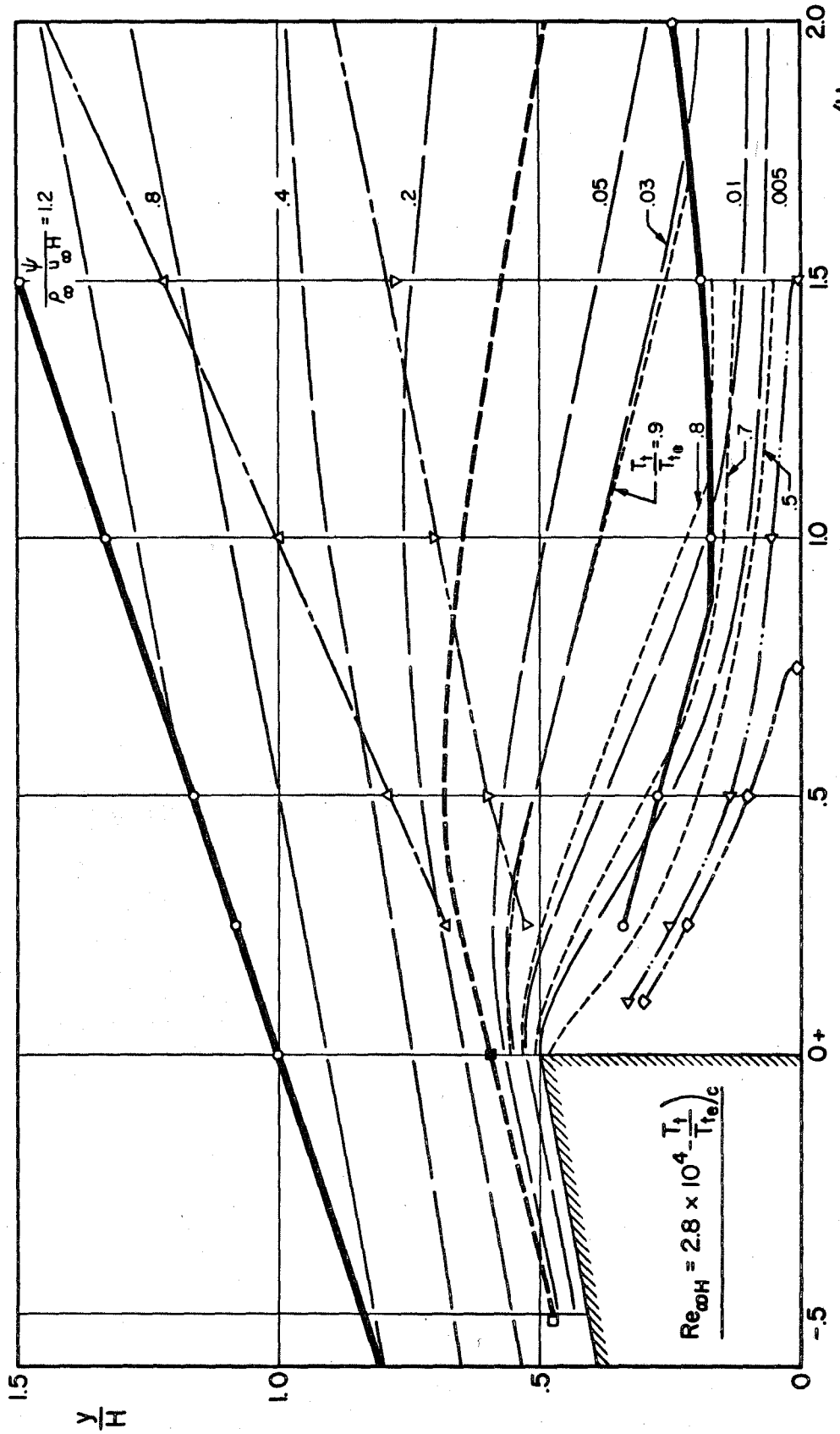

FIG. 39b-2 FLOW FIELD MAPPING OF NEAR WAKE BEHIND 20°; COLD WALL WEDGE AT $M_\infty = 6$ ($H = .3$, $T_w/T_0 = .19$)

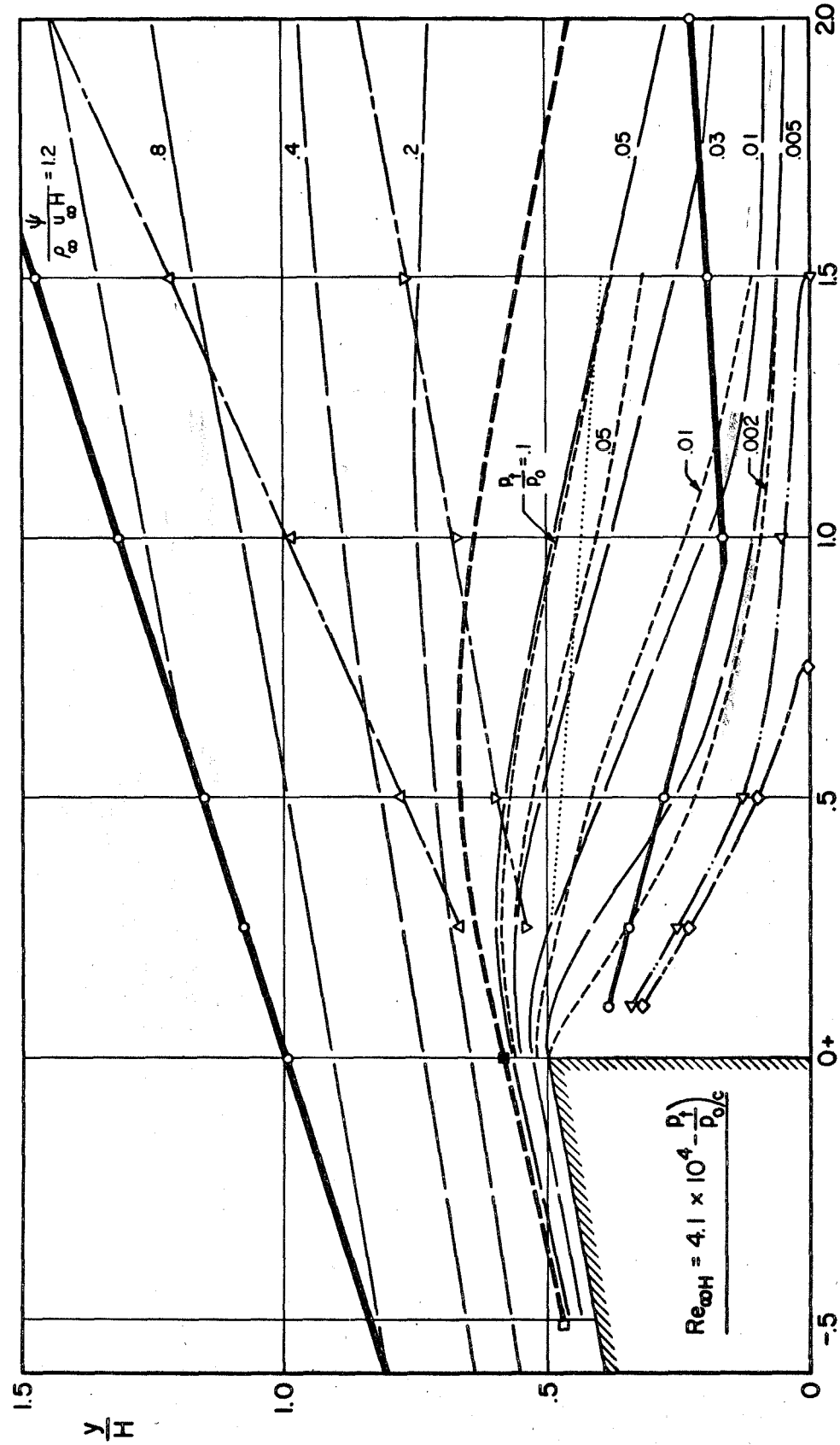

FIG. 39c-1 FLOW FIELD MAPPING OF NEAR WAKE BEHIND 20°; COLD WALL WEDGE AT $M_\infty = 6$ ($H = .3$, $T_w / T_0 = .19$)

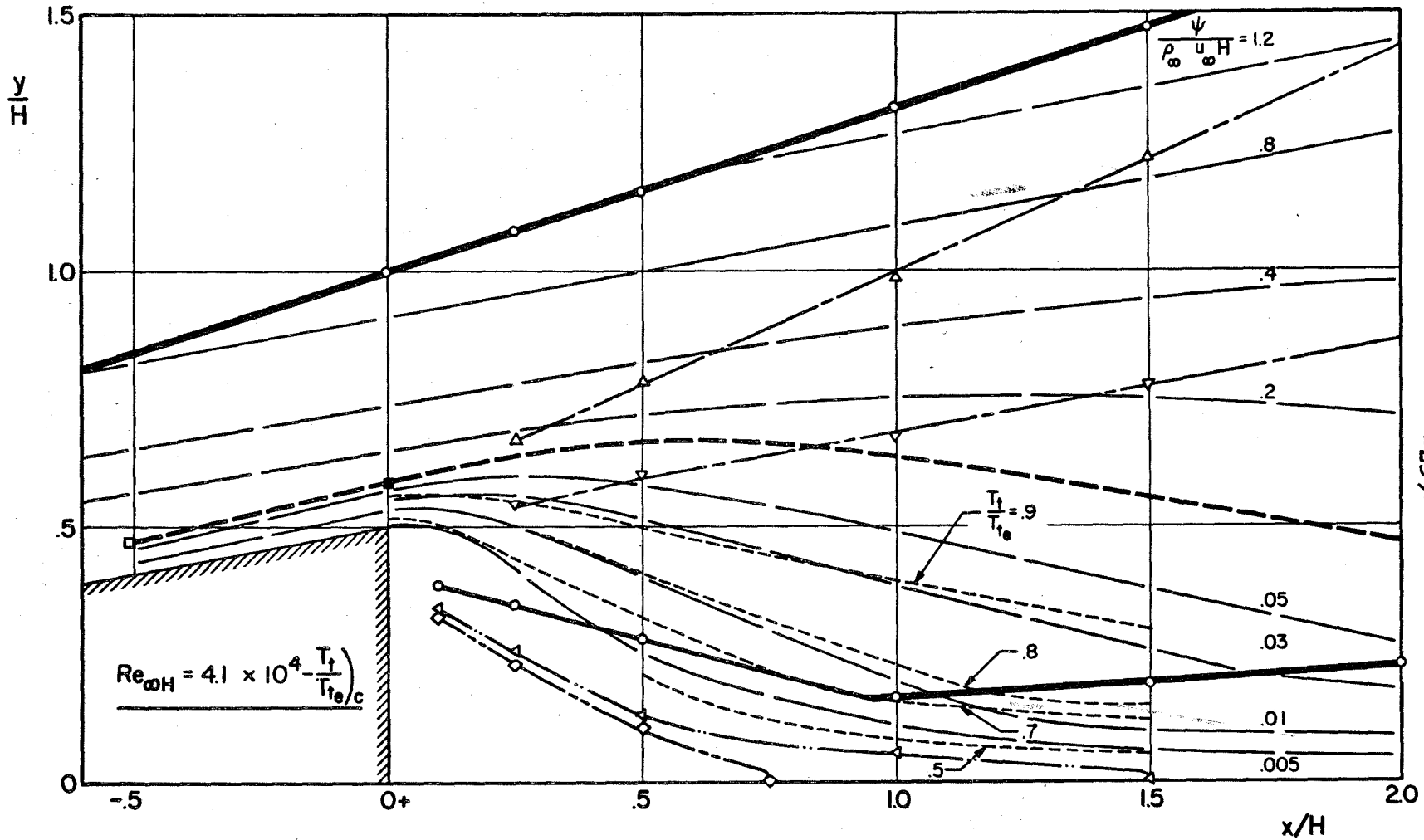

FIG. 39c-2 FLOW FIELD MAPPING OF NEAR WAKE BEHIND 20°, COLD WALL WEDGE AT $M_\infty = 6$ ($H = .3$, $T_w / T_0 = .19$)

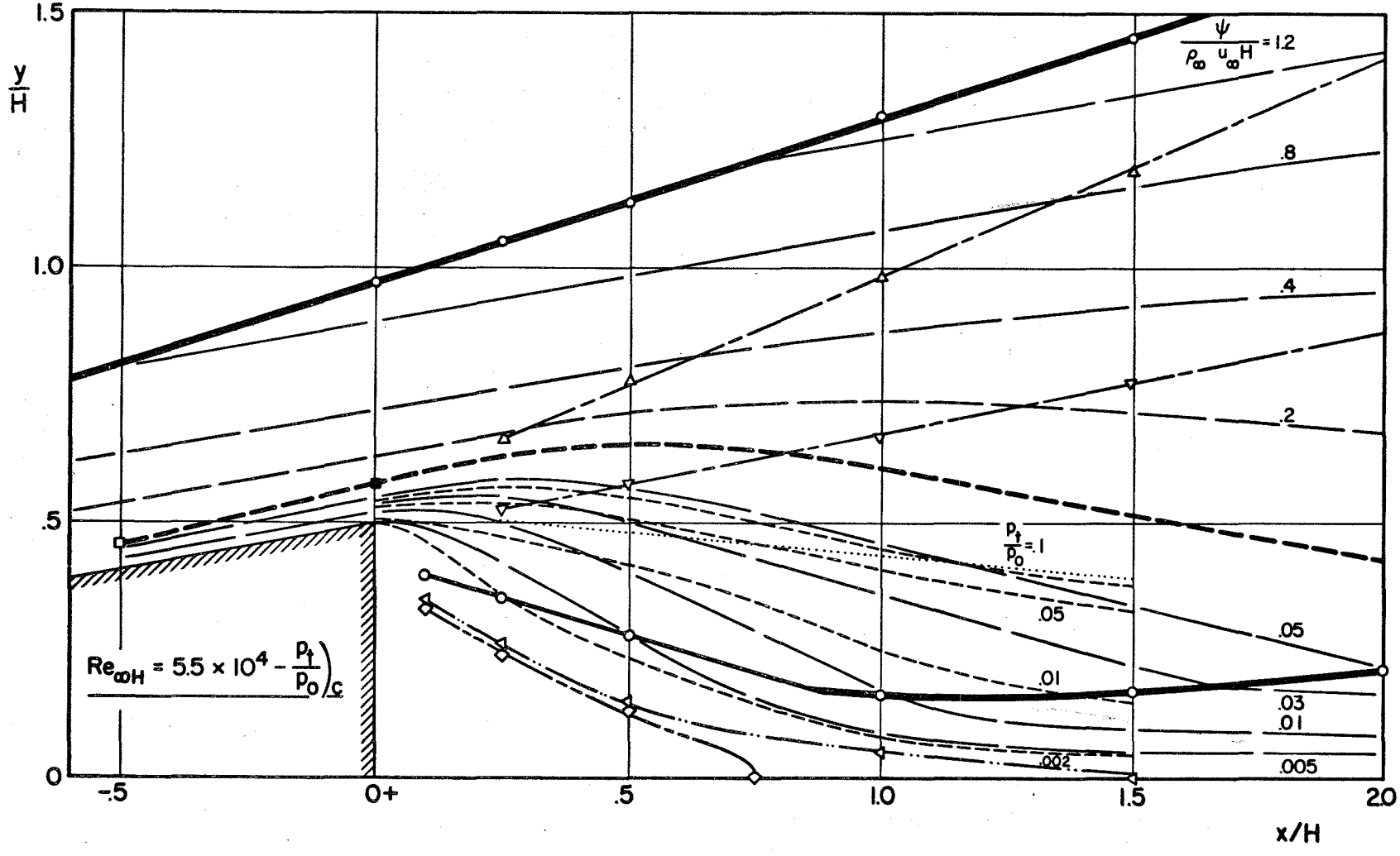

FIG. 39d-1 FLOW FIELD MAPPING OF NEAR WAKE BEHIND 20°, COLD WALL WEDGE AT $M_\infty = 6$ ($H = .3$, $\frac{T_w}{T_0} = .19$)

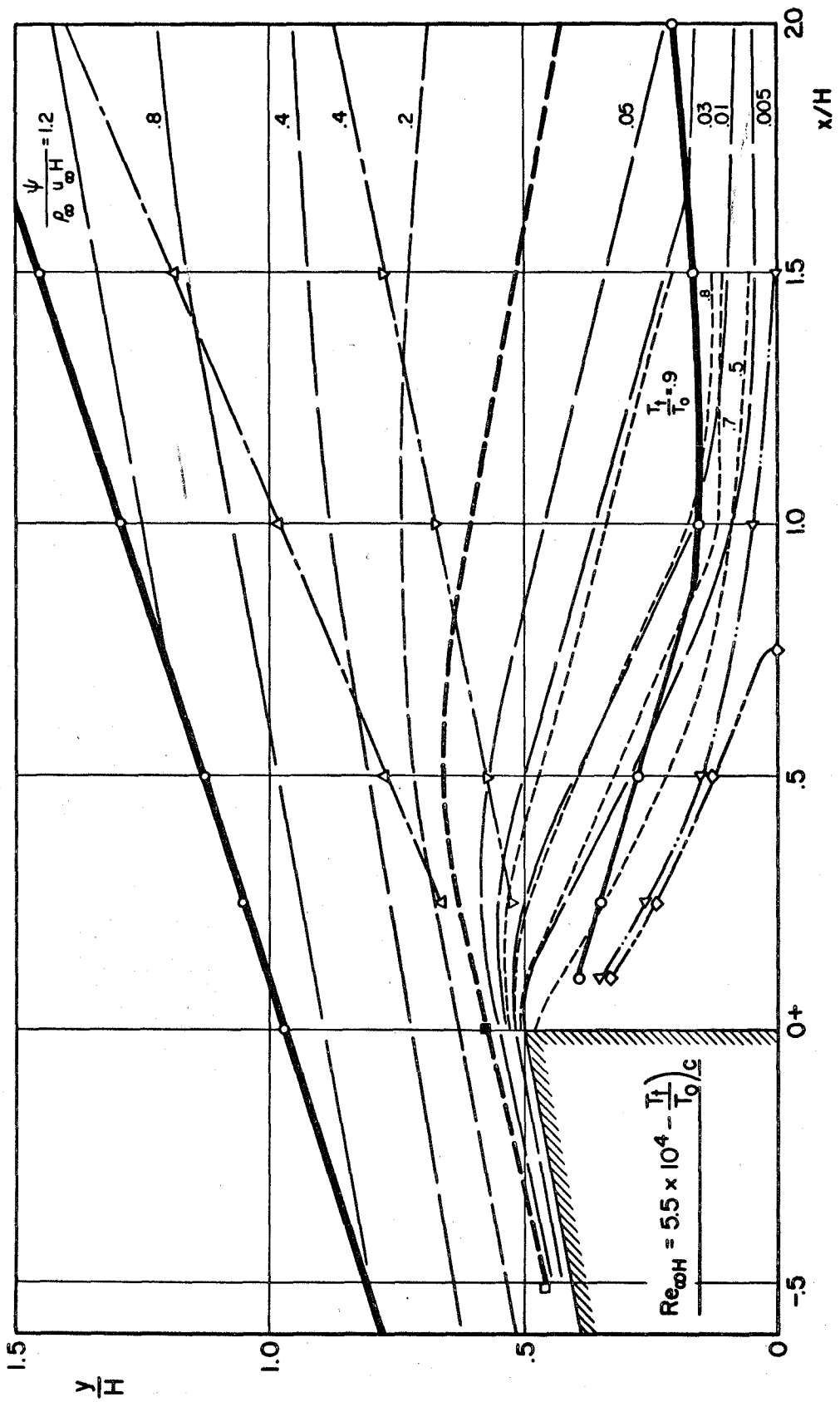

FIG. 39d-2 FLOW FIELD MAPPING OF NEAR WAKE BEHIND 20°, COLD WALL WEDGE AT $M_\infty = 6$ ($H = .3$, $\frac{T_w}{T_o} = .19$)

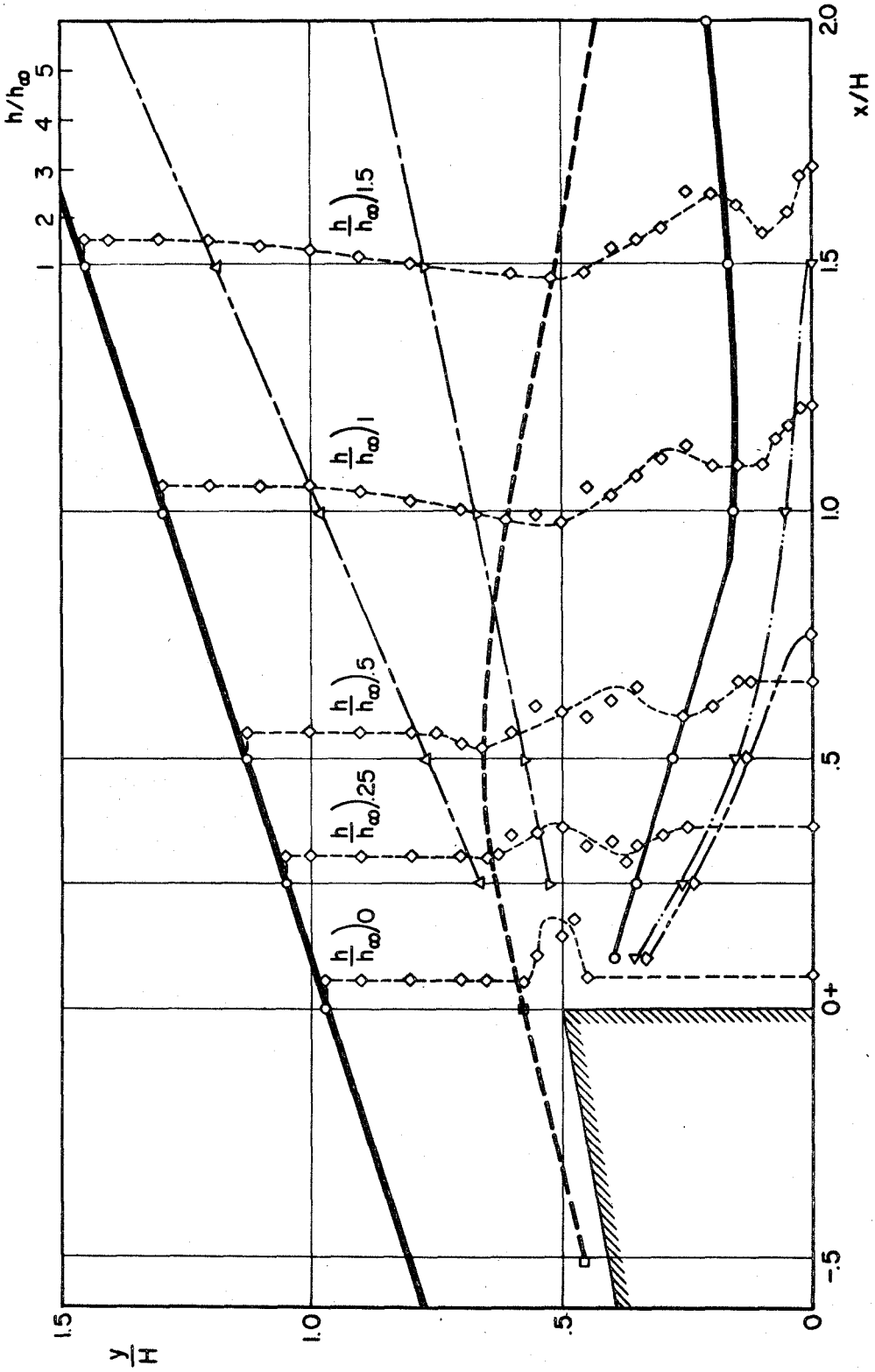

FIG.40 TYPICAL STATIC ENTHALPY PROFILES FOR NEAR WAKE BEHIND 20°, COLD WALL WEDGE

AT $M_\infty = 6$ & $Re_{\infty H} = 5.5 \times 10^4$ ($H = .3$, $\frac{T_W}{T_0} = .19$)

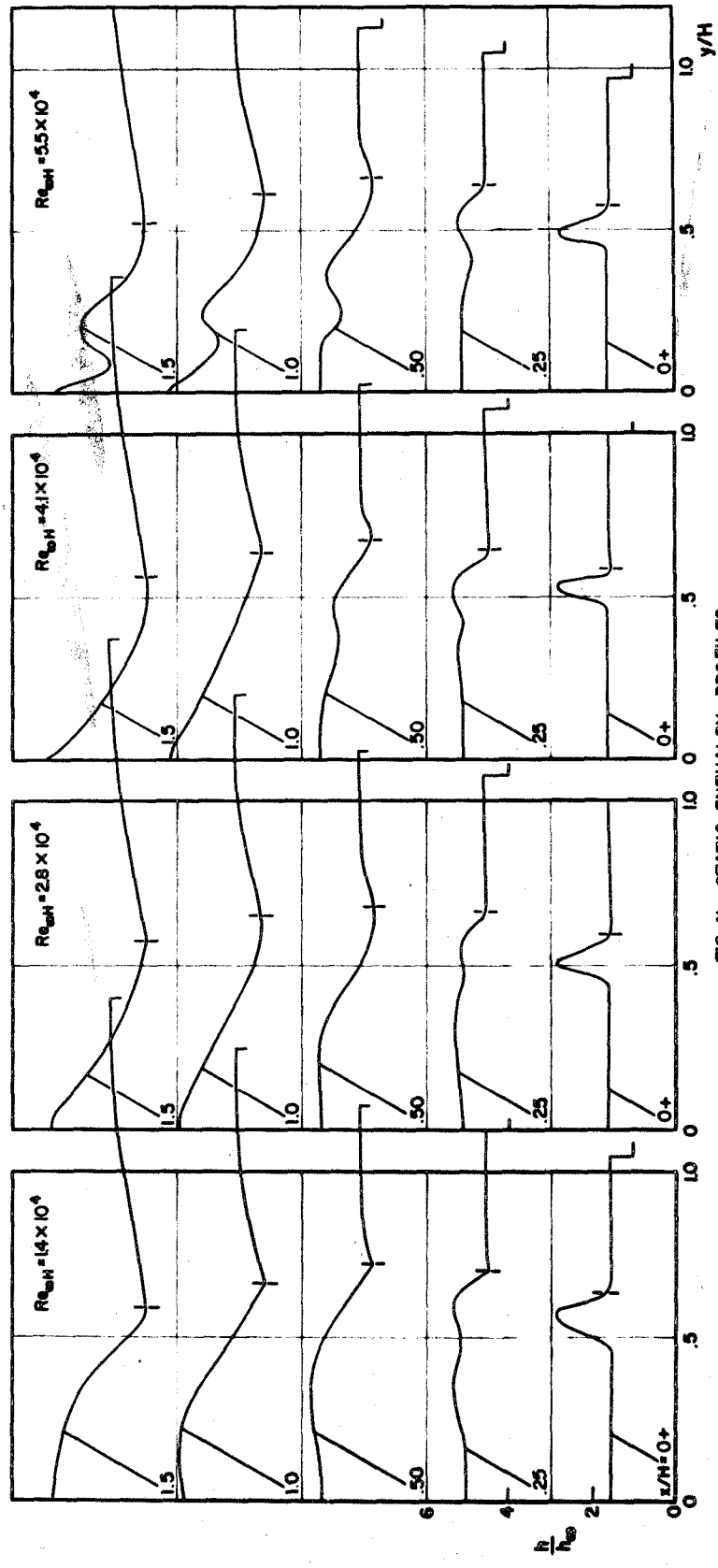

FIG. 41a STATIC ENTHALPY PROFILES
20° WEDGE MODEL-H=.3-COLD WALL

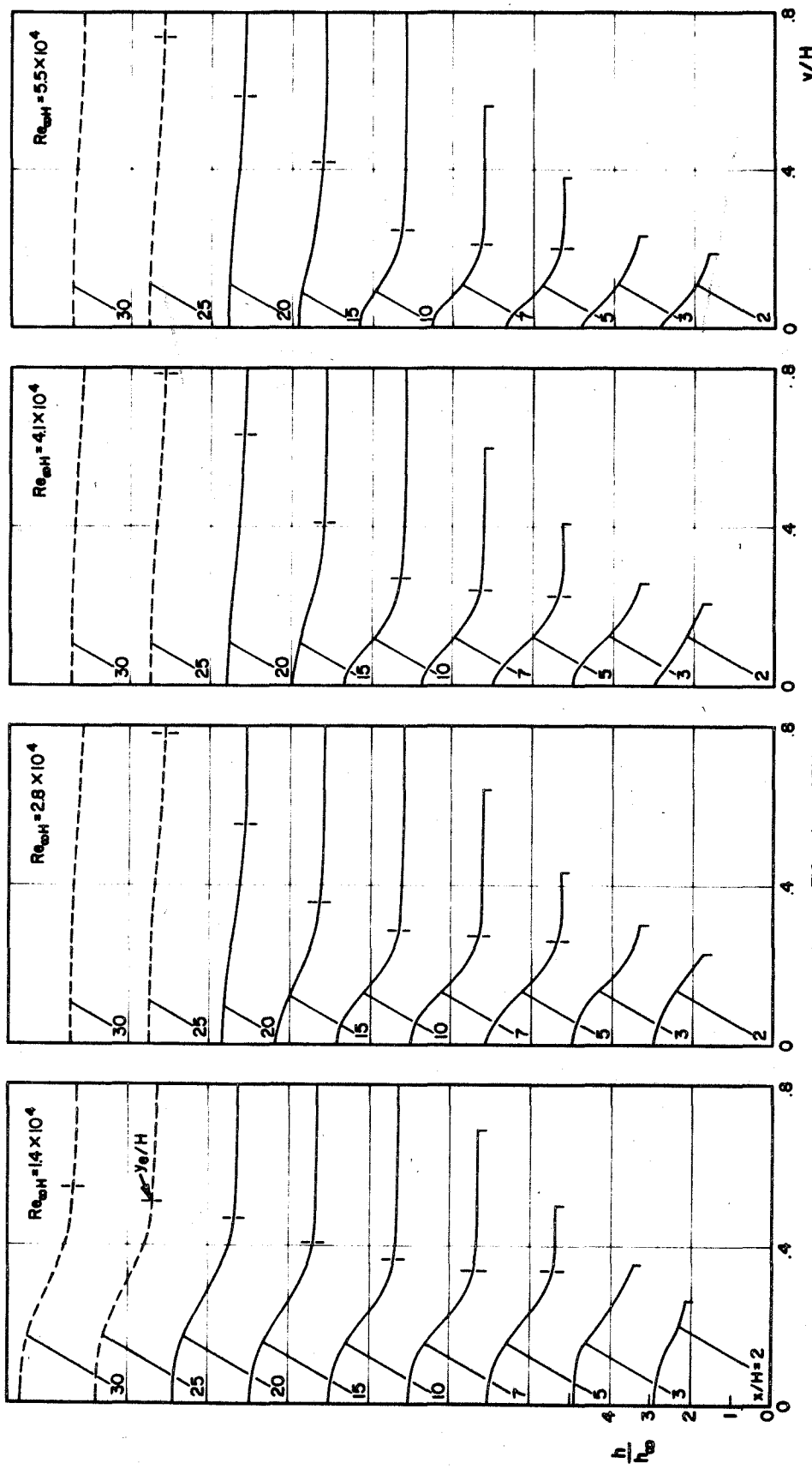

FIG. 41b STATIC ENTHALPY PROFILES
20° WEDGE MODEL-H=.3-COLD WALL

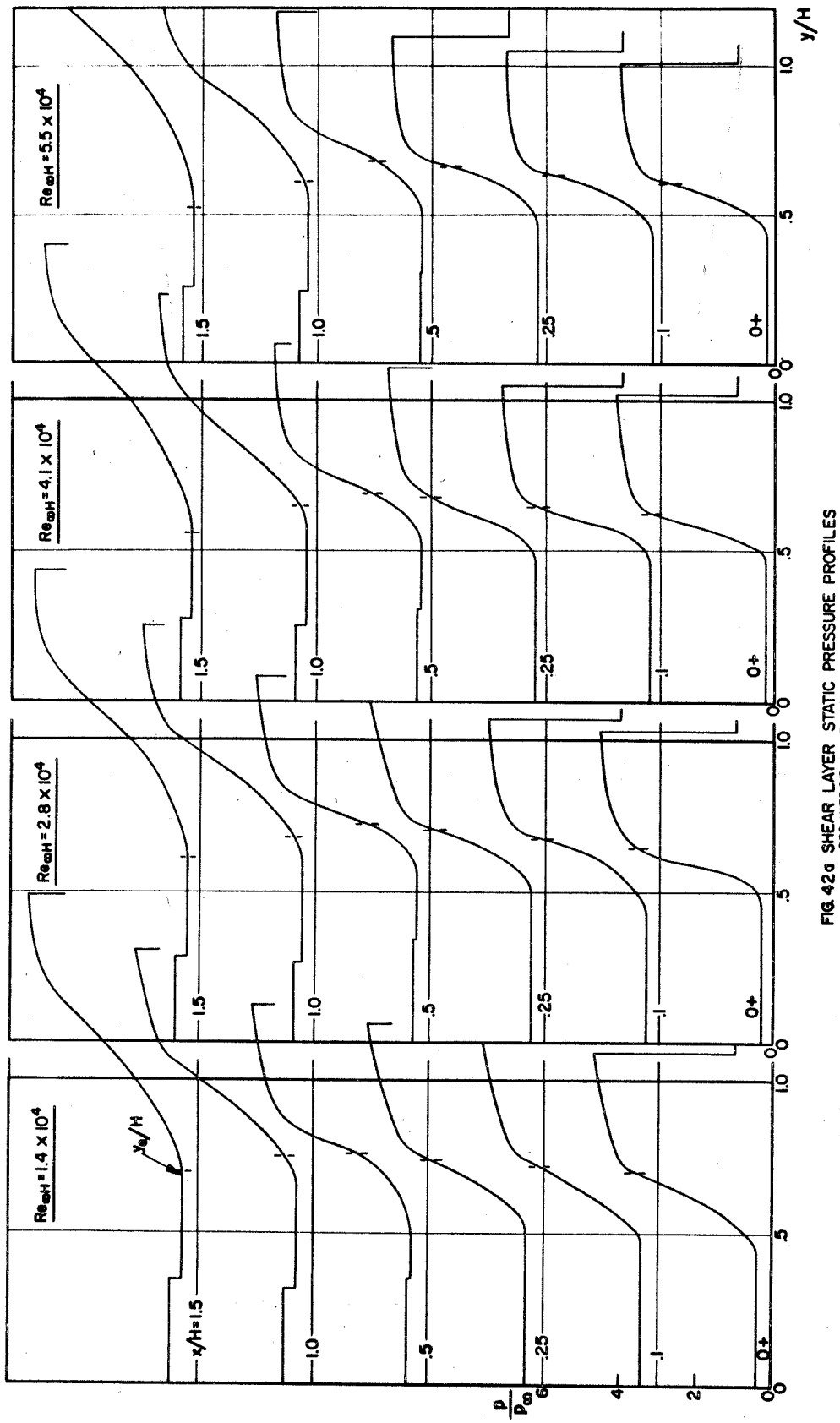

FIG. 42a SHEAR LAYER STATIC PRESSURE PROFILES
20° WEDGE-H=.3-ADIABATIC WALL

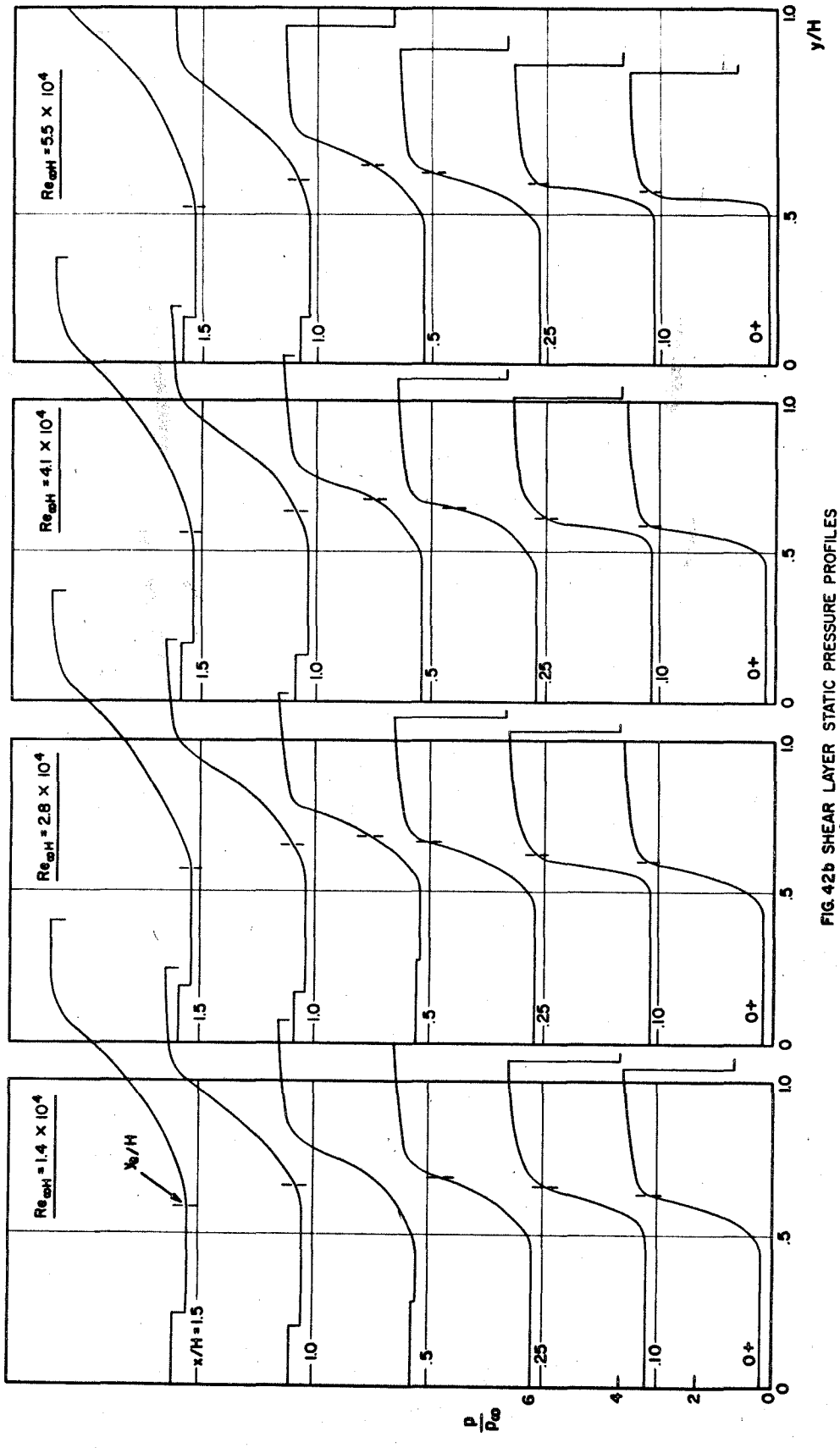

FIG. 42b SHEAR LAYER STATIC PRESSURE PROFILES
20° WEDGE - H = .3 - COLD WALL

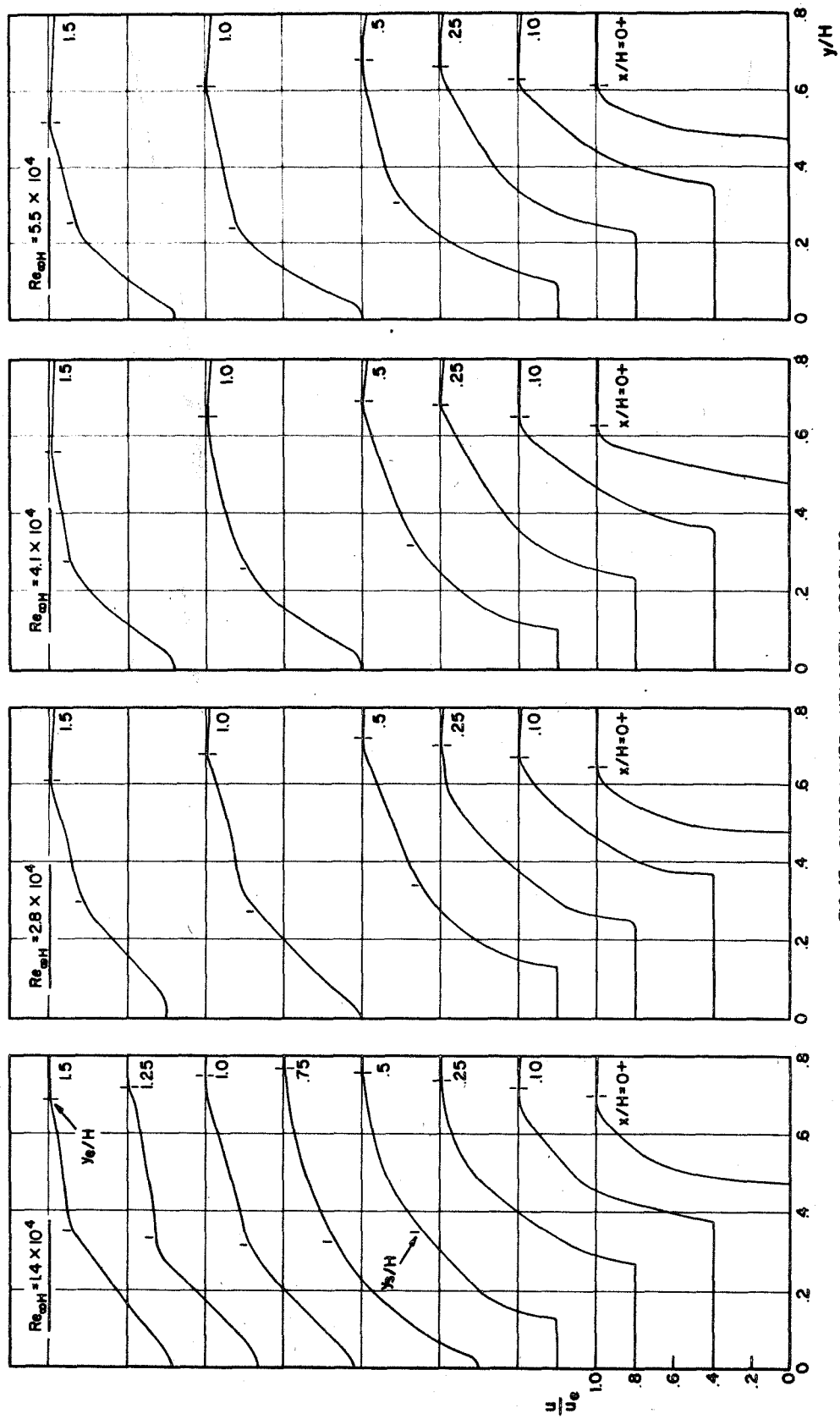

FIG. 43a SHEAR LAYER VELOCITY PROFILES
20° WEDGE-H=.3- ADIABATIC WALL

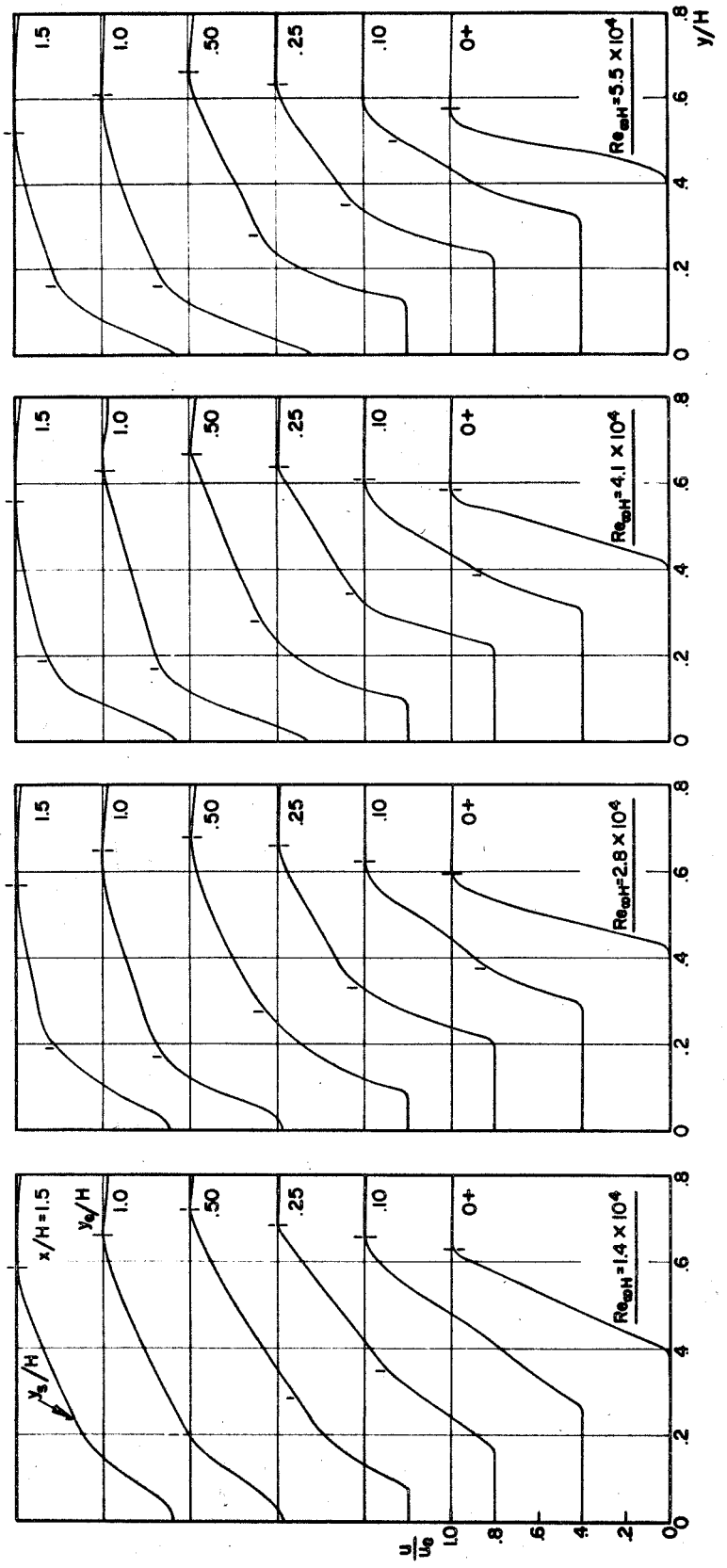

FIG. 43b SHEAR LAYER VELOCITY PROFILES
20° WEDGE-H=.3-COLD WALL

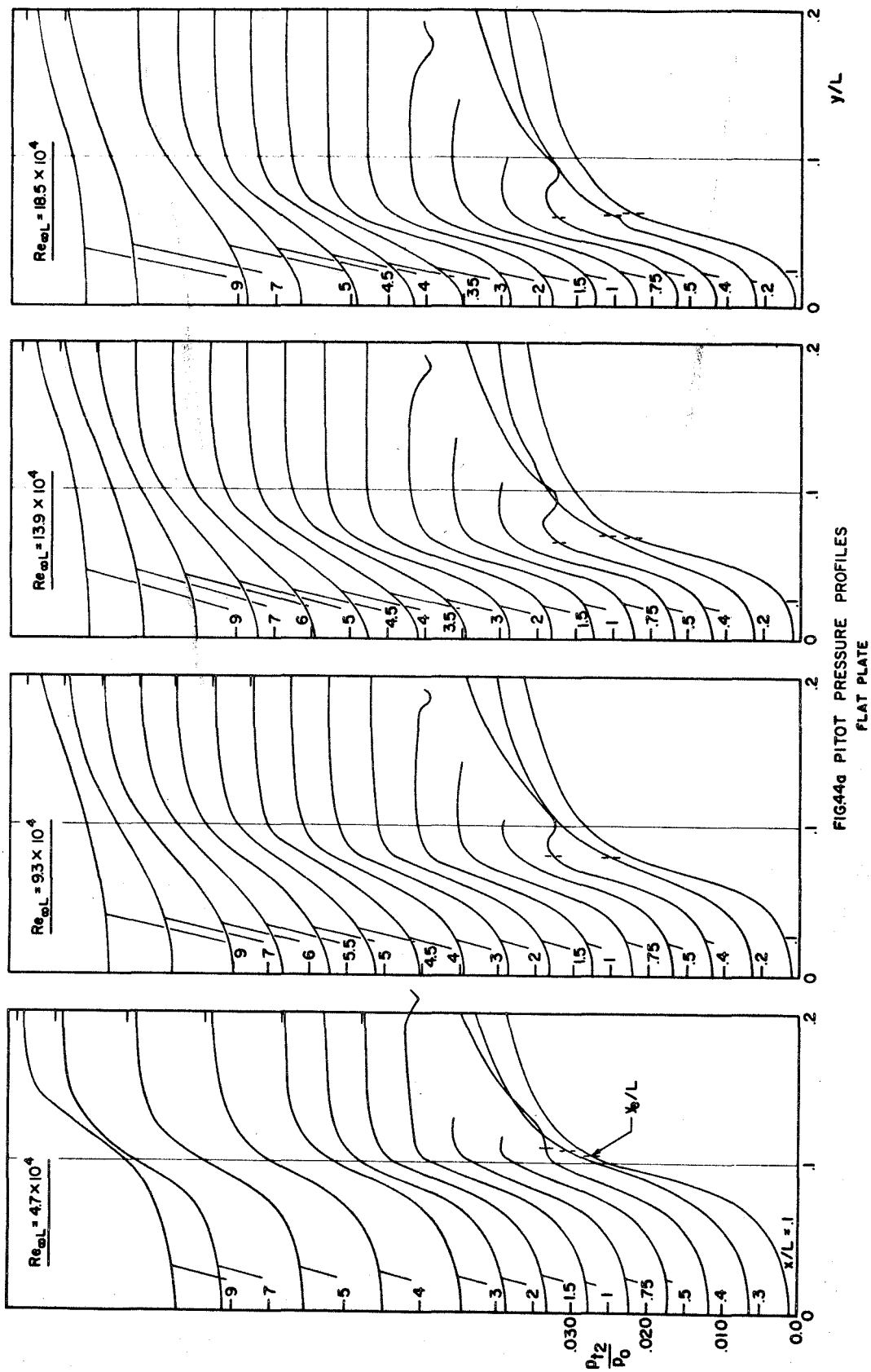

FIG.44a PITOT PRESSURE PROFILES
FLAT PLATE

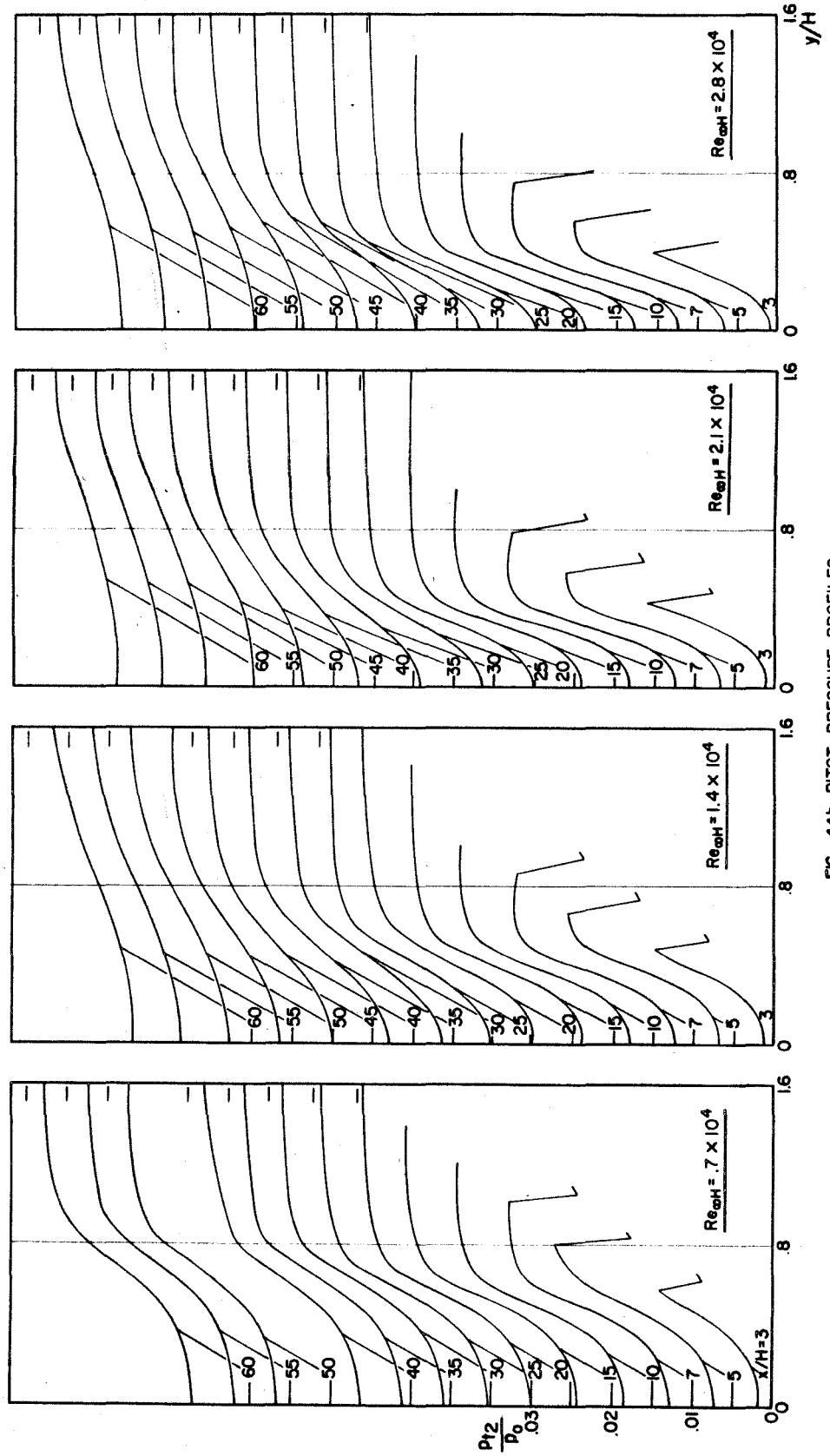

FIG. 44b PITOT PRESSURE PROFILES
20° WEDGE-H=.15

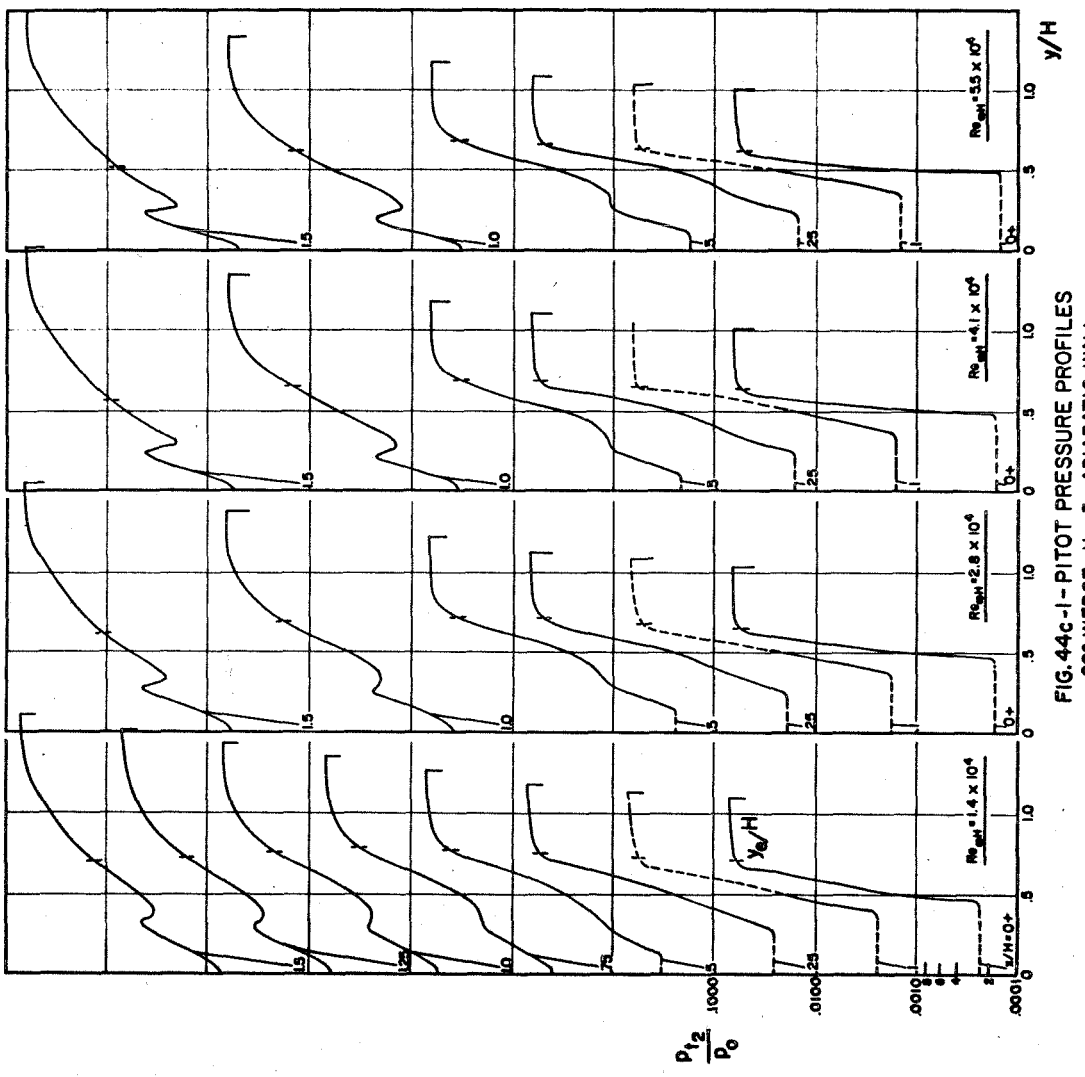

FIG. 44c-1- PITOT PRESSURE PROFILES
20° WEDGE-H=.3- ADIABATIC WALL

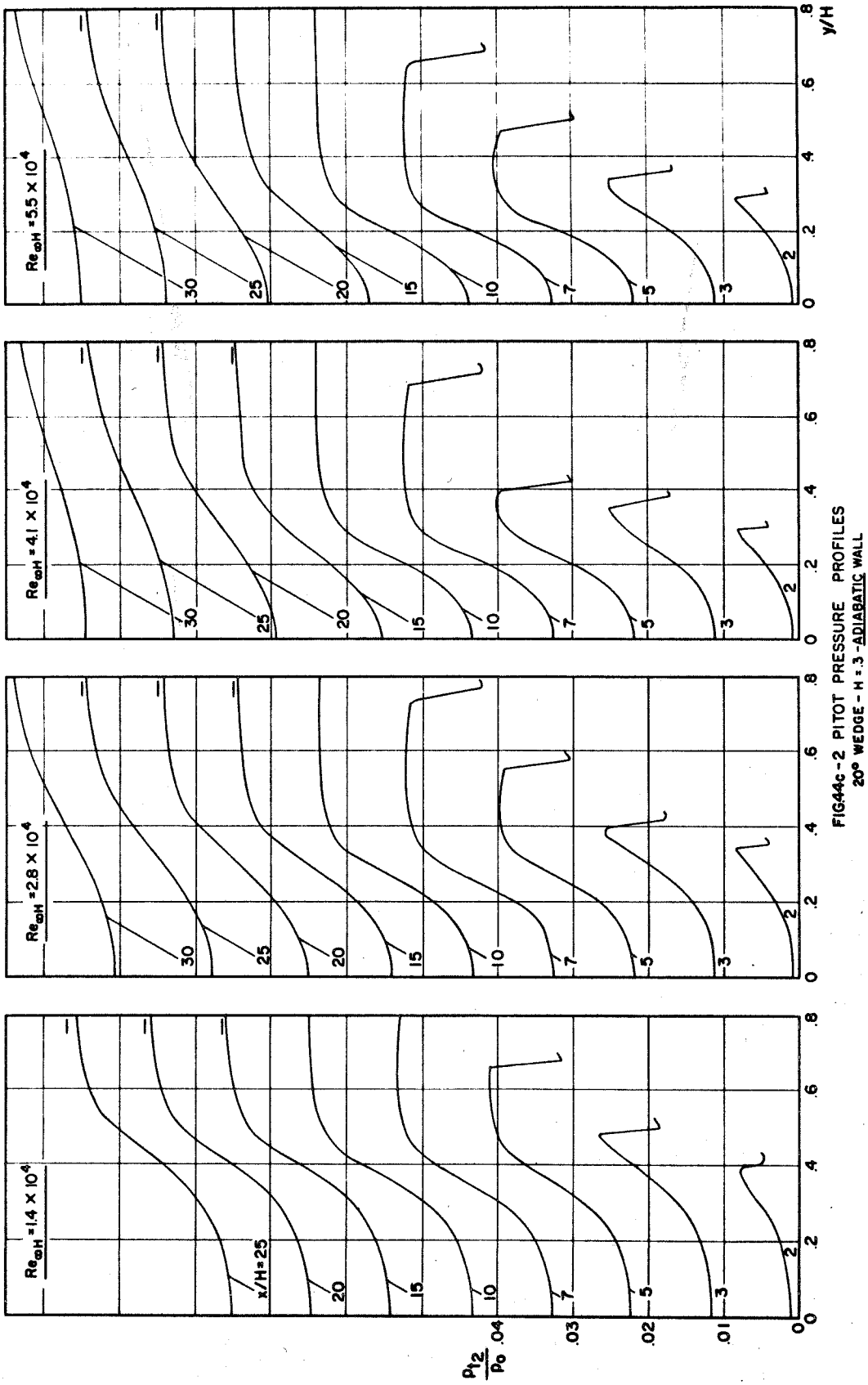

FIG44c-2 PITOT PRESSURE PROFILES
20° WEDGE - H = .3 - ADIABATIC WALL

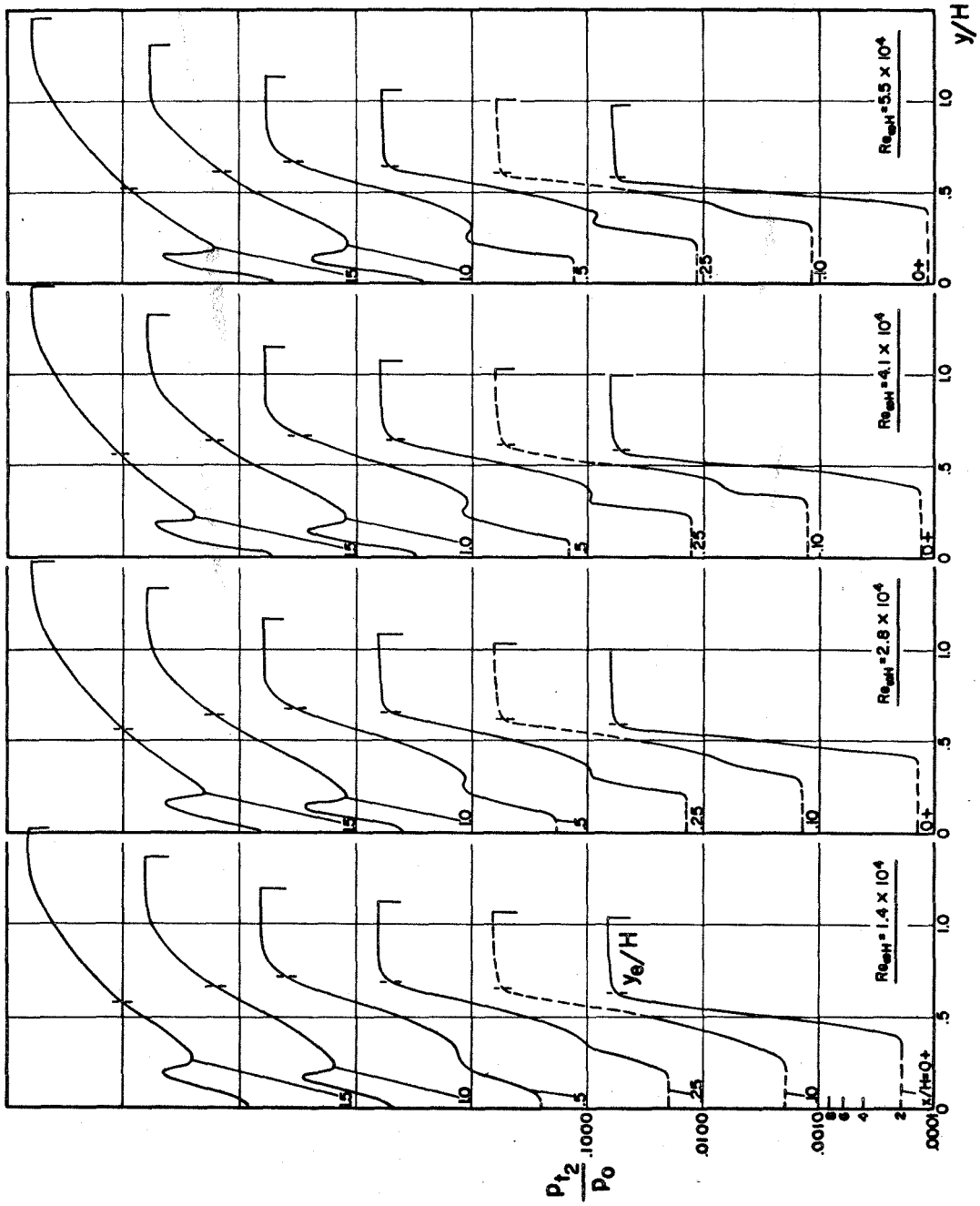

FIG.44d-I PITOT PRESSURE PROFILES
20° WEDGE-H=.3-COLD WALL

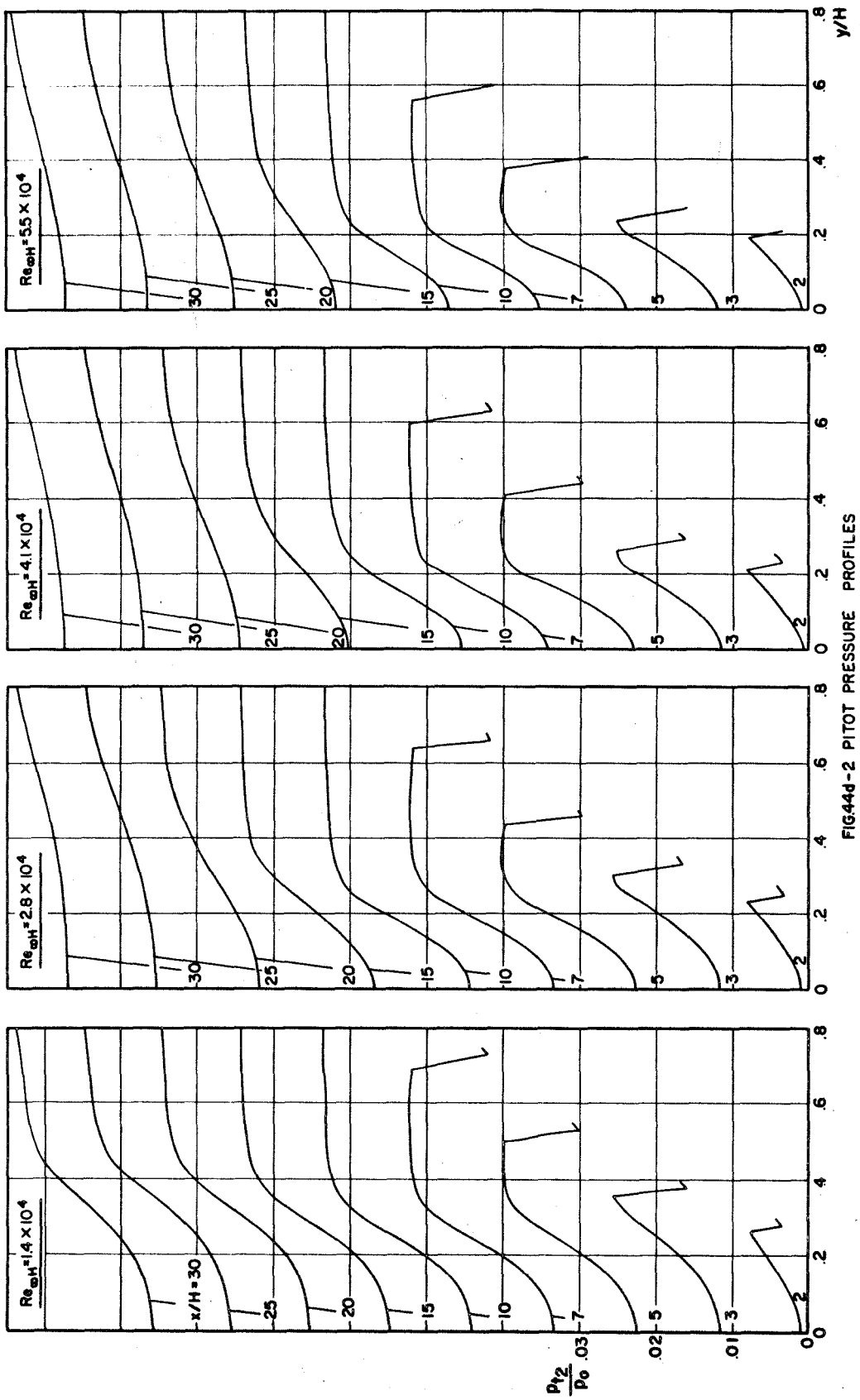

FIG.44d-2 PITOT PRESSURE PROFILES
20° WEDGE MODEL-H=3-COLD WALL

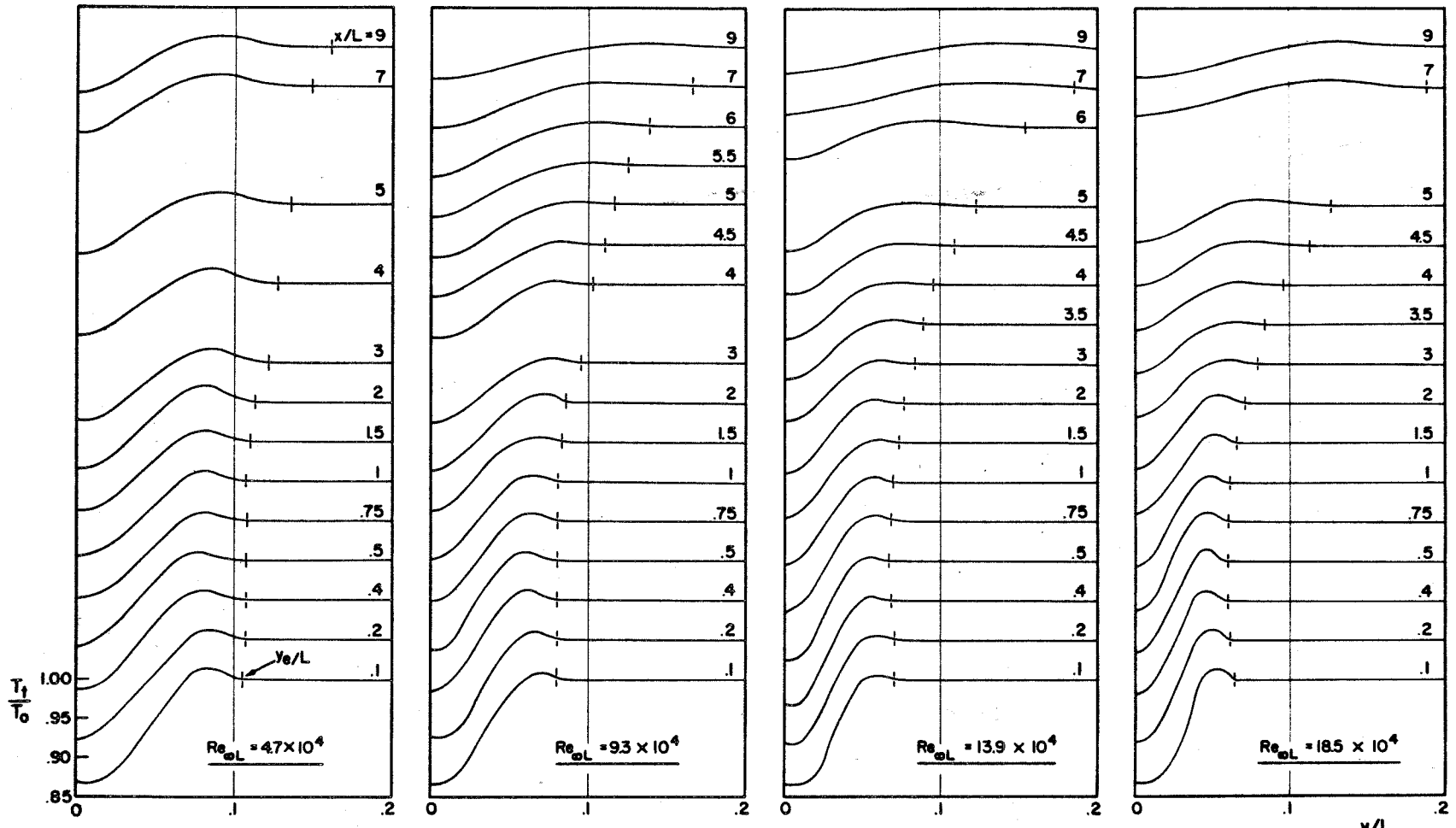

FIG.45a TOTAL TEMPERATURE PROFILES
FLAT PLATE

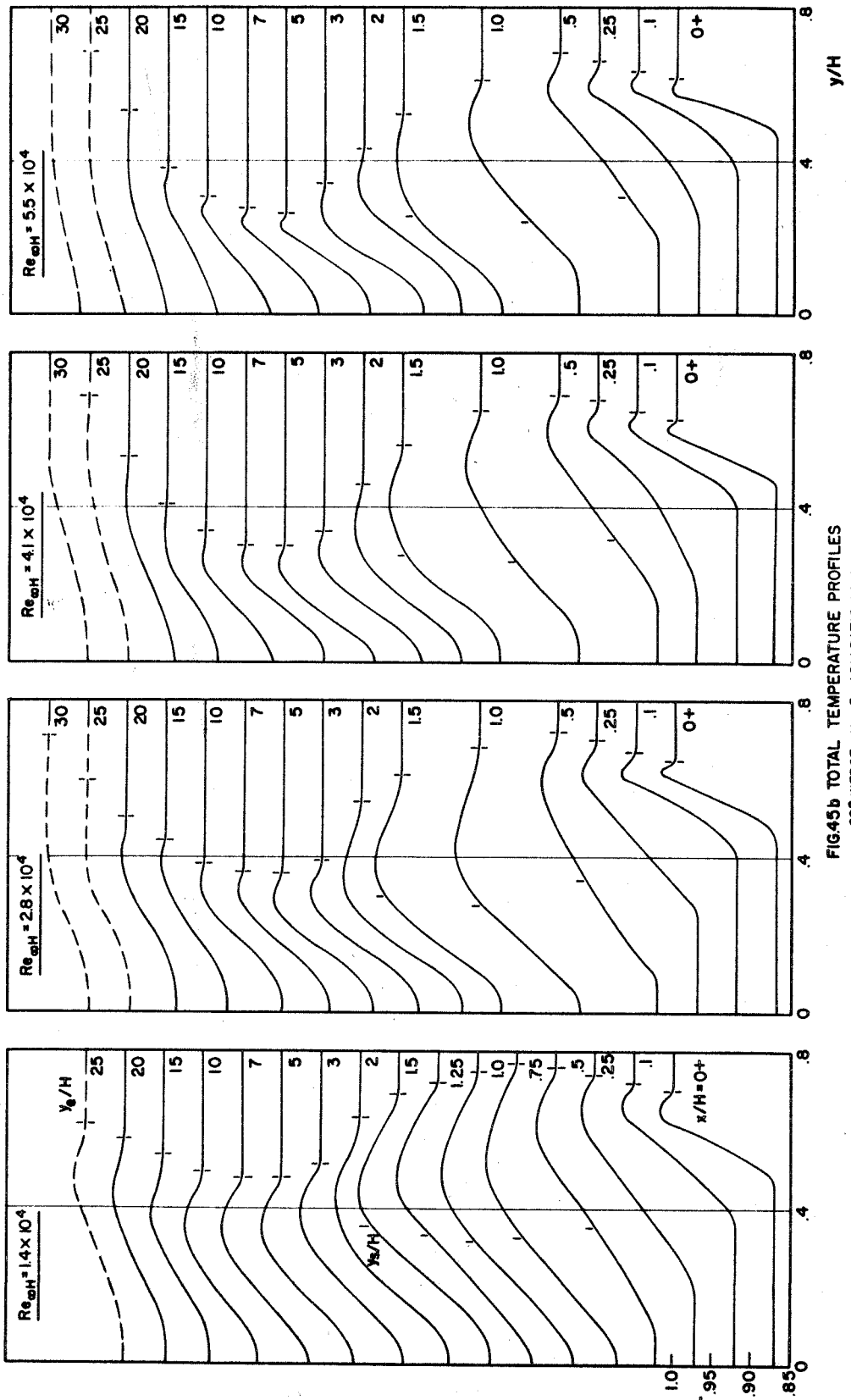

FIG.45b TOTAL TEMPERATURE PROFILES
20° WEDGE - H = .3 - ADIABATIC WALL

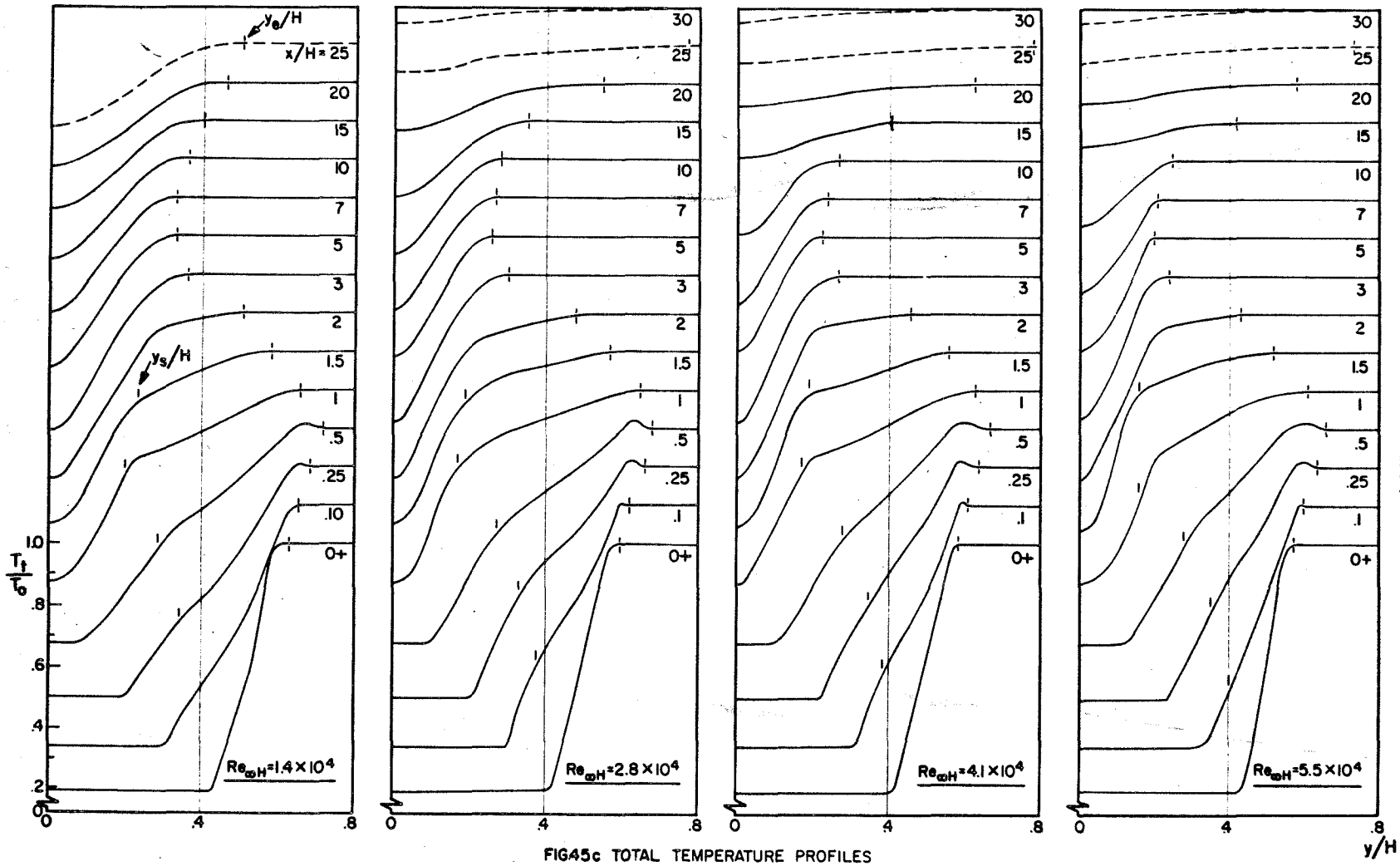

FIG45c TOTAL TEMPERATURE PROFILES
20° WEDGE MODEL-H=.3-COLD WALL